NUREG/CR-6820

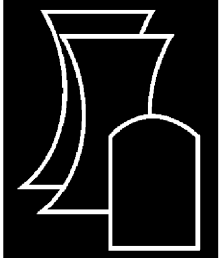

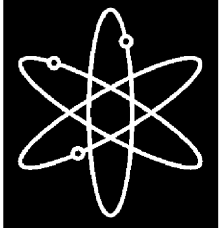

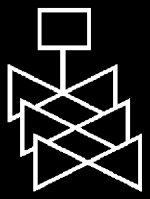

Application of Surface Complexation Modeling to Describe Uranium (VI) Adsorption and Retardation at the Uranium Mill Tailings Site at Naturita, Colorado

U.S. Geological Survey

U.S. Nuclear Regulatory Commission
Office of Nuclear Regulatory Research
Washington, DC 20555-0001

AVAILABILITY OF REFERENCE MATERIALS IN NRC PUBLICATIONS

NRC Reference Material

As of November 1999, you may electronically access NUREG-series publications and other NRC records at NRC's Public Electronic Reading Room at http://www.nrc.gov/reading-rm.html. Publicly released records include, to name a few, NUREG-series publications; *Federal Register* notices; applicant, licensee, and vendor documents and correspondence; NRC correspondence and internal memoranda; bulletins and information notices; inspection and investigative reports; licensee event reports; and Commission papers and their attachments.

NRC publications in the NUREG series, NRC regulations, and *Title 10, Energy*, in the Code of *Federal Regulations* may also be purchased from one of these two sources.

1. The Superintendent of Documents
   U.S. Government Printing Office
   Mail Stop SSOP
   Washington, DC 20402–0001
   Internet: bookstore.gpo.gov
   Telephone: 202-512-1800
   Fax: 202-512-2250
2. The National Technical Information Service
   Springfield, VA 22161–0002
   www.ntis.gov
   1–800–553–6847 or, locally, 703–605–6000

A single copy of each NRC draft report for comment is available free, to the extent of supply, upon written request as follows:

Address: Office of the Chief Information Officer,
Reproduction and Distribution
Services Section
U.S. Nuclear Regulatory Commission
Washington, DC 20555-0001
E-mail: DISTRIBUTION@nrc.gov
Facsimile: 301–415–2289

Some publications in the NUREG series that are posted at NRC's Web site address http://www.nrc.gov/reading-rm/doc-collections/nuregs are updated periodically and may differ from the last printed version. Although references to material found on a Web site bear the date the material was accessed, the material available on the date cited may subsequently be removed from the site.

Non-NRC Reference Material

Documents available from public and special technical libraries include all open literature items, such as books, journal articles, and transactions, *Federal Register* notices, Federal and State legislation, and congressional reports. Such documents as theses, dissertations, foreign reports and translations, and non-NRC conference proceedings may be purchased from their sponsoring organization.

Copies of industry codes and standards used in a substantive manner in the NRC regulatory process are maintained at—

The NRC Technical Library
Two White Flint North
11545 Rockville Pike
Rockville, MD 20852–2738

These standards are available in the library for reference use by the public. Codes and standards are usually copyrighted and may be purchased from the originating organization or, if they are American National Standards, from—

American National Standards Institute
11 West 42nd Street
New York, NY 10036–8002
www.ansi.org
212–642–4900

Legally binding regulatory requirements are stated only in laws; NRC regulations; licenses, including technical specifications; or orders, not in NUREG-series publications. The views expressed in contractor-prepared publications in this series are not necessarily those of the NRC.

The NUREG series comprises (1) technical and administrative reports and books prepared by the staff (NUREG–XXXX) or agency contractors (NUREG/CR–XXXX), (2) proceedings of conferences (NUREG/CP–XXXX), (3) reports resulting from international agreements (NUREG/IA–XXXX), (4) brochures (NUREG/BR–XXXX), and (5) compilations of legal decisions and orders of the Commission and Atomic and Safety Licensing Boards and of Directors' decisions under Section 2.206 of NRC's regulations (NUREG–0750).

DISCLAIMER: This report was prepared as an account of work sponsored by an agency of the U.S. Government. Neither the U.S. Government nor any agency thereof, nor any employee, makes any warranty, expressed or implied, or assumes any legal liability or responsibility for any third party's use, or the results of such use, of any information, apparatus, product, or process disclosed in this publication, or represents that its use by such third party would not infringe privately owned rights.

NUREG/CR-6820

Application of Surface Complexation Modeling to Describe Uranium (VI) Adsorption and Retardation at the Uranium Mill Tailings Site at Naturita, Colorado

Manuscript Completed: April 2003
Date Published: December 2003

Prepared by
J.A. Davis, G.P. Curtis

U.S. Geological Survey
Menlo Park, CA 94025

J.D. Randall, NRC Project Manager

Prepared for
Division of Systems Analysis and Regulatory Effectiveness
Office of Nuclear Regulatory Research
U.S. Nuclear Regulatory Commission
Washington, DC 20555-0001
NRC Job Code W6813

ABSTRACT

The objective of this study was to demonstrate a surface complexation modeling approach at the field scale for estimating K_d values and the retardation of a sorbing radionuclide with complex aqueous chemistry. The Uranium Mill Tailings Remediation Act (UMTRA) site near Naturita, Colorado was chosen for study, because it had a well-developed and definable uranium(VI) plume in a shallow alluvial aquifer and had spatially variant chemical conditions that we believed would be important in influencing U(VI) transport and retardation. It was shown in laboratory batch and column experiments with Naturita sediments that the adsorption and retardation of U(VI) by the Naturita sediments was strongly influenced by the dissolved carbonate concentration (alkalinity). A Generalized Composite surface complexation model (GC-SCM) was developed for the Naturita aquifer background sediments (NABS) based on fitting batch U(VI) adsorption data. With only two surface reactions (four surface species), the GC-SCM without electrical double layer terms was able to accurately simulate K_d values for U(VI) adsorption on the Naturita aquifer sediments over the observed range of pH and dissolved carbonate and U(VI) concentrations. For the range of Naturita aquifer chemical conditions, alkalinity was more important than either variable pH or U(VI) concentration in influencing U(VI) mobility. K_d values ranged from 0.29 to 22 mL/g when calculated for all Naturita groundwater analyses using the SCM. Low K_d values were associated with portions of the U(VI) groundwater plume containing high concentrations of dissolved U(VI) and alkalinity. Higher K_d values were associated with low concentrations of dissolved U(VI) and alkalinity.

In addition to the common experimental technique of batch adsorption studies, methods were investigated to estimate U(VI) K_d values in the field. Such methods are needed for: 1) validation of SCM model parameters for transport simulations within performance assessment (PA) models, and 2) estimation of initial conditions for adsorbed radionuclides for transport simulations describing previously contaminated sites. It was shown that isotopic exchange and desorption extraction methods can be an important part of a field characterization and modeling program. GC-SCM-predicted U(VI) K_d values generally agreed to within a factor of 2 to 3 with experimental estimates of the K_d values of the U-contaminated sediments. This agreement with the experimental determinations of sorbed U(VI) in the contaminated portion of the Naturita alluvial aquifer provides confidence in the predictive capability of the GC-SCM, which was developed from data with uncontaminated Naturita sediments. Another approach used to validate the GC-SCM was the determination of *in-situ* K_d values by suspending NABS samples in wells with U-contaminated groundwater for periods of time ranging from 3-15 months. *In-situ* (field) K_d values were calculated from groundwater measurements of dissolved U(VI) and U extracted from the suspended sediment samples. The *in-situ* K_d values in 17 wells ranged from 0.5 to 12 mL/g, with the K_d values decreasing with increasing alkalinity. There was close agreement between these measured *in-situ* K_d values and model-predicted K_d values using the GC-SCM.

Transport simulations conducted for the field scale demonstrated the importance of using the SCM to describe U(VI) adsorption rather than a constant-K_d modeling approach. A major conclusion from the transport simulations was that PA modelers must recognize not only that variable chemical conditions can cause a range of K_d values to be observed, but also that the spatial distribution of K_d values within that range is not likely to be a random function or a normal distribution. In plumes with chemical gradients, the spatial distribution of K_d values can be quite complex and be characterized by significant spatial character. The linkage of traditional contaminant-transport models and reactive-contaminant-transport models to models for dose assessment in PA was investigated. It was shown that a constant-K_d modeling approach is not always conservative compared to using an SCM to described radionuclide retardation in PA. Transport simulations with a rate-controlled U(VI) adsorption model agreed well with those that used the local chemical equilibrium approximation. The simulations also showed that predicted U(VI)

transport was nearly identical whether or not surface charge was explicitly considered within the GC-SCM.

The challenge in applying the surface complexation concept in the environment is to simplify the SCM, such that predicted adsorption is still calculated with mass laws that are coupled with aqueous speciation, while lumping parameters that are difficult to characterize in the environment in with other parameters. In order to be applied by solute transport modelers and within PA applications, the complexity of the adsorption model needs to be balanced with the goal of using the simplest model possible that is consistent with observed data. This can be achieved with the semi-empirical, site-binding GC modeling approach used in this report and previously demonstrated for modeling Zn retardation in a sand and gravel aquifer (Kent et al., 2000). The GC-SCM is a compromise between the simple constant-K_d approach and more complex SCM that are difficult to apply to the environment at present. Historically, solute transport modelers have lacked the necessary expertise to apply the SCM modeling approach and many have believed that the SCM approach is too complex to be applied. While it is true that the most complex SCM are too difficult to apply at present, it is demonstrated in this study that the GC modeling approach can be easily applied to simulations of radionuclide transport at the field scale and included with PA modeling. The GC modeling approach is preferable to completely empirical approaches, such as the constant-K_d model or adsorption isotherms, because the important linkage between surface and aqueous species (and associated thermodynamic data) is retained in the modeling through the coupling of mass action equations. This linkage also provides a framework for conducting uncertainty analyses that is based on process level parameters rather than on ranges of K_d values that result from lumping together multiple processes. In the authors' opinion, the current operational paradigm that employs constant-K_d values to describe the retardation of radionuclides at the field scale introduces more uncertainty than is necessary. This uncertainty could be reduced and more completely understood in the future with the use of the GC-SCM approach.

CONTENTS

FIGURES

TABLES

1 APPLICATION OF SURFACE COMPLEXATION MODELING TO DESCRIBE RADIONUCLIDE SORPTION IN COMPLEX SYSTEMS: SCIENTIFIC BACKGROUND AND OBJECTIVES

1.1 Introduction

Public and private organizations in the Unites States and other nations are cleaning up hundreds of sites contaminated with uranium (U), plutonium (Pu), and other contaminants that were released to the environment or that remain in temporary storage facilities (Crowley and Ahearne, 2002). These wastes contain high levels of radionuclides with long half-lives, and in most cases, the wastes will be disposed of in engineered facilities constructed underground in specific types of geologic formations. The most likely pathway for radionuclides to reach the biosphere from these repositories is by transport of dissolved radionuclides in groundwater (or transport of colloidal particles with adsorbed radionuclides).

In addition to the nuclear waste disposal problem, numerous sites throughout the United States are contaminated by radionuclides, especially U and thorium (Th) and their by-products, due to mining, milling and other industrial processes (Morrison and Cahn, 1991). The United States Nuclear Regulatory Commission (USNRC) is responsible for the regulatory oversight of site remediation and clean up, and possible release of sites for public or unrestricted use. Licensing decisions are made based on performance assessment (PA) calculations that utilize numerical models to estimate the increase in radioactivity exposure to the biosphere at selected locations. Contamination is often limited to the soils, subsurface sediments, and shallow aquifers at these sites.

Prediction of the fate and transport of radionuclides is of paramount importance in evaluating remediation schemes and in quantifying the risk of contamination to human or ecosystem health (USEPA, 1999). To make a calculation of radioactive exposure risk in PA, it is necessary to calculate the total amount of each radionuclide that will be present at selected locations as a function of time. A solute transport model is typically used to describe the physical processes of advection and dispersion that may transport radionuclides in groundwater from the source location to a site of ingestion. In addition to these hydrophysical processes, the transport of many radionuclides can be strongly influenced by reactive chemical processes, including aqueous complexation, sorption, precipitation and dissolution, and redox reactions. However, in practice, many reactive transport models ignore the chemical complexity of aqueous complexation and sorption processes and utilize the distribution coefficient (constant K_d) approach to describe the retardation of radionuclide contaminants (Bethke and Brady, 2000; USEPA, 1999). Although sorption is only a part of the overall PA calculations, retardation of radionuclide transport in the far-field geosphere zone may be extremely important in reducing the risk of biosphere exposure of certain radionuclides to levels that are in compliance with regulations.

The transport of actinide elements and other radionuclides in porous media can be strongly influenced by the competitive effects of the formation of mobile solution complexes and immobile adsorbed species. These elements can form many species in natural waters as a result of hydrolysis and complexation reactions. The distribution of aqueous species can be highly dependent on chemical conditions, especially pH and the concentrations of complexing ligands, such as carbonate ions (Clark et al., 1995; Waite et al., 1994). In natural waters, important complexing ligands for U(VI) include hydroxide, carbonate and dissolved organic carbon; such ligands may compete with adsorption sites for complexation of UO_2^{2+} (and other actinyl ions) and decrease the extent of adsorption via the formation of nonadsorbing aqueous complexes. The influence of some ligand interactions can be very complex, as demonstrated by the observed increased

adsorption of metals in the presence of certain ligands (Davis and Leckie, 1978). However, in some cases, the effects of complexing ligands can be modeled in a straightforward way by assuming that the aqueous complexes formed do not adsorb. For example, Kohler et al. (1996) showed that the adsorption of U(VI) on quartz in the presence of fluoride (F) ligands could be modeled as a competition between the quartz surface and aqueous F for complexation of U(VI).

The origin of K_d as an empirical modeling parameter can be traced to descriptions of ion exchange and ion chromatography in chemical engineering practice, primarily applied to alkali and alkaline earth cations that have extremely simple aqueous chemistry. Unfortunately, hydrologic modelers later assumed that this simple chemistry could be extended to essentially all inorganic contaminants and radionuclides. Perhaps the first application to transport in groundwater systems was that of Higgins (1959), who assumed that radionuclides resulting from underground nuclear explosions would adsorb via an ion exchange mechanism, with "variable pH between pH 2 and 9 having a very small effect on K_d values". Baetslé (1967), using logic still common today, argued that an exact knowledge of sorption isotherms was needed for accurate modeling of radionuclide transport, but in the interest of computational efficiency, a constant K_d approach could be applied.

The K_d concept works well when applied to trace concentrations of un-ionized, hydrophobic organic molecules, but its application to inorganic contaminants is problematic because the parameter is so sensitive to aqueous chemical conditions. For example, the K_d for U(VI) adsorption on ferrihydrite at pH 8 decreases by *four orders of magnitude* as the partial pressure of carbon dioxide gas, pCO_2, increases from its value in air (0.032%) to 1% (see Section 5). This is an important variation to understand, because the pCO_2 in aquifers commonly reaches values of 1-5%, while most K_d values have been determined in laboratory experiments equilibrated with or exposed to air. Moreover, pCO_2 often increases with transport after groundwater recharge, and this spatial/temporal trend in chemical conditions can greatly affect U(VI) retardation (see Section 9), as well as the retardation of other actinides.

The quality of thermodynamic data for radionuclide solubilities and aqueous speciation has been steadily increasing in recent years and the data are now available in critically reviewed compilations (Grenthe et al., 1992; Silva et al., 1995; Langmuir, 1997). In contrast, the choice of K_d values in PA modeling is generally made based on expert judgement of available experimental data for individual radionuclides and various rock materials. The expert judgement may include an evaluation of laboratory measurements of K_d values from batch or column experiments with site-specific materials in contact with solutions of varying chemical composition. In addition to measurements with site-specific materials, databases of K_d values have been assembled for the sorption of radionuclides on a variety of single mineral phases (Turner, 1995), natural materials, including soils and rock powders (USEPA, 1996; McKinley and Scholtis, 1995; Sheppard and Thibault, 1990; Looney et al., 1987; Baes and Sharp, 1983; Isherwood, 1981), and engineered barrier materials pertinent to nuclear waste disposal (Berry, 1992; Krupka and Serne, 1996).

One of the potentially large uncertainties in PA model calculations arises from the choice of K_d values for individual radionuclides. Depending on the type and purpose of the PA modeling study, either a single K_d value may be chosen for each radionuclide or a probability distribution function (PDF) may be derived that encompasses a range of K_d values. The uncertainty in the choice of K_d values or in the PDF arises from several sources, e.g. 1) experimental error, 2) extrapolation or interpolation of values to chemical conditions or rock types other than those used in actual experimental measurements of K_d, and 3) the scaling of K_d values measured for rock powders to the values expected for intact rocks in the site-specific, geologic setting.

Constant K_d models for adsorption do not adequately account for spatial variability in the composition of adsorbing phases or for variable chemical conditions, such as pH, ionic strength, alkalinity, or concentrations of complexing ligands that may be encountered along a groundwater flow path (Davis et al., 1998; Kohler et al., 1996). For a variety of reasons, the range of K_d values that may need to be considered for each radionuclide/rock combination can be quite large. One can consider spatial and temporal variability in chemical conditions in PA modeling with K_d values by separating the calculations into separate blocks of time or hydrologic units in space. Although the effects of changes in chemical conditions on the solubilities of radionuclides can usually be calculated in a straightforward manner, the effects of variable chemical conditions on adsorption and the choice of K_d values is more complex (Davis et al., 2002; USEPA, 1999; Kohler et al., 1996). In order to be "conservative", large ranges of K_d values may need to be estimated by expert judgement in order to account for possible changes in chemical conditions and for other sources of error. The uncertainties in these ranges are difficult to assess quantitatively without doing large numbers of experiments.

1.2 Surface Complexation Modeling

Although a number of variations in the modeling approach have been developed, there are four fundamental tenets in all surface complexation models (SCM) (Davis and Kent, 1990):

- Mineral surfaces are composed of specific chemical functional groups that react with dissolved solutes to form surface species (coordinative complexes or ion pairs), in a manner analogous to complexation reactions in homogeneous solution.

- The equilibria of adsorption reactions can be described by mass action equations. If desired, correction factors to these equations may be applied to account for variable electrostatic energy, using electrical double layer theory.

- The apparent binding constants determined for the mass action equations are empirical parameters related to thermodynamic constants by the rational activity coefficients of the surface species.

- Electrical charge at the surface is determined by the chemical reactions of the mineral functional groups, including acid-base reactions and the formation of ion pairs and coordinative complexes.

In contrast to models using constant K_d, SCM have the capability of describing changes in contaminant adsorption as chemical conditions and aqueous speciation vary, and SCM can be readily incorporated within solute transport models (Kent et al., 2000; Kohler et al., 1996; and see Section 9). Previous investigations have shown that the SCM concept can be applied to great advantage in natural systems by employing a simple Generalized Composite (GC) approach to describe metal or radionuclide adsorption (Davis et al., 2002; Davis, 2001; Kent et al., 2000; Davis et al., 1998). In the GC approach, the surface of the mineral assemblage is considered too complex to be quantified in terms of the contributions of individual phases to adsorption. Instead, it is assumed that adsorption can be described by SCM equilibria written with "generic" surface functional groups, with the stoichiometry and formation constants for each SCM mass law determined by fitting experimental data for the mineral assemblage (Davis et al., 2002; Davis et al., 1998).

Fortunately, the uncertainty in K_d values that arises from variations in the chemical composition of groundwater or mineralogical composition of the adsorbent phases along a flow path can be reduced with the use of surface complexation modeling (SCM) to describe adsorption (Kent et al., 2000; Kohler et al., 1996). In addition, certain large sources of uncertainty (e.g., scaling from K_d values measured for rock powders to the surfaces of a fractured rock system) can be more easily addressed with SCM, because SCM is based on

defining radionuclide adsorption per unit surface area rather than per unit mass.

SCM could be of significant value to PA if it was used to determine the range of K_d values that need to be considered and provide a scientific basis for the range of values chosen. Uncertainties in SCM parameters can be less than the uncertainties in K_d values (when considered as robust over a range of chemical conditions), and SCM uncertainties may be more easily quantified. For example, a recent report on batch studies of U(VI) adsorption on montmorillonite presented K_d values that ranged by more than 4 orders of magnitude over the pH range of 6.5 to 8.5 (Pabalan and Turner, 1996). Davis et al. (1998) and Kent et al. (2000) showed that the K_d values for Zn^{2+} in a sand and gravel aquifer varied by about two orders of magnitude because of variable chemical conditions in the groundwater. In each of these cases the datasets could be described by an SCM with a small number of independent parameters that remained constant and had comparatively little uncertainty in their values.

Using a range of 4 orders of magnitude in the uncertainty of K_d values (Pabalan and Turner, 1996) in PA calculations could lead to increased costs for waste cleanup at an industrial site or to rejection of an alternative waste disposal scenario. If used properly, SCM for radionuclide adsorption has the potential to increase the confidence and scientific credibility of PA transport modeling, by reducing the uncertainty in quantifying retardation and providing a means of quantifying that uncertainty. In addition, SCM has the potential to lower the estimated remediation costs of sites contaminated with radionuclides (or the feasibility of a disposal scenario) by decreasing the uncertainty of K_d values (and the associated safety factor applied in PA modeling).

The use of equilibrium geochemical models to calculate radionuclide solubilities and aqueous speciation is well established in the PA field. Surface complexation modeling is an extension of this thermodynamic modeling approach to include the reactions between dissolved species and the functional groups (ligands) present on mineral surfaces. The adsorption reactions are included as part of the network of chemical reactions that require equilibration, rather than as a condition-dependent partitioning coefficient, like K_d. Once the model is calibrated, it allows predictive calculations for a range of geochemical conditions without changing the values of the stability constants for radionuclide adsorption. The adsorption equations can be included efficiently in transport simulations in which there are chemical gradients in the subsurface environment rather than constant chemical conditions (Kent et al., 2000; Kohler et al., 1996; see Section 9).

1.3 Project Goals

Uranium ore processing on the Colorado Plateau resulted in a number of inactive mill tailing sites at which there is contamination of groundwater (USDOE, 1996). The groundwater at many of these sites is contaminated with U and often other species including vanadium, selenium and molybdenum. The USDOE is responsible for clean up of many of these sites as dictated by the Uranium Mill Tailings Remediation Act (UMTRA). At many of the sites, USDOE is proposing that sites will be cleaned up by natural flushing. A critical aspect of risk assessment and assessing the performance of natural flushing at these sites is estimating the migration of U(VI) in aquifers. In USDOE transport model simulations for these sites, retardation of U(VI) is almost always estimated based on a distribution coefficient, K_d, or a range of K_d values that is meant to describe the partitioning of U(VI) between the solid and aqueous phases. However, as mentioned above, K_d values, especially those for U(VI), are dependent on geochemical conditions within the aquifer, which often vary temporally and spatially (e.g., see Section 3). Simulations with a constant K_d can therefore introduce considerable uncertainty into the risk assessment or evaluation of remediation alternatives. Thus, in addition to hydrogeological characterization of field sites, a detailed knowledge of geochemical conditions within contaminated aquifers is required to make accurate U(VI) transport simulations.

The objective of this project was to demonstrate that, despite the complexities inherent at field sites and in modeling sorption by natural mineral assemblages, the surface complexation concept can currently be utilized to great advantage by employing the simpler GC modeling approach to describe U(VI) sorption and retardation (and thus, by extension, for other adsorbing radionuclides). In this report we present a GC model for simulating U(VI) sorption by subsurface sediments collected from the alluvial aquifer at the UMTRA site near Naturita, Colorado. In Sections 6, 7, and 9, it is shown that this simple, semi-empirical site-binding model can be readily applied within a reactive transport model for U(VI) or to predict *in-situ* K_d values, which allows temporal and spatial variations in geochemical conditions within the aquifer to be accurately considered in model simulations.

1.4 Overview of Report

Studies have been designed within this project to enable development of a GC modeling approach for description of U(VI) adsorption by subsurface materials collected from the alluvial aquifer at the UMTRA site at Naturita, Colorado (USDOE, 1995). The studies were completed under conditions of variable aqueous chemistry, which causes significant variation in the speciation of U(VI), as described in Section 2. The geochemical characteristics of the field site and its hydrogeology are summarized in Section 3. Physical and chemical characteristics of Naturita alluvial sediments both upgradient and within the region of U contamination are described in Sections 4, 5 and 6. A large composite sample of the aquifer sediments upgradient of the U contamination was collected during the study (referred to as the NABS sample, for Naturita Aquifer Background Sediments). Results of U(VI) sorption experiments with the NABS sediment sample (and K_d values) are given in Section 5. In addition, Section 5 includes development of the GC model to describe U(VI) sorption (and K_d values) as a function of solution conditions (pH, U(VI) concentration, and alkalinity (or partial pressure of CO_2). Section 6 describes the sorption of U(VI) to several individual sediment samples collected at various locations throughout the region of U contamination at the Naturita site. These samples were collected during the installation of monitoring wells, and groundwater chemical data were also determined at the same locations (sections 3 and 6), enabling the calculation of *"field-K_d values"* for these samples.

Aliquots of the NABS sample were suspended in selected monitoring wells for durations of 3 to 15 months during the study. Sorption of U(VI) by these samples suspended in the groundwater is described in Section 7. K_d values were determined for these samples and compared to those predicted by the GC model for U(VI) sorption.

The results of laboratory studies of U(VI) transport through columns packed with a grain size fraction of the NABS sample are summarized in Section 8. These studies were conducted under conditions of variable pH, U(VI) concentration, and alkalinity (or partial pressure of CO_2). The experimental results are compared with a reactive transport model that considers U(VI) aqueous complexation and sorption as predicted by the GC model. Section 9 describes the development of a detailed reactive transport model for the Naturita site. The model includes U(VI) aqueous complexation and sorption reactions consistent with the GC model and takes into account the spatial and temporal variations in groundwater chemical conditions at the site. Section 10 illustrates the sensitivity of the U(VI) transport calculations at the Naturita site to the description of U(VI) sorption, including a comparison of the predictions by the GC model with those of a constant K_d model.

Section 11 presents PA dose calculations for the Naturita site using the reactive transport model that includes the GC model to describe U(VI) sorption. The results demonstrate that it is relatively simple to include the surface complexation modeling concept within the groundwater pathway component of PA modeling.

Section 12 summarizes the conclusions of the project and discusses the significance of the project results to PA modeling. The project impacts the evaluation of appropriate methods to determine K_d values for radionuclides, the choice of models to describe radionculide sorption, and the extent of adsorption uncertainties on PA modeling. The study has also has implications for cost-effective evaluations of groundwater remediation scenarios and for the evaluation of environmental risk at licensed sites contaminated with U.

2 URANIUM(VI) AQUEOUS SPECIATION AND EQUILIBRIUM CHEMISTRY

2.1 U(VI) Solubility and Aqueous Speciation

The mobility of uranium(VI) in water-rock systems is dependent both upon its ability to form insoluble precipitates and upon its tendency to adsorb to solid substrates, particularly at relatively low total uranium (U) concentrations. The geochemical conditions that lead to significant mobility are those under which strong aqueous complexes are formed that are weakly adsorbed. For example, under alkaline conditions, uranyl-carbonato complexes are formed that are weakly adsorbed (Waite et al., 1994). Considerable advances have been made recently in developing a coherent set of thermodynamic data for describing the solution and mineral equilibrium chemistry of U (Grenthe et al., 1992; Silva et al., 1995; Langmuir, 1997). These advances allow better comparison of models for U(VI) adsorption, because consistent thermodynamic data can be used for the aqueous reactions in experimental systems.

In a previous report, we showed the complex distribution of U(VI) aqueous species as a function of pH in equilibrium with the partial pressure of CO_2 present in air (Davis, 2001). In this report we present aqueous speciation calculations relevant to the chemical conditions present in the alluvial aquifer at the Uranium Mill Tailings and Remediation Act (UMTRA) site at Naturita, Colorado. The calculations presented in this report and in Davis (2001) were made using the thermodynamic data given in Tables 2-1 and 2.2, unless indicated otherwise, which are generally consistent with the NEA database for uranium (Grenthe et al., 1992; Silva et al., 1995). However, during the preparation of this report, new results were published regarding the aqueous species, $CaUO_2(CO_3)_3^{2-}$ and $Ca_2UO_2(CO_3)_3^{0}$(aq) (Brooks et al., 2003). The existence of these species was proposed in earlier investigations (Bernhard et al., 2001; Kalmykov and Choppin, 2000), and the more recent results (Brooks et al., 2003) seem to confirm the existence of these species. Aqueous speciation calculations with the thermodynamic data of Bernhard et al. (2001) ($\log \beta_{113} = 25.4$; $\log \beta_{213} = 30.55$) suggest that these species could be the predominant aqueous species in many groundwater systems (Brooks et al., 2003). In this section we present aqueous speciation calculations with and without these species to demonstrate their potential importance in Naturita groundwaters. However, these new aqueous species were not considered further in this report, except for one set of calculations in Section 5. Alternative speciation and modeling calculations that consider these new aqueous species will be presented in subsequent publications from our group (e.g., Davis et al., 2003a; Kohler et al., 2003; Curtis et al., 2003a; Curtis et al., 2003b).

The solubility of well-crystallized schoepite, β-$UO_2(OH)_2$, in an artificial groundwater typical of uncontaminated conditions in the Naturita alluvial aquifer is illustrated in Figure 2-1. In the calculations, the solution is at equilibrium with a partial pressure of CO_2(g) of 0.01 atm (or 1%), which is typical of the aquifer conditions upgradient of the U contamination at the site. At equilibrium with schoepite, the aqueous speciation is dominated by the multinuclear mixed hydroxy carbonate complex, $(UO_2)_2CO_3(OH)_3^-$, in the pH range 5.75 to 7. The mononuclear di- and tri-carbonato complexes predominate at pH>7. The pH values in the Naturita aquifer mostly occur within the range of 6.8 to 7.2 (see Section 3). The minimum predicted solubility under these conditions is about 20 μM at pH 5.75, but the solubility at pH 7 exceeds 200 μM.

At low total dissolved U(VI) concentrations (e.g. 2×10^{-8}M), typical of the conditions upgradient of the U contamination at Naturita, the mixed hydroxy carbonate complex, $(UO_2)_2CO_3(OH)_3^-$, would not comprise a significant fraction of total dissolved U(VI) (Fig. 2-2A). At the prevailing CO_2 partial pressure of 1%, the aqueous speciation of U(VI) in the neutral to alkaline pH

range is predominantly the dicarbonato complex. The highest dissolved U(VI) concentrations observed at the Naturita site are about 10 μM and the highest partial pressures of CO_2 (5-10%) are found in the same region of the aquifer. Fig. 2-2B shows the aqueous speciation of U(VI) in an artificial Naturita groundwater solution with 10 μM dissolved U(VI) and at equilibrium with a partial pressures of CO_2 of 5%. Under these conditions, the mononuclear di- and tri-carbonato complexes predominate within the pH range 6 to 8.

Figure 2-3 illustrates the change in U(VI) aqueous speciation as a function of the partial pressure of CO_2 at a constant pH of 7.0 and a total dissolved U(VI) concentration of 1 μM. Note that at equilibrium with air ($\log pCO_2 = -3.5$), the predominant species is the multinuclear mixed hydroxy carbonate complex, $(UO_2)_2CO_3(OH)_3^-$. At a partial pressure of CO_2 of 0.2% and higher, the predominant species changes to the dicarbonato complex. Most aquifers have partial pressures of CO_2 greater than 0.5% (Hem et al., 1985).

2.1.1 Calculation with new aqueous ternary complexes, $Ca_{1,2}UO_2(CO_3)_3$

Figure 2-4 shows the significant difference in aqueous U(VI) speciation that results when the aqueous ternary complexes, $CaUO_2(CO_3)_3^{2-}$ and $Ca_2UO_2(CO_3)_3^0$(aq), are included in the calculation of equilibrium. Note that in contrast to the results presented in Figure 2-2A, the aqueous species, $Ca_2UO_2(CO_3)_3^0$(aq), is now the predominant species at pH values less than 7.8. The chemical conditions for the calculations shown in Figure 2-4 are nearly the same as in Figure 2-2A, except that the total dissolved Ca was determined for each pH value, using the assumption of equilibrium between the aqueous phase and calcite. Calculations with a total U(VI) concentration of 10^{-5}M yield essentially the same relative distribution of species as a function of pH, because none of the multinuclear U(VI) aqueous species become important. Again, this result contrasts with the similar calculations performed without the new ternary aqueous species (Fig. 2-2B), where the mixed hydroxy carbonate complex, $(UO_2)_2CO_3(OH)_3^-$, was important.

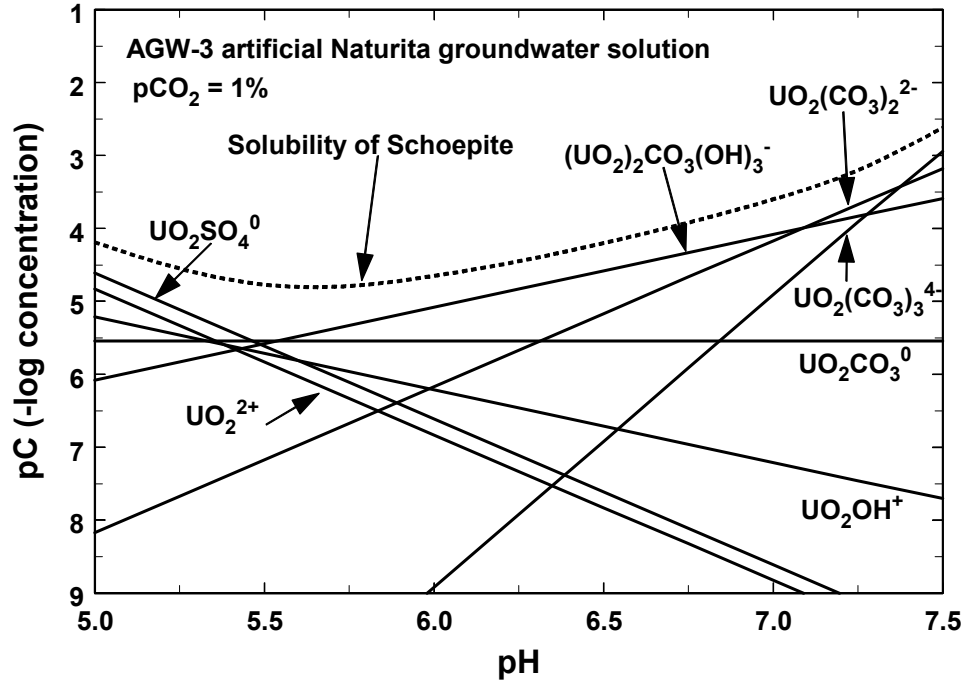

Figure 2-1. Solubility of β-$UO_2(OH)_2$, showing the pC (-log concentration) of predominant aqueous species as a function of pH in an artificial groundwater solution (see Sections 3 and 5) in equilibrium with a partial pressure of CO_2 of 10^{-2} atm (pCO_2 = 1%).

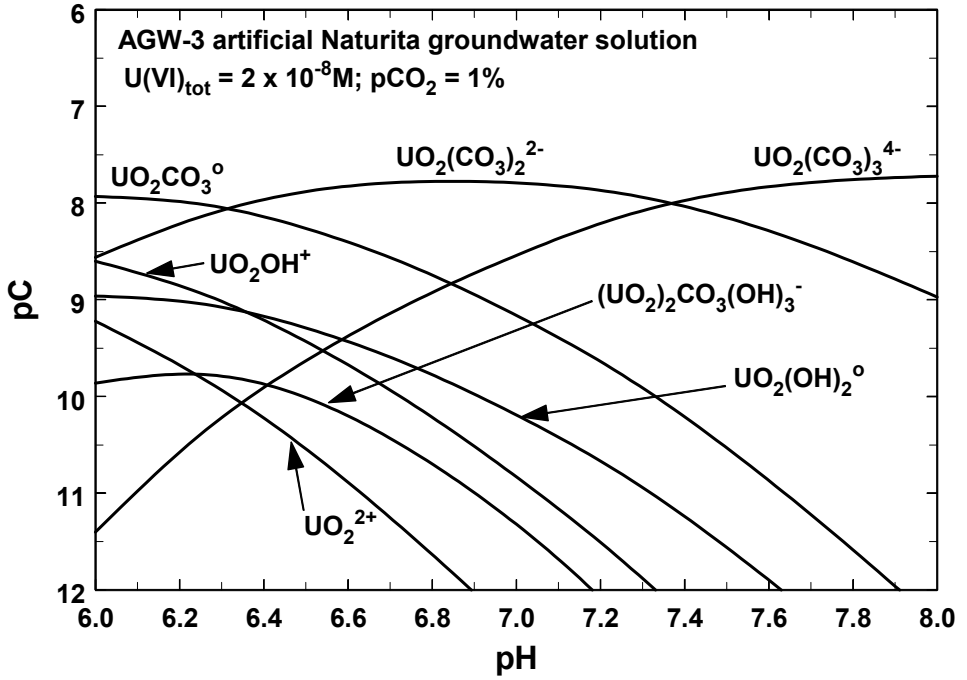

Figure 2-2A. Dissolved speciation of U(VI) as a function of pH in an AGW-3 artificial groundwater solution equilibrated with a partial pressure of CO_2 of 10^{-2} atm (pCO_2 = 1%). Total dissolved U(VI) = 2 x 10^{-8}M. Conditions typical of Naturita groundwater upgradient of uranium contamination (see Section 3).

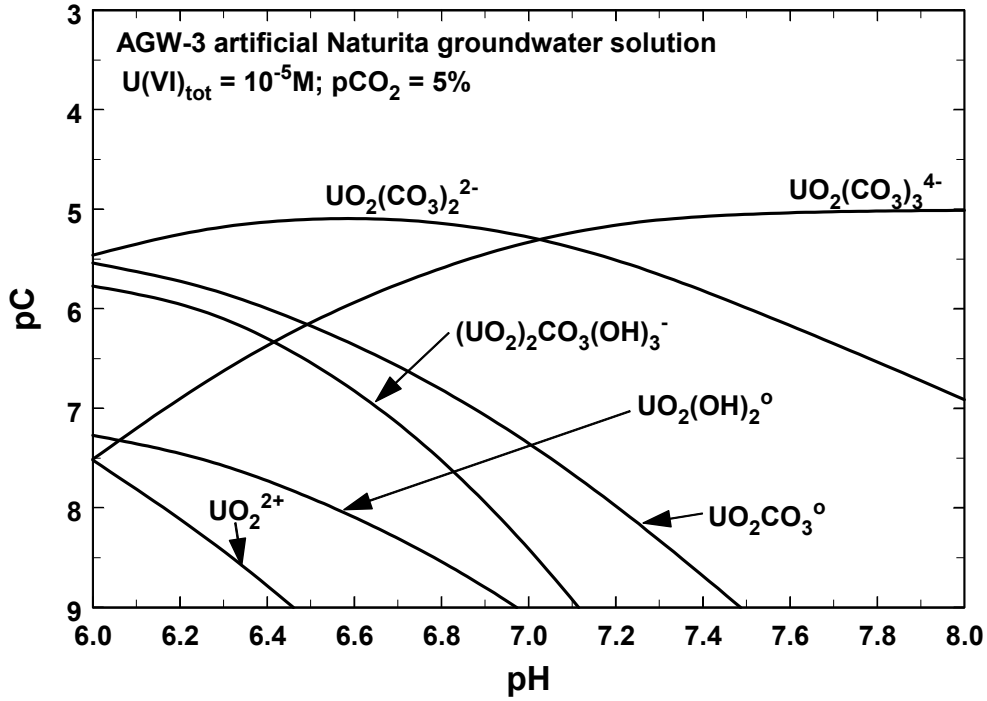

Figure 2-2B. Dissolved speciation of U(VI) as a function of pH in an AGW-3 artificial groundwater solution equilibrated with a partial pressure of CO_2 of $10^{-1.3}$ atm (pCO_2 = 5%). Total dissolved U(VI) = 10^{-5}M. Conditions typical of Naturita groundwater at center of uranium contamination (well NAT-26 - see Section 3).

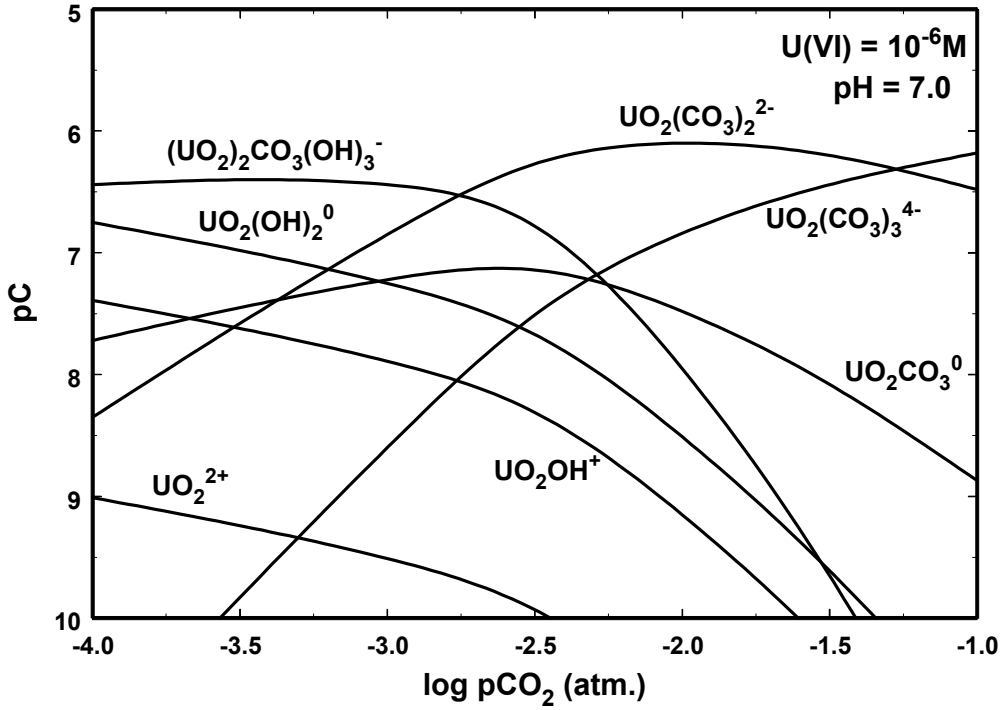

Figure 2-3. Dissolved speciation of U(VI) as a function of the partial pressure of CO_2 at pH 7 and a total dissolved U(VI) concentration of 1 μM.

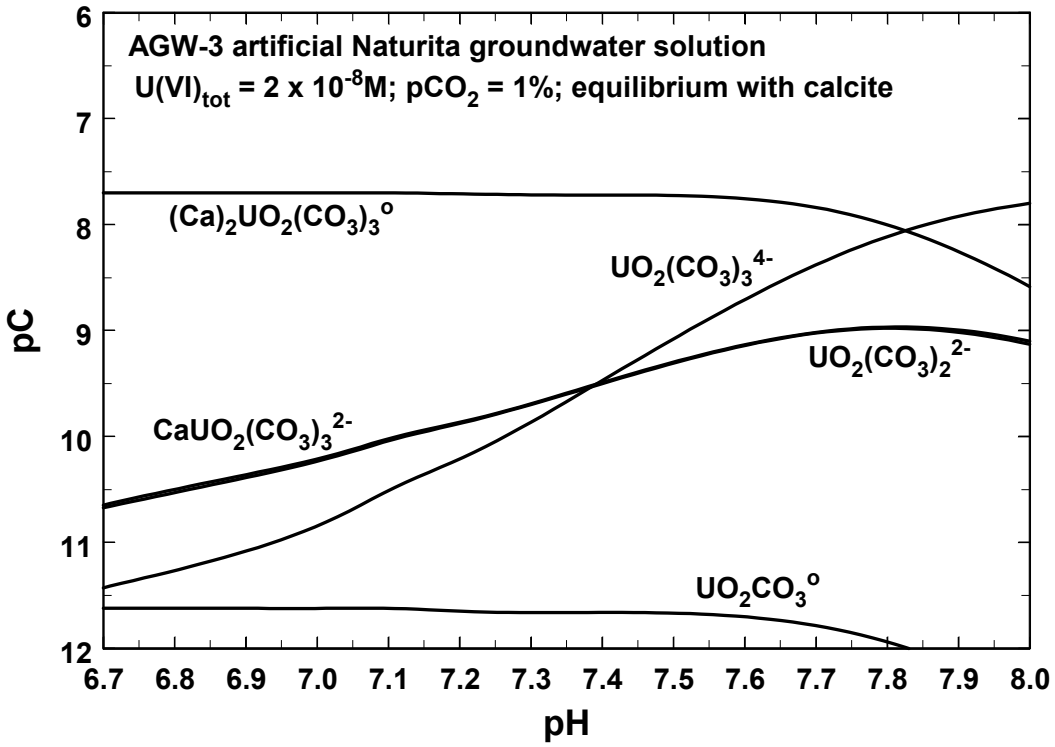

Figure 2-4. Dissolved speciation of U(VI) as a function of pH in an AGW-3 artificial groundwater solution equilibrated with calcite and a partial pressure of CO_2 of 10^{-2} atm (pCO_2 = 1%). Total dissolved U(VI) = 2 x 10^{-8}M. Calculations include the ternary aqueous complexes, $CaUO_2(CO_3)_3^{2-}$ and $Ca_2UO_2(CO_3)_3^{0}$(aq), and can be compared with Fig. 2.2A which does not include these aqueous species. Calculations differ from those in Fig. 2.2A in that equilibrium with calcite was used to determine the amount of dissolved Ca as a function of pH, whereas total dissolved Ca was constant in Fig. 2.2A. The calculated concentrations of $CaUO_2(CO_3)_3^{2-}$ and $UO_2(CO_3)_2^{2-}$ are nearly the same such that the curves lie almost on top of each other.

Table 2-1. Formation Constants for U(VI) and U(IV) Solution Species

Reaction	log ß* (I = 0)[a]
$UO_2^{2+} + H_2O \Leftrightarrow UO_2OH^+ + H^+$	-5.20
$UO_2^{2+} + 2H_2O \Leftrightarrow UO_2(OH)_{2,aq} + 2H^+$	-11.50[b]
$UO_2^{2+} + 3H_2O \Leftrightarrow UO_2(OH)_3^- + 3H^+$	-20.00[c]
$UO_2^{2+} + 4H_2O \Leftrightarrow UO_2(OH)_4^{2-} + 4H^+$	-33.0
$2UO_2^{2+} + H_2O \Leftrightarrow (UO_2)_2OH^{3+} + H^+$	-2.70
$2UO_2^{2+} + 2H_2O \Leftrightarrow (UO_2)_2(OH)_2^{2+} + 2H^+$	-5.62
$3UO_2^{2+} + 4H_2O \Leftrightarrow (UO_2)_3(OH)_4^{2+} + 4H^+$	-11.90
$3UO_2^{2+} + 5H_2O \Leftrightarrow (UO_2)_3(OH)_5^+ + 5H^+$	-15.55
$3UO_2^{2+} + 7H_2O \Leftrightarrow (UO_2)_3(OH)_7^- + 7H^+$	-31.00
$4UO_2^{2+} + 7H_2O \Leftrightarrow (UO_2)_4(OH)_7^+ + 7H^+$	-21.9
$UO_2^{2+} + CO_3^{2-} \Leftrightarrow UO_2CO_{3,aq}$	9.67 [d]
$UO_2^{2+} + 2CO_3^{2-} \Leftrightarrow UO_2(CO_3)_2^{2-}$	16.94
$UO_2^{2+} + 3CO_3^{2-} \Leftrightarrow UO_2(CO_3)_3^{4-}$	21.60
$3UO_2^{2+} + 6CO_3^{2-} \Leftrightarrow (UO_2)_3(CO_3)_6^{6-}$	54.0
$2UO_2^{2+} + CO_3^{2-} + 3H_2O \Leftrightarrow (UO_2)_2CO_3(OH)_3^- + 3H^+$	-0.86
$3UO_2^{2+} + CO_3^{2-} + 3H_2O \Leftrightarrow (UO_2)_3CO_3(OH)_3^+ + 3H^+$	0.66
$11UO_2^{2+} + 6CO_3^{2-} + 12H_2O \Leftrightarrow (UO_2)_{11}(CO_3)_6(OH)_{12}^{2-} + 12H^+$	36.43
$H^+ + CO_3^{2-} \Leftrightarrow HCO_3^-$	10.329 [d]
$2H^+ + CO_3^{2-} \Leftrightarrow H_2CO_3^* \ (\equiv CO_2(aq) + H_2O)$	16.683 [d]
$CO_2(g) + H_2O \Leftrightarrow H_2CO_3^* \ (\equiv CO_2(aq) + H_2O)$	-1.472 [d]
$UO_2^{2+} + NO_3^- \Leftrightarrow UO_2NO_3^+$	0.3
$UO_2^{2+} + Cl^- \Leftrightarrow UO_2Cl^+$	0.17
$UO_2^{2+} + 2Cl^- \Leftrightarrow UO_2Cl_{2,aq}$	-1.1
$UO_2^{2+} + SO_4^{2-} \Leftrightarrow UO_2SO_{4,aq}$	3.15
$UO_2^{2+} + 2SO_4^{2-} \Leftrightarrow UO_2(SO_4)_2^{2-}$	4.14
$SO_4^{2-} + H^+ \Leftrightarrow HSO_4^-$	1.98 [d]

Table 2.1 (continued)

Reaction	log ß* (I = 0)[a)]
$UO_2^{2+} + PO_4^{3-} \Leftrightarrow UO_2PO_4^-$	13.23
$UO_2^{2+} + PO_4^{3-} + H^+ \Leftrightarrow UO_2HPO_{4,aq}$	19.59
$UO_2^{2+} + PO_4^{3-} + 2H^+ \Leftrightarrow UO_2H_2PO_4^+$	22.82
$UO_2^{2+} + PO_4^{3-} + 3H^+ \Leftrightarrow UO_2H_3PO_4^{2+}$	22.46
$UO_2^{2+} + 2PO_4^{3-} + 4H^+ \Leftrightarrow UO_2(H_2PO_4)_{2,aq}$	44.04
$UO_2^{2+} + 2PO_4^{3-} + 5H^+ \Leftrightarrow UO_2(H_2PO_4)(H_3PO_4)^+$	45.05
$PO_4^{3-} + H^+ \Leftrightarrow HPO_4^{2-}$	12.35 [d)]
$PO_4^{3-} + 2H^+ \Leftrightarrow H_2PO_4^-$	19.562 [d)]
$PO_4^{3-} + 3H^+ \Leftrightarrow H_3PO_{4,aq}$	21.702 [d)]
$UO_2^{2+} + SiO_2(OH)_2^{2-} + H^+ \Leftrightarrow UO_2SiO(OH)_3^+$	21.54 [e)]
$SiO_2(OH)_2^{2-} + 2H^+ \Leftrightarrow Si(OH)_{4,aq}$	23.14
$SiO_2(OH)_2^{2-} + H^+ \Leftrightarrow SiO(OH)_3^-$	13.33
$2SiO_2(OH)_2^{2-} + 2H^+ \Leftrightarrow Si_2O_3(OH)_4^{2-} + H_2O$	27.28
$2SiO_2(OH)_2^{2-} + 3H^+ \Leftrightarrow Si_2O_2(OH)_5^- + H_2O$	38.18
$UO_2^{+2} + 4H^+ + 2e^- \Leftrightarrow U^{+4} + 2H_2O$	8.89 [f)]
$U^{+4} + 5CO_3^{-2} \Leftrightarrow U(CO_3)_5^{-6}$	33.9 [f)]
$U^{+4} + SO_4^{-2} \Leftrightarrow USO_4^{+2}$	6.58 [f)]
$U^{+4} + Cl^- \Leftrightarrow UCl^{+3}$	1.72 [f)]
$U^{+4} + 4H_2O \Leftrightarrow U(OH)_4 + 4H^+$	-12.0 [f)]
$U^{+4} + H_2O \Leftrightarrow UOH^{+3} + H^+$	-0.65 [f)]

a) Values from Grenthe et al. (1992), unless otherwise indicated.
b) Silva (1992), log K = -11.5 was used, reference gives log K ≤ -11.5
c) Sandino and Bruno (1992)
d) Silva et al. (1995)
e) Moll (1997)
f) Langmuir (1997)

Table 2-2. Solubility Products for Uranium Solid Phases

Reaction	log K_{so}^{*} (I = 0)[a)]
Schoepite: β-$UO_2(OH)_2(s) + 2H^+ \Leftrightarrow UO_2^{+2} + 3H_2O$	4.93
Rutherfordine: $UO_2CO_3(s) \Leftrightarrow UO_2^{+2} + CO_3^{-2}$	-14.49 [b)]
Soddyite: $(UO_2)_2(SiO_4)_2H_2O(s) + 4H^+ \Leftrightarrow 2UO_2^{+2} + H_4SiO_4 + 2H_2O$	5.74 [b)]
Uranophane: $Ca(H_3O)_2(UO_2)_2(SiO_4)_23H_2O(s) + 6H^+ \Leftrightarrow Ca^{+2} + 2UO_2^{+2} + 2H_4SiO_4 + 5H_2O$	9.42 [b)]
Carnotite: $K_2(UO_2)_2(VO_4)_2(s) \Leftrightarrow 2K^+ + 2UO_2^{+2} + 2VO_4^{-3}$	-56.3 [b,c)]
Tyuyamunite: $Ca(UO_2)_2(VO_4)_2(s) \Leftrightarrow Ca^{+2} + 2UO_2^{+2} + 2VO_4^{-3}$	-53.3 [b,c)]
Gummite: $UO_3(s) + 2H^+ \Leftrightarrow UO_2^{+2} + H_2O$	10.403
$UO_{3(C)}$: $UO_3(s) + 2H^+ \Leftrightarrow UO_2^{+2} + H_2O$	7.719
$USiO_{4(C)}$: $USiO_4(s) + 4H^+ \Leftrightarrow U^{+4} + H_4SiO_4$	-7.62 [b)]
$U_3O_{8(C)}$: $U_3O_8(s) + 16H^+ + 4e^- \Leftrightarrow 3\,U^{+4} + 8H_2O$	21.107
Uraninite: $UO_2(s) + 4H^+ \Leftrightarrow U^{+4} + 2H_2O$	-4.99 [b)]

a) Values from Grenthe et al. (1992), unless otherwise indicated.
b) Langmuir (1997).
c) Estimated value; considerable uncertainty in thermodynamic data

3 THE NATURITA UMTRA SITE: HYDROLOGY AND GEOCHEMISTRY

3.1 Introduction

Uranium (U) ore processing on the Colorado Plateau resulted in a number of inactive mill tailing sites at which there is contamination of groundwater (USDOE, 1996). The groundwater at many of these sites is contaminated with U and often other species including vanadium (V), selenium and molybdenum. The USDOE is responsible for clean up of many of these sites as dictated by the Uranium Mill Tailings Remediation Act (UMTRA). At many of the sites, the USDOE is proposing that sites will be cleaned up by natural flushing. A critical aspect of risk assessment and assessing the performance of natural flushing at many U-contaminated sites such as the UMTRA sites is estimating the migration of U(VI) in groundwater. In model simulations, retardation of U(VI) is often estimated based on a distribution coefficient, K_d, or a range of K_d values that is meant to describe the partitioning of U(VI) between the solid and aqueous phases. However, K_d values, especially those for U(VI), are dependent on the geochemistry of the aquifer, which can vary temporally and spatially. Simulations with a constant K_d can therefore introduce considerable uncertainty into the risk assessment or evaluation of remediation alternatives. Thus, in addition to hydrogeological parameters, a detailed knowledge of geochemical conditions at a contaminated site is required to make accurate transport simulations in groundwater.

Uranium occurs in the environment predominantly as U(IV) in reducing systems and U(VI) in oxic systems. In reducing waters, U(IV) forms insoluble phases and thus is relatively immobile (Langmuir, 1997). In oxic waters, U(VI) forms many soluble hydroxide and carbonate complexes which lead to increased solubility and mobility. Adsorption of U(VI) in oxic waters is sensitive to pH and partial pressure of carbon dioxide gas (pCO_2). Adsorption is generally negligible at low pH values where the uranyl cation (UO_2^{+2}) is the dominant species and increases with increasing pH usually in the pH range of 4 to 6. In the alkaline region, U(VI) is strongly adsorbed in the absence of dissolved CO_2 (Hsi and Langmuir, 1985; Prikryl et al., 2001) but in the presence of dissolved CO_2, the formation of U(VI)-carbonate complexes reduces adsorption (Hsi and Langmuir, 1985; Waite et al, 1994). At intermediate values of pH and CO_2, the extent of adsorption is determined by competition between the formation of aqueous U(VI)- carbonate complexes and surface U(VI)-carbonate complexes. The existence of these ternary surface complexes was initially postulated in order to fit adsorption data (Hsi and Langmuir, 1985) but their existence has been established spectroscopically for a variety of solids including ferrihydrite (Waite et al, 1994), hematite (Bargar et al., 1999; Bargar et al., 2000), and clay minerals. Bostick et al, (2002) recently identified ternary surface carbonate complexes in several soil samples collected from sites contaminated with U(VI). The importance of CO_2 in the formation of both aqueous and surface complexes with U(VI) illustrates that adsorption and transport of U(VI) can be strongly impacted by variable alkalinity.

The purpose of this section is to describe the hydrogeological and geochemical characteristics in the Naturita alluvial aquifer. These characteristics are used later to constrain solute transport simulations for the site (see Section 9).

3.2 Field Characterization

3.2.1 Site Description

The former U mill tailings site is approximately 3 km northwest of the town of Naturita, CO along the San Miguel River in southwestern Colorado as shown in Figure 3.1. The San Miguel River is the only perennial surface water body at the site. The Naturita area is semi arid; the estimated average annual precipitation is 9 inches (23 centimeters) and grasses and sagebrush dominate the vegetation.

The ore mill processed U and V ores at the site beginning in 1939 almost continuously until the

mill was shut down in 1958. From 1961 until 1963, a U ore upgrader was operated at the site. Uranium and V were extracted from the ore by salt roasting followed by carbonate leaching in percolation tanks. Carbonate leach tails were slurried to the western half of the Naturita site to an area of the site farthest (200 meters) from the San Miguel River and closest to the highway. Carbonate leaching residues were later sent to a second stage of sulfuric acid leaching. Acid leach tails were deposited closer to the river. Between 1977 and 1979, the mill tailings were removed from the site and between 1996 to 1998 the contaminated surface soils were excavated and transported offsite. The excavation removed soils to as deep as the water table and significantly changed the surface contours at the site.

3.2.2 Hydrogeology

Ground water at the Naturita site occurs in the alluvial deposits of the San Miguel River floodplain. This aquifer is recharged by the river to the southeast of the site and discharges into the river north of the site. Ground water flows approximately parallel to the river. The alluvial aquifer is separated from an underlying, moderately permeable sandstone aquifer (the Salt Wash Member) by a fine-grained shale (the Brushy Basin Member), which is approximately 30 m thick.

Figure 3.1 shows a map of the Naturita site that illustrates the location of the former mill yard, the extent of the former tailings pile, and all of the monitoring wells at the site. Between 1986 and 1997, USDOE installed 12 wells in the alluvial aquifer and 2 wells in the Salt Wash aquifer. All of these wells except DOE-547 and DOE-548, which are in the alluvial aquifer, were removed by the end of 1998. In 1998 and 1999, the USGS installed wells at 39 new locations and some of these new wells were clusters that included some multilevel wells. High concentrations of U are found in the ground water below and downgradient of the former tailings pile. Both water used to process the U ore and mill tailings and rain and snow that leached U from the deposited tailings could have caused the transport of U to the ground water at the site.

A well that was installed in the Salt Wash aquifer in the 1980's and subsequently abandoned by USDOE had heads that exceeded those in the alluvial aquifer indicating the potential for vertically upward flow and transport. The deep groundwaters had an average chloride (Cl) concentration of 20 □M, which was 200 times higher than Cl in background alluvial wells indicating minimal upward flow. The U(VI) in the deep groundwaters was 0.16 μM.

3.2.3 Geochemical Characterization

Groundwater samples were collected from the 12 USDOE wells between 1986 and 1997 by USDOE personnel and from the 52 USGS wells and wells DOE-547 and DOE-548 between 1998 and 2001 by USGS personnel. In this pooled data set, 474 water samples had a complete set of analytical results and 469 of the samples had charge balance errors of less than 15% and these samples were included in the calculations discussed below. The observed distribution of alkalinity, pH, and U(VI) determined by the USDOE and USGS are illustrated in the quantile plots shown in Figure 3.2. Most of the pH values ranged from 6.7 to 7.5, and the average pH was 7.1. In general, the alkalinity ranged from 2.5 to approximately 12 meq/L, although 5 samples collected between 1986 and 1992 had alkalinity values between 12 and 18 meq/L. Both pH and alkalinity are approximately normally distributed as shown in Figure 3.2. The U(VI) at the site ranged from background values of 0.01 μM to about 10 μM, although two samples had concentrations greater than 20 μM. The samples with the highest alkalinity did not coincide with the samples with highest U(VI), but in general, the concentrations of the two species were correlated (Section 9). U(VI) appears to have a bimodal distribution (Figs. 3.2c and 3.2d), which results from small concentrations in background samples and relatively large concentrations in areas impacted by the mill tailings. The minimum, maximum, mean, median, and standard deviations of the

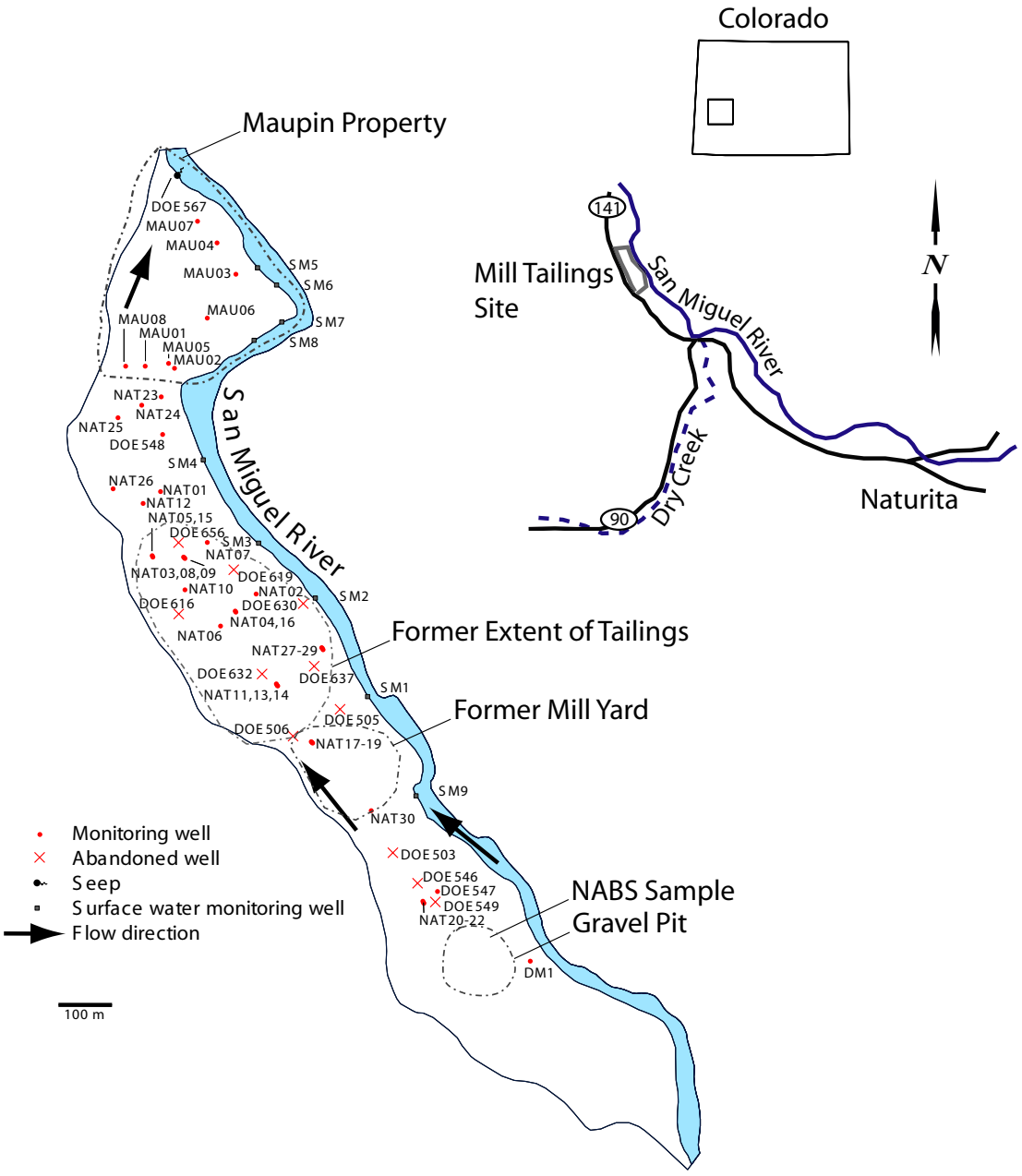

Figure 3.1 Naturita field site location, showing monitoring wells, flow direction, and U(VI) concentrations.

observed U, pH, and alkalinity values are summarized in Table 3.1. Calculated partial pressures of carbon dioxide gas ((pCO_2) in equilibrium with the groundwater ranged from from 0.0024 to 0.14 atm (0.2 to 14% of one atm); the calculated distribution is presented in Appendix A.

3.2.3.1 Spatial Distributions

Dissolved concentrations. Elevated concentrations of U(VI), alkalinity, V, and Cl were observed below and down gradient of the former U mill tailings. The concentration of each of these species is generally lower near the

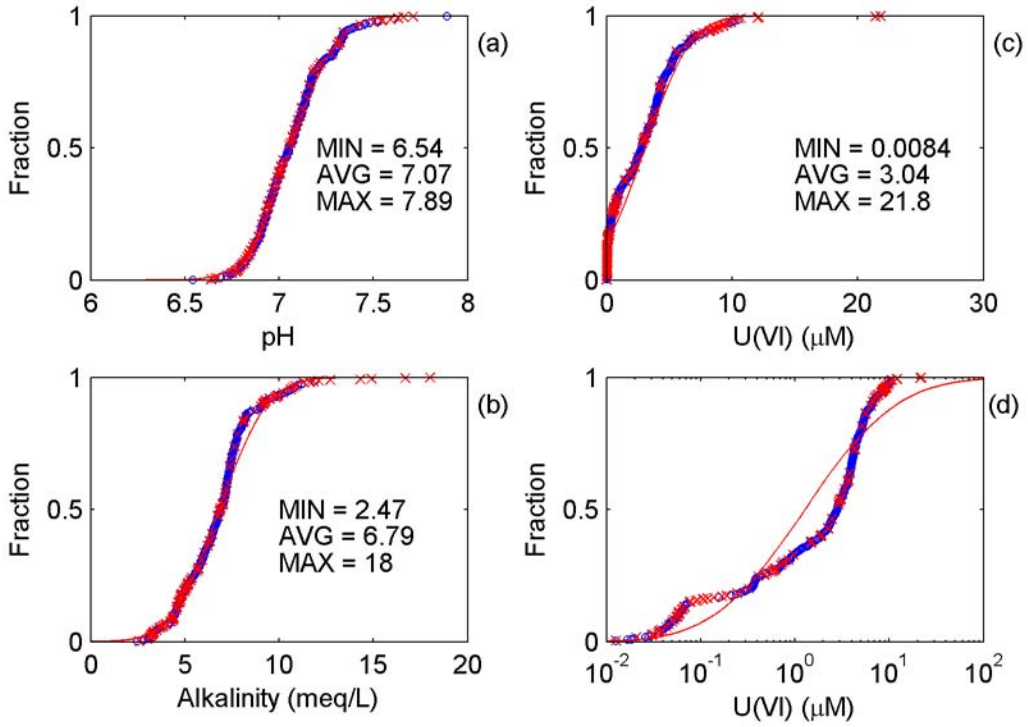

Figure 3.2 Observed cumulative distributions of pH, U(VI) and alkalinity for Naturita groundwater data collected between 1986 and 2001. USDOE data are shown by X symbols, USGS data are shown by • and the solid line represents a normal distribution. a) pH, b) alkalinity, c) and d) U(VI) concentration, linear and log scales.

San Miguel River and higher near the highway (Figure 3.3). In 1999, dissolved U(VI) was widely distributed across the site with concentrations ranging from average background values of 0.02 μM at wells DM-1, DOE-547, and NAT-20, -21, -22, to peak concentrations of 10 μM at well NAT-26; most of the impacted parts of the aquifer have U(VI) concentrations between 2 and 6 μM. Similar trends were observed for other sampling rounds.

The observed spatial distribution of alkalinity generally follows the same spatial distribution as U(VI) but the range in concentrations is much smaller. In 1999, the alkalinity values ranged from approximately 4.7 meq/L near well DOE-547 to peak values of 12 meq/L at well NAT-26. As in the case of U(VI), the zone of elevated alkalinity is widely distributed across the site. A few recent samples from well DOE-547 have had alkalinity values in the range of 2.4 to 3 meq/L; these low alkalinity values are consistent with the loss of CO_2 and precipitation of calcite in the recently developed gravel pits upgradient of well DOE-547 that have been significantly expanded since 1998.

Table 3.1 Summary of observed U(VI), pH, and alkalinity in Naturita groundwater, 1986-2001

	U(VI)	pH	Alkalinity
	(μM)		(meq/L)
min	**0.01**	**6.54**	**2.48**
max	**21.85**	**7.71**	**23.04**
avg	**3.07**	**7.07**	**6.88**
std	**2.92**	**0.19**	**2.29**
median	**2.78**	**7.05**	**6.88**
n	**469**	**469**	**469**

The groundwater had an average pH of 7.1 and ranged from 6.5 to 7.7. In general, the pH has not had a consistent spatial structure that has persisted over multiple sampling sets as is observed for U(VI) and alkalinity. The pH values from wells DM-1, DOE-547, and NAT-20, -21, -22, which are upgradient of the former mill site are approximately 1 pH unit less than that observed in the San Miguel River. In addition, the alkalinity in the background wells was nearly constant over time and had an average value of 4.7 meq/L, whereas the alkalinities in the San Miguel River varied seasonally with a range of 1.3 meq/L at high river stage to 2.6 meq/L at low river stage. The decrease in the pH and the increase in alkalinity are consistent with biological activity. This activity is assumed to occur in the riverbank and possibly in the root zone of cottonwoods and willows near the river because water samples from well DM-1, which is ~10 m from the river, are similar to those from well DOE-547 which is ~120 m from the river. The concentration of ferrous ion (Fe^{+2}) is relatively small (~ 10 μM) in the upgradient wells as well as below the former mill and tailings. Thus, although the alkalinity may be impacted by biological activity in the riverbank or hyporheic zone, the relative constancy of the Fe^{+2} and dissolved oxygen gas (O_2) concentrations over most of the site indicate that the extent of biological activity is probably limited.

There were also high V concentrations close to the highway (Figure 3.3), where concentrations approached 100 μM, whereas outside of this plume dissolved V was below detection limits. Potassium ion (K) had a nearly identically shaped plume with the exception that the concentrations were 250 μM in the center of the plume and ~ 100 μM in uncontaminated portions of the aquifer (Appendix A). One important difference between the observed distribution of U(VI) and those of K and V is that the highest concentrations of the U(VI) plume occur farther downgradient of both the V and K peak concentrations. This observation suggests that U transport is at least partially decoupled from V transport at the site.

Speciation calculations. Speciation calculations were performed using the thermodynamic data summarized in Section 2 for aqueous species and solid phase (the aqueous species, $CaUO_2(CO_3)_3^{2-}$ and $Ca_2UO_2(CO_3)_3^0(aq)$, were not considered). The calculations demonstrated that the U aqueous carbonates species, $UO_2(CO)_2^{-2}$ and $UO_2(CO_3)_4^{-4}$, accounted for more than 97% of the total U(VI) in solution in each of the 469 water samples. The percentage of each of the species ranged between approximately 5% to 95% of the total U(VI), and the $UO_2(CO_3)_2^{-2}$ species was generally the dominant species in waters with background alkalinity, while the $UO_2(CO_3)_4^{-4}$ species was predominant at higher alkalinities (see Section 2).

Speciation calculations were also conducted to evaluate the saturation indices (SI; see Langmuir, 1997) of various mineral phases, using the thermodynamic data listed in Section 2. The calculations showed that all waters are generally below saturation with respect to several U-bearing phases including uranophane ($Ca(UO_2)_2SiO_3(OH)_2$; SI<-7.7), soddyite ($(UO_2)_2SiO_22H_2O$; SI<-3.5), schoepite ($(UO_2(OH)_2H_2O$; SI<-2.8) and rutherfordine (UO_2CO_3; SI<-2.7). The uranium - vanadium (U-V) minerals carnotite ($K_2(UO_2)_2(VO_4)_2$) and tyuyamunite ($Ca(UO_2)_2(VO_4)_2$) appear to be near saturation (-0.4<SI<1.3) in the vicinity of wells NAT-03, NAT-06 and NAT-10, but well below saturation where dissolved V concentrations are at background values. The interpretation of the SI values for the U-V phases is equivocal because of uncertainty in the thermodynamic data for these minerals; in some cases these thermodynamic data were estimated (Langmuir, 1978). In addition, the saturation indices by themselves do not prove the existence or absence of a given phase. Also, extractions of contaminated sediments from NAT-03, NAT-06 and NAT-10 had extractable U concentrations that were only 10% of total extracted V (see Sections 4 and Appendix C), whereas carnotite and tyuyamunite have equimolar ratios of U to V. Finally, detailed characterization of the contaminated sediment sample NAT-06 (see Sections 4 and 6) did not identify a U-V phase

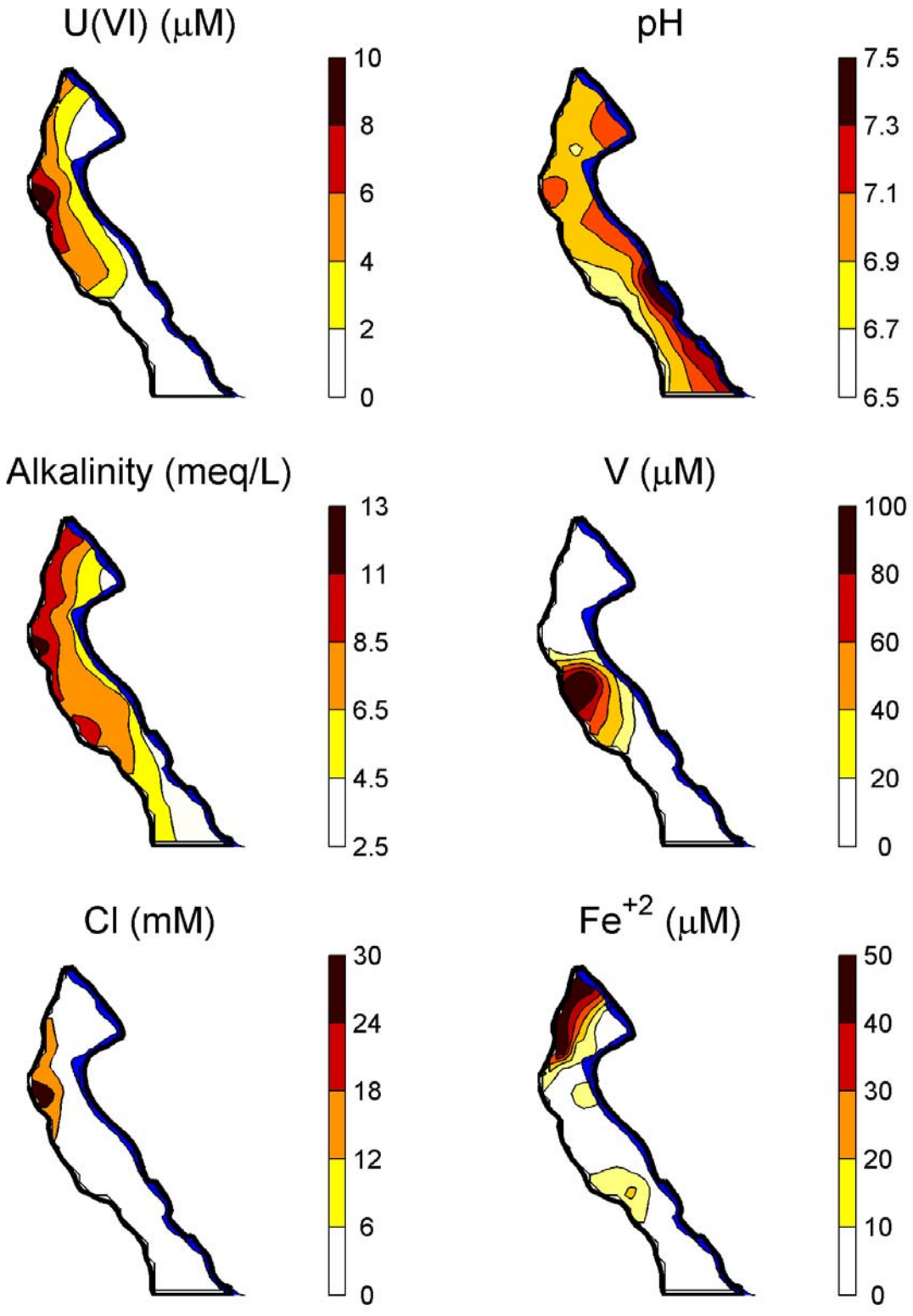

Figure 3.3. Kriged concentrations based on water samples collected in September 1999.

(Jove-Colon et al, 2003). Therefore, the transport simulations presented in Section 9 did not consider the existence of the separate U-V phases.

The groundwaters at the Naturita site are characterized by redox disequilibrium. This is demonstrated by the co-occurence of measurable dissolved O_2 and Fe^{+2}, which would not be expected under equilibrium conditions at near neutral pH values (Langmuir, 1997). The measured O_2 could result from atmospheric contamination although O_2 was observed in nearly all samples by both a dissolved oxygen meter and by Chemet. Nitrate was observed in 45 groundwater samples in the concentration range from 0.5 to 45 mg/L between 1986 and 1992; the average concentration was 7.5 mg/L. More recently, nitrate was only consistently measured at well NAT-26 where the average concentration was 2.5 mg/L. No measurable nitrite was observed in 30 samples collected from 10 wells between 1991 and 1992.

Redox speciation calculations were performed to evaluate the stability of various U(IV) phases including uraninite and U_3O_8. These calculations were are based on assuming that the Fe(III)/Fe(II) couple was at equilibrium and that the Fe(III) activity was controlled by the presence of either ferrihydrite or goethite. The calculations demonstrated that U(IV) phases were well below saturation (SI<-3) in the presence of ferrihydrite and well above saturation (SI>2) in the presence of goethite (Appendix A). The results of these calculations demonstrate the large uncertainty resulting from two different model assumptions. Rather than relying on these model simulation results, a better approach would be to experimentally investigate if U(IV) phases are present in the Naturita aquifer. Carbonate extractions on freshly collected sediments from near well NAT-25 under an inert atmosphere demonstrated that U(IV) phases were probably not important at that location (see Section 6).

3.2.3.2 Temporal Observations

One of the reasons for selecting the Naturita site for the field investigations was that a historical data set (USDOE) beginning in 1985 was available. Although all of the wells installed in the 1980's that were located in the area where tailings were deposited were destroyed, many of the new wells were placed as near as feasible to the historical wells. Comparisons are presented for three sets of wells, located roughly along a flow path, are shown in Figure 3.4. The figures show changes in U(VI), alkalinity, pH, and V, and the following general trends can be identified: (1) U(VI) decreased in the upgradient well, remained roughly constant in the middle of the domain and has increased in the downgradient pair of wells, (2) alkalinity generally decreased over time, (3) V decreased in the upgradient well and increased in the down gradient pair of wells, and (4) pH has been roughly constant. In addition to these trends, Figure 3.4 illustrates that the historical data show alkalinity values of 20 meq/L in several instances. At well DOE-616, U(VI) concentrations as high as 23 μM were observed in 1990. Thus, both U(VI) and alkalinity were 2-3 times higher in some locations in the 1980's and early 1990's than is currently observed.

3.2.3.3 Uranium Isotopic Ratios

Isotopic ratios of the isotopes ^{234}U and ^{238}U (activity of ^{234}U divided by activity of ^{238}U) were determined for two groundwater samples in March 2, 2000. For a closed system it is expected that the two isotopes ^{234}U and ^{238}U are in secular equilibrium, and the activity ratio should equal one (for details on secular equilibria, see Choppin and Rydberg (1980), and for alpha activity ratios of U isotopes in geological samples and ocean water, see Faure (1991)). A U ore as a closed system is expected to be in secular equilibrium with respect to ^{234}U and ^{238}U after approximately 10 half-lives of ^{234}U (thus, 2.46 million years). Chenoweth (1980) states that nearly all ores are essentially in radioactive equilibrium in the Uravan Mineral Belt.

The two samples chosen (from wells NAT-26 and MAU-08) had the highest dissolved U(VI) concentrations among the samples collected in

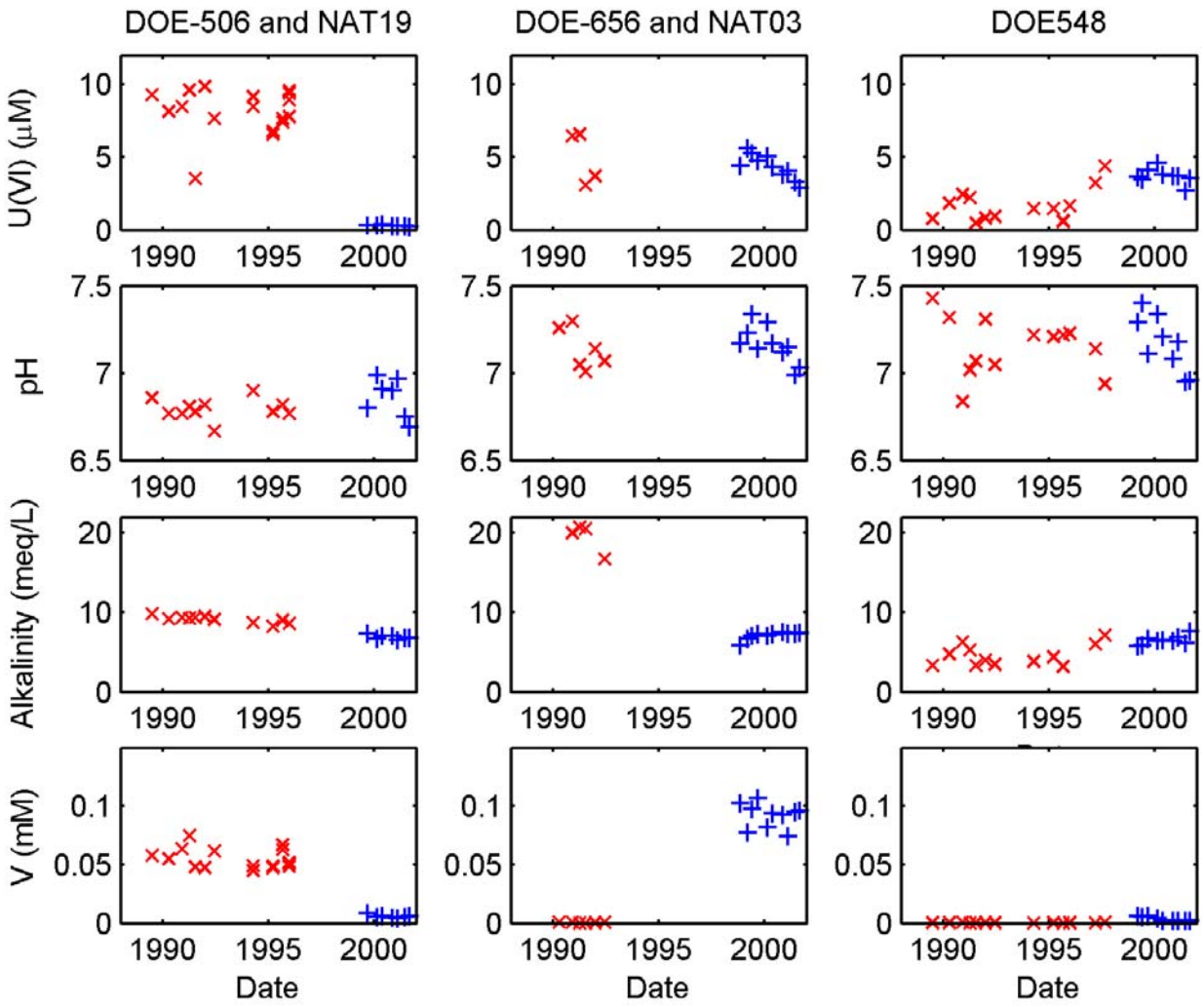

Figure 3.4 Long term monitoring observations for U(VI) and V concentrations, pH, and alkalinity.

March 2000. The measured activity ratios for these samples were 1.005±0.013 (NAT-26) and 0.960±0.021 and 1.003±0.007 for two measurements of MAU-08. Thus, the groundwater U isotopic ratios equal one within error, which is consistent with the expected isotopic ratio within the U ore.

3.3 Groundwater Flow and Conservative Transport

3.3.1 Flow Model

The shallow alluvial aquifer is bounded by the San Miguel River to the east and by the Brushy Basin member to the west (Figure 3.1). The San Miguel River is bounded to the east by an outcrop of the Brushy Basin member. The western extent of the aquifer was taken as the toe of the slope. In the upstream direction, the aquifer extends approximately 488 m upgradient of well DOE-547 to the confluence of the San Miguel River and the ephemeral Dry Creek. The aquifer is generally 2 to 4 m thick and consists of sand, gravels and cobbles. Because the aquifer is thin relative to the length of 2 km, the aquifer was approximated as a two-dimensional areal aquifer.

No flow boundary conditions were assumed on the western edge and on the bottom of the

domain along the contacts with the Brushy Basin member on the western border of the aquifer and on the eastern border of the San Miguel River. Water was allowed to flow into or out of the aquifer via contacts with the San Miguel River. Stream discharge ranges from a base flow of approximately 1.13 m^3/s (40 cfs) to peak flows resulting from snowmelt (range of 30 to 110 m^3/s). Low flow conditions are generally fairly constant and occur for approximately 8 to 9 months of the year. Pressure transducers installed in the aquifer and in the river demonstrated that the aquifer is in good hydraulic contact with the river.

Neither focused nor distributed areal recharge were included because the region is arid and preliminary groundwater flow simulations showed that including areal recharge gave a poorer match to the observed head data. Evapotranspiration (ET) may be important for the riparian woodland areas along the stream banks that support dense willow and cottonwood stands, but this was not included in the flow model because of the good hydraulic contact between the river and the aquifer.

Groundwater flow in the alluvial aquifer was simulated using a steady state flow model using MODFLOW (Harbaugh and McDonald, 1996). The steady state model avoids the need for a complex, variably saturated flow model that would be required in conjunction with the transient flow model in order to account for the transport of U(VI) in transiently saturated zones where U(VI) could be moderately adsorbed. One key limitation of the steady state model is that transient fluid sources that could be used the describe the transient source of U(VI) to the aquifer cannot be considered.

3.3.2 Estimates of Hydraulic Conductivity

Three approaches for estimating the hydraulic conductivity (K_X) were considered. These approaches included (1) slug tests, (2) migration of Cl at the site and (3) analysis of age dating results. The details of the analysis are presented elsewhere (Appendix B) and will only be summarized here. The K_X of the aquifer could not be estimated by calibrating the steady state groundwater flow model to observed heads because in the absence of flow information, the problem is ill posed.

K_X values were obtained from slug tests which tend to give local estimates of K_X (Butler, 1998). Slug tests were performed on 10 wells and each well was tested 3 to 5 times. For all 10 wells, the mean K_X obtained from the slug tests was approximately $3.53 \cdot 10^{-4}$ m/s (100 ft/day) and the data ranged by a factor of approximately 3. In addition, there was no apparent spatial distribution to the variation in K_X values. Therefore, a single K_X value was considered in the following analyses for simplicity.

K_X was also estimated from an observed Cl plume that had a peak concentration of 20 mM that was centered at well NAT-26 in 1999-2001 (Figure 3.3). In 1990, well DOE-616, which is 210 m upgradient of NAT-26, also had Cl concentrations of 20 mM but the plume was not well defined because of the limited number of wells at that time. The chloride plume was assumed to have originated from the salt roasting facilities in the mill yard and from the mill tailings. Other sources of the Cl including road salt and vertically upward flow of water from the Salt Wash Aquifer were discounted because the U(VI) and sulfate concentrations at well NAT-26 are also high. It is unlikely that road salt would have contained high sulfate and U, and the Salt Wash Aquifer had U(VI) values that were 2000 times smaller than the observed U(VI) at well NAT-26.

The hydraulic conductivity was estimated by fitting a non-reactive solute transport model to the observed Cl plume. Groundwater flow was simulated with MODFLOW (Harbaugh and McDonald, 1996), non-reactive transport was simulated with MT3DMS (Zheng and Wang, 1999) and the parameters were estimated using UCODE (Poeter and Hill, 1999). A uniform porosity equal to 0.20 was used in all of the simulations. An integral part of the parameter estimation step was to approximate the source term for the Cl. It was assumed that the earliest that the Cl was disposed of at the site was 1939

Table 3.2 Chloride ion source term descriptions and estimated hydraulic conductivity values

	Source Duration		Aquifer Extent		Parameter Estimates	
Run	Start	End	Upgradient	Downgradient	S^1	K_X
1	1939	1959	NAT-30	NAT-11	23	20
2	1939	1977	NAT-30	NAT-11	7.7	57
3	1939	1959	NAT-30	NAT-10	11	35
4	1939	1977	NAT-30	NAT-10	8.8	60

[1] S = sum of weighted squared residuals

when the salt roaster started operation. It is likely that the Cl source was present at least until 1959 when the salt roaster ceased operation, but there could have still been a significant source after 1959 because of the operation of the U ore upgrader or because of the slow leaching of Cl from the mill yard soils and from mill tailings. Similarly, the spatial extent of the Cl source was approximated as either consisting of only the mill yard or the mill yard and the full extent of the mill tailings. These four possible source terms are summarized in Table 3.2. The Cl was introduced at a constant mass-loading rate of $7.48 \cdot 10^{-12}$ moles/(m^2-s). The solute transport model was calibrated to Cl data collected between 1986 and 2001 at 12 wells illustrated in Figure 3.4. Only the K_X value was varied in the UCODE simulations.

The K_X values that gave the best match to observed Cl data in the 12 wells are summarized in Table 3.2 for each of the different assumed source terms. The K_X values for all of the simulations ranged from $0.71\text{-}2.12 \cdot 10^{-4}$ m/s (20-60 ft/d). This relatively narrow range gives some confidence in the approach given the uncertainty in the source term. In both cases when the duration of the source was constant and the extent of the source varied, nearly the same K_X value was obtained (runs 1 and 3). This results because the downstream extent of the source is relatively unimportant because most of the Cl at the downstream border of the source had already been advected downgradient of each well before the well was sampled. Figure 3.5 shows the model fit to the Cl data for a 41-year source that was distributed over the mill yard and the mill tailings. The model matches most of the data closely and predicts maximum concentrations that agree with observed maxima in the field.

The tritium-helium (^{3}H/He) ages were determined on waters sampled from 12 wells, including DM-1, NAT- 05,-03,-23, -24,-25,-26, MAU-03,-07 and -08. The observed ages can be used together with a flow and transport model to constrain groundwater model parameters (Reilly et al, 1994). The observed ^{3}H/He ages were compared with simulated ground water ages obtained using the method of Goode (1996). A K_X value was estimated for each well where the ^{3}H/He age was measured. The average K_X value was $3.1 \cdot 10^{-4}$ m/s (88 ft/day) and the standard deviation was $1.23 \cdot 10^{-4}$ m/s. This mean value is twice as large as the average K_X value estimated from the Cl migration, which is relatively good agreement. In the age simulations, it was assumed that the only source of water was the San Miguel River, and in general, the water for each well entered the aquifer upgradient of well DM-1. The presence of Cl in the older groundwaters suggests either mixing of old water with high Cl water or possibly significant recharge from the mill yard. In either case, the presence of high Cl in the oldest waters causes increased uncertainty in the K_X value estimated from groundwater age dating. Because of this uncertainty in the age dating analysis, an average value K_X of $1.59 \cdot 10^{-4}$ m/s (45 ft/d) obtained from the Cl simulations was used for the reactive transport simulations discussed below.

Figure 3.6 illustrates the simulated Cl plume for a K_X value of $1.59 \cdot 10^{-4}$ m/s. In general, the shape of the plume, including the location of the

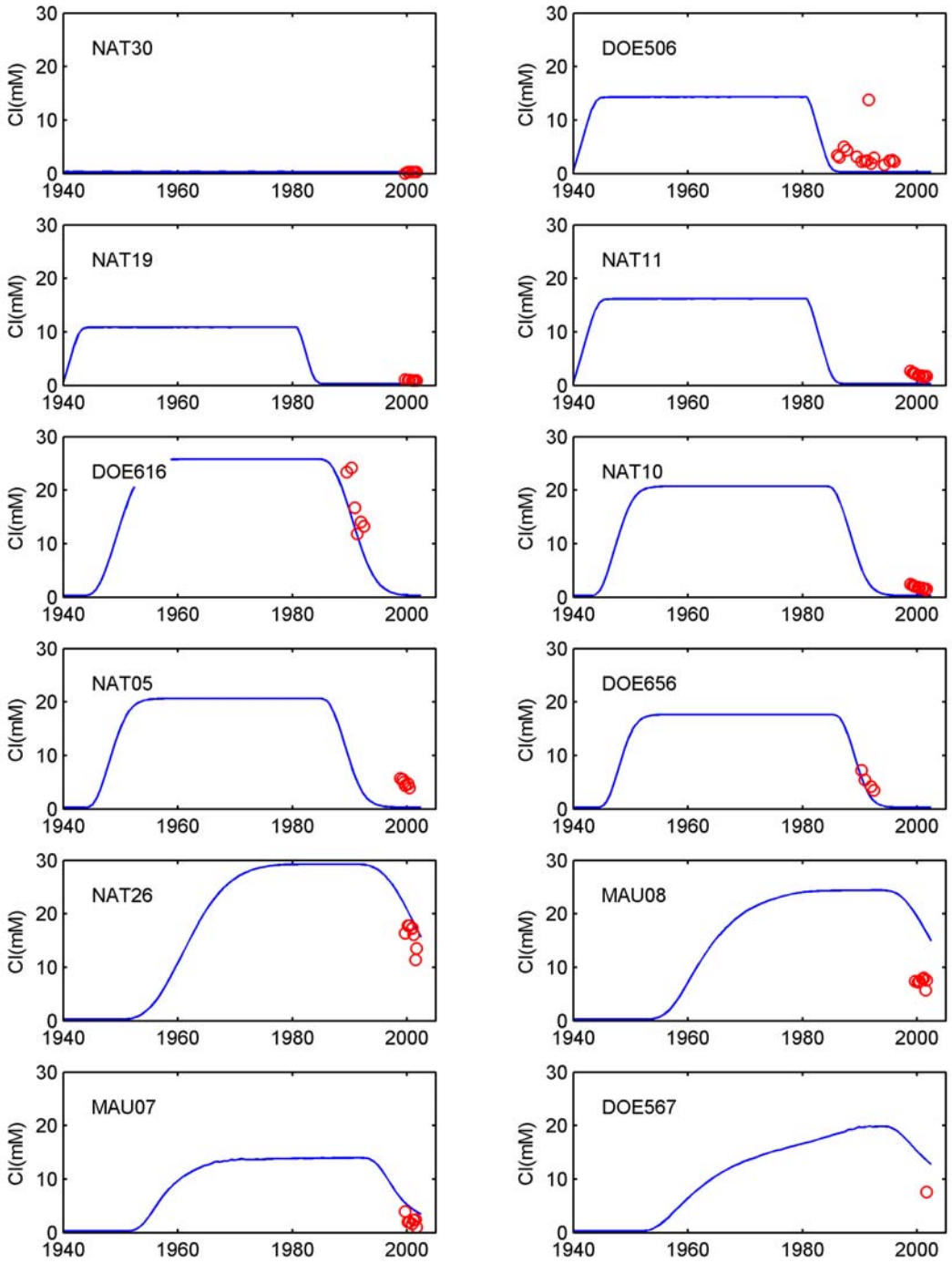

Figure 3.5 Chloride ion calibration results for run 2 (Table 3.2).

maximum Cl concentration, agrees well with the observed Cl plume (Figure 3.3). Figure 3.6 also shows that a long thin plume develops between wells NAT-25 and DOE-567. This elongated plume develops because river water short-cuts the bend in the San Miguel River near SM5 to SM8, which causes the flow to converge on the Maupin property. The velocities between wells NAT-25 and DOE-567 are approximately twice as large as upgradient near well NAT-06.

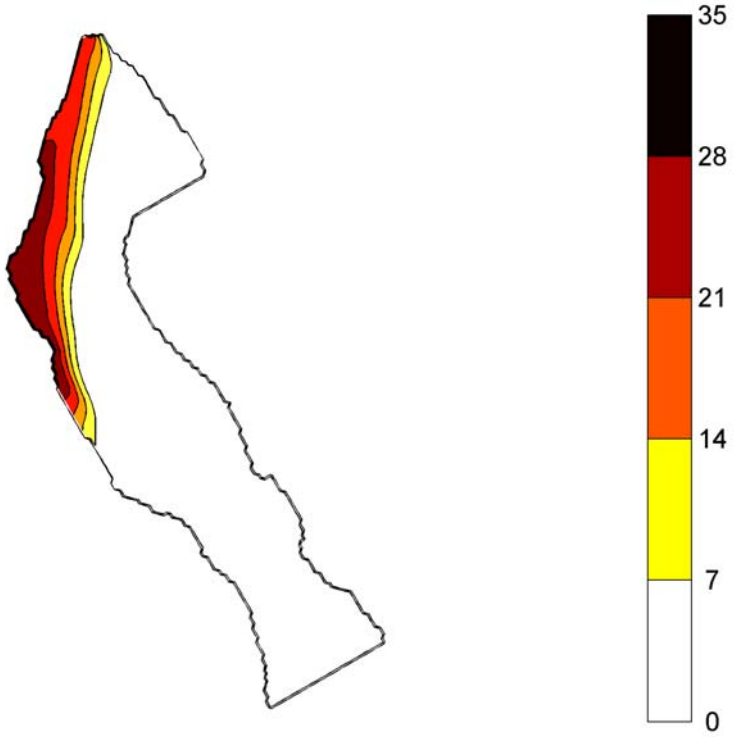

Figure 3.6. Simulated chloride ion concentrations (mM) using the calibrated flow and transport model.

4 CHARACTERIZATION OF NATURITA AQUIFER SEDIMENTS

4.1 Introduction

Uranium (U) contamination in groundwater at the Naturita UMTRA site has been observed primarily within the unconfined, shallow alluvial aquifer composed of sand, gravel, pebbles, and cobbles (see Section 3). The physical and chemical characteristics of alluvial sediments both upgradient and within the region of U contamination at the Naturita field site are described in this section. A large composite sample of the aquifer sediments upgradient of the U contamination was collected during the study (referred to as the NABS sample, for Naturita Aquifer Background Sediments). Results of U(VI) sorption experiments with the NABS sediment sample (and K_d values) are given in Section 5. In addition, Section 5 includes development of a surface complexation model to describe U(VI) sorption (and K_d values) as a function of solution conditions (pH, U(VI) concentration, and alkalinity (or partial pressure of CO_2).

Section 6 describes the sorption of U(VI) to several individual sediment samples collected at various locations throughout the region of U contamination at the Naturita site. These samples were collected during the installation of monitoring wells, and groundwater chemical data were also determined at the same locations, enabling the calculation of *"field-K_d values"* for these samples.

Aliquots of the NABS sample were suspended in selected monitoring wells for durations of 3 to 15 months during the study. Sorption of U(VI) by these samples suspended in the groundwater is described in Section 7. K_d values were determined for these samples and compared to those predicted by the surface complexation model for U(VI) sorption.

4.2 Uncontaminated Alluvial Sediment Composite Sample

4.2.1 Preparation of the NABS Sample

On July 16-17, 1998, approximately 1300 kg of material from the saturated zone of the Naturita alluvial aquifer was collected from a gravel pit located about 90 m upgradient of the site's southern boundary and 40 m from the western edge of the San Miguel River (see Fig. 4.1). The sample was considered "uncontaminated" because observations of dissolved U(VI) at well DOE547 (and decommissioned DOE wells nearby) were always very low, near the concentrations observed in the river (see Section 3). The sample was screened in the field to remove cobbles larger than 64 mm. It was visually estimated that 50 % of the material scooped by the backhoe did not pass the 64 mm screen.

Seven hundred thirty four kg of wet, <65 mm sediments were shipped in clean plastic containers to the USGS laboratories in Menlo Park, California (USA). The sediment was spread onto plastic sheets and allowed to air dry (weight of 641 kg). 141 kg of large cobbles were removed by hand from the material and the remaining sediments were sieved to separate grains <3 mm from the coarser material. 190 kg of sediments passed the 3 mm screen, representing roughly 30% (by weight) of the <65 mm material collected in the field. The 190 kg of <3 mm sediments were thoroughly mixed, and the composite sample is referred to as the Naturita Aquifer Background Sediment (NABS) sample.

4.2.2 Sediment Characterization Techniques

Grain Size Distribution. The grain size distribution of the NABS sample was determined using 1000, 500, 250, 125, and 63 μm sieves. Approximately 2 kg of material was dry sieved into the grain size fractions and weighed. The remainder of each fraction was wet sieved to wash away fine-grained material. In addition, about 95 kg of the >3 mm gravel was sieved using 5.613 mm, 9.423 mm, and 16 mm mesh screens to obtain samples of these size fractions. The upper limit of the coarsest

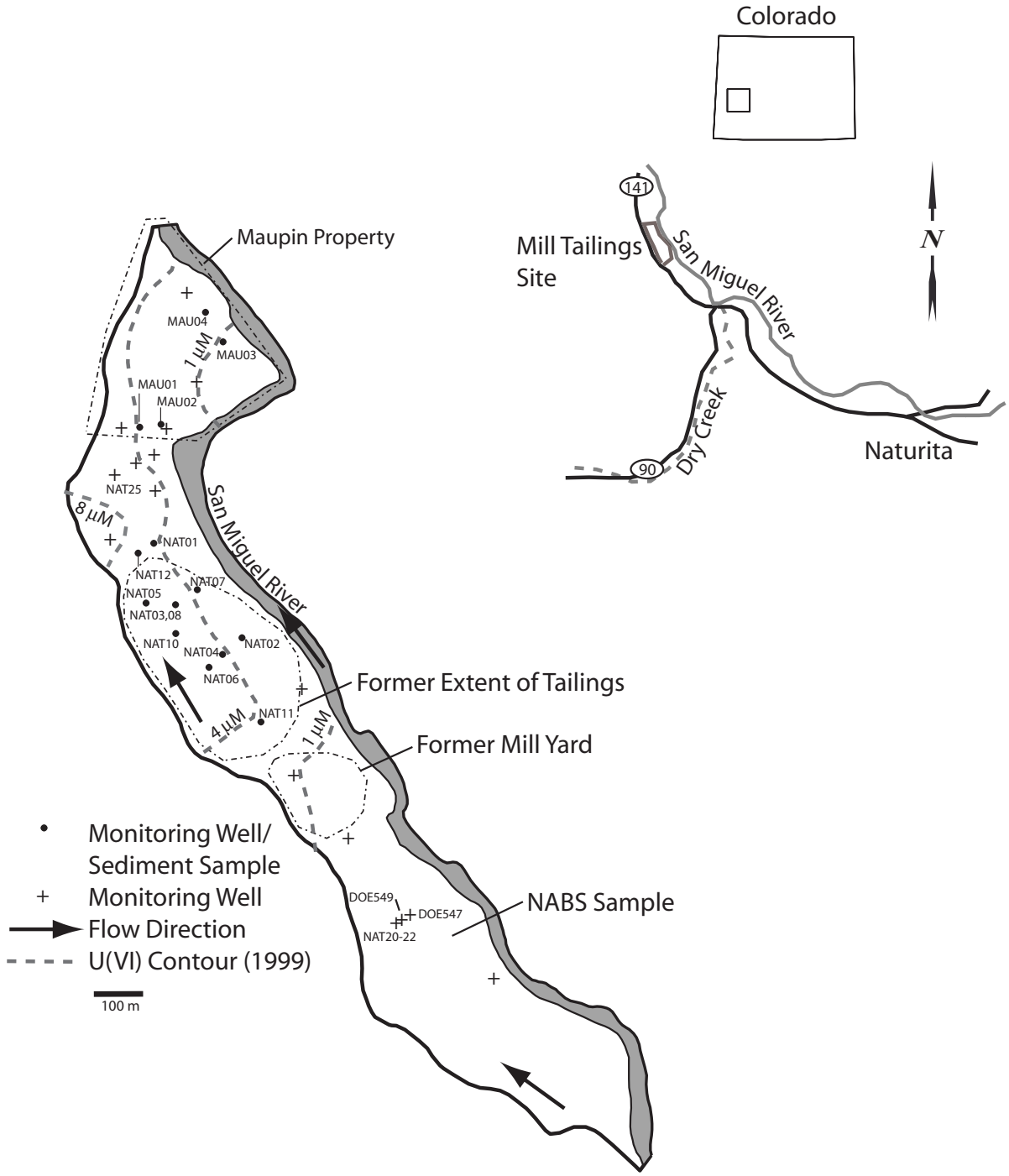

Figure 4.1 Locality map showing the location of the Naturita, Colorado UMTRA site, the former locations of the tailings and mill yard, and the locations of monitoring wells and sediment samples collected.

fraction (>16 mm) was operationally set as the size of the smallest rock worth the effort of removing by hand, which was about 5 cm long. Because of the presence of carbonate minerals, an artificial groundwater was prepared for sieving that was saturated with respect to calcite and had an ionic strength similar to that of groundwater in the Naturita alluvial aquifer ($4.19 \cdot 10^{-4}$M $NaHCO_3$, $4.50 \cdot 10^{-3}$M $CaSO_4$, $3.84 \cdot 10^{-5}$M KCl, $1.96 \cdot 10^{-3}$M NaCl, $1.15 \cdot 10^{-3}$M $MgCl_2$ and $1.70 \cdot 10^{-6}$M NaOH). As an additional step in investigating the variation of specific surface area with grain size, some of the wet sieved material underwent further washing by suspending 10 g of each fraction in 10 ml AGW, centrifuging and decanting. This process was repeated 23 times until the supernatant remained clear. The sieving waters were analyzed for dissolved calcium (Ca) before and after sieving, and these results confirm that no significant dissolution or precipitation of calcite occurred during sieving.

Surface Areas by N_2-BET gas adsorption. Specific surface areas were determined at atmospheric pressure using the flow-through method on a Micromeritics FlowSorb II (Model 2300). This method allows for accurate determination of specific surface area on granular samples of greater than 0.1 m^2/g by measuring the adsorption of nitrogen (N_2) gas. Measurements were made using the single-point method (e.g., Gregg and Sing, 1982) at a N_2 relative partial pressure of 0.3. Sample masses ranged from 1 g for the finest fraction to 20 g for the coarsest samples.

X-ray Diffraction. Bulk mineralogy of selected samples was analyzed by X-ray diffraction (XRD) by Sanpawanitchakit (2002) and Jove-Colon et al. (2003) Whole-rock mineralogy was determined semi-quantitatively. Peak height ratios of the principal minerals were used to measure the relative abundance of the phases in the samples. XRD data were collected using a Philips XRG 3100 X-ray diffractometer equipped with a graphite monochromator using Cu-Kα radiation under conditions of a 40 kV and 30 mA. XRD was carried out with 2-theta values from 2 to 60 degrees.

Scanning Electron Microscopy. The NABS sample and its grain size fractions were examined by optical and thermionic scanning electron microscopy (SEM) at the USGS Menlo Park laboratories. The SEM results (grains coated with gold/palladium) were coupled with energy dispersive spectroscopy (EDS) to give compositional information at particular surface locations.

A selection of grains was examined with a Schottky field-emission SEM (FE-SEM; LEO 982-Gemini column model). Grains were mounted to an aluminum stub with double-sided tape and examined uncoated. Thin sections were coated with gold/palladium to prevent the sample from beam damage under the 15 keV beam accelerating voltage required to collect EDS (X-ray spectra).

Uranium extraction by Carbonate Solution. The labile fraction of U(VI) in the NABS sample and its size fractions was estimated by an alkaline sodium (bi)carbonate extraction method (see Section 6 for details). The labile fraction includes the portion of U(VI) associated with the sample that equilibrates on short-time scales with dissolved U(VI) in solutions similar in composition to the Naturita groundwater, including adsorbed U(VI). Briefly, the extractant solution was $1.44 \cdot 10^{-2}$ M in $NaHCO_3$ and $2.8 \cdot 10^{-3}$ M in Na_2CO_3. Its calculated ionic strength was 0.022M, with a measured pH of 9.45 ± 0.05 (9.34 calculated for the equilibrium pH at atmospheric pressures of carbon dioxide), and its alkalinity was 20 meq/L. The extraction was carried out at room temperature for a period of 3 weeks.

4.2.3 Sediment Characterization Results

Table 4.1 shows the grain size distribution of the NABS sample, surface area measurements, and the amount of labile U(VI), as determined by the carbonate extraction method (see Section 6). In general, the amount of material in each size fraction increased with particle size, with gravels coarser than 3 mm comprising about 70% of the total mass of the <64 mm sample. The <3 mm material, which was used to prepare a large

Table 4.1 Grain size distribution, surface area, and labile U(VI) of the NABS sample and size fractions

Sample	Weight %	Surface Area (m^2/g)	Labile U(VI) (moles/g) [b]	Labile U(VI) ($moles/m^2$)	% of Labile U(VI)
NABS (<3 mm)	29.7 [a]	5.15	$8.74 \cdot 10^{-10}$	$1.69 \cdot 10^{-10}$	83.6 [c]
<63 μm	1.1	13.1	$2.50 \cdot 10^{-9}$	$1.91 \cdot 10^{-10}$	11.5
63-125 μm	1.9	7.19	$1.06 \cdot 10^{-9}$	$1.47 \cdot 10^{-10}$	8.4
125-250 μm	4.9	5.1	$6.36 \cdot 10^{-10}$	$1.25 \cdot 10^{-10}$	13
250-500 μm	6.8	3.95	$4.79 \cdot 10^{-10}$	$1.21 \cdot 10^{-10}$	13.6
0.5-1 mm	4.7	5.7	$5.36 \cdot 10^{-10}$	$9.4 \cdot 10^{-11}$	10.5
1-3 mm	10.1	6.31	$6.26 \cdot 10^{-10}$	$9.9 \cdot 10^{-11}$	26.4
3-5.6 mm	7.8	3.57	$1.28 \cdot 10^{-10}$	$3.6 \cdot 10^{-11}$	4.2
5.6-9.4 mm	10.1	3.33	$8.54 \cdot 10^{-11}$	$2.6 \cdot 10^{-11}$	3.6
9.4-16 mm	12.8	na	$7.03 \cdot 10^{-11}$	na	3.8
16-30 mm	17.6	na	$3.44 \cdot 10^{-11}$	na	2.5
30-64 mm	22.0	na	$2.57 \cdot 10^{-11}$	na	2.4

[a] <3 mm sample was 29.7% of the <64 mm sediments.
[b] From carbonate extractions (see Section 6 for methods).
[c] calculated from the sum of the size fractions <3 mm relative to the total labile U(VI) in the <64 mm sediments.

composite sample (NABS) for characterization and the U(VI) adsorption experiments, comprised 30% of the mass <64 mm.

Overall, the sediments were composed of poorly sorted, weathered and abraded rocks of many varieties. Minerals in the NABS sample are mostly quartz with lesser amounts of detrital feldspars, carbonates, magnetite, and fine clay materials. The clay fraction is highly variable, ranging mostly from intricate mixed layer illite/smectite clays to the minor presence of chlorite (Jove-Colon et al., 2003). The total carbon content of the NABS sample was 0.36% by weight, with 0.25% as inorganic carbon and 0.11% as organic carbon (Sanpawanitchakit, 2002). Extraction results suggest that carbonate minerals were 2.5% by weight, with an average composition of $(Ca_{.92}Mg_{.08})CO_3$.

Specific surface areas were determined by BET analysis for the size fractions up to 9.4 mm (Table 4.1). The finest material had the highest surface area (13.11 m^2/g), and the surface areas of the remaining fractions were surprisingly high and relatively consistent. Instead of decreasing rapidly as grain size increased, the surface areas decreased to a local minimum of 3.95 m^2/g for the 250-500 μm fraction and then increased again to 6.31 m^2/g for the 1.0-3.0 mm fraction, before finally decreasing to 3.33 m^2/g for the coarsest fraction measured (5.6-9.4 mm).

Under optical microscopic examination, the 1-3 and 0.5-1 mm fractions appeared to be composed largely of aggregates and polycrystalline lithic fragments of many types, as opposed to single crystalline grains. Figure 4.2 shows SEM micrographs taken of a grain from the 0.5-1 mm fraction. It depicts what is clearly an aggregate, with a well-rounded quartz sand grain cemented into a much finer grained groundmass. Grains in the 250-500 and 125-250 μm size fractions that contained the surface area minimum were primarily discrete, clean, rounded quartz sand grains, similar to the one in the aggregate described above. Quartz predominated in the two finest fractions (63-125 and <63 μm) as well, with a smaller amount of platey material, likely clays, visible at highest

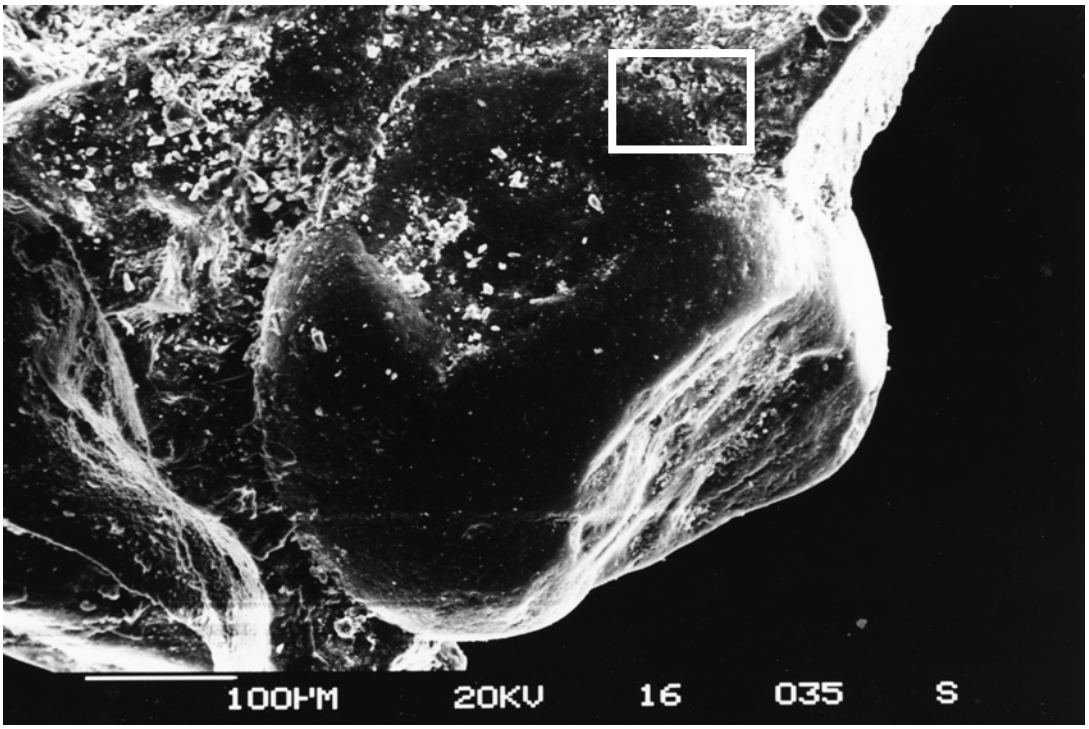

Figure 4.2 a) Close-up of a quartz grain in the 0.5-1 mm size fraction of NABS sediment cemented into a larger aggregate particle. Box shows area of enlargement for Fig. 4.2 b).

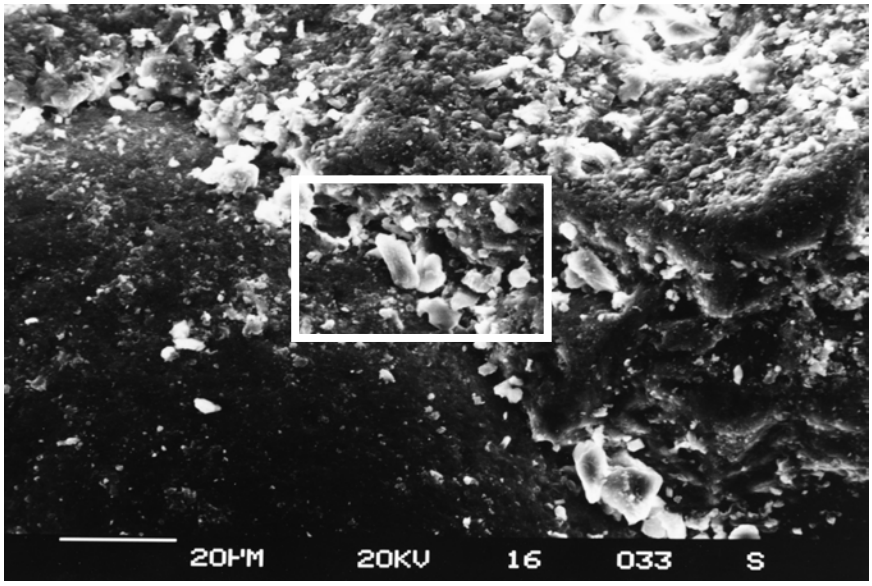

Figure 4.2 b) Boundary between the quartz grain in Fig. 4.2 a) and the cementing mineralogy. The bright trail of grains running along the boundary is composed of discrete grains of calcite mixed with clay minerals. Box shows area of enlargement for Fig. 4.2 c).

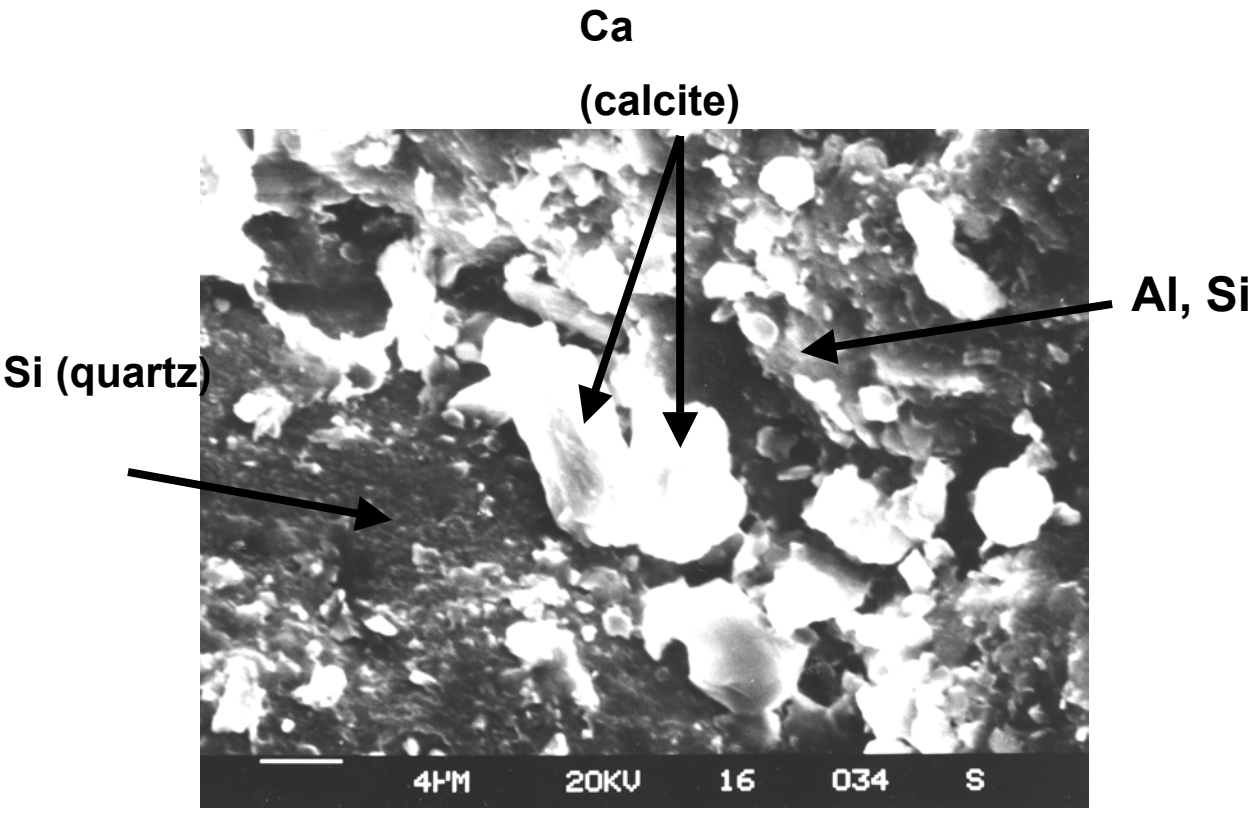

Figure 4.2 c) EDS results and inferred mineralogy in the cement.

magnification. Calcite was generally not present as cement but as individual crystals or clusters of disseminated crystals, usually between 2 and 10 μm in size. The larger grain size fractions contained significant amounts of feldspars. The full range of common feldspar twinning patterns was observed in thin section: microcline, perthite, sanidine, anorthoclase, and plagioclase. Feldspar was rarely identifiable from the <125 μm fractions.

The most common surface morphology observed was a rougher texture of angular platy shapes (Fig. 4.3), suggestive of clay mineralogy (EDS spectral analysis showed potassium, aluminum (Al), and silicon (Si)). The coating appeared to cement grains together into aggregates. The extremely textured and porous surfaces of the larger grains strongly resembled the textures of the <64 μm fraction, which may explain the relatively high surface areas measured for the 0.5-1 mm and 1-3 mm size fractions. This conclusion was further substantiated by SEM examination of thin sections: the majority of large grains had exterior coatings of adhered fine-grained minerals tens of microns thick. Using more advanced characterization methods, Jove-Colon et al. (2003) found that all grains examined exhibited iron(Fe)-rich and Al-Si-rich coatings in two of our U-contaminated samples (NAT-06 and MAU-04). The Fe-rich coatings were arranged conformably in both continuous and discontinuous modes, in some cases between the quartz interface and clay-rich coating. However, Fe-rich phases were also present as small scattered particles immersed in the clay coatings. The Fe-bearing phases were highly heterogeneous, composed mainly of mixed domains of hematite, goethite, and amorphous iron oxyhydroxides (Jove-Colon et al., 2003).

Table 4.1 shows the concentrations of labile U(VI) for the NABS sample and its size

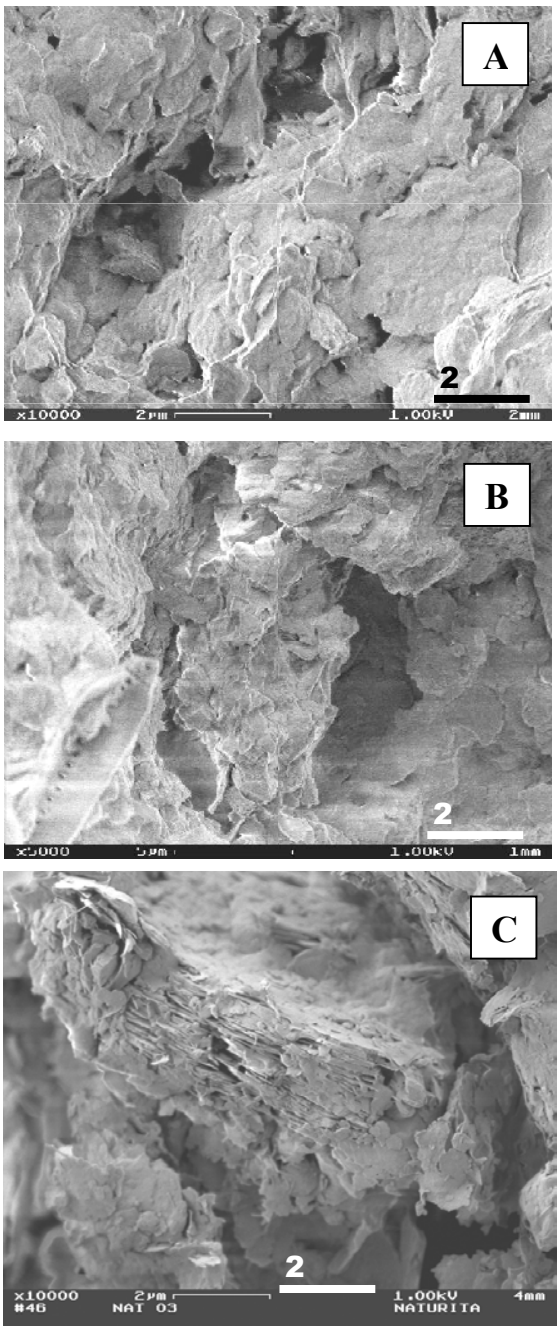

Figure 4.3 Field Emission SEM images of the grain size fraction samples prepared from the NABS sample. All grain size fractions examined had an adhered clay mineral coating covering the underlying mineral grains. For example, image A is from the <63 μm fraction while images B and C are from grains greater than 500 μm in diameter.

fractions. Labile U(VI) was measured as about 9% of the total U (2.3 mg/kg) in the NABS sample, whereas U-contaminated sediments collected at the Naturita site had much higher fractions of labile U(VI) (see Section 6). This is consistent with the hypothesis that the labile fraction is present primarily as U(VI) sorbed on the mineral surfaces. Per unit weight, the fine size fractions contained the greatest concentration of labile U(VI), as expected. However, the larger grain size fractions also contained very significant quantities of labile U(VI). When normalized to surface area, the concentrations of labile U(VI) were surprisingly similar for all of the grain size fractions <3 mm. This suggests that the coatings likely play a major role in the sorption of U(VI). Apparently, the ubiquitous presence and similarity of the coatings among the size fractions (Fig. 4.3) results in little differentiation in U(VI) sorption among the <3 mm grain size fractions.

Although the NABS <3 mm sample comprised only about 30% of the sediments <64 mm, it contained about 84% of the labile U(VI) (Table 4.1). A considerable fraction of the labile U(VI) was present in the 1-3 mm size fraction, possibly because many grains in this size range appeared to be cemented aggregates of smaller grains with significant porosity. The fact that a large fraction of the labile U(VI) was present in the NABS <3 mm composite sample suggests that the sample should provide a good representation of U(VI) sorption reactions within the Naturita alluvial aquifer.

In addition to our study of the NABS sample reported here, an additional study on an acetic acid/acetate treated (carbonate-free) NABS sample was completed by Sanpawanichakit (2002). Some characteristics of the carbonate-free sample are described in Appendix C. Sanpawanichakit (2002) characterized the surface of the carbonate-free NABS sample (some results also presented in Jove-Colon, 2003) and studied U(VI) sorption as a function of pH, U(VI) concentration, and the partial pressure of CO_2.

4.2.4 Sediment Extractions Results

Methods. Extractions of all of the <3 mm NABS samples were performed. The extraction methods and U extraction results are described in more detail in Section 6. In this section (plus in Appendix C), the results for elements other than U are presented. Briefly, the extracting solutions were: 1) artificial groundwater solutions at pH 7.9 in equilibrium with atmospheric CO_2 and near saturation with calcite; 2) hydroxylamine hydrochloride in hydrochloric acid solution at 50°C, and 3) hot concentrated nitric acid (HNO_3).

Extraction with synthetic groundwater solutions, AGW-2 and AGW-3. Some preliminary experiments were carried out to develop the methodology for the batch adsorption studies with the NABS sample (given in Section 5). An artificial groundwater (AGW-2) was designed to have a similar pH, ionic strength, and major ion chemistry as the groundwater in the Naturita alluvial aquifer, but at the atmospheric partial pressure of carbon dioxide (pCO_2). The groundwater was equilibrated with the NABS sample (and, in separate experiments, three of its grain size fractions). The changes in pH and dissolved metal concentrations were measured with time. Figure 4.4 shows that in each case, contact with the sediments increased the pH of the solution from about 6.9 to about 7.9. This change was most rapid for the finest size fraction (<63 μm) and the composite samples. The increase in pH can be attributed to the dissolution of carbonate minerals in the sediments. Calculations with the geochemical equilibrium modeling program, HYDRAQL (Papelis et al., 1988), suggest that the pH of the AGW-2 solution, in equilibrium with calcite and the atmosphere, should be 7.87. Analysis of the water after equilibration, however, did not show a significant increase in the final dissolved Ca concentration, suggesting only minimal dissolution occurred.

In light of these results, another artificial groundwater (AGW-3) was formulated with a higher initial bicarbonate concentration and an initial pH of 7.87. The pH of AGW-3 rose only slightly, to 7.93, when equilibrated with the NABS sample. The minor changes in aqueous chemical composition in these experiments are shown in Figure 4.5. The dissolved Ca concentration fluctuated somewhat, and some manganese (Mn) and Si were solubilized from the sediments into the water. To minimize these effects in the batch U(VI) adsorption experiments, the experiments were carried out with AGW-3 that was pre-equilibrated with the composite sample (see details in Section 5).

Extraction with Hydroxylamine Hydrochloride (HA*HCl) solution. The chemical composition of the NABS sample was also investigated using hydroxylamine hydrochloride-HCl (referred to as HH) extractions. HH extractions are expected to completely dissolve the more soluble phases in the sample and slightly or partially dissolve some crystalline surface phases (see description in Section 6).

The HH extraction was carried out at 50°C with 0.25 M hydroxylamine hydrochloride in 0.25 M HCl. This experiment was comprised of two parts: (i) a time series extraction of the NABS sample, and (ii) 0.5 and 72 hour extractions of the NABS sample and its grain size fractions. The time series extraction was performed using 50 g of the NABS sample and 1 L of HH solution. The 0.5 and 72 hour extractions were performed in duplicate using 1 g of sediment and 20 ml HH solution. Al, Ca, Fe, magnesium (Mg), Mn, and Si were measured using ICP-AES and matrix-matched standards.

Figure 4.6 shows the increases in solution concentration for extracted elements over the 128-hr duration of the time series extraction. The Ca concentration rose steeply and then plateaued, consistent with the expected rapid dissolution of carbonate minerals. The curve for Mg appears to be the result of two processes: rapid dissolution of Ca/Mg carbonates, followed by a slower dissolution from Fe-, Al-, and Si-bearing phases.

The results of the HH extractions of the grain size fractions show that the releases of Ca, Mg

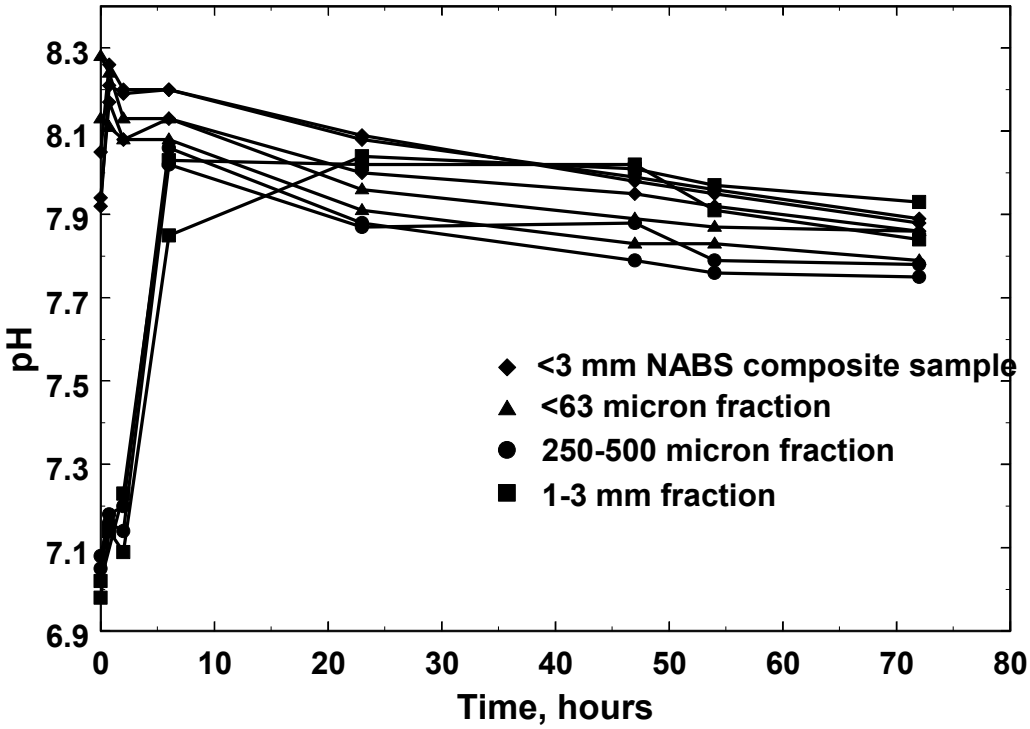

Figure 4.4 Evolution of pH in batch experiments with NABS sediment (labeled composite) and selected size fractions suspended in the artificial groundwater solution, AGW-2.

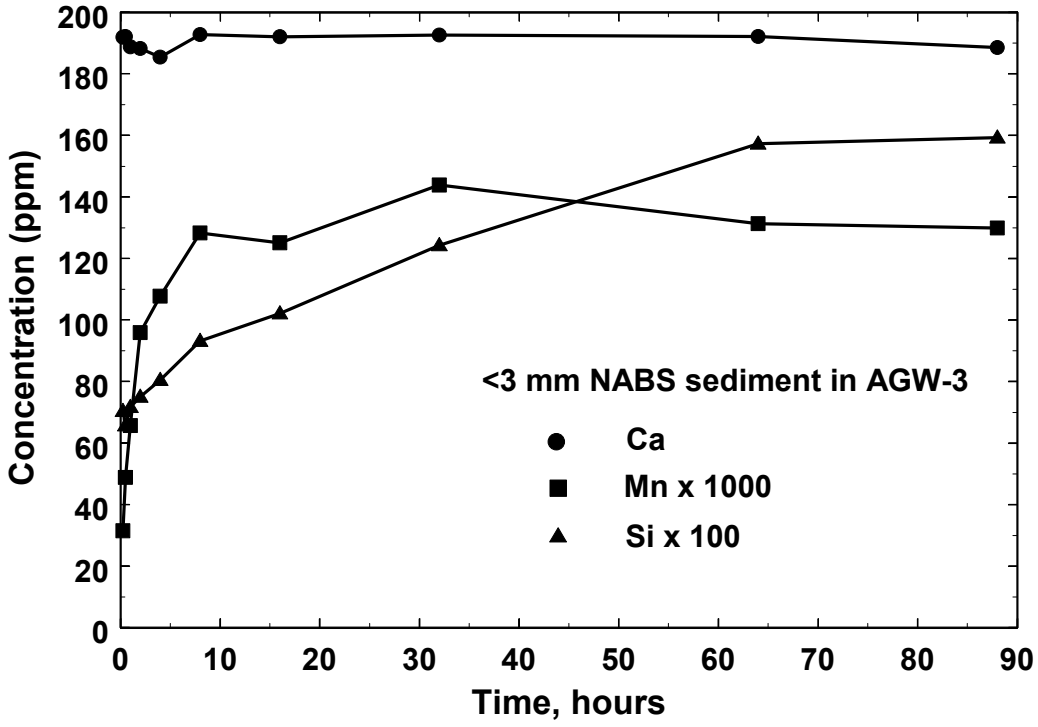

Figure 4.5 Change in the concentrations of dissolved Ca, Mn, and Si in the artificial groundwater solution, AGW-3, as a function of time after contact with the NABS sediment sample. Mn concentration multiplied by 1000, Si by 100. Concentrations given relative to the mass of NABS sediment in the experiment (ppm = mg/kg).

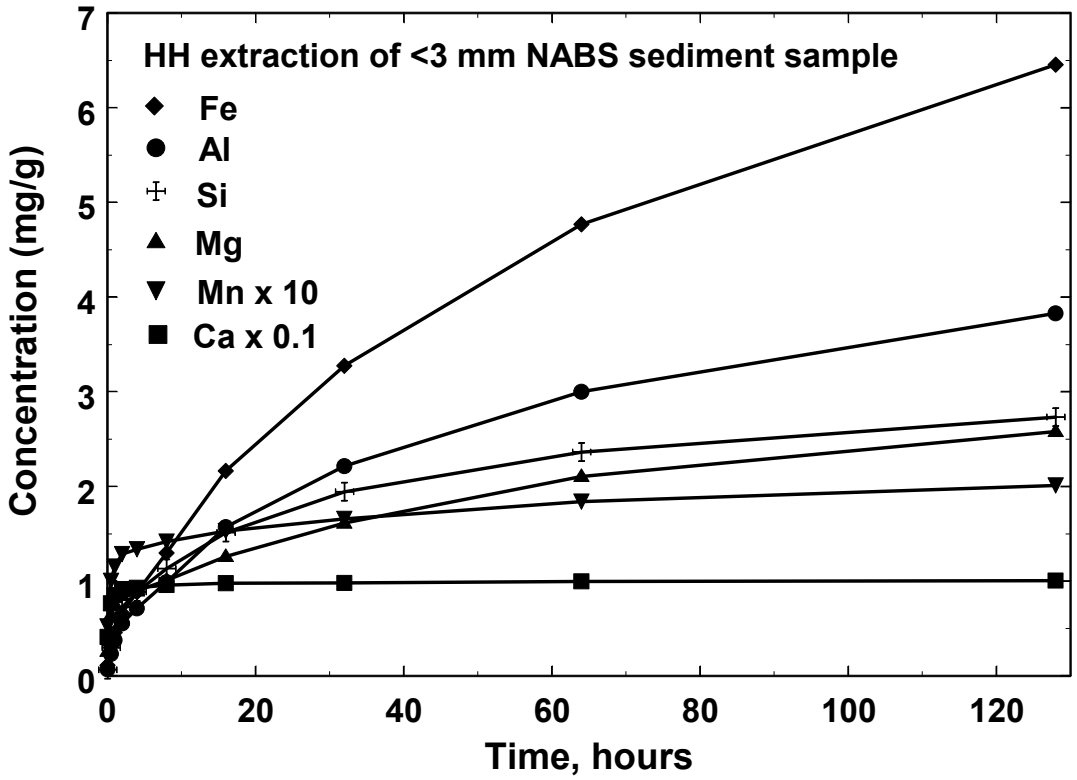

Figure 4.6 Concentrations of elements extracted from the NABS sample (per g of sediment) as a function of time in the hydroxylamine-hydrochloride extraction.

and Mn were enhanced in the finer fractions, while the dissolution of Al, Si, and Fe was slower and more evenly distributed across the size spectrum. The release of elements (in mg/g) show minima in the 250-500 μm size fraction, as was seen in the surface area distribution (Table 4.1). When normalized to surface area (see Appendix C), the minima at the 250-500 μm grain size disappears, and the relative importance of the coarser fractions as a source of dissolved Al and Fe becomes more pronounced.

Extraction with hot concentrated nitric acid. Eight subsamples of the NABS sample were refluxed in hot, concentrated nitric acid (HNO_3) for 71 hours and the average results are given in Table 4.2. The NABS subsamples were three 0.5 g samples, one 1.0 g sample, three 0.5 g samples that had been crushed with a mortar and pestle, and one crushed 1.0 g sample. While there was no significant difference in the results of the various treatments, the relative standard errors (RSE) were relatively high. Much of the variability can be attributed to the small sample masses extracted and the heterogeneity of the sample at the scale of 1 gram.

4.3 Uranium-contaminated Alluvial Sediment Samples.

U-contaminated sediments were collected from auger flights during the installation of monitoring wells in October 1998 (Fig. 4.1) or with a hand auger at a few selected locations during 2000-2001. Sample NAT-25B was collected in September 2000 with a hand auger at a location about 2 m from the monitoring well NAT-25 (Fig. 4.1). The collected sediments were drained and collected into plastic buckets. The sediments were air-dried in the laboratory, dry sieved through 3 mm nylon mesh, and stored at 4°C in the dark.

Table 4.2. Elements Dissolved by Nitric Acid Extraction of the NABS Sample

Element	Average	% RSE
	(mg/g)	
Al	11.8	28.9
Ca	12.2	25.4
Cr	0.00674	31.6
Cu	0.0126	18.2
Fe	16.1	20.1
K	2.09	24.8
Mg	4.06	21.5
Mn	0.276	29.3
Na	0.446	36.9
P	0.370	38.0
Pb	0.0337	29.1
Si	0.166	15.4
Sr	0.0611	21.8
U	0.000837	36.9
Zn	0.0639	14.6

4.3.1 Characterization Results

Table 4.3 shows the specific surface area, total U content, and carbon content of the contaminated Naturita sediment samples and the NABS sample. The total U content of the sediment was determined by γ-spectrometry (see Section 6 for method details). The surface areas of all of the <3 mm U-contaminated samples were greater than the surface area of the NABS sample (5.15 m^2/g). The reason for this is unknown, but may possibly be due to the different methods of sample collection. Comparisons and discussion of the total U content as determined by γ-spectroscopy with U extracted by various treatments of the sediments are presented in Section 6.

4.3.2 Sediment Extractions Results

Methods. The extraction methods used with the <3 mm U-contaminated sediment samples are described in detail in Section 6. Briefly, the extracting solutions were: 1) the artificial groundwater solution, AGW-3, 2) sodium bicarbonate/carbonate solution at pH 9.45, with an alkalinity of 20 meq/L, 3) hydroxylamine hydrochloride in hydrochloric acid solution at 50°C (HH), and 4) hot concentrated nitric acid.

Results. The U extraction results for each of these extractions is described in detail in Section 6. For the carbonate and HH extractions, the results for elements other than U are give in Appendix C. Table 4.4 gives the concentrations of elements extracted (either in % or ppm) in the hot concentrated nitric acid extractions.

Table 4.3: Total Uranium, Specific Surface Areas, Percent Carbon and Percent Calcite for U-contaminated Naturita Sediments and for the NABS sample

Sample	Total U [mol/g]	Surface area [m^2/g]	% Carbon by Weight		
			Total Carbon	Inorganic	Organic
NABS	$9.64 \cdot 10^{-9}$	5.2	0.36	0.25	0.11
NAT-01	$2.70 \cdot 10^{-8}$	9.0			
NAT-02	$2.29 \cdot 10^{-8}$	9.1			
NAT-03	$1.24 \cdot 10^{-8}$	13.5	1.01	0.85	0.16
NAT-04	$1.91 \cdot 10^{-8}$	14.1			
NAT-05	$1.78 \cdot 10^{-8}$	13.3			
NAT-06	$3.14 \cdot 10^{-8}$	20.0	0.55	0.19	0.36
NAT-07	$1.85 \cdot 10^{-8}$	15.4			
NAT-08	$1.28 \cdot 10^{-8}$	12.7	1.00	0.84	0.16
NAT-10	$1.55 \cdot 10^{-8}$	11.1			
NAT-11	$1.03 \cdot 10^{-8}$	17.9	0.89	0.69	0.20
NAT-12	$1.34 \cdot 10^{-8}$	12.4	0.68	0.38	0.29
MAU-01	$1.17 \cdot 10^{-8}$	13.4			
MAU-02	$2.19 \cdot 10^{-8}$	15.3	1.05	0.55	0.50
MAU-03	$2.87 \cdot 10^{-8}$	6.7			
MAU-04	$4.43 \cdot 10^{-8}$	9.7			

Table 4.4. Concentrations of Elements Extracted from Contaminated Sediments by Concentrated Nitric Acid

Sample	Uranium	Aluminum	Calcium	Vanadium	Iron	Potassium	Magnesium	Manganese	Silicon
	ppm	%	%	ppm	%	%	%	ppm	ppm
NAT-01	6.070	1.46	2.07	31.0	1.58	0.358	0.480	400	429
NAT-02	6.09	1.65	2.37	253	1.69	0.324	0.514	511	457
NAT-03	1.92	2.18	3.21	134	2.08	0.394	0.641	319	625
NAT-04	2.83	2.16	2.32	116	1.47	0.603	0.617	376	484
NAT-05	2.50	2.93	2.76	104	1.85	0.603	0.617	281	285
NAT-06	6.57	3.53	1.22	394	1.81	1.05	0.735	184	860
NAT-07	5.31	1.93	4.76	78.9	1.37	0.540	0.566	504	510
NAT-08	2.43	2.08	3.36	132	2.01	0.411	0.625	422	445
NAT-10	2.28	1.58	2.18	92.5	1.64	0.321	0.563	437	458
NAT-11	1.75	3.04	2.87	80.4	1.88	0.709	0.671	260	532
NAT-12	2.50	1.83	1.73	30.8	1.53	0.489	0.460	346	447
NAT-25B	5.67	1.27	0.29	33.0	1.05	0.316	0.274	89.7	150
MAU-01	2.24	1.82	2.15	30.0	1.62	0.418	0.505	398	421
MAU-02	4.31	2.29	2.77	35.9	1.65	0.527	0.572	401	449
MAU-03	5.02	1.00	1.97	28.4	1.36	0.220	0.375	479	379
MAU-04	10.7	1.47	1.94	25.3	1.41	0.325	0.489	439	437
NABS	0.84	1.13	1.17	28.9	1.74	0.240	0.396	274	251

Table 4.4 (cont). Concentrations of Elements Extracted from Contaminated Sediments by Concentrated Nitric Acid

Sample	Strontium ppm	Cobalt ppm	Cadmium ppm	Copper ppm	Sodium ppm	Nickel ppm	Phosphorus ppm	Lead ppm	Zinc ppm
NAT-01	186	6.90	1.61	17.9	607	7.35	352	44.9	99.2
NAT-02	174	8.82	4.00	133	615	8.09	372	65.0	204
NAT-03	190	8.54	1.39	16.5	832	9.82	488	32.2	63.3
NAT-04	153	8.05	1.87	25.6	737	7.09	273	59.5	131
NAT-05	147	6.50	-0.100	11.3	880	9.01	301	5.99	51.9
NAT-06	125	6.52	0.947	11.3	1198	8.07	353	49.3	41.4
NAT-07	146	7.23	1.37	16.6	642	7.29	248	40.2	75.7
NAT-08	167	10.5	1.33	16.5	816	8.57	455	35.1	57.1
NAT-10	114	8.62	1.75	32.4	653	9.44	329	57.0	100
NAT-11	210	8.13	1.06	14.2	1109	7.79	356	49.2	44.7
NAT-12	136	6.26	0.466	8.58	670	6.10	328	31.4	34.3
NAT-25B	46.2	3.89	-0.075	3.47	456	4.06	210	5.43	39.3
MAU-01	120	6.91	0.973	10.7	633	7.78	351	31.3	37.8
MAU-02	117	6.85	0.864	12.6	712	7.37	384	40.2	46.6
MAU-03	79.4	6.36	1.37	24.3	372	4.92	430	57.6	141
MAU-04	156	7.21	1.17	17.9	437	7.61	324	35.0	87.5
NABS	65.9	6.65	1.05	13.4	344	5.14	383	33.4	66.9

5 GENERALIZED COMPOSITE SURFACE COMPLEXATION MODELING AS A TOOL FOR ESTIMATING ADSORPTION AT FIELD SITES

5.1 Introduction

Prediction of the fate and transport of toxic metals and radionuclides is of paramount importance in evaluating remediation schemes and in quantifying the risk of the contamination to human or ecosystem health (USEPA, 1999). The transport of most of the important metal and radionuclide contaminants is strongly influenced by reactive chemical processes, including aqueous complexation, adsorption, precipitation and dissolution, and redox reactions. However, in practice, nearly all reactive transport models ignore the chemical complexity of aqueous complexation and adsorption processes and utilize the distribution coefficient (constant K_d) approach to describe the retardation of metal and radionuclide contaminants (Bethke and Brady, 2000; USEPA, 1999).

The K_d concept works well when applied to trace concentrations of non-ionic, hydrophobic organic molecules, but its application to inorganic contaminants is problematic because its value is so sensitive to aqueous chemical parameters. For example, Figure 5.1 shows the dependence of the K_d for U(VI) adsorption on ferrihydrite as a function of pH and the partial pressure of carbon dioxide gas (pCO_2). Note that the K_d value at pH 8 decreased by more than *four orders of magnitude* as the pCO_2 increases from its value in air to 1%. This is an important variation to understand, because the pCO_2 in aquifers commonly reaches values of 1-5% (Hem, 1985), while most K_d values have been determined in laboratory experiments exposed to air. Moreover, pCO_2 often increases with transport after groundwater recharge, and this spatial/temporal trend in chemical conditions can greatly affect U(VI) transport (see Section 9).

In contrast to transport models using a constant K_d, surface complexation models (SCM) have the capability of describing changes in contaminant adsorption as chemical conditions and aqueous speciation vary (Davis and Kent, 1990), and SCM can be readily incorporated (see Section 9) within solute transport models (Kent et al., 2000; Stollenwerk, 1998, 1995; Kohler et al., 1996). There are two major approaches for applying the SCM concept to model ion adsorption by soils and sediments: 1) thermodynamic surface speciation models (e.g., Weerasooriya et al., 2001; Hiemstra and van Riemsdijk, 1999), and 2) site-binding, semi-empirical models (Davis et al., 1998).

Thermodynamic surface speciation models that are developed for soils and sediments by predicting adsorption as the sum of contributions from individual mineral phases are called Component Additivity (CA) models (Davis et al., 2002; Waite et al., 2000; Davis et al., 1998; Honeyman, 1984). In the CA approach, it is assumed that a mineral assemblage is composed of a mixture of one or more reference phases, whose surface properties are known from independent studies of each phase. Model parameters for each phase can then be applied without further fitting based on a measurement of the relative amounts of each mineral surface present. This approach is given credence by the large number of investigations in the literature on ion adsorption by single mineral phases.

In the semi-empirical approach, also referred to as the Generalized Composite (GC) approach, the surface of the mineral assemblage is considered too complex to be quantified in terms of the contributions of individual phases to adsorption. Instead, it is assumed that adsorption can be described by SCM equilibria written with "generic" surface functional groups, with the stoichiometry and formation constants for each SCM mass law determined by fitting experimental data for the mineral assemblage (Davis et al., 1998; Borkovec et al., 1998).

Given the advantages of the SCM approach, why then has it not been adopted in practice for

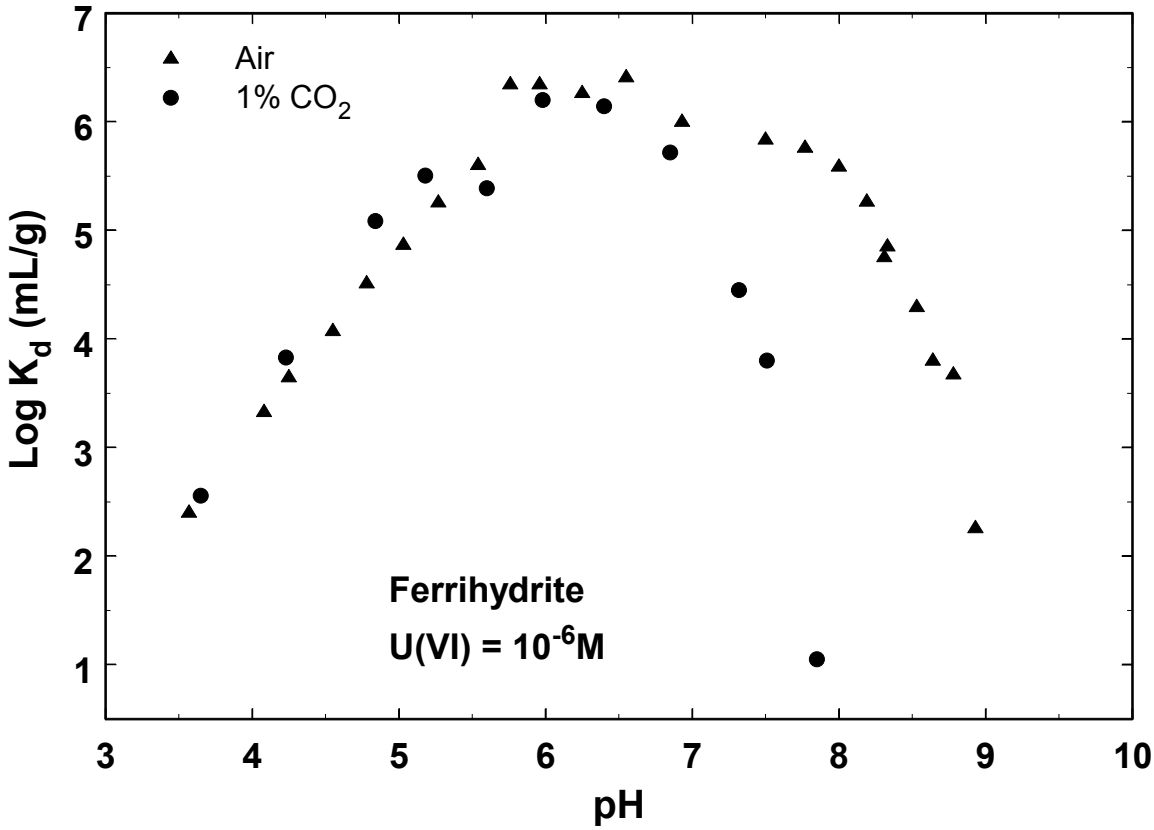

Figure 5.1 Distribution coefficients for uranium(VI) adsorption on the pure ferrihydrite surface as a function of pH and the partial pressure of carbon dioxide gas (total U(VI) concentration of 10^{-6}M).

risk assessment modeling and evaluation of remediation alternatives? The most likely reasons are:

1) a continuing evolution of our fundamental understanding of the coordination chemistry of surface complexes (e.g., see Bargar et al., 2000), leading to increasingly more complex models, and,

2) a relative lack of experience in applying the SCM concept to soil and sediments by hydrologists developing conceptual models for radionuclide transport, especially using the additive paradigm inherent in the CA approach (Sanpawanitchakit, 2002; Davis et al., 1998; Honeyman, 1984).

In this section we will demonstrate the importance of the electrical double layer terms in accurately describing the adsorption of U(VI) by the crystalline iron oxide, hematite. Iron oxides may be an important mineral phase for U(VI) adsorption in the subsurface sediments collected from the alluvial aquifer at the UMTRA site near Naturita, Colorado (Jove-Colon et al., 2003). However, it is shown that it would be difficult to apply the U(VI)-hematite SCM model parameters (and hence the CA modeling approach) to the Naturita sediments, because of the difficulty of characterizing the electrical double layer properties of iron oxide phases in the Naturita sediments. Due to this difficulty, we derive instead a GC model for simulating U(VI) adsorption by the sediments from the alluvial aquifer.

We will show that, despite the complexities mentioned above for the CA approach, the SCM concept can currently be utilized to great advantage by employing the simpler GC approach to describe adsorption in applications

to natural systems. In Sections 6, 7, and 9, it is shown that the simple, semi-empirical site-binding model that results from the GC modeling approach can be readily applied within a reactive transport model for U(VI) or to predict *in-situ* K_d values, which allows temporal and spatial variations in chemical conditions at the site to be accurately considered in model simulations.

5.2 Materials and Methods

5.2.1 U(VI) Batch Adsorption Experiments with Hematite

Hematite powder used in these experiments was synthesized from $Fe(ClO_4)_3$ following the method of Matijevic and Scheiner (1978) as described in Bargar et al. (2000). The N_2-BET surface area of the dried powder was 46.1 m^2/g. Powder X-ray diffraction spectra indicated only the presence of crystalline α-Fe_2O_3, with no evidence for goethite. Diffuse reflectance Fourier Transform infrared spectra of the hematite also showed no evidence of goethite-specific peaks.

Dried hematite powder and $NaNO_3$ were weighed into either 500 mL or 1L polyethylene bottles and milli-Q water was added to achieve a suspension of 0.2 g/L in a 0.1 M $NaNO_3$ solution. The suspensions were initially adjusted to pH 4 or 9 (where U(VI) solubility is greater than 10^{-4} M) using HNO_3 or $NaHCO_3$ and were allowed to equilibrate with humidified air. U(VI) was added dropwise as aliquots of an acidic 10 mM $UO_2(NO_3)_2$ solution while the samples were vigorously stirred. Samples were adjusted to their final pH values and then maintained by dropwise addition of 20 - 50 µL aliquots 0.1 - 0.01M HCl and/or 0.1M $NaHCO_3$. Samples were then gently agitated on a shaker for 48 hours. Prior to analysis, samples were centrifuged at approximately 40,000*g* centrifugal force for 20 minutes to concentrate the solid. Dissolved U(VI) was then measured by kinetic phosphorescence analysis (KPA). Further details of the experiments are given in Bargar et al. (2000).

5.2.2. Naturita Alluvial Aquifer Sediments

Site description. The Naturita site is located in the southwestern portion of Colorado in Montrose County, about 3 km northwest of the town of Naturita and on the west bank of the San Miguel River (see Section 3). From 1947 to 1963, the Naturita mill processed 6.4 x 10^8 kg of uranium-vanadium ore. Uranium (U) and vanadium (V) were extracted by salt roasting, followed by carbonate leaching in percolation tanks. Carbonate leach tails were slurried to the western half of the Naturita site, in the area of the site farthest (200 m) from the San Miguel River. Carbonate leach residues were later sent to a second stage of sulfuric acid percolation leaching. Acid leach tails were deposited in the eastern area of the site, closer to the river.

U contamination in groundwater at the site has been observed primarily within an unconfined, shallow alluvial aquifer composed of sand, gravel, pebbles, and cobbles (see Section 3). The aquifer is recharged by the San Miguel River in a reach about 1 km upgradient of the site. The thickness of the saturated zone of the alluvial aquifer is about 3 to 4 m (see Section 3).

Preparation of the Naturita Aquifer Background Sediment (NABS) Sample. On July 16-17, 1998, approximately 1300 kg of material from the saturated zone of the Naturita alluvial aquifer was collected from a gravel pit located about 90 m upgradient of the site's southern boundary and 40 m from the western edge of the San Miguel River (see Fig. 4.1). The sample was screened in the field to remove cobbles larger than 64 mm. It was visually estimated that 50 % of the material scooped by the backhoe did not pass the 64 mm screen.

Seven hundred thirty four kg of wet, <65 mm sediments were shipped in clean plastic containers to the USGS laboratories in Menlo Park, California. The sediment was spread onto plastic sheets and allowed to air dry (weight of 641 kg). The sediments were sieved to separate grains <3 mm from the coarser material. 190 kg of sediments passed the 3 mm screen, representing roughly 30 % (by weight) of the

Table 5.1 Composition of artificial groundwater solutions for U(VI) adsorption experiments

Name	AGW-3	AGW-5	AGW-6	AGW-7
pCO_2	0.035% (lab air)	2%	10%	0.5%
$CaSO_4$	2.33E-03	3.27E-03	3.27E-03	2.32E-03
$MgSO_4$	1.52E-03	1.52E-03	1.52E-03	1.52E-03
Na_2SO_4	9.38E-04	0	0	0
$CaCl_2$	2.38E-03	2.22E-03	0	3.95E-05
KCl	6.40E-05	6.40E-05	6.40E-05	6.40E-05
$NaHCO_3$	5.38E-04	2.41E-03	2.41E-03	2.41E-03
$CaCO_3$	0	9.27E-04	3.33E-03	8.70E-05
HCl	0	9.27E-04	1.57E-03	8.70E-05

<65 mm material collected in the field. The 190 kg of <3 mm sediments was thoroughly mixed and is referred to hereafter as the Naturita Aquifer Background Sediment (NABS).

Sediment Characterization. Only a few of the main characteristics of the NABS sediment relevant to the discussion are mentioned in this section. Detailed characterization data are presented in Section 4 and Appendix C.

5.2.3. Batch U(VI) Adsorption Experiments with Naturita Sediments

Experiments were carried out at five different pCO_2 values to determine the distribution of U(VI) between the NABS sediments and artificial groundwater solutions as a function of U(VI) concentration. The experiments were designed partly to simulate chemical conditions in the Naturita alluvial aquifer, without any dissolution or precipitation of calcite and with as little alteration of the sediment surfaces as possible. To this end, both the NABS sediments and artificial groundwater solutions were pre-treated prior to adsorption experiments so as to approximate equilibrium conditions when the U(VI)-bearing solutions were introduced.

Pretreatment of artificial groundwater solutions. Four artificial groundwater solutions (AGWs) were designed so as to approximate the major chemistry of Naturita groundwaters at various pCO_2 (Table 5.1). To prepare the solutions for use in adsorption experiments, each was placed in contact with NABS sediment in a stirred flask for at least 72 hr. 'Certified standard' grade mixed gas of appropriate CO_2 content was bubbled through the AGW solutions using a sparger. Solids were separated from the ripened solutions by filtration (0.4 μm).

For adsorption experiments, U(VI) (1000 mg/L, in 2% HNO_3) from High-Purity Standards was added to pretreated AGW to yield a solution 10^{-5} M U(VI). Other concentrations of U(VI) were obtained by dilution of this stock solution. Solutions were allowed to sit overnight to allow aqueous U(VI) speciation to approach equilibrium.

Pretreatment of NABS sediments. Two replicate weighed aliquots of NABS sample were placed into 50 ml polycarbonate centrifuge tubes in a controlled pCO_2 atmosphere within a glove bag or open to laboratory air. 30 ml of pretreated artificial groundwater solution (without added U(VI)) was added to each tube. The tubes were placed on an end-over-end rotator (14 rpm) overnight in order to pre-equilibrate the sediment surfaces. The following day the test tubes were centrifuged (25,600 RCF for 20 min) and the supernatant was removed and sampled for pH, alkalinity, and U(VI) concentration by KPA. The test tubes were weighed to determine the mass of residual AGW solution in contact with the pretreated NABS sample. Preliminary experiments showed that some cations (e.g. Si, Mn) were dissolved from the NABS sample during initial contact (see Section 4); the pretreatment helped stabilize these concentrations during the actual U(VI)

Table 5.2 Final chemical conditions in U(VI) adsorption experiments

Initial pCO_2	AGW solution	Solid/liquid Ratio (g/L)	Average final pH	Average final alkalinity (meq/L)	Final pCO_2[a]
Lab air	AGW-3	25	7.94	0.75	0.05%
0.5%	AGW-7	125	7.58	3.045	0.47%
2%	AGW-5	125	7.22	3.58	1.24%
2%	AGW-5	250	7.18	4.035	1.57%
10%	AGW-6	820	6.88	9.13	6.8%

[a] Calculated from the averaged final pH and alkalinity values

adsorption experiments. Dissolved Ca concentrations fluctuated slightly in the first hours after contact, but restabilized at the concentrations expected for equilibrium with calcite.

U(VI) Batch Adsorption Experiments. Weighed aliquots of U(VI)-bearing AGW were added to each of the pretreated NABS samples, plus to one empty (control) test tube, which were then capped and returned to the end-over-end rotator. After 96 hr the test tubes were centrifuged as above, and then sampled for pH, U(VI), and alkalinity. Experimental conditions in the batch adsorption experiments are summarized in Table 5.2. Because the experimental systems were closed, the alkalinity and pH evolved slightly during the equilibration due to mineral weathering and addition of the U(VI) stock solution. As a result, the final pCO_2 in the small head space of the centrifuge tube would be expected to be different from the pCO_2 with which the AGW solutions were initially equilibrated. Table 5.2 shows the average final pCO_2 concentrations, calculated from the measured pH and alkalinity values.

Adsorption Calculations. Calculation of U(VI) distributions in the adsorption experiments followed a straightforward material balance approach. In each case, for each sample test tube, the mass of NABS sediment added was measured and the labile (exchangeable) U(VI) content was known (see Section 6). Carbonate extractions provide a good estimate of the labile U(VI) content for contaminated sediments, however, for the low U(VI) concentrations in uncontaminated sediments, the best determination of labile U(VI) can be made by a more complex U isotopic exchange method (see Section 6). The labile U(VI) for the NABS sample determined by isotopic exchange was $5.6 \cdot 10^{-10}$ moles/g, and this value was used to include background U(VI) in the adsorption calculations. The initial and final dissolved U(VI) concentrations in the NABS pretreatment solutions were measured, allowing a calculation of the U(VI) contributed by the residual amount of pretreatment solution in contact with the NABS sample before the introduction of U(VI)-spiked AGW solution. U(VI) adsorption on the NABS sample was calculated by difference from the total labile U(VI) present in the experiment minus the dissolved U(VI) present after the 96-hr adsorption period.

5.2.4. Modeling Methods

FITEQL 4.0 (Herbelin and Westall, 1999) was used to determine the best fit of various surface reactions or combinations of reactions to the experimental data. The Davies equation was used for activity correction of aqueous species. The method recommended by Herbelin and Westall (1999, p. 6-14) for formulating problems for fitting adsorption data was used, in which adsorbed U(VI) was defined as a Type II "dummy" component. The optimization procedure minimizes the difference between experimental and calculated values of adsorbed

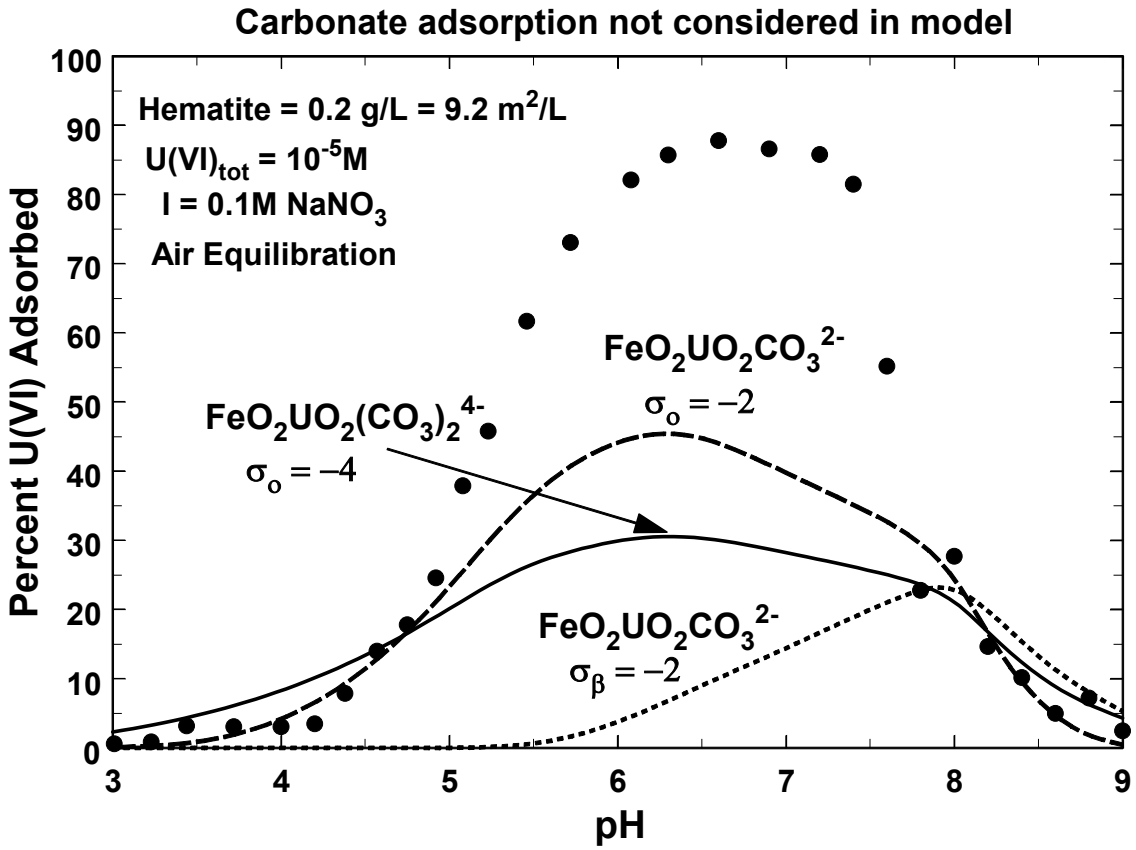

Figure 5.2 Adsorption of U(VI) on hematite as a function of pH in a $NaNO_3$ solution equilibrated with air. Data shown as dark circles. Model calculations shown for formation of the surface species, $FeO_2UO_2CO_3^{2-}$ (dashed curves) or $FeO_2UO_2(CO_3)_2^{4-}$ (solid curve). Model calculations are shown for each surface species with the net charge located in either the surface plane (σ_o) or within the mean plane of adsorbed ions (σ_β). Adsorption of carbonate anions not considered in the model calculations.

U(VI). Relative errors of 1% in the concentrations of surface sites, total U(VI), and adsorbed U(VI), and relative errors of 5% in log $[H^+]$ and log $[H_2CO_3]$ were used as FITEQL inputs.

5.3 Results

5.3.1 U(VI) Adsorption on Hematite

Figure 5.2 shows adsorption data for U(VI) on the hematite powder as a function of pH in $NaNO_3$ solutions equilibrated with air. U(VI) adsorption increases from nil at low pH to about 90% adsorbed near neutral pH. In the alkaline pH range, adsorption on iron oxides decreases due to aqueous complexation with carbonate anions (Waite et al., 1994; also see Section 2). Adsorption of U(VI) on iron oxides, such as hematite, is important to consider in this section, because Jove-Colon et al. (2003) have demonstrated a likely association of U(VI) with iron oxide nanoparticles in grain coatings in U-contaminated aquifer sediments from the Naturita site.

For the more complex thermodynamic surface speciation SCM, with electrical double layer descriptions, it is desirable to have supporting information on the surface species formed from spectroscopic studies. For U(VI) adsorption on hematite in air, it is known that the major U(VI) surface species formed are ternary surface-uranyl-carbonato complexes (Bargar et al., 2000). The spectroscopic results showed that

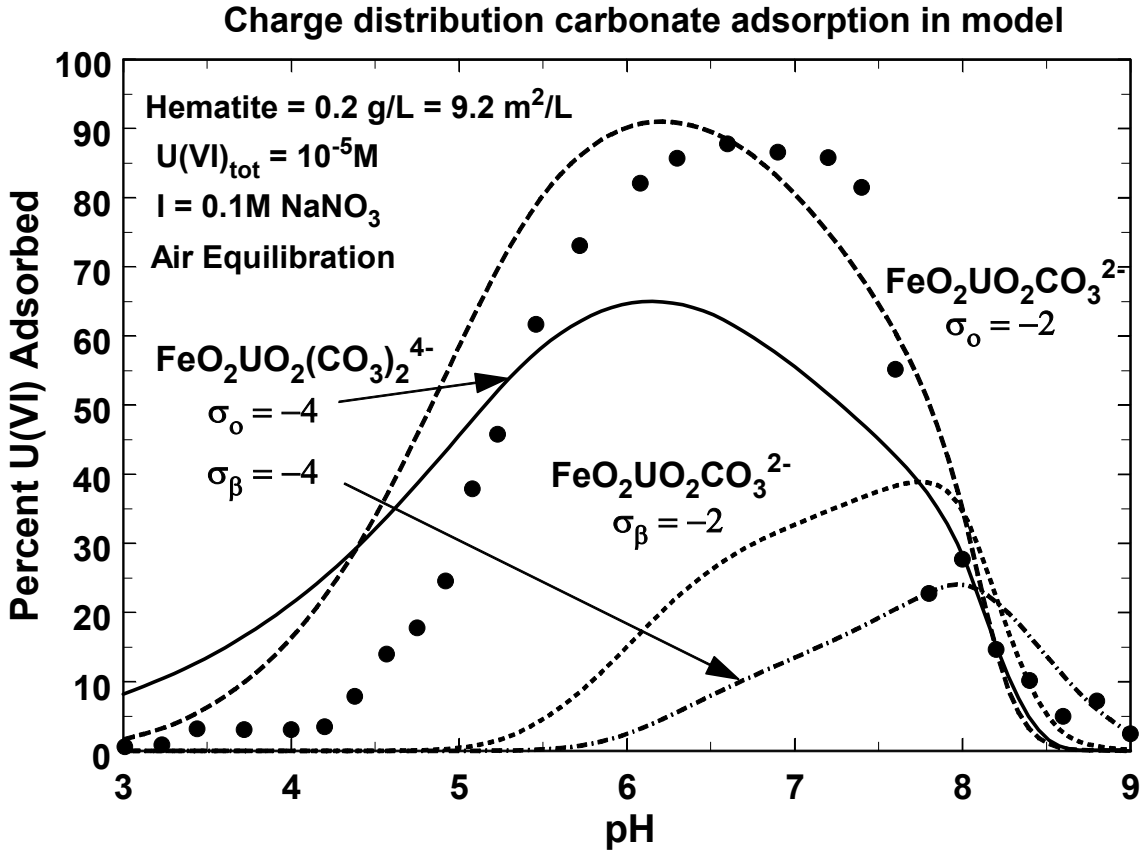

Figure 5.3 Adsorption of U(VI) on hematite as a function of pH in a $NaNO_3$ solution equilibrated with air. Data shown as dark circles. Model calculations shown for formation of the surface species, $FeO_2UO_2CO_3^{2-}$ (dashed curves) or $FeO_2UO_2(CO_3)_2^{4-}$ (solid curve and dot-dash curve). Model calculations are shown for each surface species with the net charge located in either the surface plane (σ_o) or within the mean plane of adsorbed ions (σ_β). Adsorption of carbonate is considered in the model using a charge distribution model (Davis et al., 2003) similar to the goethite-carbonate model of Villalobos and Leckie (2001).

the likely predominant surface species formed were $FeO_2UO_2CO_3^{2-}$ or $FeO_2UO_2(CO_3)_2^{4-}$ over the pH range 4-9 in systems with a total U(VI) concentration of 10^{-5}M.

Here we will demonstrate the sensitivity of the SCM calculations to electrical double layer parameters by modeling macroscopic adsorption data for U(VI)-hematite-carbonate system, using only surface species that are consistent with the spectroscopic results. A triple layer model is used to describe the data, using acid-base constants, site density, and capacitance values from Sahai and Sverjensky (1997) to describe the hematite/water interface. U(VI) SCM calculations with and without a consideration of carbonate adsorption in the model are compared to demonstrate further the importance of the electrical double layer to the U(VI) adsorption modeling. All relevant aqueous U(VI) species are considered in the model calculations (see Section 2).

Figures 5.2 and 5.3 show FITEQL model calculations for U(VI) adsorption on hematite. Because of poor fits, FITEQL would not converge when the complete U(VI) adsorption dataset was used in a model calculation. For

illustrative purposes, calculations are shown when the model was *fit to the U(VI) adsorption data in the pH range 7-9 only*, which partly explains why there are large deviations of the model curves from the data in the low pH range. Each model curve is for a single surface reaction only; none of the curves shown consider a combination of surface reactions. The calculations show the general dependence of the predicted U(VI) adsorption as a function of pH; the curves can be moved up and down the y-axis by assigning a greater or smaller formation constant for the formation of each species. The purpose, however, is to demonstrate how model calculations using the mass laws for formation of the surface species, $FeO_2UO_2CO_3^{2-}$ and $FeO_2UO_2(CO_3)_2^{4-}$, are sensitive to the "location" of the net charge within the interface.

The calculations shown in Figure 5.2 assume that carbonate anions do not adsorb at the hematite surface. The net charge of the $FeO_2UO_2CO_3^{2-}$ surface species is –2. For modeling, a choice must be made as to how to correct the mass law for formation of the species for the electrostatic component of the free energy. The net charge could be approximated as located within the surface plane (σ_o) or within the mean plane of adsorbed ions (σ_β). Calculations are shown for each of these choices (with a best fit to the adsorption data in the alkaline pH range). A model curve is also shown for the species, $FeO_2UO_2(CO_3)_2^{4-}$, with a net charge of –4 located within the surface plane (σ_o). All of the calculated curves greatly underestimate the experimental data; moreover, none of the curves has a dependence on pH that is consistent with the trend observed with the experimental data.

Figure 5.3 shows a similar set of model calculations except that the adsorption of carbonate anions is included in the model. Carbonate adsorption is known to occur on iron oxide surfaces and has a significant effect on the electrical charge and potential at the oxide-water interface (Villalobos and Leckie, 2001; Kohler et al, 1999). The carbonate adsorption decreases the surface charge and potential via adsorption and thus has a significant effect on modeling adsorption of the charged U(VI)-carbonato surface species. A much better fit to the experimental data can be obtained, while still using only the surface species indicated from spectroscopic results, once the adsorption of carbonate anions is considered within the model. A complete model of U(VI) and carbonate anion adsorption on hematite is given in Davis et al. (2003).

The sensitivity of modeled U(VI) adsorption to the electrostatic correction factor illustrates a significant practical problem in extending the detailed thermodynamic surface speciation models directly to simulations of adsorption on complex mineral assemblages in the environment. As mentioned above, mineral surfaces in the environment are coated with poorly crystalline secondary mineral coatings and natural organic materials (fulvic and humic acids), making it extremely difficult to assess quantitatively the electrostatic contribution to the free energy of adsorption. Clearly, an assumption that the electrical double layer properties of clean hematite studied in the laboratory are the same for hematite grains in sediments is likely incorrect. Thus, a major challenge in applying the surface complexation concept to the environment is presented by our poor understanding of the surface functional group composition of grain coatings and the electrical double layer at the sediment/water interface.

It is shown below, however, that the semi-empirical GC modeling approach simplifies the calculations such that adsorption can still be simulated using mass laws that are coupled with aqueous speciation, while lumping together parameters that are difficult to characterize in the environment.

5.3.2 U(VI) Batch Adsorption Experiments with the NABS sample

Preliminary experiments were carried out to determine the length of time necessary to achieve steady state solution concentrations of U(VI) in an artificial groundwater solution (AGW-3) in contact with the NABS sample or its grain size fractions. These experiments were

carried out with 10^{-6} M U(VI) added to AGW-3 solution at equilibrium with atmospheric CO_2. Under these conditions, the AGW-3 solution had an equilibrium pH of 7.94 +/- 0.05 (Table 5.2).

Because the samples are of unequal surface area, the results are best compared with a surface-area distribution coefficient, $K_a = K_d/a$, where a is the specific surface area in m^2/g. The results ofthese experiments are presented as K_d and K_a values in Figure 5.4. The results show that U(VI) adsorption continued to approach adsorptive equilibrium for at least 96 hr. The fine grain size fractions adsorbed more U(VI) per unit mass than the coarse fractions (Fig. 5.4A), but much of this difference was eliminated by accounting for surface area differences (Fig. 5.4B). The approach to U(VI) adsorptive equilibrium was slower with the larger grain sizes, perhaps due to the porosity observed in the grains.

Batch adsorption isotherm experiments with the NABS sample were conducted with reaction times of 96 hr, which appeared to allow enough time to approach steady-state dissolved U(VI) concentrations (Fig. 5.4). Because of the presence of calcite in the NABS sample, only one equilibrium pH value was obtained for each AGW-pCO_2 pair (Table 5.2). Total U(VI) added to the experiments varied from zero (in which background labile U(VI) desorption was evaluated, see Section 6) to 1 x 10^{-5} M. Figure 5.5 shows fractional adsorption of U(VI) on NABS as a function of the U(VI) concentration, pCO_2, and pH. Fractional adsorption decreases as the U(VI) concentration increases, as has been observed for quartz, aluminosilicate minerals, and iron oxides (Davis et al., 2001; Waite et al., 1994). Adsorption also decreased as the pCO_2 increased, but the decrease is not obvious in Figure 5.5 because the solid/liquid ratio in the experiments was increased as well. When plotted as the log of the U(VI) adsorption density versus the log of the dissolved U(VI) concentration (not shown), the adsorption isotherms have a slope of 0.75, consistent with isotherms determined for U(VI) on pure quartz (Kohler and Davis, 2001; Kohler et al., 1996). The aqueous conditions at the highest pCO_2 (6.8%) are in the range observed in the Naturita alluvial aquifer (see Section 3). Figure 5.6 shows the same experimental data plotted as log K_d values versus log of the dissolved U(VI) concentration.

5.3.3 GC Model for U(VI) Adsorption on Naturita Sediments

Despite the complexities of the sediments, the Generalized Composite (GC) modeling approach can be used in order to apply the surface complexation concept for modeling U(VI) adsorption. The GC approach allows simple relationships to be derived that couple the change in U(VI) adsorption with variations in U(VI) aqueous speciation. Because no electrostatic information was available for the charge and potential at the Naturita sediment surfaces, a non-electrostatic model was used. In order to simplify the model, the following choices were made: a) a total site density of 3.84 $\mu moles/m^2$ of hydroxyl groups was assumed, as recommended by Davis and Kent (1990), b) at least two types of sites (strong and weak) were assumed to exist on the surface to account for the change in adsorption with U(VI) concentration, and c) three or less U(VI) surface reactions would be used to describe the experimental data. The latter constraint was arbitrary but was adopted to simplify the model. In general, a goal of the semi-empirical GC modeling approach is to develop the simplest model possible that describes the major features of adsorption as chemical conditions are varied over field-relevant ranges (Davis et al., 1998).

Ideally, spectroscopic data are available to constrain the possible choices of surface species. Based on the studies of Jove-Colon et al (2003), it can be assumed that U(VI) adsorbs primarily to aluminol edge sites and ferrinol sites located within the ubiquitous coatings found on mineral grains. XAS and FTIR spectroscopic studies have indicated that U(VI) forms strong, edge-sharing, bidentate bonds with the surfaces of iron oxides and that the attached uranyl cation forms ternary surface complexes with carbonate anions (Bargar et al., 2000). At least nine monomeric U(VI) surface reactions are possible in a uranyl-carbonate-iron oxide system (Table

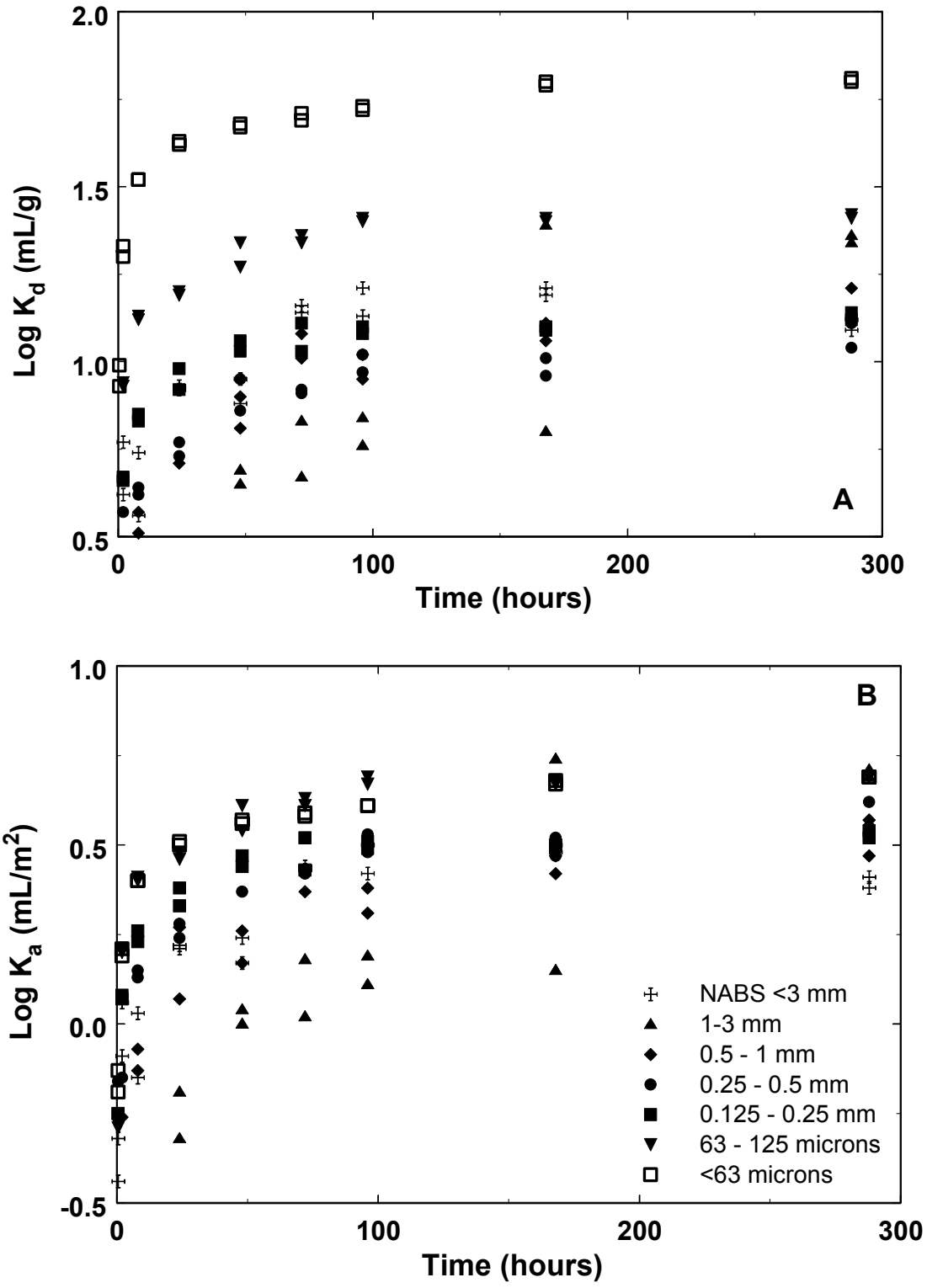

Figure 5.4 Kinetics of U(VI) adsorption by the NABS sample and grain size fractions in AGW-3 solutions equilibrated with air, containing 25 g/L of sediment and with 10^{-6}M U(VI) added to the experiment at time = 0; pH = 7.94. Part A) plotted as K_d (mL/g), and Part B) plotted as K_a (mL/m^2). Symbols are the same in Part A) and B).

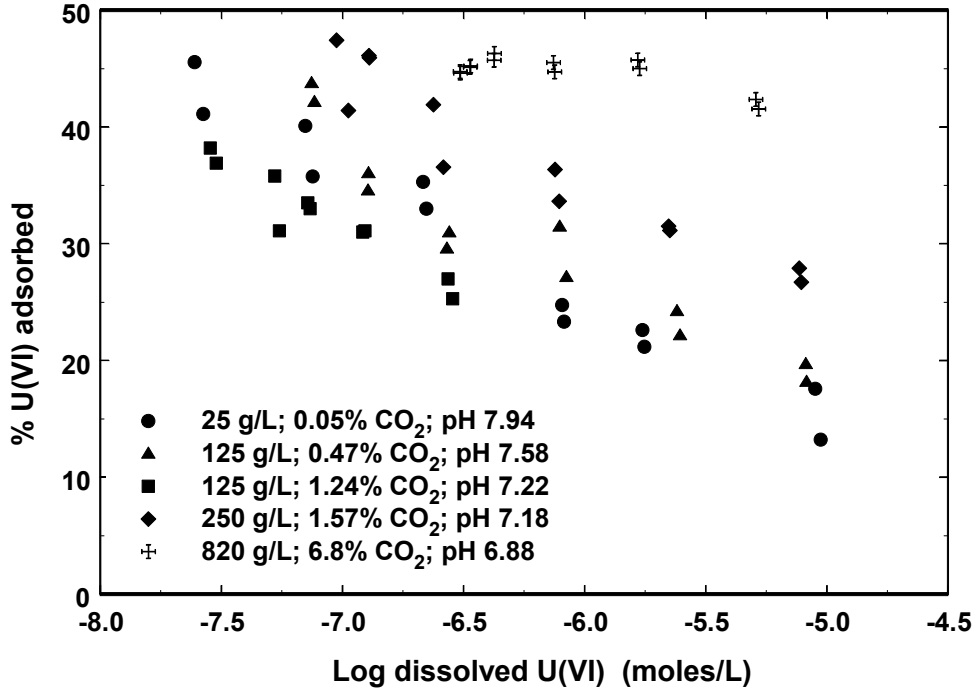

Figure 5.5 Fractional U(VI) adsorption on the <3 mm NABS composite sample as a function of the partial pressure of CO_2, pH, and solid/liquid ratio. Reaction time of 96 hr.

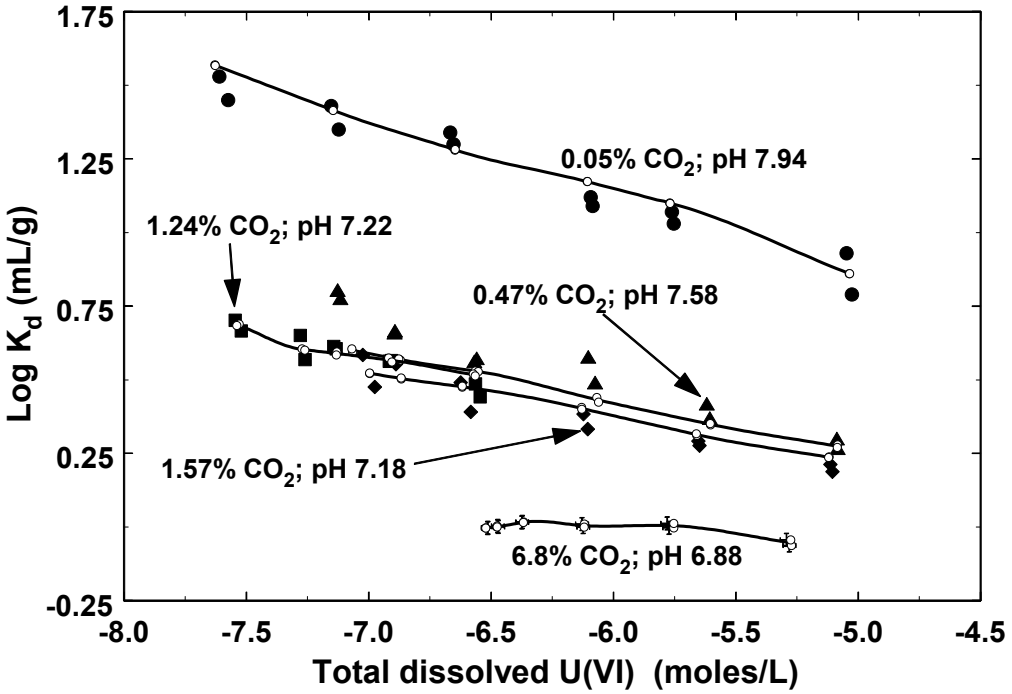

Figure 5.6 U(VI) adsorption on the <3 mm NABS composite sample as a function of the partial pressure of carbon dioxide, pH, and solid/liquid ratio expressed as log K_d values. Data points (shown as solid symbols) are the same as in Figure 5.5. Model simulations are shown as solid curves and small open symbols. These simulations did not consider the ternary aqueous U(VI) complexes, $CaUO_2(CO_3)_3^{2-}$ and $Ca_2UO_2(CO_3)_3^0(aq)$.

Table 5.3 Surface Reactions Considered for the GC Surface Complexation Model

Number	Reaction
1	$SOH + UO_2^{2+} = SOUO_2^{+} + H^{+}$
2	$SOH + UO_2^{2+} = SOUOOH + 2H^{+}$
3	$SOH + UO_2^{2+} + H_2CO_3 = SOUO_2HCO_3 + 2H^{+}$
4	$SOH + UO_2^{2+} + H_2CO_3 = SOUO_2CO_3^{-} + 3H^{+}$
5	$SOH + UO_2^{2+} + H_2CO_3 = SOUO_2OHCO_3^{2-} + 4H^{+}$
6	$SOH + UO_2^{2+} + 2H_2CO_3 = SOUO_2(HCO_3)_2^{-} + 3H^{+}$
7	$SOH + UO_2^{2+} + 2H_2CO_3 = SOUO_2(CO_3HCO_3)^{2-} + 4H^{+}$
8	$SOH + UO_2^{2+} + 2H_2CO_3 = SOUO_2(CO_3)_2^{3-} + 5H^{+}$
9	$SOH + UO_2^{2+} + 2H_2CO_3 = SOUO_2OH(CO_3)_2^{4-} + 6H^{+}$

5.3). Other U(VI)surface ternary complexes are plausible in the Naturita sediments, including phosphate and silicate ternary complexes, but these were not considered because their existence has not yet been confirmed in model systems. Bargar et al. (2000) observed multimeric surface ternary complexes of U(VI) in the carbonate/hematite system, however, these were only present within a very narrow pH range (8-8.5) and at high adsorbed concentrations (>0.4 μmoles/m^2), and therefore, U(VI) multimeric surface species were not considered. Multimeric U(VI) surface complexes also seem unlikely in the pH range and U(VI) adsorption density for Naturita sediments in this study, given that the trends observed as a function of U(VI) concentration in quartz, ferrihydrite, and hematite systems did not indicate multimeric surface complexes (Bargar et al., 2000; Davis et al., 2003; Davis, 2001). Because of the excess of surface sites over adsorbing U(VI), combined with the assumption of a non-electrostatic model, ionization reactions of the surface hydroxyl groups do not need to be considered (Davis et al., 1998). The U(VI) aqueous chemical species considered in the modeling are given in Table 2-1, with the exception that one separate set of calculations was done including the new ternary aqueous U(VI) complexes, $CaUO_2(CO_3)_3^{2-}$ and $Ca_2UO_2(CO_3)_3^{0}$(aq) (Brooks et al., 2003).

Initially it was assumed that strong sites were equal to 0.1% of the total sites. FITEQL calculations were completed to determine which single reaction (Table 5.3) would provide the best fit to the experimental data with a 2-site model. FITEQL output includes a goodness-of-fit parameter, WSOS/DF, the weighted sum of squares of the difference in value between model simulations and experimental data points, divided by the degrees of freedom (Herbelin and Westall, 1999). Lower values of WSOS/DF mean the proposed model is a better fit to the data; WSOS/DF will be referred to as "fit" below.

Representing the U(VI) adsorption data with a single reaction produced a reasonably good fit, with the best fit provided by reaction 1 (fit = 3.8). The second step in model development was to consider combinations of two reactions to represent the data. The fit to the data was improved with a second reaction, with the best combinations being reactions 1 and 2 (fit = 2.43) and 1 and 5 (fit = 2.38). However, testing showed that the results were dependent on the assumed site density for strong sites. Further testing of the ten best reactions pairs (fit at a strong site density of 0.1% of total sites) yielded an interim best fit result using reactions 2 and 4, with a strong site density of 0.02% of total sites (fit = 1.79).

The next step in the model development was a test of whether the fit to the data was improved more by adding a third site type of a third U(VI) surface reaction to the model. No improvement to the fit could be achieved by adding a third surface reaction to the model. However, the fit to the data could be improved by adding a third site type. In the final model (shown as solid

curves in Figure 5.6), reactions 2 and 4 were used with very strong sites (0.01% of the total) and strong sites (1.2% of the total), resulting in a fit of 1.51. Although there were two reactions (2 and 4) and three site types, yielding six possible U(VI) surface reactions, only four reactions were used in the model. Including reaction 2 with strong sites or reaction 4 with weak sites did not improve the fit to the data, and these reactions were not used. The final model included all aqueous reactions plus the surface reactions given in Table 5.4.

For simplicity, the reactions shown in Tables 5.3 and 5.4 are written as monodentate bonds with the surface. Because spectroscopic results show that the uranyl cation forms a bidentate bond at the surface with surface-coordinated oxygen atoms (Bargar et al., 2000), all monodentate model calculations were performed with a site density equal to 50% of the total surface hydroxyl groups, i.e., 1.92 μmoles/m^2. The reactions can also be written to form bidentate bonds (Davis et al., 2002). Use of the lower total site density affects the stability constants for the surface reactions (Table 5.4), but has a negligible effect on the goodness-of-fit to the experimental data or the choice of surface species (Davis et al., 2003).

The final model describes the batch U(VI) adsorption data quite well (Fig. 5.6), but also does an excellent job of predicting K_d values for adsorbed U(VI) on U-contaminated Naturita sediments (Sections 6 and 7). In addition, it does a good job of predicting the transport of U(VI) in the Naturita alluvial aquifer (Sections 9 and 10).

5.3.4 GC Model for U(VI) Adsorption with the Ternary U(VI) Aqueous Species

A similar procedure was followed to fit the data in which the new aqueous ternary U(VI) species, $CaUO_2(CO_3)_3^{2-}$ and $Ca_2UO_2(CO_3)_3^0$(aq), were included in the modeling calculations. As was shown in Figure 2-4 (in comparison to Fig. 2-2A), inclusion of these species has a significant effect on the calculated aqueous speciation of U(VI).

In this case, the fit to the data with two reactions showed that the best combinations were reactions 1 and 2 (fit = 6.1) or 8 and 9 (fit = 12.4). In the final model with the new ternary aqueous U(VI) species included (shown in Figure 5.7), reactions 1 and 2 were used with three site types: very strong sites (0.01% of the total – an assumed value), and strong sites (0.1% of the total – optimized value), resulting in a fit of 4.5. The GC model parameters for this case are given in Table 5.5. The reaction pairs 7 and 9 (final fit = 10.2) or 8 and 9 (final fit = 11.1) could have been chosen because these surface species are more consistent with spectroscopic data on hematite surfaces (Bargar et al., 2000). However, the reaction pair 1 and 2 was chosen as the final model because of its superior fit to the data. The results demonstrate how surface complexation model parameters are dependent on the quality of the thermodynamic data for aqueous species. More details on this modeling case (with the ternary aqueous U(VI) complexes included) are presented in Davis et al. (2003).

5.4 Discussion

Applications of the surface complexation concept to adsorption by soils and sediments are relatively rare due to the complexity of natural systems. Some examples include Turner et al. (1996), Zachara et al. (1995), Stollenwerk (1995), Davis et al. (2002, 1998), and Arnold et al. (2001). The surface properties of soil and sediment grains are significantly altered by accumulation of poorly crystalline phases of iron(III) and aluminum oxyhydroxides and silicates (Jove-Colon et al., 2003; Penn et al. 2000, Padmanabhan and Mermut, 1996; Coston et al., 1995). For surface complexation modeling, the principal difficulties posed by the coatings are that the identity, structure, composition, and electrical double layer properties of the surface are not easily determined (Davis et al., 1998).

A problem with the CA modeling approach is that model parameters for metal ion adsorption on reference minerals have generally been determined with models that correct mass action equations for coulombic effects in pure systems.

Table 5.4 Generalized Composite Surface Complexation Model for the NABS Sample[2]

Reaction[1]	Symbol	Log K (I = 0)
$UO_2^{+2} + >WOH + H_2O = >WOUO_2OH + 2H^+$	K_W	-6.74
$UO_2^{+2} + >SOH + H_2CO_3 = >SOUO_2CO_3^- + 3H^+$	K_{SC}	-8.00
$UO_2^{+2} + >SSOH + H_2O = >SSOUO_2OH + 2H^+$	K_{SS}	-2.06
$UO_2^{+2} + >SSOH + H_2CO_3 = >SSOUO_2CO_3^- + 3H^+$	K_{SSC}	-6.36

[1] WOH refers to weak sites, SOH to strong sites, and SSOH to very strong sites.
[2] Consistent with a total site density of 1.92 μmoles/m^2 of surface area and for calculations without the ternary aqueous U(VI) species, $CaUO_2(CO_3)_3^{2-}$ and $Ca_2UO_2(CO_3)_3^0$(aq).

At present, there are no methods available for determining the appropriate EDL model parameters to use in describing the surfaces of a complex mixture of phases, such as sediments. It is known that the surface charge of mineral phases in natural waters is very different from that observed in simple electrolyte solutions. For example, the adsorption of major ions in natural waters (e.g., Mg^{2+}, Ca^{2+}, CO_3^{2-}, and silicate) and the formation of organic coatings are known to cause large changes in the point-of-zero-charge (pH_{PZC}) and isoelectric point (pH_{IEP}) of mineral phases (Davis and Kent, 1990). CA modeling predictions for U(VI) adsorption on the Naturita sediments are presented and compared with GC modeling results in Davis et al. (2003).

In contrast to the CA modeling approach, GC modeling is generally applied with a non-electrostatic model (NEM), which considers surface equilibria strictly as chemical reactions, without explicit correction for electrostatic attraction or repulsion (Davis et al., 1998). In the NEM, the pH-dependent coulombic energy contribution to the mass action equation is included within the apparent binding constant. One can derive the apparent binding constants and stoichiometry of the mass action equations by fitting the *macroscopic* dependence of adsorption as a function of pH. As a consequence, the mass action equations that describe adsorption in an NEM are not expected to provide accurate representations of the stoichiometry of the reactions *at the molecular scale*, however, the surface reactions can still be coupled with aqueous speciation models to provide accurate simulations of macroscopic adsorption. Interestingly, Sanpawanitchakit (2002) had success in applying a CA non-electrostatic approach to a carbonate-free sample of the Naturita sediments.

The GC modeling approach has been applied in relatively few instances in the literature (Davis et al., 2002; Davis et al., 1998; Bradbury and Baeyens, 1997), but because of its simplicity, this approach may be the most appropriate for risk assessment modeling of sites with adsorbing inorganic contaminants (Kent et al., 2000).

Our current understanding of ion adsorption is well advanced at the molecular level in clean mineral suspensions, but our knowledge and adsorption modeling become increasingly uncertain as the physical scale increases. The inherent heterogeneity of environmental systems makes application of the truly mechanistic adsorption models difficult. In the authors' opinion, however, the current operational paradigm that employs constant distribution coefficients to describe radionuclide retardation introduces more uncertainty than is necessary and the approach ignores our well-developed knowledge of aqueous speciation and thermodynamics. (This is not universally true for all radionuclides; K_d values may work well for ions that have simple aqueous speciation, such as cesium and strontium). In many cases, where there is either temporal or spatial variation in chemical conditions, the uncertainty in simulated retardation could be reduced with

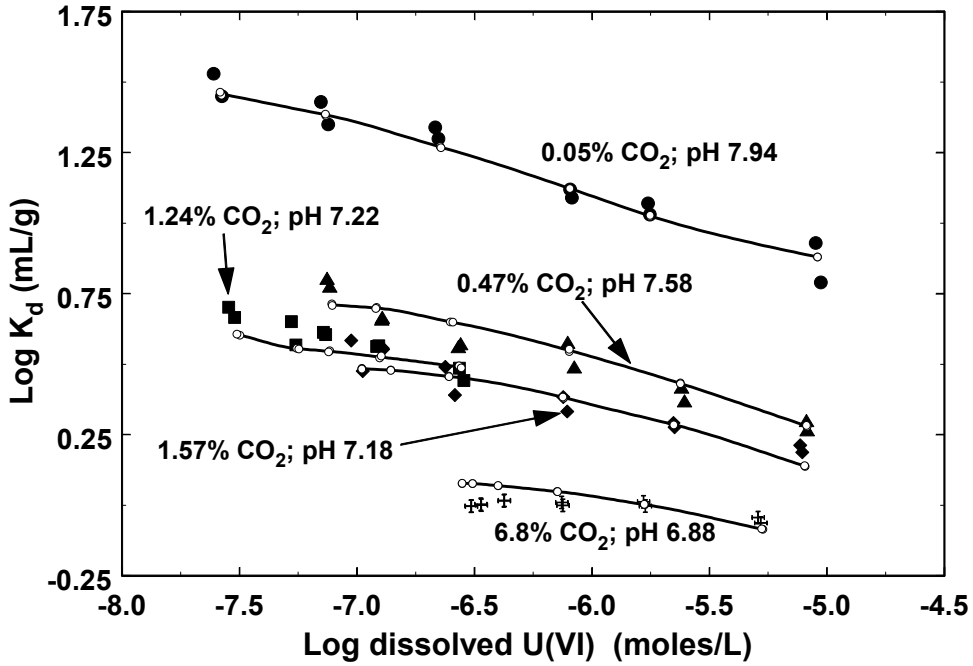

Figure 5.7. U(VI) adsorption on the <3mm NABS composite sample as a function of the partial pressure of carbon dioxide, pH, and solid/liquid ratio expressed as log K_d values. Experimental data points (shown as solid symbols) are the same as in Figure 5.5. Generalized Composite SCM simulations are shown as solid curves drawn through small open symbols and included the formation of the ternary aqueous U(VI) complexes, $CaUO_2(CO_3)_3^{2-}$ and $Ca_2UO_2(CO_3)_3^0$(aq).

Table 5.5 Generalized Composite Surface Complexation Model for the NABS Sample[2]

U(VI) Surface Reaction [1]	Log K (I=0)
$SSOH + UO_2^{2+} = SOUO_2^+ + H^+$	6.798
$SOH + UO_2^{2+} = SOUO_2^+ + H^+$	5.817
$WOH + UO_2^{2+} = SOUO_2^+ + H^+$	2.570
$SSOH + UO_2^{2+} + H_2O = SOUOOH + 2H^+$	-0.671
$SOH + UO_2^{2+} + H_2O = SOUOOH + 2H^+$	-2.082
$WOH + UO_2^{2+} + H_2O = SOUOOH + 2H^+$	-5.318

[1] WOH refers to weak sites, SOH to strong sites, and SSOH to very strong sites.
[2] Consistent with a total site density of 1.92 μmoles/m^2 of surface area and for calculations that included the ternary aqueous U(VI) species, $CaUO_2(CO_3)_3^{2-}$ and $Ca_2UO_2(CO_3)_3^0$(aq).

the use of semi-empirical site-binding models such as the GC model presented here.

The range of applicability of semi-empirical, site-binding models with respect to chemical variation is determined by the type and amount of experimental data collected. Thus, a greater emphasis needs to be placed on site-specific characterization of natural mineral assemblages and groundwater compositions expected to be encountered along major flowpaths away from nuclear repositories and other radionuclide sources to the environment. Laboratory data collection for such studies should be focused on those radionuclides (and their parent isotopes) that are expected to be important contributors of dose in the far-field regime. From a practical point of view, the limiting factor in applying either type of modeling approach may be the knowledge of the spatial and temporal variation in aqueous chemical conditions and mineral surfaces exposed along flow paths in performance assessment scenarios.

5.5 Summary and Conclusions

Adsorption of U(VI) by the Naturita sediments is strongly influenced by the pCO_2 in equilibrium with the aqueous phase. Under conditions typical of the groundwater at the field site in Naturita (pCO_2 of 2-6%, pH 7), the K_d value for U(VI) adsorption is about ¾ to one order of magnitude less than that observed when for systems equilibrated with air. This illustrates the importance of pCO_2 in experiments designed to determine K_d values; most K_d values in the literature were determined in air (USEPA, 1999).

The complexity of natural systems makes it difficult to apply our detailed molecular scale knowledge of surface speciation on single mineral phases directly to the groundwater environment. A particular problem with the more complex SCM is that the predicted adsorption can be quite sensitive to the electrical charge and potential calculated for the mineral/water interface. Our knowledge of the electrical double layer at sediment surfaces is poor, given the common occurrence of micron-thick coatings of secondary mineral phases and resistant organic materials. Another problem is that the surface composition is usually not well known in terms of mineralogical composition or surface functional groups.

Despite these complexities, the GC modeling approach allows simple relationships to be derived that couple the change in U(VI) adsorption with variation in U(VI) aqueous speciation. These relationships, written as chemical mass law equations, can be readily incorporated with reactive solute transport models. GC model parameters are derived as semi-empirical constants, calibrated by fitting a simple surface speciation model such that the major features of radionuclide adsorption are simulated as chemical conditions are varied over field-relevant ranges. The GC approach should not be extrapolated to conditions outside of the range for which adsorption data were collected for model calibration (Davis et al., 1998). However, a GC model can be used for predictive calculations that interpolate within the range of chemical conditions studied.

The GC modeling approach may be an important compromise modeling approach between the simple constant K_d approach and the most complex of SCM models. In order to be applied by solute transport modelers and within PA applications, the complexity of the adsorption model needs to be balanced with the goal of using the simplest model possible that is consistent with observed data. Historically, solute transport modelers have lacked the necessary expertise to apply the SCM modeling approach and many have believed that the SCM approach is too complex to be applied. As will be demonstrated in Sections 9-11, the GC modeling approach can be more easily applied, and as was demonstrated in this section, it does not require a burdensome program of data collection.

6 METHODS FOR ESTIMATING ADSORBED URANIUM(VI) AND DISTRIBUTION COEFFICIENTS IN CONTAMINATED SEDIMENTS

6.1 Introduction

Uranium (U) ore processing on the Colorado Plateau resulted in a number of inactive mill tailing sites at which there is contamination of groundwater near rivers (USDOE, 1996). At the UMTRA site in southwestern Colorado (Fig. 3.1), U and vanadium (V) ores were processed between 1939 and the early 1980's (USDOE, 1995). Remediation removed contaminated soil in the vadose zone below where the tailings and mill yard were located. The contaminants of major concern were U, V, and the decay products of the natural U isotopes, especially ^{226}Ra. Uranium contamination still exists in the alluvial aquifer at the site (see Section 3).

A critical aspect of risk assessment and remediation studies at many U-contaminated sites is estimating the migration of U(VI) in groundwaters (e.g. Prikryl et al., 1997; Biehler and Falck, 1999; Bain et al., 2001). In model simulations, retardation of U(VI) is often estimated based on a distribution coefficient, K_d, or a range of K_d values that is meant to describe the partitioning of U(VI) between the solid and aqueous phases. In practice, K_d values are generally chosen from literature values or calculated from the results of simple laboratory batch experiments with materials from contaminated sites, single mineral phases, mineral mixtures, crushed rock materials or on studies/observations at other U-contaminated sites. However, Lienert et al. (1994) pointed out that great care should be taken when laboratory K_d values are used to estimate in-situ field K_d values. Based on the retarded appearance of a U(VI) pulse in a well at a distance of 5 m from a river, these authors estimated a K_d value of 7±2.5 mL/g. This value is much smaller than K_d values generally obtained in laboratory experiments on mineralogical constituents of the aquifer material (quartz, calcite, K-feldspars, illite and chlorite) (USEPA, 1999; Davis, 2001).

U(VI) is relatively weakly adsorbed compared to many metal contaminants, and it forms strong aqueous complexes with carbonate. K_d values, especially those for U(VI), are dependent on geochemical conditions in aquifers, which can vary temporally and spatially. Numerous batch adsorption studies on natural and synthetic materials have demonstrated the dependence of U(VI) adsorption on pH and the concentrations of complexing ligands (e.g., carbonate) (Hsi and Langmuir, 1985; Tripathi, 1983; Waite et al., 1994; Davis et al., 2002; Arnold et al., 2001, and see Section 5). A significant problem is that many batch experiments performed in the laboratory for K_d values were equilibrated in air, and thus did not account for the fact that the partial pressure of carbon dioxide gas (pCO_2) can be as high as 5-10% in aquifers (Hem, 1985). In addition, pCO_2 may vary seasonally within aquifers (von Gunten et al., 1991; Lienert et al., 1994). Simulations with a constant K_d can, therefore, introduce considerable uncertainty into risk assessment or evaluation of remediation alternatives.

Many researchers have, over the last two decades, pointed out the limitations or inadequacies of a constant K_d approach for transport modeling (Reardon, 1981; Bethke and Brady, 2000; Koretsky, 2000). More recent transport simulations take advantage of multicomponent reactive transport models, which take the aqueous chemical speciation into account (Stollenwerk, 1995 and 1998; Gabriel et al., 1998). Surface complexation models (SCM) have provided an approach to describe the adsorption processes (through well defined stoichiometric reactions) of species of interest, rather than the simple distribution between the aqueous and solid phases (Gabriel et al., 1998; Davis and Kent, 1990). This process-oriented approach to adsorption and transport modeling better reflects the dynamic behavior of a complex aquifer system (Kohler et al., 1996; Meeussen et al., 1999; Papini et al., 1999). Thus, in addition to hydrogeological parameters, a detailed knowledge of geochemical conditions at a contaminated site is required to make accurate transport simulations in groundwater.

One important initial condition in predictive transport simulations for contaminated groundwater sites is the mass of metal contaminants associated with the soils or sediments. Several experimental studies have been conducted to evaluate the extent to which U(VI) is associated with soils. Payne and Waite (1991) determined "accessible" U in rock samples from two U ore deposits in Australia by equilibrating crushed rock materials with a synthetic groundwater, which was spiked with the isotope $^{236}U(VI)$. Approximately 20 to 25% of the total U content of the rocks participated in the isotopic exchange process with aqueous U(VI) for a time scale of days. When extracted with Tamm's acid oxalate solution, extractable U was close in value to the labile U(VI) fraction determined by isotopic exchange. Because only a small amount of U(VI) was exchangeable in NH_4Cl solutions, the authors concluded that the isotopically exchangeable U(VI) was mostly bound to the mineral surfaces by specific adsorption rather than ion exchange.

Mason et al. (1997) leached U-contaminated soils from the Fernald Environmental Management Project (FEMP) with carbonate solutions of various concentrations and pH. They found that a 0.5 M sodium bicarbonate solution was an efficient extractant for U. The amount of U released corresponded approximately to the amount of U(VI) present in the soil. Furthermore, they showed that addition of sodium peroxide oxidized U(IV) in the soil and thus increased extractable U. FEMP soils contain calcite and the pH in the extracting solutions remained high (>8.3).

Gadelle et al. (2001) tested the efficiency of surfactants and bicarbonate (among other extractants) for the extraction of U(VI) adsorbed under laboratory conditions onto Oak Ridge soils. Bicarbonate was as efficient as the surfactants as long as the pH of the extracting solutions stayed high enough to stabilize the aqueous uranyl-carbonato complexes. In addition, the bicarbonate solution dissolved the least amount of iron (Fe) compared to other extractants.

None of the studies above was focused on developing experimental methods for quantifying initial U(VI) adsorption for predictive reactive solute transport modeling. In this section, we report on various methods that were evaluated to determine the labile fraction of U(VI) adsorbed on U-contaminated sediments collected at the Naturita UMTRA site. A method was developed to assess total exchangeable U(VI) by isotopic exchange and the results were compared to the quantities of U dissolved from the contaminated sediments by various extractants. *In-situ* K_d values for the sediments are estimated, and these are compared with K_d values obtained from a surface complexation model developed to describe U(VI) adsorption by the Naturita Aquifer Background Sediment (the NABS sample, see Section 5).

6.2 Methods and Materials

6.2.1 Materials

Experiments were conducted with sediments collected from the alluvial aquifer at the UMTRA site near Naturita, Colorado (see Section 3). The Naturita site is located in southwestern Colorado in Montrose County, about 3 km northwest of the town of Naturita, and on the west bank of the San Miguel River (Figure 3.1). U contamination at the site has been observed primarily within an unconfined, shallow alluvial aquifer composed of sand, gravel, pebbles, and cobbles (see Sections 3 and 4).

Experiments were conducted with the NABS sample and with 16 samples of U-contaminated alluvial sediment. Collection and characteristics of the NABS sample are described in Sections 4 and 5. The U-contaminated sediments were collected from auger flights during the installation of USGS monitoring wells in October 1998 or with a hand auger at a few selected locations during 2000-2001 (Fig. 4.1). Sample NAT-25B was collected in September 2000 with a hand auger at a location about 2 m from the monitoring well NAT-25. Both the U-contaminated sediments and the NABS sample were air-dried, dry sieved through a 3 mm nylon

mesh and stored at 4°C in the dark. Sample NAT-25J was collected in September 2001 with a hand auger at a location about 3 m from NAT-25 and 4 m from site NAT-25B. Sample NAT-25J was neither air-dried nor sieved and was used immediately in glove bag experiments as described below.

The major mineralogical components of the Natural alluvial sediments are quartz (40-50%), feldspars (20-30%), calcite (up to 10%), dolomite (a few %), and layer silicates (muscovite). For a detailed mineralogical description of the sediments the reader is referred to the work of Sanpawanichakit (2002), Jove-Colón et al., (2003), and see Section 4. A detailed mineralogical/elemental study on the micro- and nanometer scale on single grains from a carbonate free NABS sample and the NAT-06 and MAU-04 samples was performed by Jove-Colón et al. (2003). They used several X-ray diffraction and electron microscopy techniques (SEM-EDS, SIMS, HRTEM, μ-SXRF, μ-XANES, see Table of Symbols for definitions) and found illite/smectite layer silicates and Fe (oxy-) hydroxide coatings on the mineral grains. The BET surface areas of the sediments were measured on a Tristar Micromeritics system and are given in Table 4.3.

6.2.2 Methods

Hot concentrated nitric acid extractions. A small amount of <3 mm sample was ground in a mortar. One g was weighed into a 20 mL glass scintillation vial and 12 mL of concentrated nitric acid (HNO_3) were added. After evolving CO_2(g), the vials were covered with glass bulbs, put on a hot plate and kept at a temperature below boiling. After an extraction time of several days the samples were taken to dryness over a period of approximately two days. They were then taken up in 20 mL of 0.15M HNO_3, ultrasonicated, and left quiescent for a few days before filtering (0.45 μm). Finally, samples were diluted with milli-Q water and analyzed by ICP-AES for metals and by kinetic phosphorescence analysis (KPA) for U(VI).

Hydroxylamine-hydrochloride (HH) extractions at 50°C. 200 g of 0.25M $NH_2OH{\cdot}HCl$ in 0.25M HCl at 50°C were added to 10 g of <3 mm sediment in a 250 mL bottle and placed in a water bath at 50±2°C. The bottles were shaken occasionally. After 0.5, 1, 2, 4, 8, 24, 48 and 96 hr, 3 mL samples were withdrawn and filtered (0.45 μm). For ICP-AES measurements, filtrates were diluted with 0.15M HNO_3. For U(VI) measurements (KPA), aliquots of the filtrates were converted to the nitrate salts by repeated evaporation to dryness and taking up in concentrated nitric acid, with a final reconstitution and dilution of the solution in 0.15M HNO_3, suitable for KPA analysis.

Mildly alkaline sodium (bi)carbonate extractions in the laboratory. The solution used as an extractant was $1.44{\cdot}10^{-2}$M in $NaHCO_3$ and $2.8{\cdot}10^{-3}$M in Na_2CO_3, and is referred to as the CARB solution in this section. The calculated ionic strength of CARB was 0.022M, with a measured pH of 9.45±0.05, and an alkalinity was 20 meq/L. The extractions were carried out at room temperature. 200 g of CARB solution were added to 10 g of sediment in a 250 mL bottle that was put on a shaker. After settling, a 3 mL aliquot was filtered (0.45 μm), and an aliquot was diluted with 0.15M HNO_3 for analysis by KPA and ICP-AES. Data were collected as a function of time during the extractions, with sampling times ranging from 1 hr to 12-14 days. The extractions were performed in two series. In the first series of samples (samples NAT-03, 06, 08, 11, 12, MAU-02), the pH was allowed to drift without adjustment. The pH values dropped from 9.45 in the initial CARB solution to typically 8.8-9.0. In the most extreme case (sample NAT-06), the pH drifted down to pH 8.1. In this series, the samples were kept at room temperature without shaking for 2 months, after which the pH was readjusted to its initial value of 9.45 to check if additional U(VI) would be desorbed. The samples were shaken again for a period of two days, and dissolved U(VI) was measured at the beginning and end of the two-day period.

In the second series (the remaining sediment samples), the pH was monitored and readjusted

to 9.45 at each of the first five time points. For the sixth time point, the adjustment was made 2 days before sampling. Final pH values were between 9.40 and 9.47.

Mildly alkaline sodium (bi)carbonate extractions performed at the Naturita field site. Extractions with the CARB solution were also performed in the field on sediments obtained by hand auger at NAT-25J, located about 2 m southeast of well NAT-25 (Fig. 4.1). The sediment samples were collected immediately after drilling by pushing a 3 mL syringe (with a cut-off barrel) into the core. The syringe with the sediment was then wrapped with plastic saran and put in a glove bag, which was flushed with N_2 gas to create a non-oxidizing atmosphere that would stabilize any U(IV) associated with the sediment surfaces. The first mL from the syringe was used for a CARB extraction performed outside the glove bag in ambient air. A second mL was used for a CARB extraction inside the glove bag that was continuously flushed with nitrogen, and a third mL was saved for pore water analysis and CARB extraction under laboratory conditions as described above. Unlike the other sediment samples, this set of samples (NAT-25J) was not sieved to remove grains larger than 3 mm.

Artificial groundwater extractions. The sediment samples were extracted with an artificial groundwater solution, referred to as AGW-3 (see Section 5), which had a composition based on an average well water composition for well DOE-549, a well located near DOE-547 (Fig. 4.1). However, in order to conduct experiments equilibrated with the pCO_2 in air, the alkalinity (HCO_3^-) of the water had to be significantly reduced relative to DOE-549 water. In order to keep the ionic strength near 0.02M, $CaCl_2$ was added. The composition of AGW-3 was $NaHCO_3$ $5.38\cdot10^{-4}$M, KCl $6.4\cdot10^{-5}$M, Na_2SO_4 $9.38\cdot10^{-4}$M, $MgSO_4\cdot7H_2O$ $1.515\cdot10^{-3}$M, $CaCl_2$ $2.38\cdot10^{-3}$M, and $CaSO_4\cdot2H_2O$ $2.33\cdot10^{-3}$M. The calculated pH was 7.88 (for a pCO_2 of 373ppm) with an alkalinity of 0.538 meq/L, and the calculations show that the AGW-3 solution was near saturation with calcite.

Prior to contact with the sediment samples, the AGW-3 solution was first equilibrated with the NABS sediment sample for several days. The pre-equilibration step was performed to minimize subsequent pH changes during the extraction of the samples. In the course of the pre-equilibration step, AGW-3 acquired 1.2 to 2 μg/L of dissolved U(VI) from the NABS sample.

200 g of pretreated AGW-3 solution was mixed with 10 g of a sample in 250 mL bottles at room temperature. Bottles were placed on a shaker and equilibrated for up to three weeks. The pH stayed in the range 7.8 to 8.1 for most of the sample extractions; the pH in the extractions of samples MAU-04 and NAT-06 drifted down to 7.6. After settling (or in some cases centrifuging), a 3 mL aliquot was withdrawn and filtered (0.45μm). Aliquots of the filtrates were diluted with 0.15M HNO_3 for KPA and ICP-AES analyses. U(VI) concentrations in solution were converted to desorbed U per unit mass of dried solid after corrections for: 1) U(VI) introduced with pretreated AGW-3 and 2) U(VI) introduced by dried soil solution entrained by the sediments during sampling.
Desorption experiments in AGW-3 were conducted in two batches. Batch #1 included samples NAT-03, 06, 08, 11, 12 and MAU-02; Batch #2 included samples NAT-01, 02, 04, 05, 07, 10, MAU-01, 03 and MAU-04. After the desorption experiments, samples from Batch #2 were stored in a refrigerator for 4 months for later isotope exchange experiments (see below), whereas samples from Batch #1 were discarded. For isotope exchange experiments on samples from batch #1, a second set of extractions was conducted with AGW-3, and isotope exchange experiments were conducted immediately after an 18-day extraction period.

U(VI) isotopic exchange experiments. Isotope exchange experiments were conducted by spiking sediment/water suspensions with approximately $6\text{-}9\cdot10^{-9}$ M ^{233}U (30-45 dpm/mL) as uranyl nitrate. Bottles were shaken during the first two weeks of equilibration and then equilibrated for a sampling at 10 months by occasional shaking by hand. Sampling was performed after the bottles sat quiescent for 30

min and then acidifying and filtering an aliquot of supernatant (method 2 described below). Phase separation by this method was faster than centrifuging, and adding acid before filtering prevented adsorption of U(VI) to filters. The small amount of solid remaining in the acidified supernatant did not increase the aqueous U(VI) concentration solution more than the analytical uncertainty (3%). The phase separation method was tested by comparing with two other methods with 2 sediment samples: (1) filtration of the suspensions followed by acidification, (2) 30 min of settling, followed by withdrawal of an aliquot of supernatant, which was then acidified and filtered, and (3) centrifugation followed by acidification. Results from method 2) agreed within error with the values obtained by method 3). One extraction of one sample by method 1) was 3.5% lower than the average, slightly larger than the analytical uncertainty of 3%.

^{233}U alpha activity in the supernatant was measured for each sample by liquid scintillation counting, and total dissolved U(VI) was measured twice by KPA during each experiment. Alkalinities were measured at the end of the 10-month period.

We define the concentration of labile U (C_{labile}) in each experiment by:

$$C_{labile} = \frac{A_{System}}{A} \cdot C \qquad (6.1)$$

where C_{labile} is the concentration (moles/mL) of the labile U, A_{system} is the total ^{233}U activity (dpm/mL) in the system, A is the activity of dissolved ^{233}U (dpm/mL), and C (moles/mL) is the concentration of total dissolved U(VI) measured by KPA. C_{labile} was calculated for each experiment by measuring C and the ^{233}U activity, A. A_{System} was known from the initial addition of ^{233}U activity. Corrections were made for: 1) ^{233}U and U(VI) removed during sampling (at several points in time) in the course of the AGW-3 extraction and isotope exchange experiments, 2) the contribution of the ^{233}U tracer to the total U(VI) concentration, and 3) U(VI) in the pre-equilibrated AGW-3 solution (1.8 μg/L) at the beginning of the AGW-3 extraction, and 4) U(VI) derived from evaporated sediment pore water (0.25 mL pore water per g of sediment). For the latter correction, the actual U(VI) concentration in groundwater sampled from the well was used (Table 6.1). C_{labile} (moles/mL) can be converted to C^*_{labile} in moles/g of solid by multiplying by the liquid/solid ratio in each experiment, V/w (mL/g), where V is the volume (mL) and w is the sediment mass (g).

U(VI) adsorption on the NABS sample at atmospheric pCO_2 and low U(VI) concentrations. In batch adsorption experiments at low U(VI) concentrations, the small amount of background adsorbed U(VI) on the NABS sample, C^*_{labile} must be accounted for in the mass balance for U(VI) in the experiment (see Section 5). In order to determine C^*_{labile} on the NABS sample, adsorption experiments with the addition of ^{233}U isotope only were conducted. Variable masses of NABS sample were weighed into 50mL polycarbonate centrifuge tubes with screw caps. 25 mL of AGW-3 solution with a known amount of ^{233}U activity were added to each tube, the tubes were equilibrated for 7 to 9 days, the final pH of the suspensions was measured, and the tubes were centrifuged. Aliquots of supernatant were analyzed for ^{233}U activity, total dissolved U(VI), and some samples for alkalinity.

6.3 Results

6.3.1 Total U content of sediment samples determined by γ-spectrometry

The total U content of the <3 mm sediment fractions was quantified by non-destructive measurement of the 63 keV line of ^{234}Th in secular equilibrium with ^{238}U (Table 6.1). A value of 2.3 mg/kg ($9.6 \cdot 10^{-9}$moles/g) U was found for NABS, in good agreement with the range of values for U concentrations expected for uncontaminated sediment materials. The major mineralogical constituents of the sediments from the aquifer are quartz and feldspars, for which U concentrations of 1.7 and 2.7 mg/kg, respectively, are reported in Roger and Adams (1978). All other samples, with the exception of sample NAT-11, had higher U concentrations than the NABS sample.

Table 6.1 Uranium Extraction Results and Total Uranium by γ-Spectrometry (moles/g)

Sample [1]	Extraction Method				Total U [4]	U(VI) from Porewater [5]
	AGW-3	CARB	HH [3]	HNO_3conc. [3]		
NAT-01	$7.1\pm0.4\cdot10^{-9}$	$1.44\pm0.07\cdot10^{-8}$	$2.75\pm0.14\cdot10^{-8}$	$2.55\pm0.13\cdot10^{-8}$	$2.70\cdot10^{-8}$	$8.98\cdot10^{-10}$
NAT-02	$3.0\pm0.2\cdot10^{-9}$	$8.67\pm0.43\cdot10^{-9}$	$1.83\pm0.09\cdot10^{-8}$	$2.56\pm0.13\cdot10^{-8}$	$2.29\cdot10^{-8}$	$4.68\cdot10^{-10}$
NAT-03	$3.6\pm5.0\cdot10^{-10}$	$3.21\pm0.50\cdot10^{-9}$	$6.55\pm0.50\cdot10^{-9}$	$8.07\pm0.50\cdot10^{-9}$	$1.24\cdot10^{-8}$	$1.01\cdot10^{-9}$
NAT-04	$6.7\pm5.0\cdot10^{-10}$	$4.57\pm0.50\cdot10^{-9}$	$9.32\pm0.50\cdot10^{-9}$	$1.19\pm0.06\cdot10^{-8}$	$1.91\cdot10^{-8}$	$1.00\cdot10^{-9}$
NAT-05	$1.4\pm0.5\cdot10^{-9}$	$5.33\pm0.48\cdot10^{-9}$	$9.42\pm0.48\cdot10^{-9}$	$1.05\pm0.05\cdot10^{-8}$	$1.78\cdot10^{-8}$	$9.59\cdot10^{-10}$
NAT-06	$2.1\pm0.7\cdot10^{-9}$	$1.88\pm0.09\cdot10^{-8}$	$2.82\pm0.14\cdot10^{-8}$	$2.76\pm0.14\cdot10^{-8}$	$3.14\cdot10^{-8}$	$1.32\cdot10^{-9}$
NAT-07	$6.2\pm2.9\cdot10^{-10}$	$3.30\pm0.29\cdot10^{-9}$	$1.35\pm0.07\cdot10^{-8}$	$2.23\pm0.11\cdot10^{-8}$	$1.85\cdot10^{-8}$	$5.75\cdot10^{-10}$
NAT-08	$3.8\pm5.8\cdot10^{-10}$	$3.70\pm0.58\cdot10^{-9}$	$8.01\pm0.58\cdot10^{-9}$	$1.02\pm0.06\cdot10^{-8}$	$1.28\cdot10^{-8}$	$1.16\cdot10^{-9}$
NAT-10	$4.7\pm5.6\cdot10^{-10}$	$3.30\pm0.56\cdot10^{-9}$	$8.39\pm0.56\cdot10^{-9}$	$9.57\pm0.56\cdot10^{-9}$	$1.55\cdot10^{-8}$	$1.12\cdot10^{-9}$
NAT-11	$-0.9\pm6.4\cdot10^{-10}$	$2.29\pm0.64\cdot10^{-9}$	$5.09\pm0.64\cdot10^{-9}$	$7.33\pm0.64\cdot10^{-9}$	$1.03\cdot10^{-8}$	$1.27\cdot10^{-9}$
NAT-12	$2.1\pm0.6\cdot10^{-9}$	$5.51\pm0.58\cdot10^{-9}$	$9.17\pm0.58\cdot10^{-9}$	$1.05\pm0.06\cdot10^{-8}$	$1.34\cdot10^{-8}$	$1.17\cdot10^{-9}$
NAT-25B	$6.7\pm0.5\cdot10^{-9}$	$1.87\pm0.09\cdot10^{-8}$	$2.39\pm0.12\cdot10^{-8}$	$2.38\pm0.12\cdot10^{-8}$	$2.29\cdot10^{-8}$	$9.97\cdot10^{-10}$
MAU-01	$1.3\pm0.3\cdot10^{-9}$	$3.65\pm0.28\cdot10^{-9}$	$7.33\pm0.37\cdot10^{-9}$	$9.41\pm0.47\cdot10^{-9}$	$1.17\cdot10^{-8}$	$5.63\cdot10^{-10}$
MAU-02	$4.0\pm0.2\cdot10^{-9}$	$1.09\pm0.05\cdot10^{-8}$	$1.60\pm0.08\cdot10^{-8}$	$1.81\pm0.09\cdot10^{-8}$	$2.19\cdot10^{-8}$	$4.11\cdot10^{-10}$
MAU-03	$9.4\pm0.5\cdot10^{-9}$	$1.77\pm0.09\cdot10^{-8}$	$2.56\pm0.13\cdot10^{-8}$	$2.11\pm0.11\cdot10^{-8}$	$2.87\cdot10^{-8}$	$2.02\cdot10^{-10}$
MAU-04	$1.50\pm0.08\cdot10^{-8}$	$3.58\pm0.18\cdot10^{-8}$	$5.15\pm0.26\cdot10^{-8}$	$4.49\pm0.22\cdot10^{-8}$	$4.43\cdot10^{-8}$	$2.53\cdot10^{-10}$
NABS [2]	$2.46\pm0.12\cdot10^{-10}$	$8.74\pm0.44\cdot10^{-10}$	$2.12\pm0.11\cdot10^{-9}$	$3.54\pm0.18\cdot10^{-9}$	$9.64\cdot10^{-9}$	$6.30\cdot10^{-12}$

[1] Surface areas of samples are given in Table 4.3.
[2] HH extraction was 193 hr; CARB extraction was 3 weeks.
[3] Error estimated at 5%.
[4] From γ-spectroscopy, based on the 63 keV line of ^{234}Th. Estimated error 10%.
[5] The porewater correction is based on 0.25 mL water per g of dry solid.

6.3.2 Hot concentrated nitric acid extractions

A large fraction of the total U in each sample was released during extraction with hot concentrated nitric acid (Table 6.1). It would be expected that all adsorbed and surface-precipitated U would be dissolved by the extraction, but it is unknown to what extent the hot acid attacks the sediment matrix and dissolves U from the crystalline material. For samples NAT-01, -02, -06, -07, -25B, and MAU-04, the extracted U was the same as the total U within error. A straight line plot (not shown) of total U concentration versus U released by the hot HNO_3 extraction had a slope of 0.82±0.07, an intercept of $(6\pm1)\cdot10^{-9}$ moles/g, and a correlation coefficient (r^2) of 0.90.

6.3.3 Hydroxylamine-Hydrochloride extractions (HH)

The HH method is commonly used to estimate the amount of nanocrystalline, hydrous ferric oxide (HFO) that is present in sediment and soil samples. A 30 min treatment completely dissolves HFO, whereas crystalline minerals, such as goethite or hematite, are only dissolved slightly (Chao and Zhou, 1983; Coston et al., 1995; Fuller et al., 1996). The release of U from

the Naturita sediment samples during HH extractions at 50°C was essentially complete after approximately 8 hr. Dissolved Fe did not reach a maximum concentration in the extractions, even after 96 hr, reflecting the continuous dissolution of Fe-bearing minerals. However, dissolved V and Mn exhibited a trend like U, in that the release was essentially complete after a period of time, 8 and 24 hr for V and Mn, respectively.

U dissolved by the HH extractions was similar to that extracted by concentrated HNO_3 for many of the samples (Table 6.1), although some samples showed less extraction by HH. For samples MAU-03 and MAU-04, U extracted by HH was the same as total U within error. A plot (not shown) of total U concentration versus U released by the HH extraction had a slope of 0.72±0.04, an intercept of $(9\pm1)\cdot10^{-9}$ moles/g, and an r^2 of 0.95. No correlation was observed between extracted Fe and extracted U, V, or manganese (Mn). In addition, no correlation was observed between extracted Fe or U and the specific surface area of the sediment samples. Jove-Colón et al. (2003) found no clear association of U with Fe by SIMS analysis on the surfaces of individual grains selected from the NAT-06 and MAU-04 samples, which had the highest U extracted by HH. However, for a carbonate-free (acetic acid/sodium acetate treated) NABS sample onto which U(VI) was adsorbed in the laboratory, these authors found a good correlation of U(VI) with Fe on a single grain surface and confirmed the hexavalent oxidation state of adsorbed U.

6.3.4 Sodium (bi)carbonate extractions

The objective of the CARB extractions was to quantitatively desorb U(VI) from the sediment surfaces by strong aqueous complexation of U(VI) with carbonate with minimal dissolution of the crystalline matrix. Steady-state concentrations of dissolved U(VI) were achieved after 5 days of extraction with the CARB solution. Extracted U (in moles/g) is given in Table 6.1; errors caused by uncertainty in the porewater contribution was significant for some samples (e.g., 28% for sample NAT-11). During the first 2 days of extraction, the pH and Ca^{2+} concentration in the extract decreased, indicating that a small amount of calcite was likely precipitated. For all samples except NAT-06, the pH remained higher than 8.6 throughout the extraction and speciation calculations with HYDRAQL (Papelis et al., 1988) show that more than 96% of the dissolved U(VI) was present as $UO_2(CO_3)_3^{4-}$, which does not adsorb (Waite et al., 1994; Davis, 2001). For sample NAT-06, pH decreased during the extraction from 9.4 to 8.1 during the first 300 hr (Fig. 6.1). After 1850 hr of extraction for sample NAT-06, the pH was adjusted from 8.1 to 9.4. The pH adjustment had no measurable effect on the concentration of dissolved U(VI) (Fig. 6.1). Dissolved Ca decreased due to additional calcite precipitation (note the pH decreased again after the initial pH adjustment upward). Dissolved V increased after the adjustment of pH, suggesting that an anionic V species was incompletely desorbed. The fact that the extracted U did not change after the pH adjustment indicates that U(VI) desorption during the first 5 days of the extraction was complete.

Extractions with CARB solution are relatively mild compared to the concentrated nitric acid and HH extractions, and the CARB extractions were not expected to cause significant dissolution of the mineral matrices. A comparison of the total U concentration versus U extracted by the CARB solution is shown in Figure 6.2. Linear regression analysis gave a slope of 0.94±0.08, an intercept of $1.1\pm0.1\cdot10^{-8}$ moles/g, and an r^2 of 0.90. CARB extractions of the NABS sample yielded values of $5.7\cdot10^{-10}$ moles/g and $8.7\cdot10^{-10}$ moles/g for one and three weeks extraction times, respectively (Table 6.1). Later, another three-week extraction on duplicate samples gave a value of $7.1\pm0.4\cdot10^{-10}$mol/g (see Section 7). The y-axis intercept of the regression line (Fig. 6.2) yields a total U concentration very close to that of the NABS sample. This result may be interpreted to mean that the Naturita sediments have a "background" U concentration of about $1\cdot10^{-8}$ moles/g, and because the NABS sample had very little U dissolved by the CARB solution, most of the

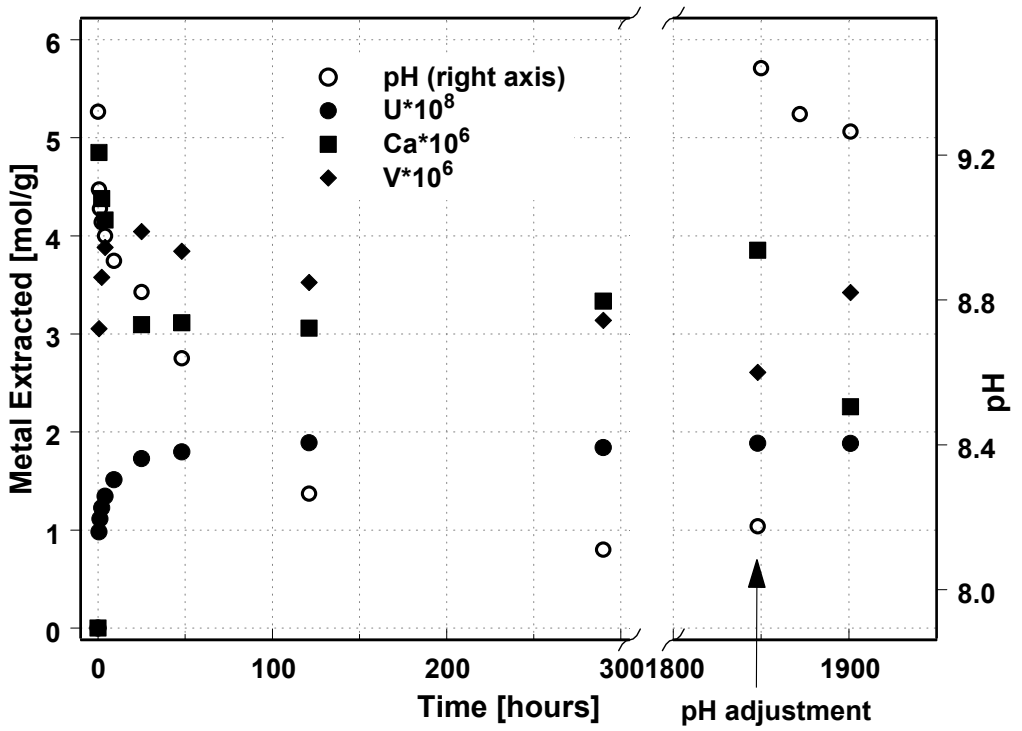

Figure 6.1 Evolution of chemical conditions with time in the sodium (bi)carbonate (CARB) extraction of the NAT-06 sediment sample.

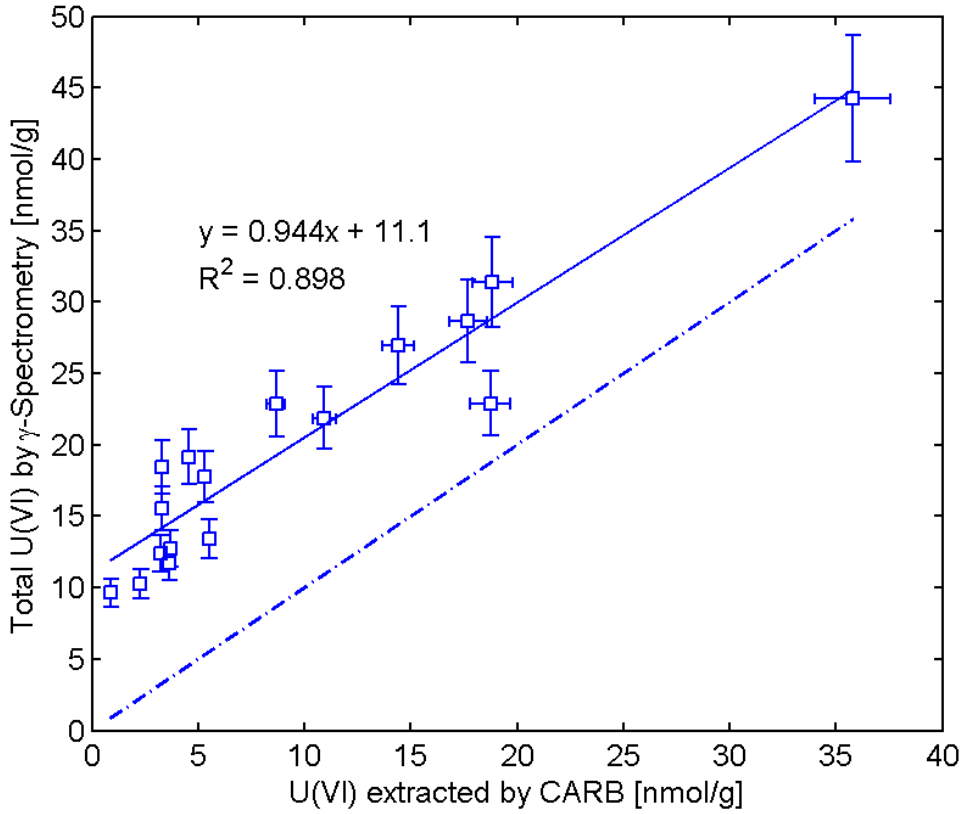

Figure 6.2 Relation between the total U concentrations in sediment samples determined by γ-spectroscopy and U extracted by the sodium (bi)carbonate solution (CARB).

"background" U can be assumed to be located within crystalline matrices. A fraction of the "background" U was dissolved in the concentrated nitric and HH extractions (Table 6.1).

6.3.5 Artificial groundwater solution extractions

Dissolved U(VI) concentrations increased rapidly over the first 48 to 96 hr of contact with AGW-3 solution. After that time, a steady slow release of U(VI) was observed for most samples. For some samples, the U(VI) released during the extraction by AGW-3 solution was equivalent to that expected from re-dissolution of U(VI) derived from evaporated porewater within experimental error (Table 6.1; samples NAT-03, -04, -08, -10 and -11). However, for cases with higher U content, e.g., samples NAT-01, -02, -05, -06, -07, -12, -25B, MAU-01, -02, -03 and -04, the increase in U(VI) concentration in the extract can clearly be attributed to U(VI) desorption from the sediments beyond that expected from re-dissolution of U(VI) in former porewater.

Comparing the values among the four extraction methods (Table 6.1), it is clear that the two hot acidic treatments were most efficient in dissolving U from the sediments as expected. However, the CARB extraction was also quite efficient, and for some of the samples, U extracted by the CARB solution approached the values obtained by the acidic treatments (e.g., samples NAT-06, NAT-25B, MAU-03 and MAU-04). This may be interpreted to mean that most of the contaminant U in these samples was present as sorbed U(VI) that could be easily desorbed with the CARB solution. As expected, the AGW-3 extractions released the least amount of U.

6.3.6 Isotopic exchange experiments

There were two objectives for the isotope exchange experiments: (1) obtain a K_d value for U(VI) adsorption in suspensions equilibrated with air, and (2) quantify the amount of isotopically exchangeable U(VI) in the U-contaminated samples, hereafter referred to as "labile U". Isotopic exchange was initiated at the end of the AGW-3 extractions, after dissolved U(VI) was approaching steady-state concentrations. Spiking a suspension near equilibrium with ^{233}U(VI) tracer and observing the activity of ^{233}U in aqueous solution over time is a method for determining a distribution ratio, R_d, for a contaminated sediment sample (Payne et al., 2001; Payne and Waite, 1991). If chemical equilibrium is achieved during the isotopic exchange experiment, R_d equals K_d. In the discussion below, we use only the term, K_d, although equilibrium may not have been achieved in all cases.

The quantity of isotopically exchangeable U(VI) in each experiment can be obtained from the mass balances for U(VI) and ^{233}U(VI). Because of the oxic conditions, it is assumed that no ^{233}U(VI) was reduced by the sediment surfaces and that no dissolved U(IV) was present. The amount of labile U in each experiment can be determined from Equation 1. The labile fraction of total U in each experiment includes all U atoms that participate in dynamic processes (sorption, desorption, precipitation, dissolution, oxidation, reduction) that achieve near equilibrium with the aqueous phase. Within the time scale of the experiment, ^{233}U(VI) tracer is distributed between the aqueous and sediment phases by these dynamic processes, and at isotopic equilibrium, it can be assumed that all U(VI) isotopes *in the labile fraction* are distributed in a similar manner.

The labile fraction of total U and U(VI) K_d values U were determined for each of the 15 U-contaminated sediment samples (except NAT-25B) and for the NABS sample (Figs. 6.3 and 6.4). Addition of the ^{233}U(VI) spike to the AGW-3 solution equilibrated with the sediment samples increased the total dissolved U(VI) concentration in the suspensions by 0.9% to 11.7%, with an average of 6.0±3.5%. Depending on the sediment sample, ^{233}U activity in solution decreased 30% to 80% from its initial value during the first 24 hr. In general, the approach to a near-constant ^{233}U activity in solution occurred on a similar time scale (several

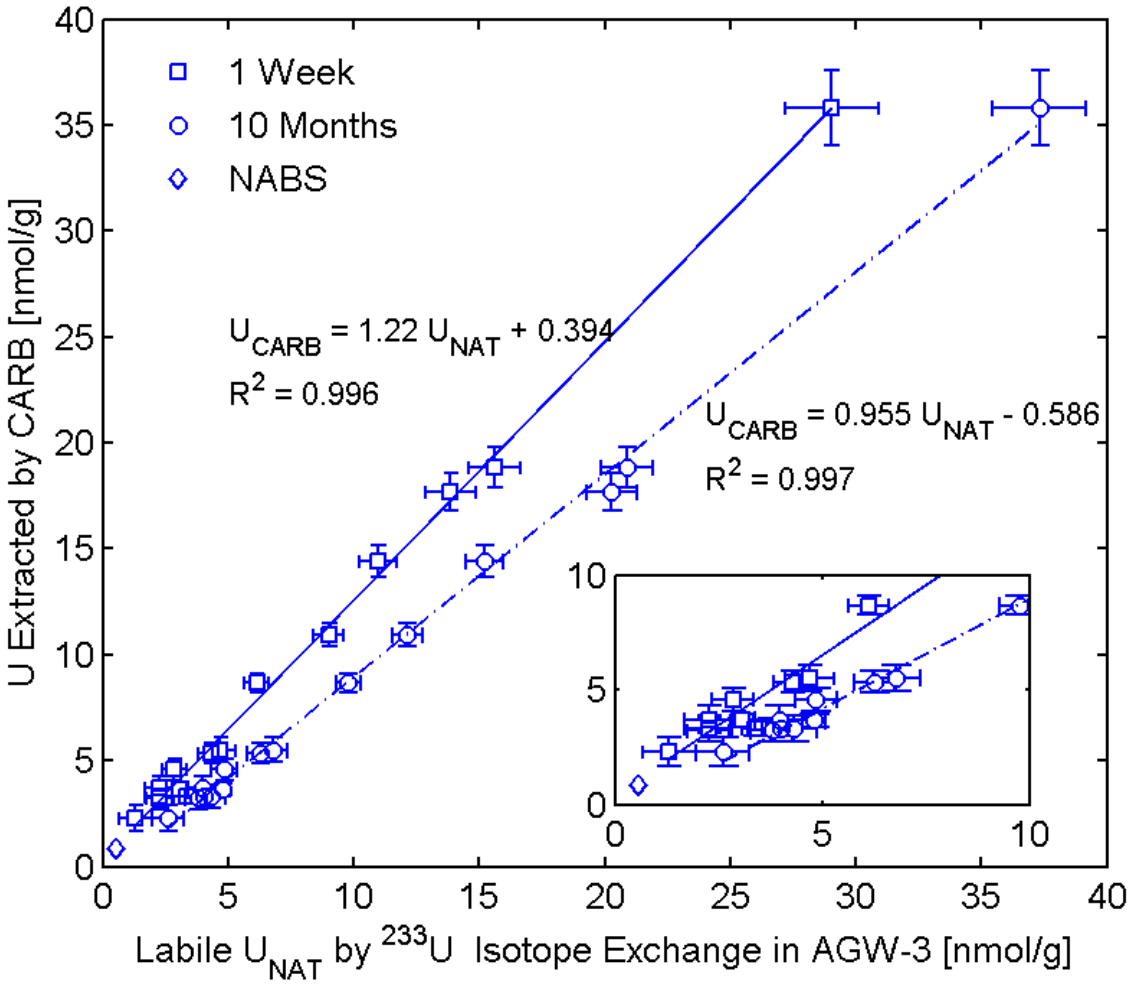

Figure 6.3 Relation between labile U(VI) determined by isotopic exchange measurements and U extracted by the CARB solution for 15 U-contaminated sediment samples and the NABS sample.

days) as U(VI) release in the AGW-3 and CARB extractions.

The total dissolved U(VI) concentrations increased very slowly with time during the isotopic exchange experiments. The change in total dissolved U(VI) after one week of isotopic exchange increased an average of 6.4% for all of the sediment samples. After approximately 10 months of isotopic exchange the total dissolved U(VI) concentration increased an average of 45% from the values after one week (range of 20% to 84%). During the 10-month period, the distribution of ^{233}U between the sediments and solution remained within 7% of its distribution after one week for 11 of the 15 U-contaminated samples.

For the NABS sample, the purpose of isotopic exchange experiments was to determine the concentration of labile U (background sorbed U(VI)) that would significantly affect the U(VI) mass balance in experiments at low U(VI) concentrations (see Section 5). Samples were equilibrated for 7-9 days. For this series of experiments, a plot of the labile U(VI) concentration (moles/mL) of a particular sample versus its solid/liquid ratio (g/mL) yielded a slope (equal to C^*_{labile}) of $5.57 \pm 0.22 \cdot 10^{-10}$ moles/g.

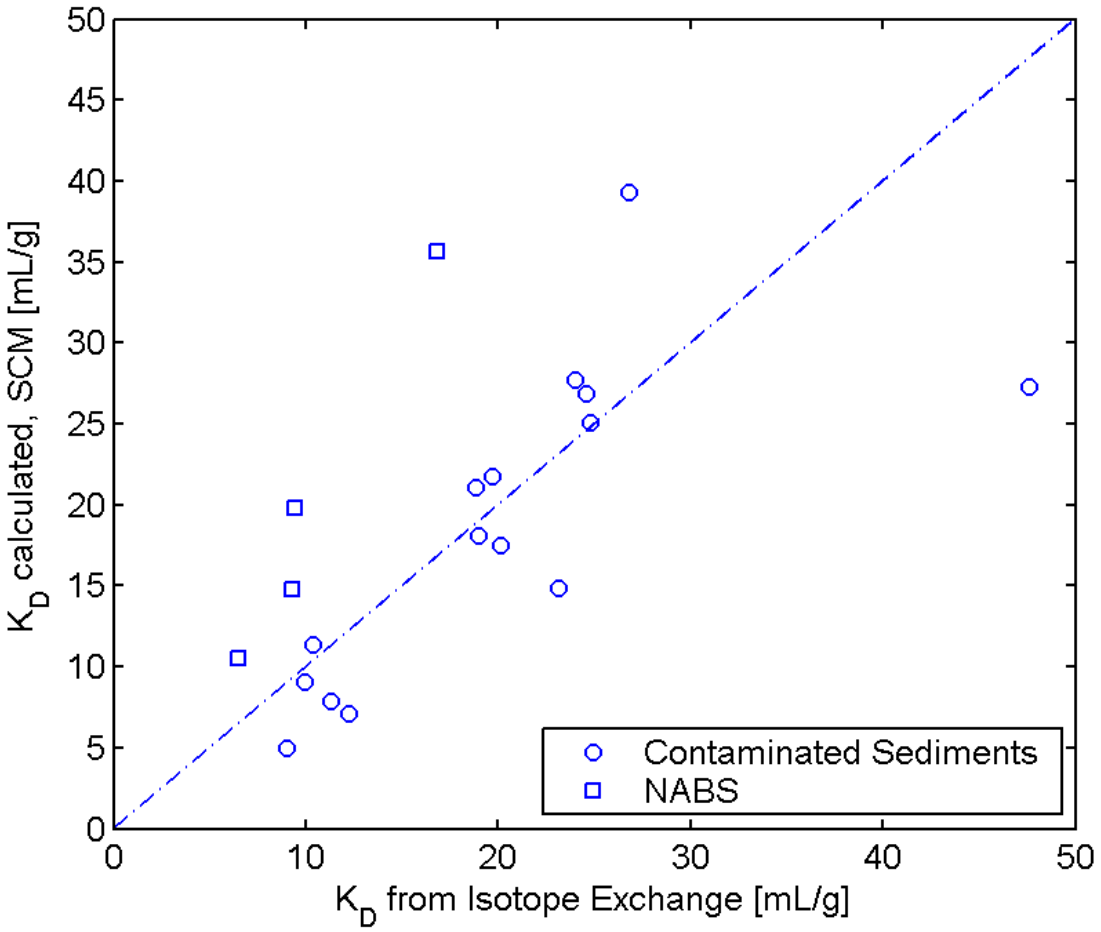

Figure 6.4 Comparison of K_d values for sediment samples determined by isotope exchange experiments and K_d values calculated from the SCM developed from U(VI) adsorption data with uncontaminated sediments (Section 5). Conditions: pH 7.9, equilibration with air.

6.3.7 Sodium (bi)carbonate extraction of the NAT-25J sample

An experiment was conducted in the field to determine if exposure to air influenced the amount of U being extracted by the CARB solution. A sub-sample of sample NAT-25J, was extracted under a continuously flowing atmosphere of nitrogen gas, and the results were compared to CARB extractions of other sub-samples after exposure to air in the field and several weeks later in the laboratory. Since the U-contaminated sediments extracted in the laboratory (described above) were air-dried, U(IV) on sediment surfaces could have been oxidized prior to extractions. If this occurred, U(VI) extracted by the CARB solution might be interpreted as desorption of U(VI) from the sediments, when in fact the U had been present as U(IV) in the subsurface prior to sampling. By performing the CARB extraction in the field under a nitrogen atmosphere, directly after sampling NAT-25J, oxidation of U(IV) would be minimized. U(IV) is highly insoluble, even in the presence of high carbonate concentrations HYDRAQL (Papelis et al., 1988) calculations indicate a solubility on the order of 10^{-8} M for U(IV) under CARB extraction conditions, assuming that $UO_{2(am)}$ is the controlling phase ($K_{s,0} = 10^{-4.15}$, Langmuir, 1997). Measured concentrations in the extracts were greater than $2 \cdot 10^{-7}$ M.

Table 6.2 shows the results for the extractions of sample NAT-25J. In general, the results for the N_2(g)-headspace extractions agreed well with

Table 6.2. Results of sodium (bi)carbonate (CARB) extractions of the fresh sediment sample, NAT-25J.

Sample #	U extracted in the field Atmosphere		Lab extracted
	N_2-headspace [1)]	Air-headspace [1)]	Air-dried
	moles/g	moles/g	moles/g
1	$4.84 \cdot 10^{-9}$	$3.82 \cdot 10^{-9}$	$3.92 \cdot 10^{-9}$
2	$4.46 \cdot 10^{-9}$	$4.84 \cdot 10^{-9}$	$4.31 \cdot 10^{-9}$
3	$9.89 \cdot 10^{-9}$	$3.89 \cdot 10^{-9}$	$7.43 \cdot 10^{-9}$
4	$3.30 \cdot 10^{-9}$	$3.97 \cdot 10^{-9}$	$3.19 \cdot 10^{-9}$
5	$4.96 \cdot 10^{-9}$	$7.34 \cdot 10^{-9}$	$4.10 \cdot 10^{-9}$
6	N/A [2)]	N/A [2)]	$4.59 \cdot 10^{-9}$

[1)] See text.
[2)] Not analyzed.

the extractions conducted in the laboratory after air-drying. Out of 5 samples tested in the field, one air-headspace extract had a significantly higher dissolved U(VI) concentration than the corresponding N_2(g)-headspace extract, suggesting possible oxidation of U(IV) on the sediment, but this higher value was not corroborated by laboratory extraction of the air-dried sample. One of the air-headspace field samples was approximately half of the corresponding N_2(g)-headspace value, but again the air-headspace field value was not corroborated by the laboratory air-dried extraction (Table 6.2). The variation in U extracted with the CARB solution in the experiment are likely due to sample inhomogeneities, and this might be expected because the samples were not air-dried, sieved, and mixed as a composite like the other samples. Despite the variability in U extracted, the comparison of air-headspace and N_2(g)-headspace extractions suggests that the U extracted was predominantly present as U(VI) on the NAT-25J sample. However, as this test was only performed on one sample, the presence of U(IV) in the subsurface cannot be ruled out at other locations at Naturita. In September 2001, water sampled from well NAT-25 had a dissolved Fe(II) concentration (measured in the field) of 0.05 mg/L and dissolved oxygen was 0.08 mg/L. However, these conditions were not typical for NAT-25. Over a two-year period prior to sampling, values for dissolved Fe(II) ranged between 0.35 and 1.1 mg/L and for dissolved oxygen between 0.19 and 0.83 mg/L, conditions typical of many wells throughout the alluvial aquifer at Naturita, which consistently exhibits these mildly reducing conditions (see Section 3). Dissolved oxygen in recharging river water is depleted in groundwater within a short distance from the river, but conditions do not become more reducing with distance downgradient. A few wells have Fe(II) concentrations approaching 2 mg/L, e.g., 1-2 mg/L at MAU-02 and MAU-04, but most are less than 500 μg/L (see Section 3).

The U(VI) extracted from NAT-25B sediments by the CARB solution was approximately 3.7 times larger than that extracted from the NAT-25J samples, even though the samples were collected at the same depth at locations only 5 m apart. One reason for this difference in extracted U(VI) may have been caused by temporally variable chemical conditions at the NAT-25 well. In June 2000, when the NAT-25B sample

was collected, the groundwater at well NAT-25 had a dissolved U(VI) concentration of 1840 μg/L (7.7 μM) and an alkalinity of 10.3 meq/L. In contrast, in September 2001 when the NAT-25J sample was collected, the U(VI) concentration was 920 μg/L (3.9 μM) and the alkalinity was 8.8 meq/L. Speciation calculations using the SCM from Section 5 show that the variable chemical conditions may account for 50% of the observed difference in extracted U(VI). In addition, the two samples may have had different surface areas.

6.4 Discussion

One objective of the experiments was to determine whether U(VI) adsorption on the U-contaminated sediments could be characterized and compared with U(VI) adsorption measurements on uncontaminated Naturita sediment (see Section 5). The isotopic exchange experiments provide a means of determining the K_d values of the contaminated Naturita sediment samples under a relatively uniform set of conditions: equilibration with AGW-3 and in equilibrium with the pCO_2 in air. In addition, the labile fraction of sediment U(VI) can be compared with the sediment extraction results to determine if any of the methods provides a good estimate for sorbed U(VI) on U-contaminated sediments. Furthermore, if U(VI) adsorption on the contaminated sediments can be quantified, then it is possible using the dissolved U(VI) concentrations at the wells to calculate *in-situ* K_d values for the alluvial aquifer. Payne et al. (2001) used Tamm's acid oxalate extractions to measure accessible U and determined *in situ* K_d values at the Koongarra U deposit in Northern Australia. These authors also confirmed the fraction of labile U(VI) by isotopic exchange methods.

6.4.1 Comparison of U(VI) K_d values at atmospheric pCO_2

Use of the ^{233}U tracer in the isotopic exchange experiments allows a direct determination of the K_d value for each sediment sample. The following equation holds:

$$K_d = C_s/C \qquad (6.2)$$

where C_s is the concentration of sorbed U(VI) on the sediment in moles/g, C is the dissolved U(VI) concentration in moles/mL, and K_d has the units mL/g. K_d can be determined solely by ^{233}U activity measurements according to equation (6.3):

$$K_D = \frac{V}{w} \cdot \left(\frac{C_{labile}}{C} - 1 \right) = \frac{V}{w} \cdot \left(\frac{A_{System}}{A} - 1 \right) \qquad (6.3)$$

where V/w is the solution to solid ratio of the system in mL/g and the other parameters are as defined above (Eq 6.1). It is important to note that C_{labile} only refers to the labile fraction of U(VI) that participates in isotope exchange processes and does not include U fixed in the mineral matrix.

K_d values for the contaminated sediment samples ranged from 9 to 27 mL/g (with the exception of sample NAT-06, 48 mL/g). Possible causes for the range in K_d values are variations in the specific surface area and surface mineralogy of each sample and variations in alkalinity and total U(VI) concentration in each experiment. At a particular pH, increasing alkalinity stabilizes the aqueous uranyl-carbonate complexes and thus reduces K_d values (Davis et al., 2002), whereas increasing specific surface area is assumed to increase K_d values. In the discussion below it will be shown that the observed range in K_d values among these samples can be accounted for to a large extent when solution speciation (especially alkalinity) in conjunction with the surface complexation model from Section 5 is used to estimate the K_d values.

The range of K_d values for the contaminated sediments compares well with the range (6.2 to 32 mL/g) measured for the NABS sample in isotopic exchange experiments. In the NABS experiments, the main variables were the total concentration of U(VI) and the alkalinity. Comparable K_d values were also found in the U(VI) batch adsorption experiments equilibrated with air (see Section 5).

6.4.2 Comparison of labile sediment U(VI) with sodium (bi)carbonate extraction results

If there was no oxidation of U(IV) on the sediments during air drying, then it is likely that the measured labile fraction of sediment U(VI) is equivalent to sorbed U(VI), since U(VI) solid phases were undersaturated in the Naturita groundwaters (see Section 3). The CARB extraction was designed to desorb U(VI) without dissolving the crystalline matrix, so a comparison of these results is warranted. Figure 6.3 shows plots of U(VI) extracted by the CARB solution versus the labile fractions of sediment U(VI) determined by isotopic exchange for either 1 week or 10 months of isotopic exchange. U(VI) extracted by the CARB solution is very well correlated with results obtained for both sets of isotope exchange data. For the 1-week exchange data, the slope, intercept and r^2 of the linear regression line are 1.22±0.02, $3.9\pm2.2\cdot10^{-10}$moles/g, and 0.996, respectively, indicating that the CARB extracted U(VI) was, on average, 22% greater than that determined by isotopic exchange for 1 week. After 10 months, the labile fraction estimated from isotope exchange was within 5% of the CARB extraction data, but slightly higher. The corresponding values of a linear regression line are 0.96±0.01, $-5.9\pm2.0\cdot10^{-10}$moles/g, and 0.997 for slope, intercept and r^2, respectively. The proximity of the slope to one suggests that both methods likely access essentially the same reservoir of U(VI). These results are encouraging because they suggest that the CARB extraction method is a very practical, inexpensive, and simple experimental technique to determine the labile U(VI) in contaminated sediments.

For the NABS sample, 7 to 9 days of isotopic exchange yielded a concentration of labile U(VI) of $5.6\cdot10^{-10}$ moles/g, in excellent agreement with the value obtained from the 1-week CARB extraction of $5.8\cdot10^{-10}$ moles/g. The 3-week CARB extraction gave a somewhat higher value of $8.74\cdot10^{-10}$ moles/g (Table 6.1).

6.4.3 *In-situ* field K_d values for U(VI)

Conditions within the contaminated portion of the alluvial aquifer at Naturita varied spatially, with pH values ranging from 6.8 to 7.4, alkalinities from 5 to 10 meq/L, calculated pCO_2 of 2 to 10%, and dissolved U(VI) concentrations from $1\cdot10^{-7}$M to $1\cdot10^{-5}$M (see Section 3). The increased levels of CO_2(g) in the aquifer are believed to be the result of biological activity that occurs primarily after river water recharges the alluvial aquifer. Because of the lower alkalinities and pCO_2, the K_d values measured in the isotopic exchange experiments are expected to be higher that those that apply under the Naturita field conditions, since formation of aqueous uranyl-carbonate complexes at higher alkalinities should lower the K_d values (see Section 5). Table 6.3 gives estimates of *in-situ* K_d values, based on the measured U(VI) concentrations in groundwater and the estimates of sorbed U(VI) from the CARB extractions and isotopic exchange experiments conducted with the sediments from the same location. With the exception of samples MAU-03 and MAU-04, note how the *in-situ* K_d values (Table 6.3) are considerably smaller than the laboratory values reported above (9-48 mL/g).

In practice, most K_d values used in performance assessment modeling of U(VI) transport in groundwater are based on laboratory adsorption experiments with uncontaminated sediments in systems equilibrated with atmospheric pCO_2 (USEPA, 1999). The CARB extraction can be very useful for studies of U-contaminated sites because the extraction can provide an independent estimate of sorbed U(VI) under actual field conditions, so that K_d values can be calculated under *in-situ* conditions.

6.4.4 Comparison with K_d values estimated from the U(VI) surface complexation model

A non-electrostatic surface complexation model (SCM) was developed in Section 5 to describe U(VI) adsorption by the NABS sample at various U(VI) concentrations pH values, and pCO_2. The 3-site model, with a total of four

Table 6.3 Comparison of model-predicted K_d values with experimental K_d values for field conditions at the Naturita field site.

Sample	K_d [mL/g] Model-predicted	K_d [mL/g] CARB	K_d [mL/g] Isotope Exchange
NAT-01	1.62	4.01	4.24
NAT-02	2.38	4.63	5.22
NAT-03	2.63	0.80	0.941
NAT-04	2.69	1.14	1.21
NAT-05	1.89	1.39	1.63
NAT-06	2.63	3.56	3.95
NAT-07	3.41	1.44	1.75
NAT-08	1.74	0.80	0.857
NAT-10	1.86	0.73	0.961
NAT-11	2.09	0.45	0.513
NAT-12	1.54	1.18	1.46
MAU-01	1.33	1.62	2.13
MAU-02	4.01	6.66	7.38
MAU-03	3.21	21.9	25.1
MAU-04	3.57	35.4	36.9
NABS [1)]	3.29	16.1	10.3
NABS [2)]	9.11	47.2	30.1

[1)] For averaged conditions as reported for NAT-20, -21 and –22: Alkalinity = 4.721 meq/L, pH 6.989, and $5.43 \cdot 10^{-8}$M U(VI) (12.9 μg/L).
[2)]For conditions reported for DOE-547, November 27, 2000, Alkalinity = 2.48 meq/L, pH 7.16, and $1.85 \cdot 10^{-8}$M U(VI) (4.4 μg/L).

U(VI) surface species, was successful in describing the adsorption data. Two of the surface species were ternary uranyl-carbonato surface complexes. The existence of uranyl-carbonato ternary surface complexes in suspensions of solids has been confirmed through spectroscopic techniques (Bargar et al., 1999, 2000; Bostick et al., 2002).

K_d values computed with the SCM can be compared with two sets of K_d determinations for the U-contaminated sediments presented above: (1) K_d values observed at the end of the AGW-3 extractions, and (2) K_d values calculated for the *in-situ* field conditions. In the case of the AGW-3 extractions, experimental values for the specific surface area, pH, alkalinity, total dissolved U(VI), and solid-solution ratio in the laboratory experiments were used as input to the SCM calculations. Figure 6.4 compares the model-predicted K_d values with those determined at the end of isotope exchange experiments in AGW-3 solution. Many of the model-predicted K_d values agree very well with the measured ones and all are within a factor of two (note the linear K_d scale in Fig. 6.4). The fact that the only sediment characterization involved in the model input was the specific surface area leads to the hypothesis that the variability in the U(VI) K_d values is largely due to variation of aqueous chemical conditions. Pabalan et al. (1998) and Davis et al. (2002) have observed that a wide range of K_d values for U(VI) obtained for many different solid phases could be reduced to a single parameter, K_a, in units of mL/m^2, that varies primarily with aqueous conditions. K_a values are obtained by

dividing K_d by the specific surface area of the solid phase.

Observed and model-predicted K_d values for the <3 mm material under *in-situ* conditions are listed in Table 6.3. The model predictions were performed using field data (pH, alkalinity, dissolved U(VI), Na^+, K^+, Mg^{2+}, Cl^-, SO_4^{2-}) for each individual well in conjunction with the measured specific surface areas of the contaminated sediment samples. Equilibrium with calcite was assumed in the simulations. These model-predicted K_d values are compared with "observed" K_d values determined from both the CARB extractions and the isotopic exchange K_d values. The model-predicted K_d values generally agree to within a factor of 2 to 3 with the estimates from the experimental data, which is a very encouraging result. The exceptions are K_d values for the MAU-03 and MAU-04 samples, for which the model-calculated values are about an order of magnitude lower than those estimated from the experimental data.

A possible reason for the discrepancies in the model-predicted values for the MAU-03 and MAU-04 samples is that these wells are the only ones at the site located in a downgradient, marshy area with cottonwood and willows trees. The average dissolved oxygen is 0.2 mg/L at MAU-03 and 0.7 mg/L at MAU-04, and the average Fe(II) concentrations are 1.34 mg/L and 0.05 mg/L, respectively. The average Fe(II) concentration for all wells is 0.47 mg/L. The Fe(II) concentration (1.25 mg/L) measured at well MAU-04 in the field in the fall of 1998 was higher than at other locations in the alluvial aquifer, and springs emanating from near the water table downgradient of MAU-03 and MAU-04 had red Fe-bearing precipitates. Although the glove-bag CARB extractions conducted in the field suggested that there was little U(IV) associated with the NAT-25J sediment sample (Table 6.2), it is possible that there was U(IV) associated with the MAU-03 and MAU-04 sediments at the time of sampling in 1998. Because the sediments were later air-dried, U(IV) in surface coatings was likely oxidized to U(VI) and then desorbed during the CARB extractions or the isotopic exchange experiments. This could lead to overestimates of *in-situ* U(VI) K_d values in the experimental "observations" in comparison to the model-predicted values.

Comparison of *in-situ* U(VI) K_d values in the uncontaminated portion of the aquifer is complicated by several factors, especially the choice of groundwater concentrations of U(VI), alkalinity and pH. Also, for the NABS sample, there is a factor of approximately 1.6 between the K_d values determined by the carbonate extraction (3-week) and isotopic exchange methods. The NABS sample was collected by a backhoe at the edge of a gravel pit that had been excavated to the groundwater table. Unfortunately, groundwater samples were not collected at the same time and location. The model-predicted value of 3.3 mL/g for the NABS sample in Table 6.3 is based on an average groundwater composition (U(VI) 12.9 μg/L, alkalinity 4.72 meq/L, and pH 6.99) from wells NAT-20, NAT-21 and NAT-22 (Fig. 4.1), which are in the uncontaminated area near well DOE-547. Model calculations show that the predicted K_d values are particularly sensitive to alkalinity at values below 4 meq/L. For example, at well DOE-547, the historical average chemical conditions from 1986 to 2002 are pH 7.1, alkalinity 4.1 meq/L, and U(VI) 12 μg/L. These conditions yield a model-predicted K_d value of 4.1 mL/g. Aerial photographs of the site indicate that the gravel mining operation expanded after 1997 near the location where the NABS sample was collected. After 1999, the average chemical conditions for 8 groundwater samples at well DOE-547 were pH 7.3, alkalinity 3.1 meq/L, and U(VI) 12 μg/L. The decrease in alkalinity and increase in pH are consistent with the loss of $CO_2(g)$ from standing water in the gravel pit. The model-predicted K_d value for this average composition is 8.1 mL/g. One water sample collected in November 2000 at well DOE-547 had an alkalinity of 2.48 meq/L, pH 7.16, and U(VI) 4.4 μg/L, which yields a model-predicted K_d value of 9.11. The latter predicted value agrees better with the observed K_d of 10.3 mL/g determined from isotopic exchange measurements and average water composition. The model calculations presented here were done using the model

calibrated without consideration of the ternary aqueous U(VI) complexes, $CaUO_2(CO_3)_3^{2-}$ and $Ca_2UO_2(CO_3)_3^0$(aq) (Brooks et al., 2003). For comparison, the extraction and isotopic exchange results are compared with the model that included the ternary aqueous U(VI) complexes in Kohler et al. (2003).

6.5 Summary and Conclusions

K_d values are dependent on the chemical composition of the solution phase and the nature of the solid materials. Variability in K_d values has been the subject of several studies (Waite et al., 1994; Davis et al., 2002; USEPA, 1999; Pabalan et al., 1998; Altmann et al, 2001; Turner and Sassman, 1996; Prikryl et al., 2001; Barnett et al., 2002). Methods are needed to estimate K_d values in the field for validation of SCM to be used in risk assessment transport models and to constrain the initial conditions in transport modeling.

This study shows that isotopic exchange and desorption extraction methods that are custom-designed for the appropriate chemical scenario can be an important part of a field characterization and modeling program. The experimental determinations of sorbed U(VI) in the Naturita alluvial aquifer build confidence in the semi-empirical SCM developed from experimental data with uncontaminated sediments (Section 5) and improve the credibility of the initial conditions of U(VI) transport simulations for the aquifer (Sections 9 -11).

7 COMPARISON OF FIELD AND MODEL-PREDICTED URANIUM (VI) K_d VALUES

7.1 Introduction

Simulations of reactive transport processes in groundwater often require many parameters as model inputs. These parameters include hydraulic parameters and descriptions of boundary conditions as well as reaction parameters that describe the chemical reaction network. While hydrologic parameters are usually obtained from field tests such as pump tests, slug tests, or tracer tests coupled with model calibration, it is less clear how chemical reaction parameters should be determined. For chemical reaction processes, parameter values could be based on a variety of sources ranging from tabulated thermodynamic data to laboratory-derived parameters using site-specific materials to field-determined values. The appropriate method used to obtain reaction parameters may depend on the nature of the chemical reaction being modeled. For example, tabulated values of equilibrium constants may be adequate for simulating aqueous complexation reactions and solubility constraints (Grenthe et al. 1992,Allison et al., 1991,Smith and Martell 1976). On the other hand, field-derived parameters or model-calibrated values may be required to describe complex redox reaction networks (Essaid et al. 1995,Smith et al., 1996,Mayer et al. 2001). In the middle of the spectrum, laboratory or field experiments using site-specific materials could be used to obtain reaction parameter estimates for adsorption reactions. This study compares hexavalent uranium (U(VI)) adsorption measured under field conditions with adsorption calculated from a surface complexation model (SCM) developed from laboratory batch experiments.

In oxic environments, the most stable valence of uranium is U(VI) which forms soluble U(VI) bearing solids (Grenthe et al. 1992). Thus, at circumneutral pH values the mobility of U(VI) can be controlled by adsorption reactions. Adsorption of U(VI) in oxic waters is sensitive to the pH and the carbonate activity and therefore to the partial pressure of CO_2 (P_{CO2}). This sensitivity arises because of changes in both aqueous and surface speciation. Adsorption is generally small at low pH values where the dominant species is the UO_2^{+2} cation. Adsorption increases with increasing pH usually in the pH range of 4 to 6 and U(VI) hydrolysis species in solution become increasingly dominant (Hsi and Langmuir 1985,Waite et al. 1994,Pabalan et al. 1998,Davis et al., 2002). In the alkaline region, U(VI) is strongly adsorbed in the absence of dissolved CO_2 (Hsi and Langmuir 1985,Prikryl et al. 2001) but in the presence of dissolved CO_2, the formation of aqueous U(VI)-carbonate complexes can cause adsorption to be negligible (Hsi and Langmuir 1985,Waite et al. 1994,Davis et al., 2002). At intermediate values of pH, the extent of adsorption is particularly sensitive to P_{CO2} because of the formation of both aqueous U(VI)-carbonate complexes and ternary surface U(VI)-carbonate complexes. The existence of these ternary surface complexes was initially postulated in order to fit adsorption data (Hsi and Langmuir 1985,Waite et al. 1994) but their existence has been established spectroscopically for a variety of solids (Bargar et al., 1999,Bargar et al. 2000,Bostick et al. 2002).

The simplest approach to describe adsorption of U(VI) by a sediment is to use a K_d value defined by

$$K_d = \frac{U_{ADS}}{U_{AQU}} \qquad (7.1)$$

where U_{ADS} is the amount of U(VI) adsorbed, and U_{AQU} is the amount of U(VI) dissolved the groundwater at equilibrium. However, in cases where there is significant chemical variability, a single K_d value is of limited value (Reardon 1981,Bethke and Brady, 2000). This is particularly true for U(VI), which has both complex aqueous and surface chemistry (Grenthe et al. 1992,Pabalan et al. 1998,Davis et al, 2002). Alternatively, surface complexation models (SCMs) have been used in many laboratory studies to describe adsorption of U(VI) by a variety of solids under conditions of

variable pH and sometimes P_{CO2}. Initially, SCMs were used to describe U(VI) adsorption by well-characterized metal oxides and clay minerals (Hsi and Langmuir 1985,Waite et al. 1994,Pabalan et al. 1998,Tripathi 1983,McKinley et al. 1995,Turner et al. 1996,Turner and Sassman 1996). More recently, several studies have used SCMs to describe U(VI) adsorption by soils and sediments (Davis et al.,2002,Prikryl et al. 2001,Turner et al. 1996,Waite et al. 2000,Arnold et al. 2001,Barnett et al., 2002). The success of these laboratory studies with complex soils and sediments is encouraging. However, none of these studies has tested the use of SCMs to describe U(VI) sorption under variable chemical conditions in a field environment .

SCMs have been used in several instances to describe adsorption in reactive transport models in the presence of variable chemical conditions. The models used have varied in terms of the number of reactive site types, the reaction stoichiometery, and whether or not an electrical double layer was used. Kohler et al. (Kohler et al. 1996) examined variable pH, ligand concentration and U(VI) concentration and calibrated a nonelectrostatic SCM to three laboratory column experiments. The calibrated reactive transport model was able to quantitatively predict the effects of a complexing ligand (fluoride) and variable pH. Stollenwerk used a diffuse double layer SCM to simulate molybdate transport in laboratory columns (Stollenwerk 1995) and at the Cape Cod field site (Stollenwerk 1998). Kent et al., (Kent et al. 2000) successfully simulated Zn transport in a sand and gravel aquifer with variable pH using a nonelectrostatic SCM. However, under field conditions, similar success has not yet been demonstrated for uranium which has more complex aqueous and surface speciation than either molybdate or Zn. In addition, an agreement between simulated and observed concentration distributions in field studies could be somewhat fortuitous because of the complexitity of applying reactive transport models to natural systems where boundary conditions and the source terms are often uncertain. The objective of this study was to compare K_d values determined in the field with those predicted by an SCM for U(VI) adsorption developed under laboratory conditions. Independently testing a laboratory SCM under field conditions is a valuable task that can increase the credibility of the conceptual model for adsorption used in reactive transport simulations.

7.2 Experimental Methods

7.2.1 Site Description

The field studies were conducted at the site of a former uranium mill located along the San Miguel River approximately 3 km north of the town of Naturita, Colorado, USA (Figure 7.1). A detailed description of the site is presented in Section 3 and therefore only the main characteristics are summarized here. A uranium mill that was operated at the site between 1941 and 1961 processed uranium ores with both sodium carbonate and sulfuric acid and produced uranium concentrates. Mill tailings were deposited and remained on the site until they were removed in 1979. Between 1986 and 1996, the U.S. Department of Energy (DOE) installed and monitored 12 wells in the alluvial aquifer at the site; all but two of these wells (including DOE547) were abandoned during surface remediation activities between 1996 and 1998 when contaminated soils were removed from the site. Beginning in 1998, the USGS installed seventeen 5.1-cm diameter wells and thirty 1.25-cm diameter wells at the site. All of the wells were installed in the shallow, unconfined aquifer that consists of cobbles, gravels, sands and some fine material. The saturated thickness of the aquifer ranged from 1 to 4 m and the depth to groundwater ranged from 1 to 3 m.

Figure 7.1 illustrates a map of the field site including the locations of all of the active groundwater wells, which were sampled approximately every 4 months between October, 1998 and September 2001. The field and laboratory methods used for groundwater sample analysis and a complete description of the geochemical conditions in the aquifer are presented in Section 3. The distribution of

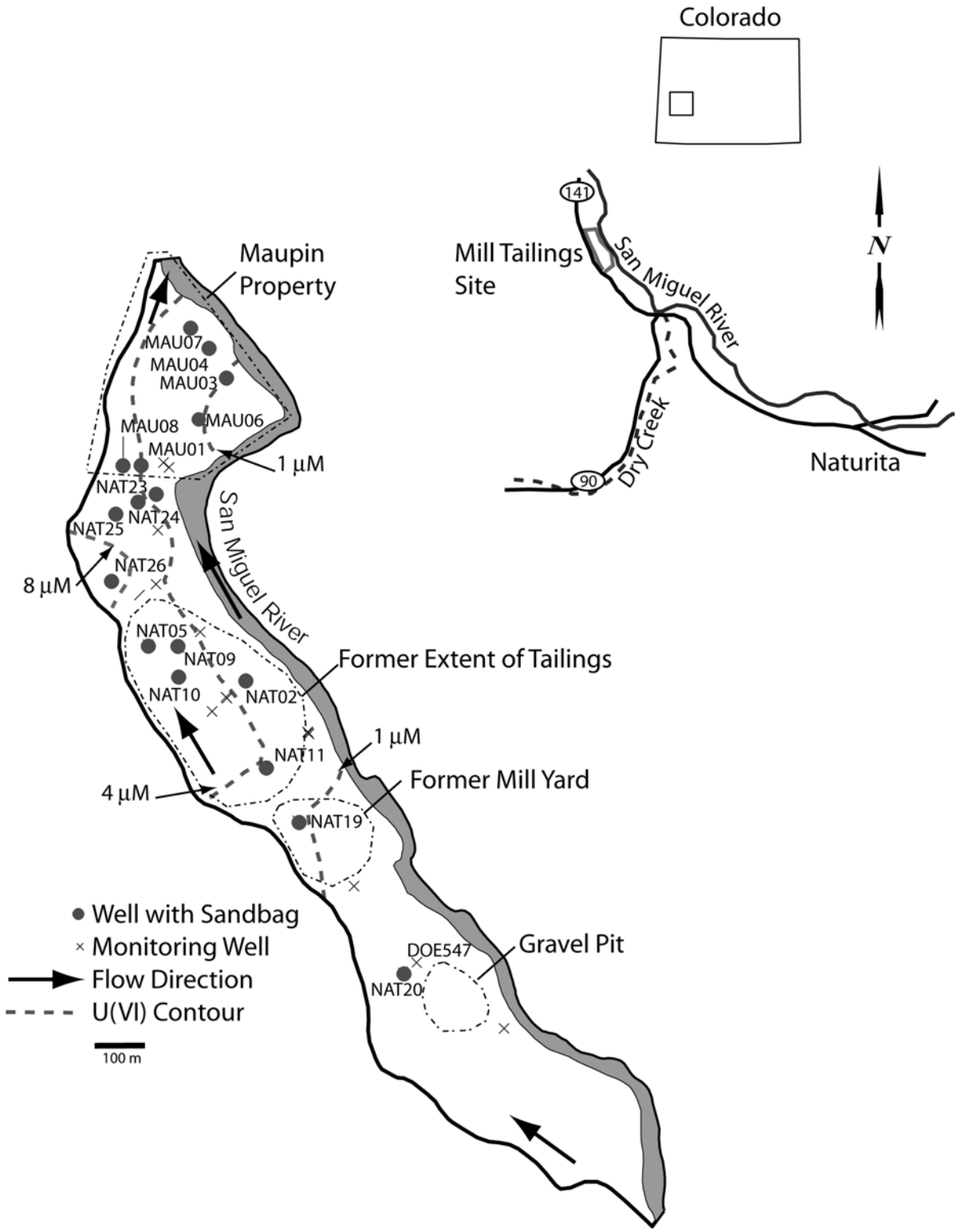

Figure 7.1 Naturita UMTRA site illustrating the locations of wells where sandbags were deployed, U(VI) contours, the extents of the former tailings piles and mill site, and the gravel pit.

U(VI) observed in June 2000 when the field experiments described below were started is also shown in Figure 7.1. At that time, the U(VI) concentration at the site varied from average background values of 0.02 μM at DOE547 to maximum concentrations of 10.2 μM at NAT26. These two wells also had the minimum and maximum measured alkalinities of 3.3 and 11 meq/L for wells DOE547 and NAT26, respectively. The observed spatial distribution for alkalinity was similar in shape to that for the dissolved U(VI) concentration (Section 3). The pH values at the site were between 6.8 and 7.2 and did not illustrate a discernable spatial pattern. The partial pressure of CO_2 calculated from the pH and alkalinity values ranged from 0.01 to 0.08 atmospheres (Section 3).

7.2.2 Experimental Approach

Adsorption experiments were conducted using a composite sediment sample <3 mm diameter prepared from approximately 1300 kg of sediment collected below the water table at a gravel pit approximately 300 m upgradient of the former U(VI) millyard (Figure 7.1). The sample was screened in the field to remove cobbles greater than 6.4 cm and then screened again in the laboratory to remove gravels greater than 3 mm. The material that passed through the 3 mm screen is referred to as Naturita aquifer background sediment (NABS). Adsorption of U(VI) by NABS was measured in the laboratory for variable pH and P_{CO2} and the adsorption data and a surface complexation model are presented in Section 4.

In situ K_d values were measured on samples of NABS material that were suspended in each of the seventeen 5.1-cm wells shown in Figure 7.1. Each sample had approximately 10 g of NABS that was bundled with a 50 μm opening nylon mesh fabric held closed with a cable tie. Four or five bags were placed in a coarse polyethylene mesh (~0.8 cm opening), which was attached to a 1.25-cm PVC pipe placed in the wells. All of the samples were installed in the wells in June 2000 except for samples at NAT23 and MAU06 which were installed in September 2000. The sandbags were suspended in the screened interval at 0.5 m above the bottom of the well except for the samples at NAT26. At this well, the sandbags were initially suspended at 0.5 m from the bottom of the well but they were found to be above the unusually low groundwater surface in September of 2000 when the water was only approximately 0.25 m deep in the well. The bags were subsequently lowered to the bottom of the well in NAT26. The sandbags were sampled in September and November 2000, and March and September 2001. Samples were taken by removing a sandbag from each well and shipping them to the laboratory where the bags were frozen at –2ºC until analysis. In most instances, groundwater was sampled each time a sandbag was removed from a well. Two casing volumes were purged from the well prior to sampling the well.

An important assumption of the field tests conducted in this study is that the water in the well bore that contacts the sandbags was equivalent in composition to the formation water as measured by the well sampling.

7.2.3 Sediment Analysis

Frozen samples were thawed and the sand was removed from the bags and placed in a laminar flow hood to dry. Weights were recorded before and after drying to determine the residual water content of the sandbag. The dried samples were thoroughly mixed so that a representative sample could be obtained and subsampled for various analyses. The amount of U(VI) adsorbed to natural sediments can be measured by isotopic exchange experiments which equates the amount of adsorbed U(VI) with the labile pool of U that equilibrates with a known U isotope on the time frame of hours to months (Payne et al. 2001). In Section 6 the isotopic exchange method was used to quantify U(VI) adsorbed by contaminated sediments obtained from the Naturita site. Moreover, it was demonstrated that the amount of U(VI) extracted from the contaminated sediments by a carbonate solution (as described below) was in excellent agreement with the amount of adsorbed U(VI) determined by isotopic exchange.

In this study, the relatively simple carbonate extraction method was used to measure U(VI) adsorbed by samples that had been suspended in the wells. The carbonate extraction solution (CARB) had a pH of 9.45, an alkalinity of 20 meq/L and an ionic strength of 0.02 M. Duplicate 2 g samples of dry sand were extracted with 40 g of carbonate solution. Samples were mixed on a shaker table, and a 1.5 mL solution aliquot was removed after 24, 170, 336, and 504 hours. Each aliquot was filtered through a 0.45 μm filter and acidified to 1% HNO_3 with concentrated trace metal grade HNO_3. Throughout the experiment, the pH of the carbonate extractions remained above 9.3. The results for the time series experiments showed that U(VI) extracted after 336 and 504 hours were indistinguishable; only results obtained after 504 hours are presented below. The U(VI) content in the extracts was analyzed by kinetic phosphorescence analyzer (KPA) which had an instrumental precision of less than 3%.

Separate 1g subsamples were also ground in mortar and pestle and extracted by hot concentrated nitric acid (HNO_3) which dissolves both adsorbed and precipitated (or co-precipitated) U(VI) on grain surfaces. However, the method does not fully dissolve U from rock fragments. Thus, this method was included to evaluate if poorly crystalline phases containing U(VI) formed in the sandbags under field conditions. Samples were refluxed on a hot plate with 10-12 mL HNO_3 over the course of 4 days (~32 hours total reflux time) until the sand was light gray in color. The samples were then heated uncapped and reduced to almost dryness. After samples had cooled, they were resuspended in 20 mL 1% HNO_3, then filtered (0.45 μm) and further diluted for analysis of U(VI) by KPA.

Gamma spectroscopy was used to determine the total U concentrations on subsamples of about 6-7 g of the sandbag samples (Section 6). Samples were counted until the relative counting error was ≤ 10%. This method determines the total U content of the sample which includes surficial U(VI) (adsorbed and precipitated) and U within the interior of rock fragments.

All U extraction data were corrected for U(VI) present on sandbags that result from evaporated interstitial groundwater. This correction was calculated from the gravimetrically determined residual water content of the samples and the U(VI) concentration in groundwater at each well. The U(VI) extraction data were also corrected for the U(VI) in the NABS sample as described below.

Extractable iron and specific surface area were measured to evaluate if any detectable changes in these sediment properties occurred while the sandbags were in the wells. Samples were extracted with a hydroxylamine hydrochloride solution, a technique that has been used to determine the levels of Fe oxides present in aquifer sediments (Fuller et al. 1996, Coston et al., 1995). Duplicate 1 g samples were extracted with 20 g of 0.25 M $NH_2OH{\cdot}HCl$ in 0.25 M HCl at 50°C. Solution aliquots (1.5 mL) were taken at 1.0, 24, and 96 hours and immediately filtered through a 0.45 μm filter and diluted (~15x) with 1% HNO_3 for ICP analysis. The Brunaur Emmett Teller (BET) surface area was determined by analysis of N_2 gas adsorption on 3 g samples using a Tristar Micromeritics system. This method gave surface areas that had a precision of less 5% for replicate analyses.

7.2.4 Surface Complexation Model

A surface complexation model (SCM) was presented in Section 5 for describing U(VI) adsorption by the NABS sample as a function of pH and alkalinity. The SCM consists of four U(VI) surface reactions, which are listed in Table 7.1. The solution speciation reactions and equilibrium constants were identical to those used in other modeling studies (Davis et al., 2002, Davis 2001, see Table 2.1). The SCM was developed using the semi-empirical generalized composite approach based on the assumptions that the complex aquifer sediments have generic rather than mineral-specific surface sites that adsorb U(VI), and that electrical double layer considerations can be ignored for simplicity (Davis et al., 2002,Kent et al. 2000,Davis 2001,Davis et al. 1998,Westall et al., 1998). Model-predicted K_d values were computed from

Equation 1. The dissolved U(VI) concentration was equal to that determined from the groundwater analyses and the adsorbed concentration was calculated from the observed aqueous geochemical data and the SCM using a geochemical equilibrium model (Herbelin and Westall 1994). The model calculations used the measured U(VI), pH, alkalinity, and ionic strength and assumed equilibrium with calcite. The model calculations presented here were done using the model calibrated without consideration of the ternary aqueous U(VI) complexes, $CaUO_2(CO_3)_3^{2-}$ and $Ca_2UO_2(CO_3)_3^0$(aq) (Brooks et al., 2003). For comparison, the results of this study are also presented with the model that included the ternary aqueous U(VI) complexes in Curtis et al. (2003a).

The calculations also used the surface area of the NABS sample because it was found that the surface area did not change significantly when the sandbags were in the wells. The calculations assumed that the sandbags were in local adsorptive equilibrium with groundwater in the well bore and that the wellbore was an open system relative to the aquifer. This assumption is analogous to the local equilibrium assumption used in reactive transport modeling (Rubin, 1983). Thus, the groundwater chemistry in the wells can vary over time and, if adsorption is sufficiently fast, the calculations remain valid. Batch experiments with NABS samples show that steady-state concentrations are achieved in less than 96 hours (Section 4). In Section 9 it is shown that for the geochemical conditions in the Naturita aquifer, the model K_d values were most sensitive to alkalinity and least sensitive to pH.

7.3 Extraction Results

7.3.1 Sediment Characterization

Hydroxylamine hydrochloric acid extraction results. As described below, U uptake by the sandbag samples after 3 months was nearly identical to that observed after 14 months, and therefore most of the analyses were conducted on samples after 3 months of exposure. This includes the analyses conducted on the solids to evaluate the possibility of any changes in sediment characteristics.

The groundwaters at Naturita contain small concentrations (0.1 to 2 ppm in a few wells) of Fe^{+2} (Section 3) and oxidation and precipitation of this iron on the sediment in the sandbags could have increased the ferrihydrite content of the sediment. Alternatively, reductive dissolution could decrease the ferrihydrite content (Lovley and Phillips 1986,Lovley and Phillips 1988). If the ferrihydrite content changed by precipitation or dissolution, the adsorption of U(VI) could also change because U(VI) is strongly sorbed to ferrihydrite (Waite et al. 1994). Iron content extractable by the hydroxylamine hydrochloride solution was used as a measure of the abundance of ferrihydrite in the aquifer sediments (Coston et al., 1995).

Table 7.1: Surface Complexation Model Reactions and Equilibrium Constants Used in Model-Predicted K_d Calculations[a]

U(VI) Surface Reaction	Log K[b]
$>WOH + UO_2^{+2} + H_2O = >WOUO_2OH + 2H^+$	-6.74
$>SOH + UO_2^{+2} + H_2CO_3 = >SOUO_2CO_3 + 3H^+$	-8.00
$>SSOH + UO_2^{+2} + H_2O = >SSOUO_2OH + 2H^+$	-2.06
$>SSOH + UO_2^{+2} + H_2CO_3 = >SSOUO_2CO_3 + 3H^+$	-6.36
[a]See Section 5 for model details. Total site density of 1.92 μmoles/m^2 of monodentate sites was assumed (= 3.84 μmoles/m^2 hydroxyl groups). Distribution of sites was 98.79% weak (>WOH), 1.2% strong (>SOH) and 0.01% very strong (>SSOH). [b]Apparent stability constant for the surface reaction.	

A 30-minute treatment completely dissolves ferrihydrite whereas crystalline iron oxides such as goethite and hematite dissolve more slowly (Chao and Zhou 1983). After one hour of extraction, the average amount of Fe dissolved for the 17 samples was 11.3±0.8 μmol/g which is within error of the measured Fe content of 10.0±0.5 μmol/g for the NABS sample before sandbag deployment. The 10 % increase in Fe-oxide content was not large enough to have a significant impact on U(VI) adsorption.

Surface Area. The BET surface area of the NABS sample prior to placement in the sandbags was 5.15 m^2/g (Section 4). The BET surface area was measured on three sandbag samples after approximately 90 days of exposure to contaminated groundwater. The measured surface areas were 5.1 m^2/g for a sample from NAT19, 5.2 m^2/g for a sample from NAT26 and 5.0 m^2/g for a sample from MAU03. All of these values are very close to the surface area of the parent material indicating that there were negligible changes in surface area caused by suspension of the material in the groundwater. The nearly constant surface area results are also consistent with the nearly constant Fe extraction results suggesting the changes in the samples were small over the course of the experiments.

7.3.2 Uranium Extractions

Sandbag samples from three wells were analyzed after approximately 90, 160, 250, and 460 days to evaluate the long term U(VI) uptake by the sediment samples in the field. Samples were analyzed from NAT19, which is located upstream of the most highly contaminated zone, NAT05, which had high dissolved U(VI) and high vanadium concentrations, and NAT25, which had a high dissolved U(VI) concentration and no detectable vanadium (Section 3). Figures 7.2a-c show the U(VI) concentration, pH, and alkalinity values observed in the three wells during the time the sandbags were deployed in the field. The samples were extracted with CARB solution and analyzed to determine adsorbed U(VI) and the results are shown in Figure 7.2d. No corrections were made to the CARB extractable U(VI) because the CARB method gave results that were nearly identical to the results obtained by isotopic exchange (Section 6). Adsorbed U(VI) for the four NAT19 samples decreased slightly from 8.0×10^{-9} mole/g to 5.6×10^{-9} mole/g as the dissolved U(VI) concentration in groundwater decreased from 0.36 to 0.22 μM. Adsorbed U(VI) in the four NAT05 samples varied by less than 20%. For the NAT05 and NAT25 samples, adsorbed U(VI) reached a maximum value after 250 and 160 days, respectively, and then decreased with exposure time. After 460 days the adsorbed U(VI) was similar to its value after 90 days. A comparison of Figure 7.2d with Figures 7.2a and 2b shows that the adsorbed U(VI) coincided with variations in dissolved U(VI) and alkalinity. Thus, the extraction data suggest that adsorbed U(VI) adjusted to the temporal changes in groundwater chemistry which is consistent with the assumption of local equilibrium between adsorbed and dissolved U(VI).

Because adsorbed U(VI) had generally reached a steady-state value after 3 months, detailed analyses of the sandbag samples were conducted for a single time point. The earliest sampling time for each well was chosen because these samples would be least likely to be influenced by secondary processes such as weathering reactions. The sampling date, residence time and results for the extractions of U(VI) with CARB and HNO_3 and the analysis of total U are listed in Table 7.2. The results showed an increase in U content relative to the NABS sample for most samples. The amount of U measured by these methods generally increased in the order CARB<HNO_3<total, as was also observed for contaminated sediments collected at the site (Section 6). A regression of the amount of U extracted by the CARB solution and the hot concentrated HNO_3 analyses had a slope of 1.38, an intercept of 0.09, and a correlation coefficient (r^2 value) of 0.83 (results not shown). The total U analyses showed an increase of at most 9×10^{-9} mole/g and this value is approximately the same as was measured in the CARB and HNO_3 extractions. Even though there was a small increase relative to the background U, the total U measurements indicated that the precipitation of a new phase that was not extracted by the CARB and HNO_3

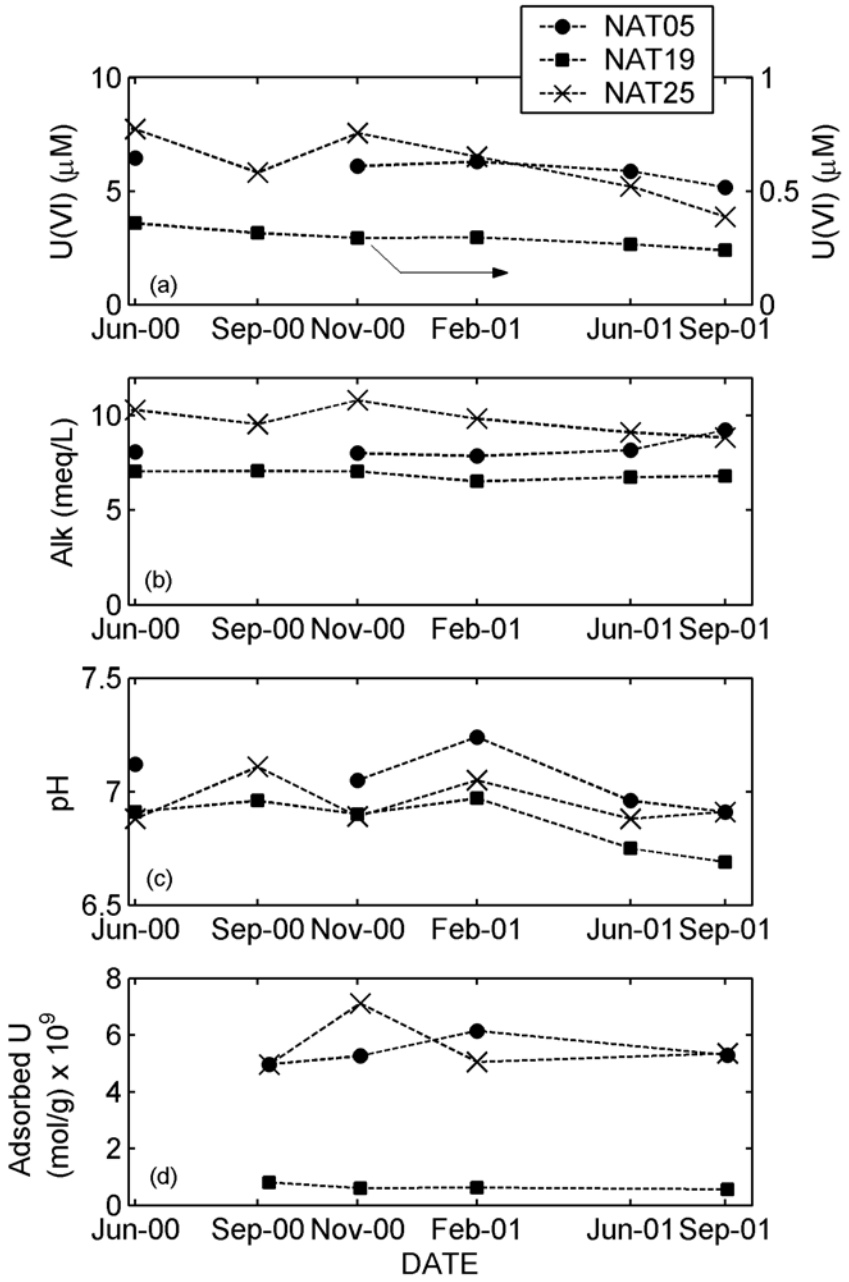

Figure 7.2. Extracted U(VI) from NABS sediment aliquots suspended in wells NAT05, NAT19 and NAT25 for variable contact times.

solutions did not occur to a great extent.

The HNO_3 extraction data listed in Table 7.3 can be used to evaluate if any new U-bearing phases formed while the sandbags were in the field. Hot HNO_3 dissolves both adsorbed U(VI) and U held in crystalline phases of secondary coatings (Lenhart and Honeyman 1999). Using the results for the HNO_3 extractions, the increase in U retained in crystalline phases during the sandbag deployment can be estimated. The background U in secondary crystalline phases of the NABS sample equals the difference between the HNO_3 and CARB extraction results:

$$U_{CRYST,NABS} = U_{HNO3,\ NABS} - U_{CARB,\ NABS} \quad (7.2)$$

The increase in U retained in crystalline and adsorbed phases during sandbag deployment U can be estimated by correcting the HNO_3 extraction results for $U_{CRYST,NABS}$:

$$U_{HNO3,CORR} = U_{HNO3} - U_{CRYST,NABS} \quad (7.3)$$

Figure 7.3 compares the values of $U_{HNO3,CORR}$ with U_{CARB}, the increase in crystalline U is the difference between the two quantities. The amount of adsorbed U(VI) determined from the CARB extractions was on average 30% less than the U extracted by HNO_3 (after background correction). This indicates that, in comparison to adsorbed U(VI), relatively little U was incorporated into the sediments by (co)precipitation with crystalline phases during contact with groundwater in the field. In addition, some of the 30% difference between HNO_3 and CARB-extractable U could have been caused by diffusion of U(VI) into small pores within the sediments, since it is possible that HNO_3 dissolves some particles, releasing U(VI) adsorbed in deep pore spaces, whereas U(VI) must desorb and diffuse out of the porous matrix during CARB extractions.

7.4 *In-situ* and Model-Predicted K_d Values

U(VI) K_d values are strongly influenced by the formation of soluble U(VI) carbonate complexes. Therefore, model K_d values vary at the site because the chemical composition of the groundwater at the site varies spatially and at some wells, the chemical composition changed slowly over time.

Table 7.2. U Extraction Results for the NABS and Sandbag Samples

				Uranium Content (moles/g x 10^9)		
Sample	**Sandbag Installation**	**Sample Date**	**Contact Time (days)**	**Carbonate Extraction**	**Nitric Acid Extraction**	**Total U**
NABS				**0.71±0.04**	**3.7±0.2**	**12±1**
MAU-01	**6/24/2000**	**9/10/2000**	**78**	**4.2±0.5**	**8.4±0.1**	**20±2**
MAU-03	**6/24/2000**	**9/21/2000**	**89**	**2.7±0.4**	**6.8±0.1**	**15±1**
MAU-04	**6/24/2000**	**11/30/2000**	**159**	**3.2±0.2**	**7.9±0.1**	**14±1**
MAU-06	**9/21/2000**	**11/30/2000**	**70**	**0.83±0.09**	**5.0±0.1**	**10±1**
MAU-07	**6/24/2000**	**9/21/2000**	**89**	**4.8±0.4**	**12±1**	**16±2**
MAU-08	**6/24/2000**	**9/14/2000**	**82**	**5.3±0.3**	**9.7±0.1**	**19±1**
NAT-02	**6/24/2000**	**9/12/2000**	**80**	**3.1±0.4**	**6.4±0.1**	**14±1**
NAT-05	**6/24/2000**	**9/20/2000**	**88**	**3.6±0.4**	**8.1±0.1**	**14±2**
NAT-09	**6/24/2000**	**9/20/2000**	**88**	**2.9±0.2**	**6.4±0.1**	**14±1**
NAT-10	**6/24/2000**	**9/20/2000**	**88**	**3.7±0.5**	**8.5±0.1**	**14±1**
NAT-11	**6/24/2000**	**9/16/2000**	**84**	**3.5±0.5**	**6.8±0.1**	**15±2**
NAT-19	**6/24/2000**	**9/20/2000**	**88**	**0.74±0.08**	**3.5±0.04**	**11±1**
NAT-20	**6/24/2000**	**9/20/2000**	**88**	**0.50±0.02**	**3.9±0.04**	**8.9±0.9**
NAT-23	**9/20/2000**	**11/30/2000**	**71**	**8.5±0.3**	**15±0.2**	**21±2**
NAT-24	**6/24/2000**	**9/13/2000**	**81**	**5.7±0.6**	**12±1**	**20±2**
NAT-25	**6/24/2000**	**9/15/2000**	**83**	**6.2±0.4**	**8.4±1**	**17±2**
NAT-26	**6/24/2000**	**9/10/2000**	**78**	**4.9±0.3**	**12±1**	**15±1**

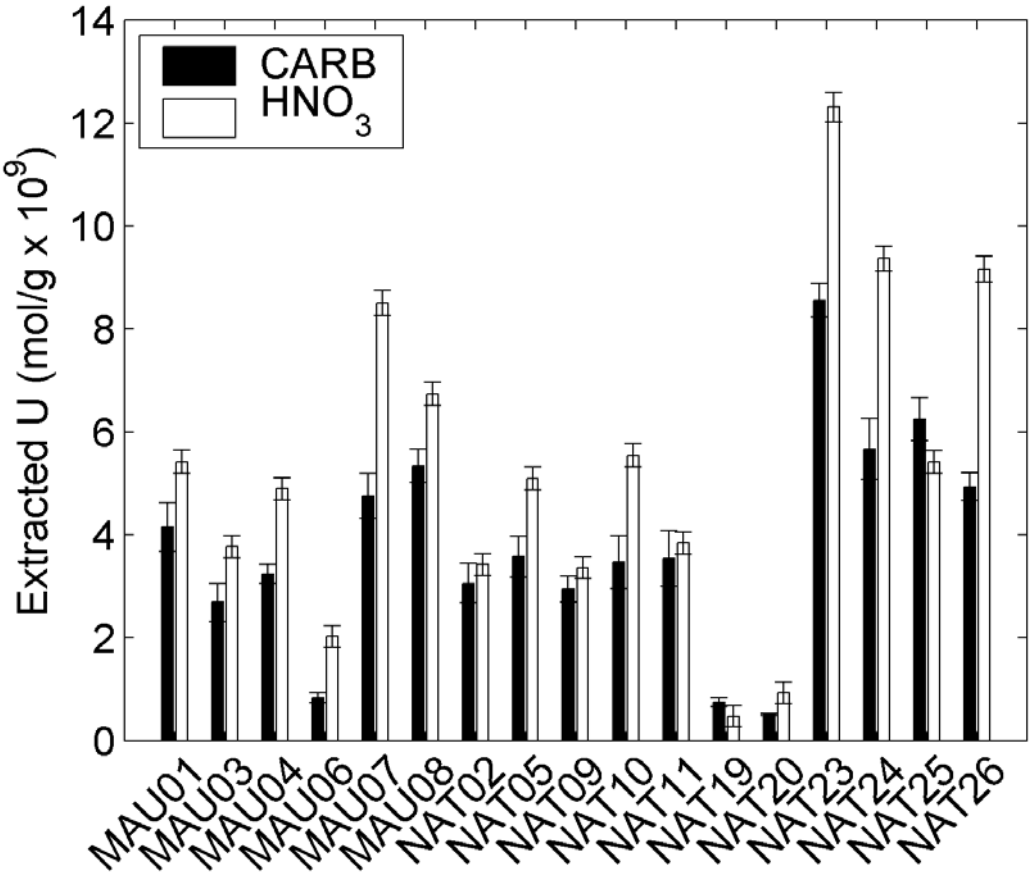

Figure 7.3 Comparison of adsorbed U(VI) determined by carbonate extraction with U extracted by concentrated HNO_3 after correction for background crystalline U.

The *in situ* K_d values were calculated using equation 1, the adsorbed U(VI) determined from carbonate extraction results in Table 7.2 and the dissolved U(VI) concentrations in Table 7.3. It was assumed that all U released by the extractions was present in the sediments as U(VI), because it was previously found that carbonate extractions conducted in the field on fresh sediments collected near NAT25 under a nonoxidizing atmosphere gave similar results as extractions performed on air-dried samples (Section 6). The *in situ* K_d values were compared with model K_d values calculated from the measured groundwater composition and the SCM. Comparisons were made for 3 samples that were exposed to contaminated groundwater for various lengths of time and for 17 samples that were deployed in wells that had spatially variable chemical conditions.

Model and *in situ* K_d values are compared in Figure 7.4 for sandbags from NAT05, NAT19 and NAT25 that were analyzed after approximately 90 to 460 days of contact with contaminated groundwater in Figure 7.4. The *in situ* K_d values ranged from 0.64mL/g for samples from NAT25 to 2.4mL/g for samples from NAT19. The model K_d values for the same samples ranged from 0.68mL/g to 2.0 mL/g. The model calculations show that smaller K_d values for NAT25 result primarily from the higher alkalinity but also from the higher U(VI) concentration. All of the points fall slightly below the ideal 1:1 line as the simulated values slightly under predicted the *in situ* K_d values. A regression of the data has a slope of 0.78 ± 0.06 mL/g and an intercept of 0.034 ± 0.08 mL/g.

Table 7.3: Dissolved U(VI), Alkalinity, and pH for Wells with Deployed Sandbags

Well	Dissolved U(VI) (μM)	Alkalinity (meq/L)	pH
MAU-01	3.14	7.48	6.95
MAU-03[1]	1.12	4.46	7.14
MAU-04	0.76	4.62	7.14
MAU-06	0.62	4.66	7.08
MAU-07[1]	2.38	6.96	6.95
MAU-08	6.21	9.40	6.98
NAT-02	1.63	6.32	7.33
NAT-05[1,2]	6.09	8.02	7.05
NAT-09[3]	3.62	7.18	7.08
NAT-10[1]	4.15	7.58	7.03
NAT-11	3.71	7.92	6.85
NAT-19	0.32	7.08	6.96
NAT-20	0.04	3.94	6.98
NAT-23	6.72	6.64	6.90
NAT-24	3.74	7.22	6.96
NAT-25	5.82	9.56	7.11
NAT-26	9.86	10.4	7.07

[1]Water composition is an average of samples taken in June and November 2000.
[2]Water composition for well NAT15-1, located ~2.5 m upgradient of well NAT-05.
[3]Water composition for well NAT-08, located ~2.5 m upgradient of well NAT-09.

At a finer level of comparison, the model predictions also accounted for small temporal changes in the geochemical conditions at wells NAT25 and NAT19. The *in situ* K_d at NAT25 increased by a factor of 2.2 from 0.64 mL/g to 1.4mL/g and the model K_d increased by a factor of 1.4. The increase in the model K_d at NAT05 is caused by both the factor of 2 decrease in U(VI) in groundwater and the 22% decrease of alkalinity (Figure 7.2). For samples from NAT19, the *in situ* K_d values ranged from minimum values of 2.1 mL/g to maximum values of 2.4 mL/g. This difference coincided with a 33 percent decrease in dissolved U(VI) and a nearly constant alkalinity. The SCM predictions suggest that these changes in aqueous concentrations account for most of the observed change in the *in situ* K_d values at NAT19. For the sample from NAT05, the model K_d values also track the changes in *in situ* K_d in most cases even though the changes in K_d are smaller. The observation that the *in situ* K_d values adjusted to the observed change in chemical conditions in the groundwater supports the local equilibrium assumption that was made in calculating the model K_d value.

The effect of variable chemical conditions on simulated and *in situ* K_d values was also evaluated by comparing K_d values determined on samples from the seventeen wells distributed across the site. Figure 7.5 illustrates a plot of the *in situ* versus model K_d values for samples that were exposed to groundwater for approximately three months in most cases. The error bars for the *in situ* K_d values are the differences between duplicate samples and the error bars for the model K_d values are the

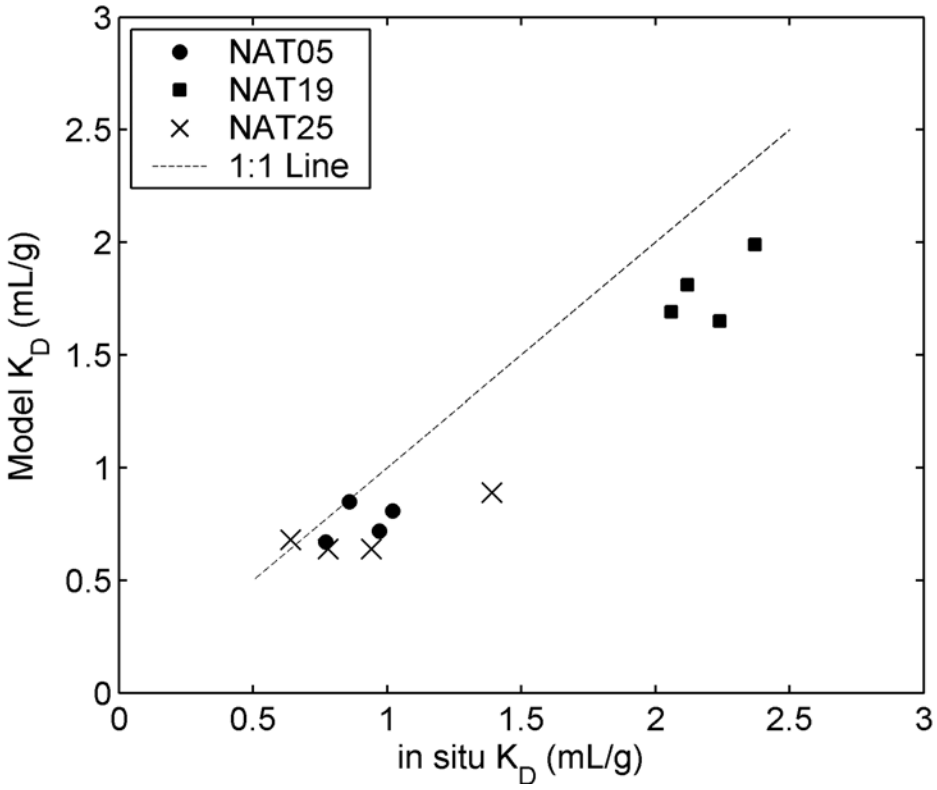

Figure 7.4 Relation between *in-situ* U *(*measured) and model-predicted K_d values for samples contacted with groundwater for varying amounts of time.

standard deviations of model K_d values calculated from 4 to 5 water analyses that were collected within 9 months of when the sandbags were sampled. The *in situ* K_d values ranged from 0.47 mL/g for NAT26 to 12.3 mL/g for NAT20. NAT26 had groundwater with both the high alkalinity and high U(VI) concentration. Conversely, the maximum *in situ* K_d value was observed at NAT20 which had groundwater with the lowest alkalinity and U(VI) concentration. The inset in Figure 7.5 shows that the good agreement includes the cluster of points with K_d values in the range of 0.5 to 2.5 mL/g. The *in situ* and model K_d values agree within a factor of 2 or are within the error estimates for all samples except for the sample from NAT20.

Several factors could impact the *in situ* K_d value at NAT20. First, the model K_d values are most sensitive to alkalinity, especially for alkalinity values below 5 meq/L. Within 9 months of when the sandbag sample from NAT20 was collected, the average alkalinity of the groundwater in NAT20 was 4.4 meq/L, whereas the average alkalinity in well DOE547, which is located only 50m from NAT20, was 3.3 meq/L. The reason for the different alkalinity values is unclear but it could result from precipitation of calcite at the free water surface of a new gravel pit upgradient of DOE547. At NAT 20, the observed chemical conditions together with the SCM predict an average K_d of 4.1 mL/g. For comparison, the average model K_d at DOE547 was 8.1 mL/g. One water sample collected in November 2000 at DOE547, had an alkalinity of 2.48meq/L, a pH of 7.2, and a U(VI) concentration of 0.008 μM which, together with the SCM, yields a K_d of 12.1. This latter model value agrees closely with the *in situ* K_d for the sandbag sample from NAT20. Thus, the K_d values for waters with low U and low alkalinity such as at NAT20 and DOE547 are particularly sensitive to the alkalinity and U(VI) concentrations used in the calculation.

A second possibility for the difference between the *in situ* and the model K_d values is that the model K_d is sensitive to the equilibrium constant

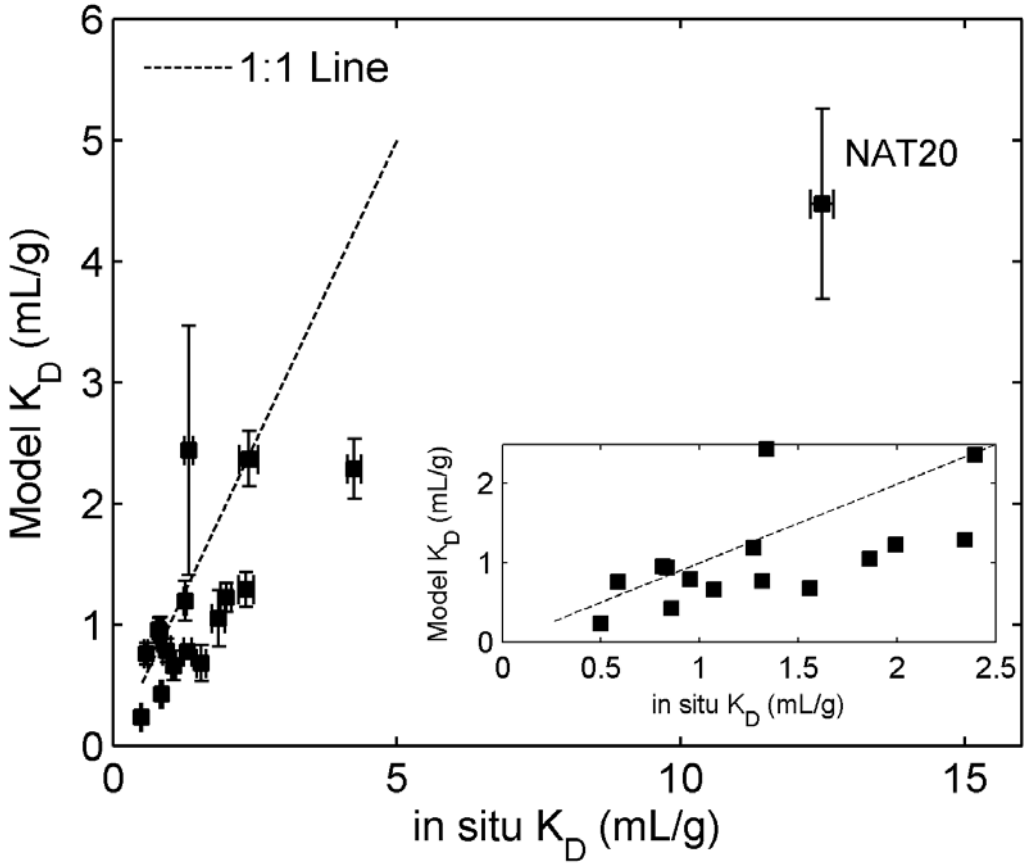

Figure 7.5. Relation between in-situ U(measured) and model-predicted K_d values.

for the adsorption reaction with the very strong site included in the SCM (Table 7.1). For low alkalinity and low U(VI) concentration, U(VI) adsorption is dominated by the reaction:

$$>SSOH + UO_2^{+2} + H_2O = >SSOUO_2OH + 2H^+ \quad (4)$$

where >SSOH represents the low-abundance, high affinity adsorption sites. An increase in the log K for the formation of $>SSOUO_2OH$ of 0.3 log units would give an exact match between the *in situ* and model K_d values and an increase of 0.17 log units would give a value within the uncertainty of the observed K_d value. Such a change in the equilibrium constant would have a small effect on the model K_d values for the remaining 16 samples because the >SSOH sites are relatively unimportant at the higher U(VI) concentrations in the contaminated groundwaters.

7.5 Summary and Conclusions

This study compares U(VI) K_d values measured under field conditions with K_d values calculated from an SCM developed from laboratory sorption data (see Section 5). *In-situ* U*(*field) K_d values were calculated from groundwater measurements of dissolved U(VI) and U extracted from the sandbag sediment samples using a sodium (bi)carbonate solution at pH 9.45. U(VI) K_d values for samples taken after 3 months of exposure to contaminated groundwater were indistinguishable from samples taken after 15 months. The K_d values from 17 wells ranged from 0.5 to 12 mL/g, and the K_d values decreased with increasing groundwater alkalinity, consistent with increased formation of U(VI)-carbonate complexes at higher alkalinities. The *in-situ* K_d values were compared with K_d values predicted by the SCM. The comparison demonstrated a close agreement

between the model-predicted and measured *in-situ* K_d values. In addition, *in-situ* K_d values measured at 3 wells at varying exposure times between 90 and 400 days agreed with model-predicted K_d values, even though some of the K_d values varied by a factor of approximately 2 due to temporally variable chemical conditions. Thus, the SCM was effective at accounting for the effects of variable alkalinity and U(VI) concentrations in the groundwater on U(VI) K_d values.

The good agreement between the *in situ* and model K_d values was achieved with a relatively simple SCM that included only 4 U(VI) adsorption reactions. In contrast, SCMs for model oxides studied under batch conditions in the laboratory often include more adsorption reactions and also account for surface ionization, sometimes consider adsorption of CO_2, and usually include corrections for an electrical double layer (Waite et al. 1994,Pabalan et al. 1998, Lenhart and Honeyman 1999). In contrast, the generalized composite SCM used in this study does not include CO_2 adsorption, surface ionization, nor does it account for an electrical double layer. However, the SCM used provides the important link between aqueous speciation and sorption via the mass action laws for the adsorption reactions. This connection accounts for the ability of the model to give a good agreement to the *in situ* K_d values obtained at locations with variable alkalinity, U(VI) concentrations and pH values with a modest number of parameters.

The observation that the model K_d values agreed well with the K_d values measured under field conditions is encouraging. The implication is that adsorption reactions could be studied at other sites by suspending uncontaminated sediments in wells with contaminated water. The experiments are relatively simple and could be conducted at modest cost as a part of site characterization. Results from these site-specific studies with site-specific sediments could be useful in reducing uncertainty in model predictions used in risk or performance assessments and could help document the process of natural attenuation. The approach, however, is not without its simplifications.

Probably the most important simplification is that because the NABS sample used in the sandbags was derived from a homogenized background sediment sample, the natural geochemical heterogeneity of aquifer sediments is circumvented. At the Naturita site, this issue was considered and it was found that the SCM developed for NABS agreed with K_d values determined by CARB extraction within a factor of 3 (Section 6). Together, the demonstration that the laboratory SCM applies to both uncontaminated and contaminated sediments increases the credibility of reactive transport simulations that use the SCM approach to describe adsorption.

8 URANIUM(VI) TRANSPORT IN COLUMNS PACKED WITH NATURITA ALLUVIAL AQUIFER SEDIMENTS

8.1 Introduction

Column experiments were conducted to assess if the surface complexation model (SCM) developed in Section 5 was able to account for the transport of U(VI) under variable chemical conditions in well-controlled laboratory experiments, as has also been studied by Barnett et al. (2000). The columns were packed with a grain size fraction of the NABS sample used in the batch adsorption studies (Section 5). The chemical conditions spanned a range that nearly encompassed the variability of alkalinity, pH and U(VI) concentration observed in the field (Section 3). We assessed the applicability of the SCM by comparing predicted breakthrough of U(VI) with four sets of experimental results.

8.2 Materials and Methods

8.2.1 Preparation of Sediments for Column Studies

The material used in the column experiments was a sized and washed fraction of the NABS sample. The characteristics of the NABS sample are described in Sections 4 and 5. The sized material used in the column studies is referred to as the NAT-COL sample.

Batches of the NABS sample were dry sieved through 500 and 125 μm sieves. Material between these two screen sizes was retained. The retained material was then wet sieved through the 125 μm screen with two artificial groundwater solutions, referred to as AGW-1mod and AGW-3. The purpose of the wet sieving was to remove fine particles that might clog column frits or otherwise cause experimental problems. The composition of the AGW-3 solution is described in Section 5. The AGW-1mod solution had lower alkalinity and pH than AGW-3 (0.44 and 7.78, versus 0.54 and 7.89, respectively), and a higher dissolved Ca^{2+} concentration (7 mM versus 4.71 mM in AGW-3). Most of the wet sieving was conducted with AGW-3; AGW-1mod was used only in one initial sieving.

Wash waters (AGW-3) were collected in a bucket, and suspended particles <125 μm in the wash water were allowed to settle. The clear supernatant of the wash water was then reused for the next washing cycle. In addition to the wet sieving, two sedimentation steps on the washed material were performed in AGW-3 in a glass cylinder with the purpose of further removal of fine-grained particles. The washed sediments were air dried in the laboratory. Two batches of 3863 g (Batch #1) and 4084 g (Batch #2) were obtained. For the column experiments described below, only material from Batch #1 was used.

The BET specific surface areas were measured on a Micromeritics TriStar 3000 system. Complete adsorption isotherms were recorded. Specific surface areas were calculated from BET-plots for the range of $0 < p/p_0 \leq 0.2$ atm.

8.2.2 Methods for Column Studies

The column set-up was similar to that described in Kohler et al. (1996) but with some minor modifications. Two ISCO 500D syringe pumps with 500 mL capacity were used. A vertical flow-through pH combination electrode (Cole-Parmer U-05992) was put in-line a few cm downstream of the column outlet, before the fraction collector. The electrode was connected to an Orion SA720 pH meter, and the pH was monitored and recorded at one-min intervals on a PC. The pH electrode was calibrated prior to and at the end of experiments with pH buffers 4, 7 and 10 pumped at the same flow rate as in the experiment. It was noted that the pH electrode was sensitive to pressure changes and this was accounted for in the calibration. The column was a Millipore (Millipore Vantage L VL 22X250) 22 mm inner diameter glass column with adjustable pistons with 1 mm diameter bores and 5 μm end meshes. The length of the packed beds depended on the experiment and was either 13.3

cm or 6.5cm (see below). Experiments were conducted at a flow rate of either 10 or 1 mL/hr.

Some experiments were conducted at partial pressures of CO_2 (pCO_2) greater than in air (0.28% and 2.0%). These experiments required additional modifications in the experimental methods, as it was known that CO_2 gas could permeate through the thin walls of 0.025 and 0.05 cm Teflon tubing. This could cause an increase in pH in the column influent, resulting in changes to dissolved U(VI) speciation and possibly calcite precipitation. To avoid these problems, the entire loading loop was immersed in an electrolyte bath of the appropriate artificial groundwater solution that was sparged with gas at the same pCO_2. In addition, all 0.05 cm Teflon tubing between 1) the pumps, 2) the thick walled Teflon reservoirs, and 3) up to the entrance of the column was guided through 0.95 cm (3/8 inch) Tygon tubing, through which a flow of approximately 60 mL/minute of the gas at the same pCO_2 was maintained.

For experiments conducted under atmospheric conditions, a sucrose solution of density 1.2 g/mL was filled into pump 1, which was used to displace the electrolyte solution from the reservoirs (see Kohler et al., 1996). Pump 2, which was used to displace the pulse solution out of the loading loop, was filled with milli-Q water. For experiments under increased pCO_2, sparged electrolyte solution was filled into both pumps and care was taken that electrolyte from pump 1 did not reach the second Teflon reservoir (Kohler et al., 1996).

Various artificial groundwater solutions were used in the column experiments. Table 8.1 shows the initial compositions of the artificial groundwater solutions. The solutions had similar compositions as those used in batch experiments (Table 5.1), except that chloride was replaced by sulfate. This allowed direct analysis of dissolved U(VI) in the column effluent samples by kinetic phosphorescence analysis (KPA), avoiding any chloride interferences. The solutions were kept slightly undersaturated with respect to calcite for each set of chemical conditions. An automated fraction collected effluent samples that were analyzed for tritium tracer (HTO) by liquid scintillation counting on a Beckman LS 6500 system and for dissolved U(VI) by KPA.

The NAT-COL sediment sample was filled into the column as a thick paste made up in AGW-3COL solution. Once packed, the column was wrapped into aluminum foil to block out light and prevent biological growth. The column was pretreated with AGW-3COL solution (or the solution suitable for the given conditions, see Table 8.1) at a flow rate of 10 mL/hr for several days, and the outflow was collected until approximately 1L was accumulated. The pretreated AGW-3COL that had been in contact with column material was subsequently used to make up the pulse solution, and was also loaded into the Teflon reservoirs as the eluant for experiments.

The solutions were kept in equilibrium with the appropriate pCO_2 before being transferred to the Teflon reservoirs. The pulse solution was spiked with a small volume of a U(VI) stock solution and HTO as a non-reactive tracer. Concentrations in the pulse solutions were 10^{-6}M or 10^{-5}M for U(VI) and approximately 10 nanocuries/mL for HTO. The volume of the pulse was typically 140±5 mL. The flow rate was 10 mL/hr in the experiment designated COL25, and 1 mL/hr in experiments COL26, -27, -28, and -29. After the pulse, the column was eluted with the pre-treated (sediment-contacted) artificial groundwater solution at the same flow rate. During some experiments the laboratory and column temperatures were recorded. A summary of all column experiments conducted is given in Table 8.2.

8.3 Experimental Results

8.3.1 Nitrogen gas adsorption isotherms

Figure 8.1a shows a nitrogen adsorption isotherm for the NAT-COL sample from Batch #1. Figure 8.1b shows the corresponding BET plot. Two samples from Batch #1 and one sample from Batch #2 were analyzed; the mean surface area was 3.06 m^2/g with a standard deviation of 0.05 m^2/g for the three samples. The

Table 8.1 Composition of Artificial Groundwater Solutions used in Column Experiments and Uranium(VI) Species Distribution[1]

Artificial Groundwater	AGW-3COL	AGW-3COL3	AGW-3COL1
pCO_2	373 ppm	0.28%	2.0%
Sodium [M]	$2.41 \cdot 10^{-3}$	$3.00 \cdot 10^{-3}$	$3.65 \cdot 10^{-3}$
Potassium [M]	$6.4 \cdot 10^{-5}$	$6.4 \cdot 10^{-5}$	$6.4 \cdot 10^{-5}$
Magnesium [M]	$1.52 \cdot 10^{-3}$	$1.52 \cdot 10^{-3}$	$1.52 \cdot 10^{-3}$
Calcium [M]	$4.71 \cdot 10^{-3}$	$4.71 \cdot 10^{-3}$	$4.71 \cdot 10^{-3}$
Sulfate [M]	$7.19 \cdot 10^{-3}$	$7.06 \cdot 10^{-3}$	$6.26 \cdot 10^{-3}$
Bicarbonate [M], (added as $NaHCO_3$)	$5.38 \cdot 10^{-4}$	$1.40 \cdot 10^{-3}$	$3.65 \cdot 10^{-3}$
$Alk_{initial}$ [meq/L], calculated	0.538	1.40	3.65
$pH_{initial}$, calculated	7.85	7.41	6.99
Calcite undersaturation, calculated[2]	0.815	0.801	0.817
Ionic strength [M] calculated	0.0218	0.0223	0.0227
Equilibrated with Calcite			
Alk [meq/L], calculated	0.562	1.51	3.93
pH, calculated	7.90	7.45	7.02
Ca^{2+} [M], calculated	$4.74 \cdot 10^{-3}$	$4.79 \cdot 10^{-3}$	$4.88 \cdot 10^{-3}$
Ionic strength [M], calculated	0.0218	0.0225	0.0231
Major Species in % (total U(VI) =10^{-5}M)			
$(UO_2)_2(OH)_3(CO_3)^-$	67.0	31.0	3.4
$UO_2(CO_3)_3^{4-}$	9.3	38.6	53.8
$UO_2(CO_3)_2^{2-}$	21.9	27.8	39.4
$UO_2CO_3^0{}_{aq}$	0.0	2.2	3.2

[1] U(VI) speciation calculated with HYDRAQL (Papelis et al., 1988) using the thermodynamic data given in Section 2.
[2] $\{Ca^{2+}\}\{CO_3^{2-}\}/K_{sp}$ for calcite

Table 8.2 Summary of Column Experiments

Experiment	Mass of Solid [g]	Pore Volume [mL]	Length [cm]	Pulse volume [mL]	U(VI) pulse concentration [M]	pCO_2
COL25	79.4±0.4	20.4±0.3	13.25±0.05	138.6±0.5	$9.5 \cdot 10^{-6}$	373 ppm
COL26	38.6±0.4	9.95±0.3	6.4±0.05	144.3±0.5	$1.0 \cdot 10^{-5}$	373 ppm
COL27	39.8±0.4	9.36±0.3	6.5±0.05	144.1±0.5	$1.23 \cdot 10^{-5}$	2%
COL28	40.4±0.4	10.24±0.3	6.5±0.05	143.9±0.5	$1.0 \cdot 10^{-6}$	2%
COL29	40.1±0.4	10.0±0.3	6.5±0.05	144.5±0.5	$1.0 \cdot 10^{-5}$	0.28%

BET C parameter ranged from 670 to 730 (Gregg and Sing, 1982). The reproducibility was quite good between the two batches and two samples of batch #1. However, the error of the measurement is in the range of 10%, and so the value was rounded up to of 3.1 m^2/g for all calculations. This value is smaller than that found for the 125-250 and 250-500 μm grain size fractions of the NABS sample (5.1 and 3.95 m^2/g, respectively, Table 4.1). The difference is likely caused by the removal of fine material from the NABS sample during the wet sieving and washing pretreatment of the NAT-COL sample.

8.3.2 Total U concentration by γ-Spectrometry and HH Extractable U

Total U concentration by γ-spectrometry and extractable U by hydroxylamine-hydrochloride (HH) were determined on the NAT-COL sample, using the methods described in Section 6. A total U content of $6.6 \cdot 10^{-9}$ moles/g was found, somewhat smaller than the U content of the <3 mm NABS sample ($9.6 \cdot 10^{-9}$ moles/g). HH-extractable U ($1.1 \cdot 10^{-9}$ moles/g) was considerably smaller than total U, indicating that most of the U was within the crystalline matrix in the NAT-COL sample, rather than adsorbed (see Section 4).

8.3.3 U(VI) Adsorption Isotherm on the NAT-COL Sample

A U(VI) adsorption isotherm was determined for the NAT-COL sample in AGW-3 solution at pH 7.9±0.1 at the pCO_2 in air (Fig. 8.2). The slope of the log-log plot is 0.82, with a correlation coefficient of 0.995. The isotherm can be interpreted as a Freundlich isotherm, $\log q = \log K_f + (1/n) \cdot \log C$, where q is the adsorbed U(VI) and C is dissolved U(VI), and the slope equals the coefficient (1/n). Log-log isotherms with slopes different than 1 indicate non-linear adsorption. It is interesting to note that very similar values for 1/n of 0.85±0.02 were obtained for uranium adsorption on quartz at the acidic pH values near 4 (Kohler et al., 1996; Kohler and Davis, 2001).

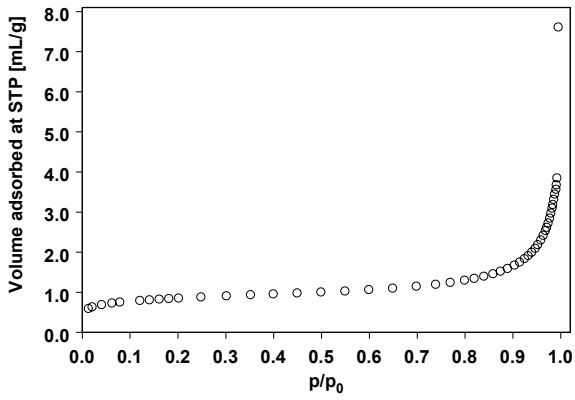

Figure 8.1a. Nitrogen gas adsorption isotherm of the NAT-COL sample.

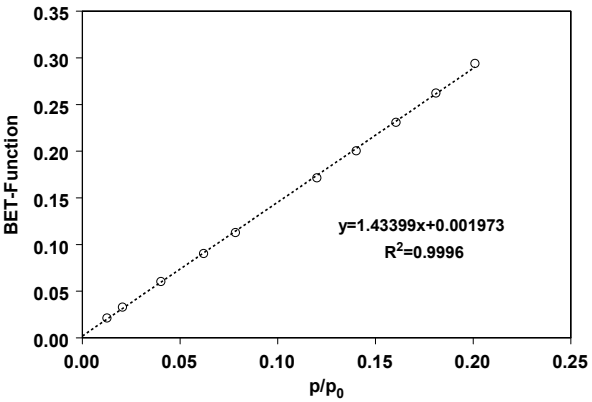

Figure 8.1b. BET-plot for the NAT-COL sample.

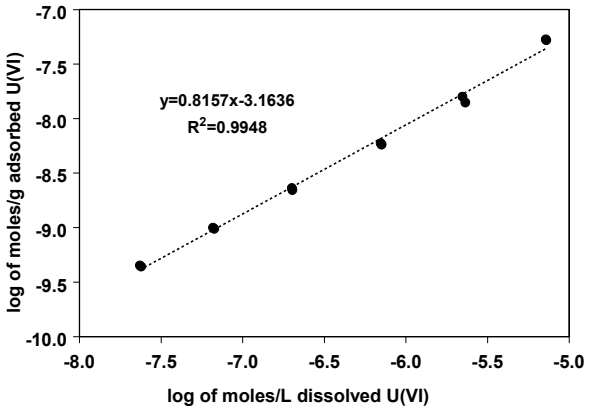

Figure 8.2. Adsorption isotherm of U(VI) on the NAT-COL sample at pH 7.9 and at the pCO_2 in air.

8.3.4 Column Characteristics

A linear packing density of 6.024 g/cm was determined from a preliminary column experiments with 150 g of Naturita sediment and a column length, L, of the packed bed of 24.9 cm. Experiments COL25 and COL26 (Table 8.2) had packed bed lengths of 13.25 cm and 6.4 cm, respectively. Based on the packing density of 6.024 g/cm, the mass of sediment for COL25 and COL26 was calculated to be 79.82 g and 38.55 g, respectively. The porosity, n, of the packed bed was calculated from the column geometry (2.2 cm inner diameter and measured packed bed length) and the mass of sediment packed given above, assuming a value of 2.65 g/cm^3 for the sediment density. A value of n = 0.402 was obtained, which is independent of column length.

For the average linear pore water velocities, $v = Q/(A \cdot n)$, where A is the column cross-sectional area (3.80 cm^2) and Q is the flow rate (Table 8.3). Values of $1.81 \cdot 10^{-3}$ cm/sec and $1.81 \cdot 10^{-4}$ cm/sec were calculated for v in experiments COL25 and COL26, respectively (Table 8.3). The hydrodynamic dispersion coefficients, D_h, for COL25 and COL26 were estimated based on the tritium (HTO) breakthrough curves, according to the graphical method described in Bear (1979). Values for D_h are given in Table 8.3, together with the Peclet numbers (Pe = $v \cdot L/D_h$).

The normalized HTO breakthrough curves for both experiments are shown in Figure 8.3. As expected, the slower flow rate led to greater dispersion. Despite the shorter column length in experiment COL26, the spreading of the breakthrough for the slow flow rate was wider than in experiment COL25 if measured in units of pore volumes.

Values for the dispersivity (α) and the molecular diffusion coefficient (D_m^*) of HTO in the porous medium were obtained from a plot of D_h vs. v, according to:

$$D_h = \alpha \cdot v + D_m^*$$

The slope, α was $4.4 \cdot 10^{-2}$ cm and the intercept, D_m^* was $3.1 \cdot 10^{-6}$ cm^2/sec. Thus, The diffusion coefficient of HTO in the porous medium was approximately one order of magnitude smaller than in pure water ($2.4 \cdot 10^{-5}$ cm^2/sec; Nakayama and Jackson, 1963).

8.3.5 Influence of Flow Rate on U(VI) Transport

Figure 8.4 shows the effect of the flow rate, Q, on the transport of U(VI) through the column filled with the NAT-COL sample. Breakthrough curves for U(VI) were normalized to the pore volume because different lengths for the packed media were used in the two experiments (Table 8.2). Both experiments were conducted at a total U(VI) inlet concentration of $1 \cdot 10^{-5}$M. Pulses of approximately 140 mL were used in each experiment, which corresponded to pulse lengths of 7 and 14 pore volumes for experiments COL25 and COL26, respectively. Both breakthrough curves are of the same general asymmetric shape, with a relatively steep rising limb and a long tail. In experiment COL25, U(VI) breakthrough (half height of the rising limb) occurred at about 9 pore volumes, earlier than in experiment COL26 (about 14 pore volumes). This demonstrates that the time scales of the sorption/desorption processes (reaction kinetics) and/or mass transfer processes (diffusion into pore spaces) are of the same order or exceed the residence time in the column experiments (2 and 10 hr for COL25 and COL26, respectively). In batch sorption experiments with the NABS sample, U(VI)

Table 8.3 Estimated Hydrodynamic Parameters for Experiments COL25 and COL26

Experiment	Q [mL/hr]	v [cm/sec]	D_h [cm^2/sec]	Pe
COL25	**10**	**$1.82 \cdot 10^{-3}$**	**$8.29 \cdot 10^{-5}$**	**291**
COL26	**1**	**$1.82 \cdot 10^{-4}$**	**$1.11 \cdot 10^{-5}$**	**105**

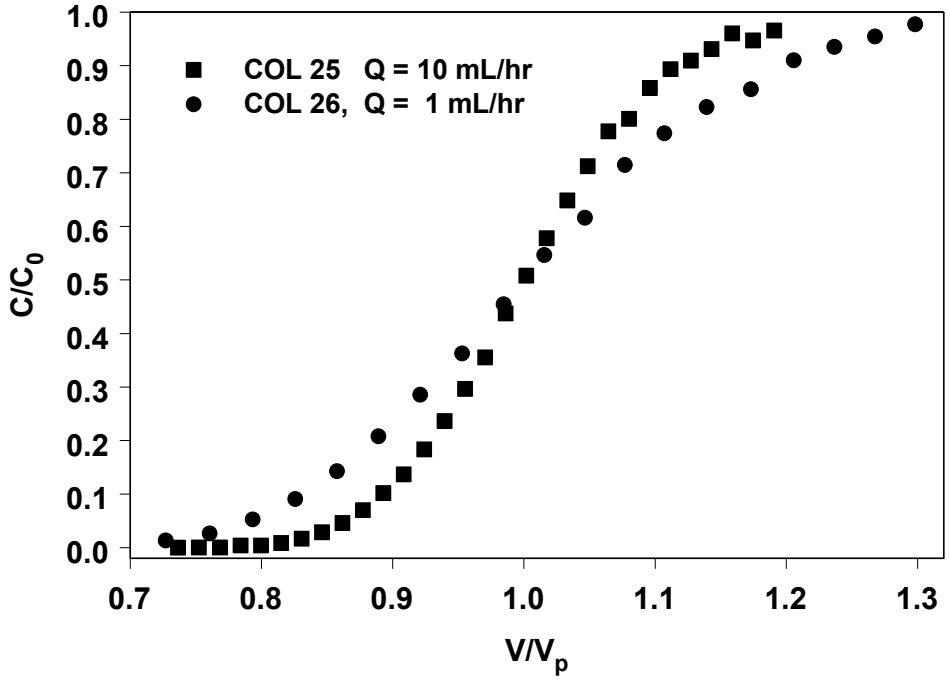

Figure 8.3. Breakthrough curves for the tritium tracer (HTO) in experiments COL25 and COL26, illustrating the dispersion of the non-reactive tracer at two different flow rates and column lengths. C = HTO concentration; C_o = inlet HTO concentration; V = volume of eluant passing through a column beginning with the pulse; V_p = column pore volume

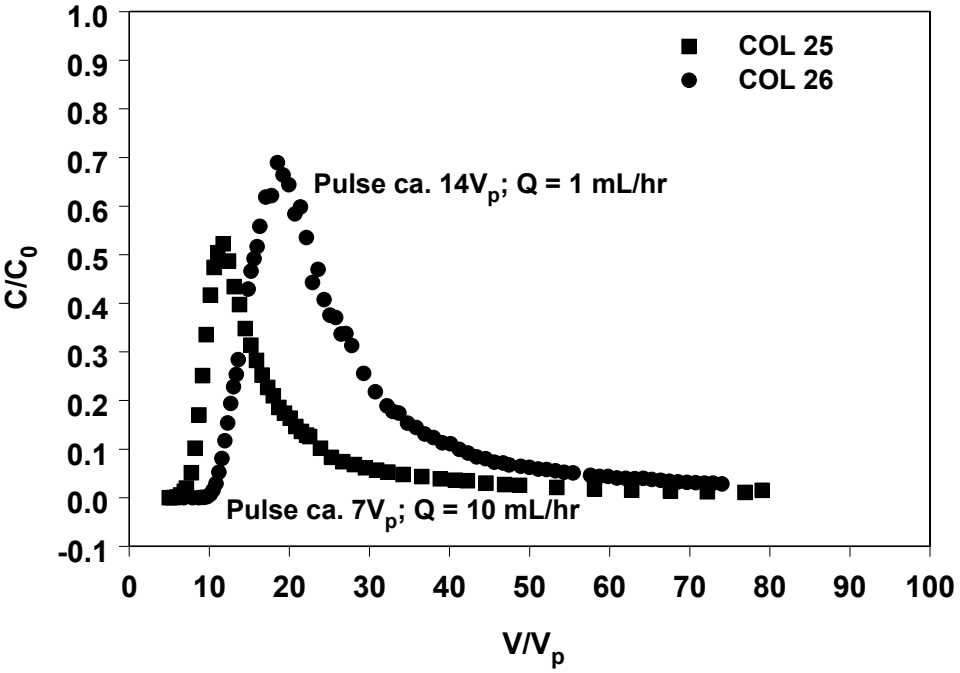

Figure 8.4. Breakthrough curves of U(VI) in experiments COL25 and COL26 at flow rates of 10 and 1 mL/hr. C = aqueous U(VI) concentration; C_o = inlet U(VI) concentration; V = volume of eluant beginning with the pulse; V_p = column pore volume.

uptake was near completion after approximately 4 days (Section 5). However, a direct comparison of the two systems is not straightforward, because different solid/liquid ratios exist in the column and batch experiments, which affects the surface site density distribution in per volume of water. Since the U(VI) sorption on the NAT-COL sample is non-linear (Fig. 8.2), asymmetrical breakthrough curves were expected.

8.3.6 Influence of variable chemical conditions on U(VI) transport

Figure 8.5 shows the effect of variable U(VI) inlet concentration on U(VI) transport. Breakthrough of the leading edge for an inlet concentration of 10^{-5}M U(VI) was approximately at 4 pore volumes (37.4 mL), whereas breakthrough at 10^{-6}M U(VI) occurred at 6 pore volumes (61.4 mL). The U(VI) inlet concentration was the only significant difference in conditions between these two experiments (COL27 and COL28); both were conducted at 2% pCO_2. An earlier breakthrough at the higher U(VI) inlet concentration is expected based on the non-linearity of the sorption isotherm (Fig. 8.2) and an assumption of local equilibrium. Temperature stability problems in the laboratory likely caused the scatter in data observed around the top of the breakthrough curve for the 10^{-6}M U(VI) inlet concentration.

Figure 8.6 shows the effect of pCO_2 on the breakthrough of U(VI), under otherwise nearly identical conditions. For comparison, the breakthrough curves of the non-reactive tracer, HTO, are also shown in the figure. All U(VI) breakthrough curves exhibited rather steep rising limbs and relatively long trailing tails. Increasing the pCO_2 from atmospheric to 2% resulted in a nearly 4-fold decrease in retardation of the U(VI) leading edge of breakthrough (from 14.9 pore volumes in experiment COL26 to 4.2 pore volumes for COL27). In the hypothetical case of a linear U(VI) isotherm and local equilibrium, the observed change in retardation (by a factor of 3.5) is consistent with a decrease in the K_d value by a factor of 4.5 at the observed porosity of 0.4.

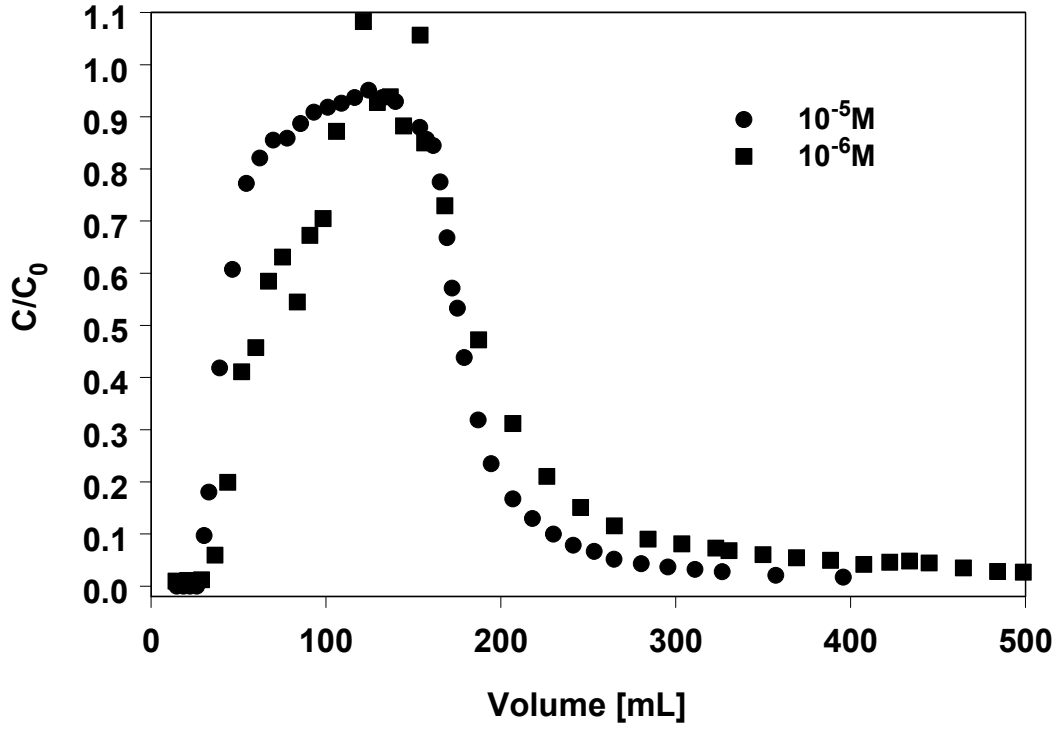

Figure 8.5. Influence of U(VI) inlet concentration, C_0, on the breakthrough of U(VI) in experiments COL27 and COL28. C = concentration of aqueous U(VI).

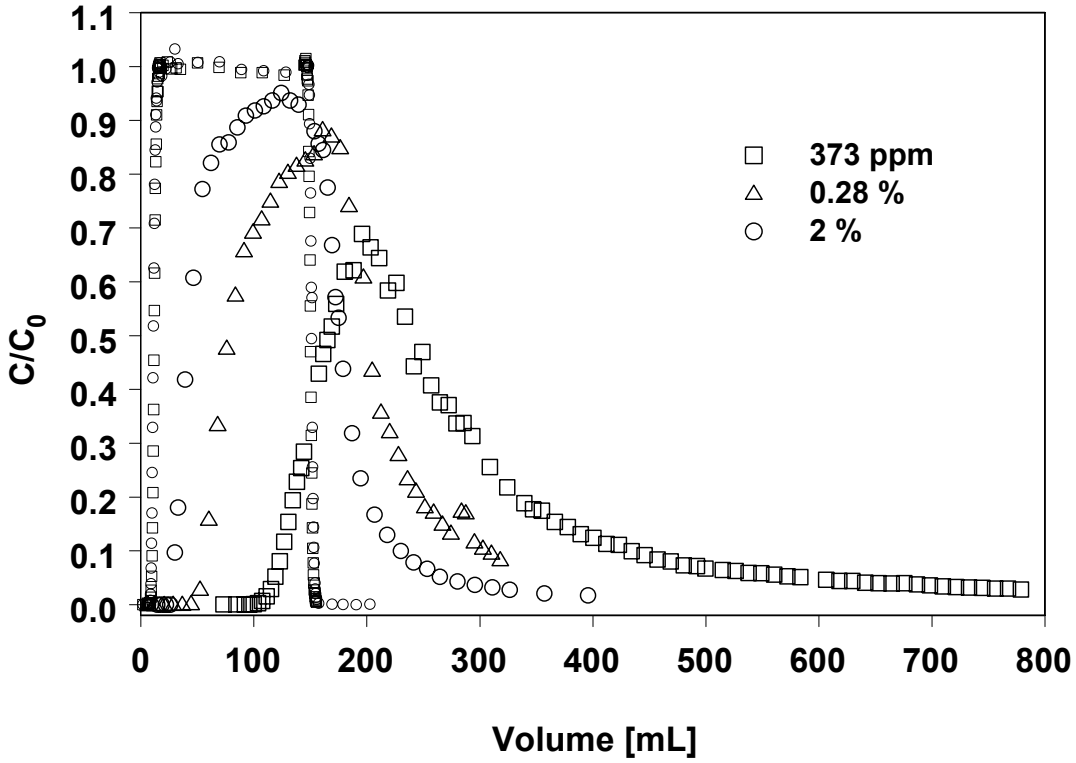

Figure 8.6. Breakthrough of U(VI) at various partial pressures of CO_2. The rectangular pulse shapes are the pulses of the non-reactive tritium (HTO) tracer. Experiments COL26, COL27, and COL29. C = concentration of aqueous U(VI); C_o = inlet U(VI) concentration.

The observation of the decrease in U(VI) transport at higher pCO_2 is significant and clearly demonstrates the potential importance of temporal and spatial variations in alkalinity on the mobility of U(VI). With increasing pCO_2, the mononuclear uranyl-carbonate complexes become the predominant species in the solutions, and the binuclear mixed hydroxy-carbonate complex decreases in concentration (see Table 8.1). Observations of pCO_2 in the range of 1-5%, caused by microbiological activity, are quite common in groundwater/aquifer systems (Hem, 1985). For the Naturita aquifer, pCO_2 values of 2 to 10% were estimated (Section 7), and this causes a range of U(VI) K_d values of more than an order of magnitude (Section 5).

8.3.7 Flow Interruption Experiments

Experiment COL29 was a flow interruption experiment. The purpose of this type of experiment is to obtain information on reaction kinetics and/or mass transfer processes. When the flow into the column is stopped at some point in time, slow chemical reaction kinetic or mass transfer processes will continue to evolve toward local equilibrium. If the column is not at local chemical equilibrium when the flow is stopped and later resumed, a step change in U(VI) concentration may be observed at the outlet of the column. Breakthrough curves of this type can then be analyzed and simulated by reactive transport models to gain additional information about the slow processes (Brusseau et al., 1989; Koch and Flühler, 1993).

Flow was interrupted twice during the experiment (Fig. 8.7). The first interruption occurred at elution volume of approximately 190 mL. Because the interruption occurred during the relatively steep decrease in U(VI) concentration as the pulse was eluting, the increase in U(VI) concentration is hard to discern but is still visible slightly below 200 mL. However, the second flow interruption at 280 mL led to a sharp increase in U(VI) concentration in the tail of the pulse. Both

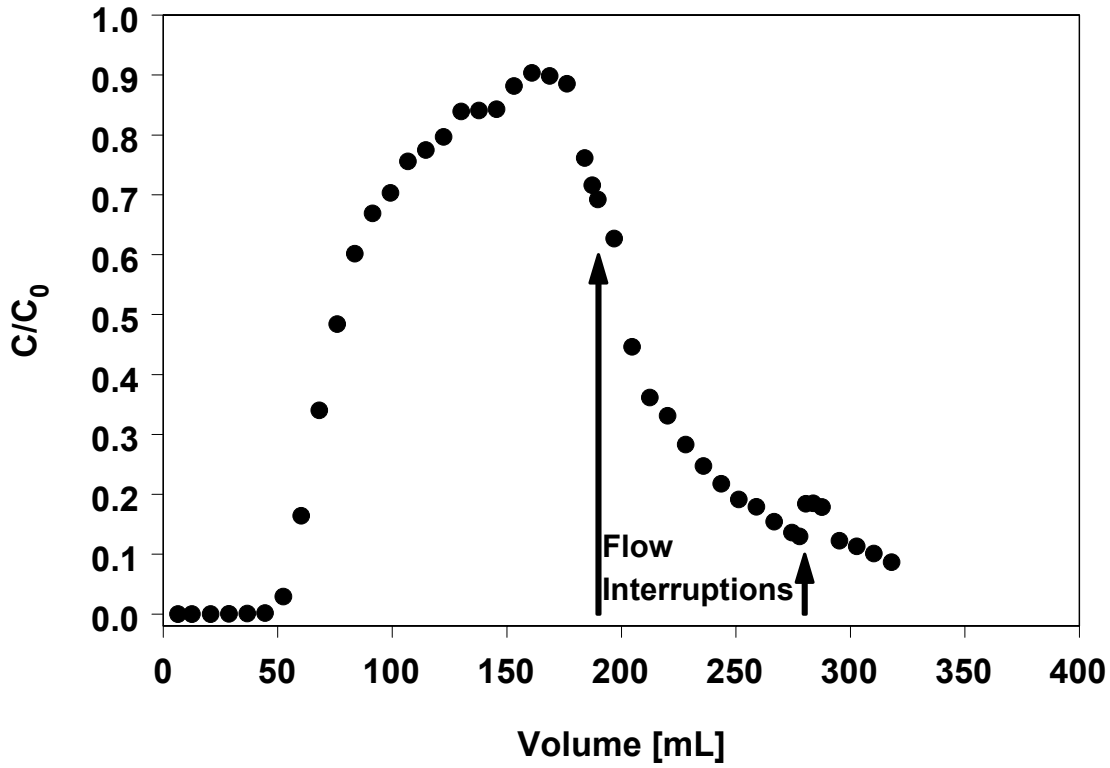

Figure 8.7. Flow interruption experiment (COL29) with the NAT-COL sample. Flow was stopped for 100±5 hours at elution volumes of 190 mL and 280 mL. C = concentration of aqueous U(VI); C_o = inlet U(VI) concentration.

interruptions lasted approximately four days (10 pore volumes).

Figure 8.8 shows the profile of the major metal concentrations in the effluent during the elution. The concentrations remained essentially stable (within the analytical error of 5%). It appears that slight increases in dissolved Ca and Si concentrations were observed during the interruptions of the flow at 190 and 280 mL elution volume, presumably due to dissolution of mineral phases, such as calcite, quartz, or feldspars.

8.4 Model Results

Model predictions were performed using the surface complexation model (SCM) developed for the NABS sample in Section 5 (the version of the model that did not consider formation of the aqueous species, $CaUO_2(CO_3)_3^{2-}$ and $Ca_2UO_2(CO_3)_3^{0}$(aq)). The difference in specific surface area between the NABS and NAT-COL samples was accounted for by assuming that the site densities of the two samples were equal per unit surface area. No other adjustments were made to the SCM model. Model predictions were made to evaluate if the SCM model calibrated from the batch sorption experiments with the NABS sample was capable of describing the U(VI) retardation observed in the column experiments with the NAT-COL sample.

8.4.1 Batch U(VI) Adsorption Isotherm

The agreement between the experimentally observed adsorption isotherm (see Fig. 8.2) and a model-predicted isotherm is illustrated in Figure 8.9. At low dissolved U(VI) concentration, the simulated adsorbed concentrations are approximately a factor of two (~0.3 log units) greater than the measured concentrations. At the highest dissolved U(VI) concentrations, there was near perfect agreement between the model predictions and the measured values. The SCM was calibrated to describe

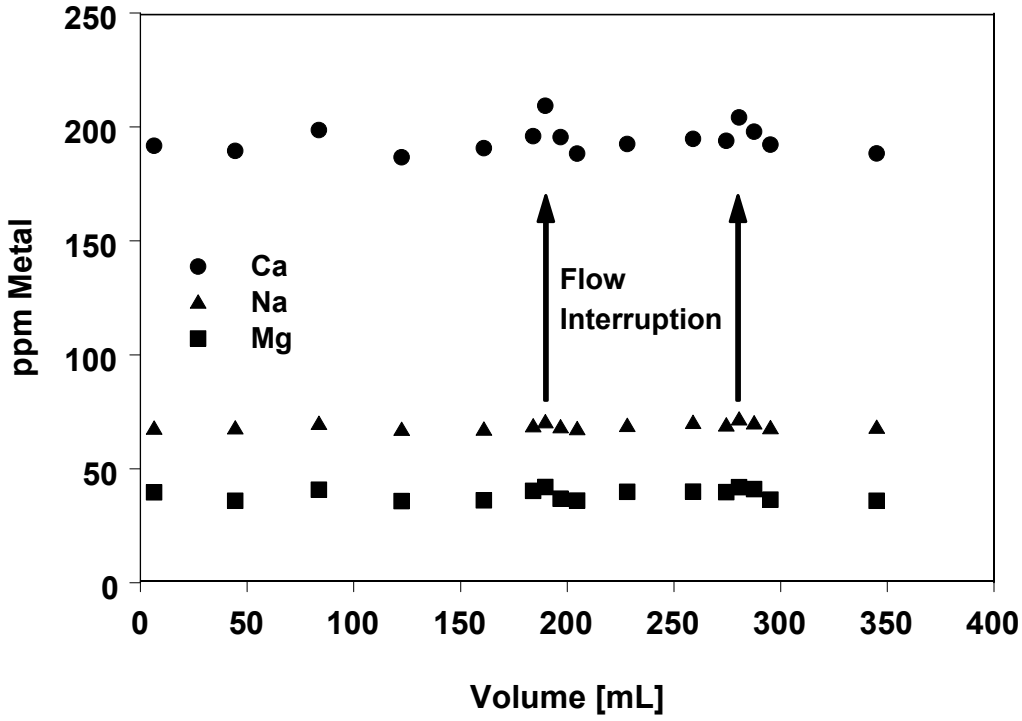

Figure 8.8a. Metal concentrations in the column effluent of experiment COL29. Slight increases in the Ca^{2+} concentration occurred at the times of flow interruption.

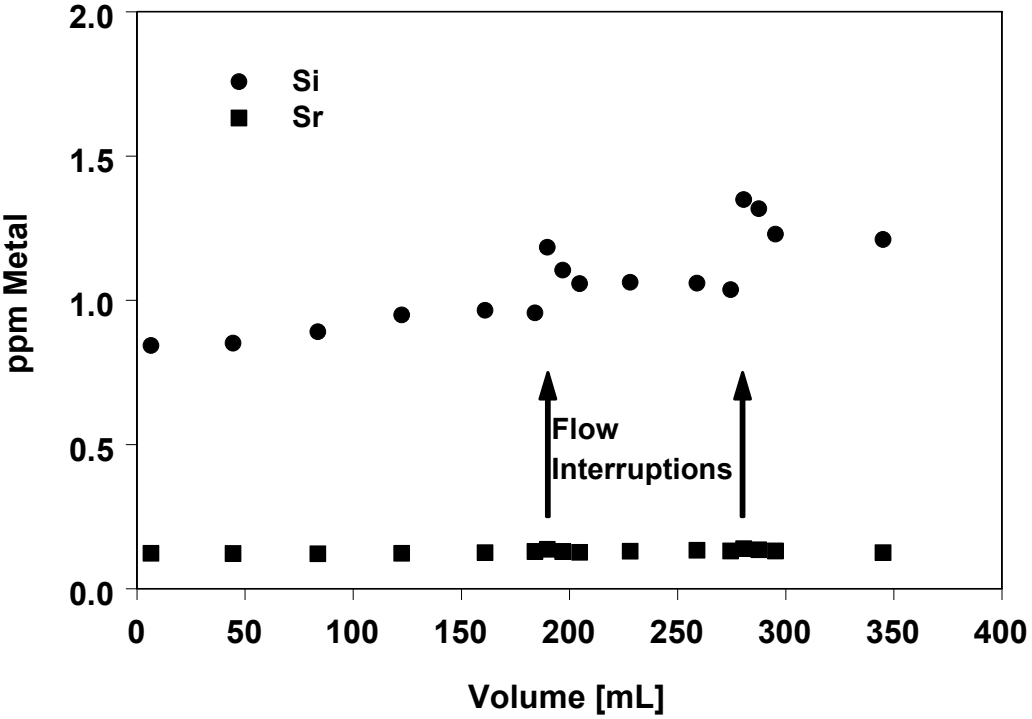

Figure 8.8b. Dissolved Sr and Si concentrations in the column effluent of experiment COL29. Slight increases in the Si concentration occurred at the times of flow interruption.

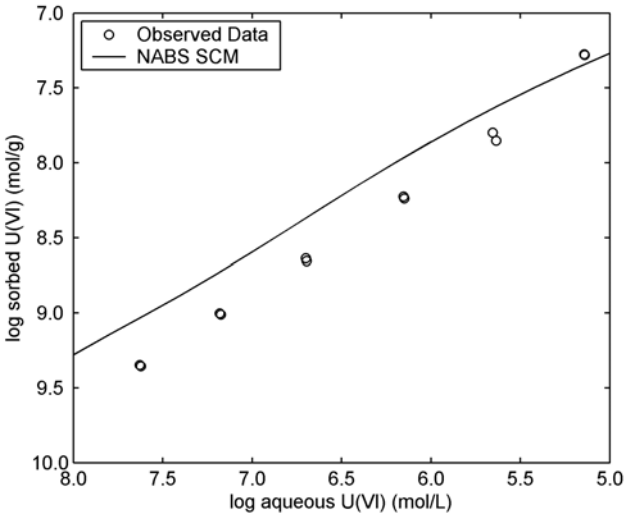

Figure 8.9. Comparison of U(VI) adsorption isotherm predicted with the SCM developed for the NABS sample and the observed U(VI) adsorption data with the NAT-COL sample.

U(VI) adsorption over a wide range of conditions, and the average error between the experimental data points and model predictions is of the order of 0.15 log units for the NABS sample (Section 5). Thus, the agreement between the experimental data for the NAT-COL sample and the model predictions was slightly worse, but still seems good given the extensive washing to the NAT-COL sample and the 40% decrease in the surface area.

8.4.2 U(VI) Retardation as a Function of Chemical Conditions

Model predictions were performed for experiments COL26 to COL29 using the local equilibrium assumption (LEA). Experimental results for COL25 were not simulated, because it seems likely that U(VI) transport in that experiment was affected by rate-controlled processes at the higher flow rate.

Figure 8.10 compares the observations and predictions of U(VI) breakthrough. In general there is good agreement between the predictions and the data. This is particularly true for experiments COL27 and COL28 which were conducted at 2% pCO_2, pH 7 and at two different U(VI) inlet concentrations. In both cases, the leading edge of the observed breakthrough curve is matched very closely by the model-predicted curves. However, in both cases, there is more tailing in the data than is indicated by the model-predicted curves. This may result because the model has only three sites, and therefore cannot completely reproduce the non-linearity of the adsorption isotherm at the very low U(VI) concentrations that occur during the tailing. An alternative explanation is that slow sorption kinetics causes the observed tailing.

For experiments COL26 and COL29, there is generally a good fit of the model curves to the data, although not as good as for experiments COL27 and COL28. In both cases, the model predicts approximately 15-20% greater U(VI) retardation than was observed in the experiments. The causes for the differences are not known. It is possible that kinetic factors are more important at the higher pH values, as this has been observed in U(VI) column experiments with pure quartz powders (Curtis et al., 1999).

The model predictions account for most of the observed variability in retardation. The pore volumes required for breakthrough of the leading edge of the U(VI) pulses increased from 4.2 to 7.2 to 14.9 as the pCO_2 decreased from 2% to 0.28% to 0.037%. As discussed previously, these changes are consistent with an observed increase in the K_d value by a factor of 4.5. The model predictions suggest that the change in aqueous chemical conditions should cause an increase in the K_d value by a factor of 4.6. Thus, most of the observed variability in K_d values was captured by the model predictions without changing the values of any SCM model parameters.

8.5 Summary

Experiments were conducted to investigate the effects of variable chemical conditions on U(VI) transport through columns packed with sediments from the Naturita alluvial aquifer. Experiments were conducted with a size fraction (125-500 μm) of the NABS sample (Section 4).

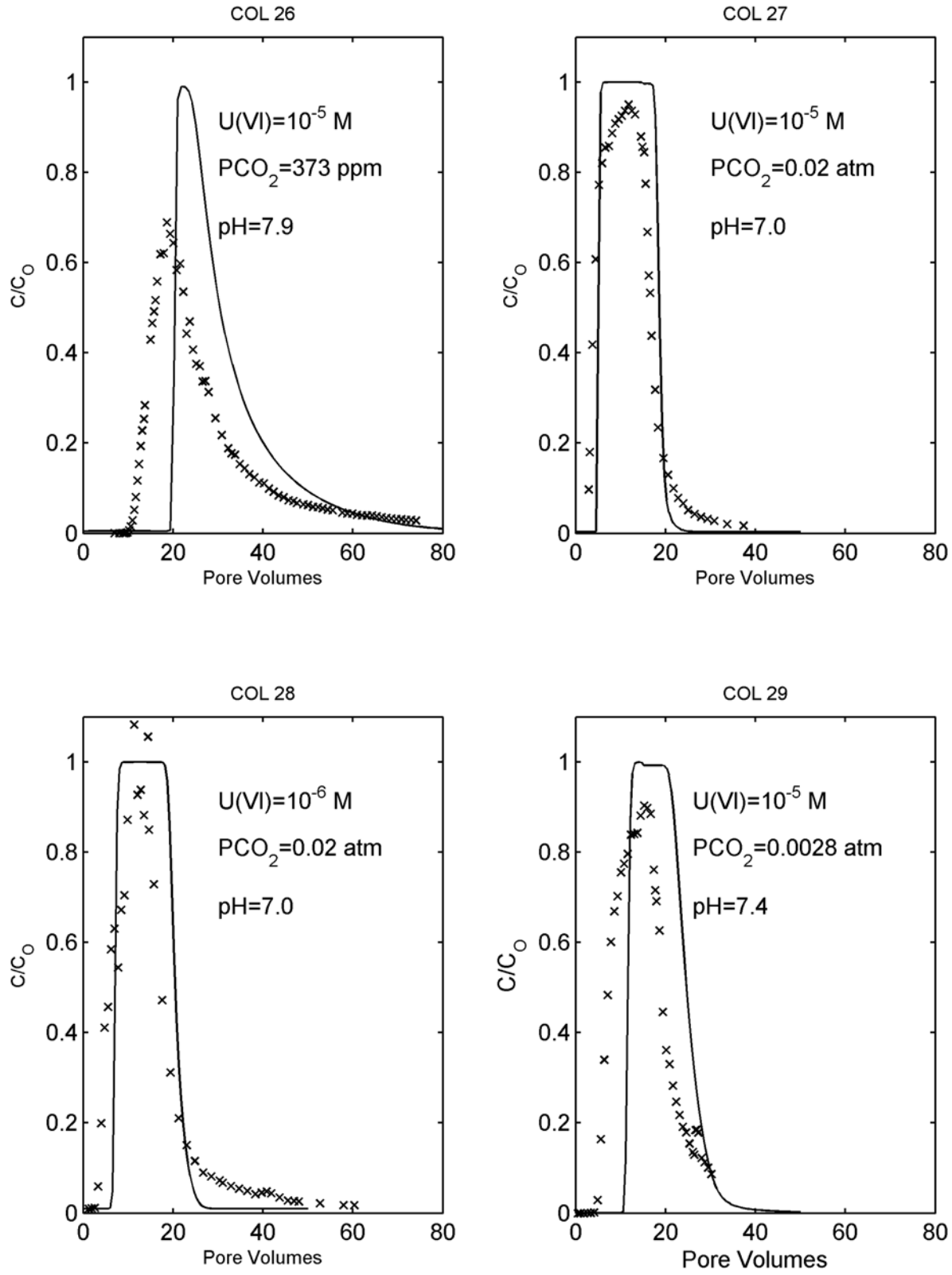

Figure 8.10. Comparison of experimental U(VI) breakthrough curves through columns packed with the NAT-COL sample with curves predicted by a transport model that includes the SCM developed from batch experiments with the NABS sample.

The sized fraction, referred to as the NAT-COL sample, had a specific surface area that was 40% less than that of the NABS sample. U(VI) adsorption onto the NAT-COL sediment at pH 7.9 and atmospheric CO_2 could be described by a Freundlich isotherm, and the slope of the isotherm agreed well with that observed for pure quartz powder. Batch adsorption data collected for the NAT-COL sample was predicted well using the SCM model calibrated for the NABS sample with the assumption that the site densities per unit surface area were the same for both samples. The SCM predicted U(VI) adsorption very well at high U(VI) concentrations (10^{-5} M), but overpredicted adsorption by a factor of 2 at lower U(VI) concentrations (10^{-7} M).

Column experiments conducted by the introduction of pulses of U(VI) demonstrated that U(VI) retardation is significantly affected by variable chemical conditions, especially variable pCO_2 and pH. Because of the presence of calcite in the NABS sample, the pCO_2 and pH values were not varied independently. The transport model predictions strongly suggest that dissolved carbonate is the most important chemical variable in the Naturita alluvial aquifer. The pore volumes required for the breakthrough of the leading edge of the U(VI) pulses increased from 4.2 to 7.2 to 14.9 as the pCO_2 decreased from 2% to 0.28% to 0.037%. This observed variation was predicted by the SCM, assuming local chemical equilibrium and without adjusting any SCM parameters.

9 REACTIVE TRANSPORT MODELING OF URANIUM(VI) IN THE ALLUVIAL AQUIFER AT THE NATURITA UMTRA SITE

9.1 Introduction

Transport of U(VI) in laboratory columns has been successfully modeled by Kohler et al. (1996) using a surface complexation model (SCM). These authors examined variable pH, ligand concentration and U(VI) concentration, and calibrated a non-electrostatic SCM to 3 column experiments packed with well characterized quartz powder. The calibrated reactive transport model that incorporated the SCM predicted the effects of a complexing ligand (fluoride) and variable pH on U(VI) adsorption and retardation. However, the SCM modeling approach has only been used in a few field scale applications. Stollenwerk calibrated a diffuse layer SCM to simulate molybdate (Mo) transport in laboratory columns (Stollenwerk, 1995), and then successfully predicted Mo transport at the Cape Cod field site (Stollenwerk, 1998). Kent et al. (2000) successfully simulated the pH-dependent transport of Zn in the same sand and gravel aquifer with a non-electrostatic SCM. Similar success has not yet been demonstrated for U(VI), which has more complex aqueous and surface speciation than either Mo or Zn.

Reactive transport modeling was performed to demonstrate that the observed distribution of dissolved U(VI) within the Naturita alluvial aquifer could be reproduced using independently determined hydraulic properties of the aquifer and independently determined adsorption properties of the Naturita aquifer background sediment sample (the NABS sample, see Section 5). The simulations did require that the source term be approximated.

This section describes: (1) the effect of variable chemical conditions at the Naturita site on U(VI) transport, (2) application of the reactive transport model to reproduce the current existing conditions, (3) results of a sensitivity analysis that evaluates the effects of SCM parameters, hydraulic conductivity, and background U(VI) concentrations on predicted U(VI) transport, and (4) results of simulations that test some of the assumptions made in formulating the conceptual model for reactive transport. Simulations were performed using RATEQ (Curtis, 2003), which couples reactive transport to MODFLOW (Harbaugh and McDonald, 1996) and MT3DMS (Zheng and Wang, 1999). Selected simulation results were confirmed with FITEQL (Herbelin and Westall, 1994) and PHREEQC (Parkhurst and Appelo, 1999).

9.2 Conceptual Reactive Transport Model

The conceptual reactive transport model extends the conceptual model of flow and non-reactive transport (see Section 3) by accounting for chemical reactions that occur in the aquifer. Both aqueous complexation and surface complexation reactions were included. The aqueous reactions were described in Section 2, and these account for the formation of both U(VI) hydrolysis species and U(VI)-carbonate species, with the exception that the aqueous species, $CaUO_2(CO_3)_3^{2-}$ and $Ca_2UO_2(CO_3)_3^0(aq)$ (Brooks et al., 2003), were not considered here. For comparison, model simulations that consider these aqueous species are given in Curtis et al. (2003b). The adsorption reactions were accounted for by including the SCM developed for the NABS sample from laboratory experiments (see Section 5). The SCM consists of 4 reactions and 3 different site types that are listed in Table 9.1 as Model 1. The three site types are described as: very strong, strong, and weak sites, corresponding to the strength of their U(VI) binding (Table 9.1). The different site types are used to describe non-linear isotherms commonly observed for cations on oxides (Davis and Kent, 1990; Kohler et al., 1996). The SCM includes seven parameters. There are four equilibrium constants for the adsorption reactions (i.e., K_W, K_{SC}, K_{SS}, and K_{SSC} in Table 9.1) and three site concentrations (i.e., $>WOH_T$, $>SOH_T$, and $>SSOH_T$). The SCM was previously shown to give model K_d values that agreed with field observations within a factor of

Table 9.1: Generalized Composite Surface Complexation Model for U(VI) Adsorption by the NABS sample[1]

Reaction	Symbol[2]	Log *K*	k_f
Model 1: Reactions written in terms of the UO_2^{+2} aqueous species			
$UO_2^{+2} + >WOH + H_2O = >WOUO_2OH + 2H^+$	K_W	-6.74	$5 \cdot 10^8$
$UO_2^{+2} + >SOH + H_2CO_3 = >SOUO_2CO_3^- + 3H^+$	K_{SC}	-8.00	$3 \cdot 10^{15}$
$UO_2^{+2} + >SSOH + H_2O = >SSOUO_2OH + 2H^+$	K_{SS}	-2.06	$1 \cdot 10^{12}$
$UO_2^{+2} + >SSOH + H_2CO_3 = >SSOUO_2CO_3^- + 3H^+$	K_{SSC}	-6.36	$6 \cdot 10^{15}$
Model 2: Reactions written in terms of the $UO_2(CO_3)_2^{-2}$ aqueous species			
$UO_2(CO_3)_2^{-2} + >WOH + H_2O = >WOUO_2OH + 2H^+ + 2CO_3^{-2}$		-23.68	$2 \cdot 10^3$
$UO_2(CO_3)_2^{-2} + >SOH = >SOUO_2CO_3^- + H^+ + CO_3^{-2}$		-8.53	$1 \cdot 10^5$
$UO_2(CO_3)_2^{-2} + >SSOH = >SSOUO_2CO_3^- + H^+ + CO_3^{-2}$		-6.62	$3 \cdot 10^5$
$UO_2(CO_3)_2^{-2} + >SSOH + H_2O = >SSOUO_2OH + 2H^+ + 2CO_3^{-2}$		-19.00	$3 \cdot 10^6$

[1] See Section 5 for model details. Total site density of 1.92 μmoles/m^2 of monodentate sites was assumed (= 3.84 μmoles/m^2 hydroxyl groups). Distribution of sites was 98.79% weak (>WOH), 1.2% strong (>SOH) and 0.01% very strong (>SSOH).

[2] The symbols are used in Figures 9.7, 9.8, and 9.9 to identify different model parameters.

2 to 3 (see Sections 6 and 7). The concentration of adsorption sites was calculated from the average surface area of the aquifer sediments of 12.4 m^2/g (Section 4) and total surface site density of 1.92 μmoles/m^2 (Section 5). The SCM was developed for the NABS sample, which was screened to remove particles that had a diameter >3 mm. As described in Section 4, the NABS sample was a sized fraction of a large composite sample collected with a backhoe. The composite sample was estimated to contain about 50% cobbles (>64mm) that were removed in the field. Based on a particle size analysis of the <64 mm fraction, it was estimated that NABS sample represented 15% of the aquifer sediments (Section 4). Assuming that the relatively large fraction of sediments >3 mm in the alluvial aquifer had an insignificant adsorption capacity, a total solids concentration of 1190 g/L of groundwater was calculated for the reactive transport modeling.

The transport simulations assumed that the groundwater was in equilibrium with the calcite that is present in the aquifer (Section 4). Groundwater samples were in equilibrium with calcite (Section 3). It was assumed that the effects of the variable aqueous carbonate concentration, and therefore the dominant effects on U(VI) mobility, could be simulated by only considering calcite equilibria. The simulations did not consider the dissolution equilibria of other elements, such as V, K, Mg or Si. The simulations also did not consider the transport of Na, Cl, or sulfate ions, which are the major contributors to ionic strength.

Several assumptions were made in applying the SCM to the field scale simulations. These include the assumptions that: (1) local chemical equilibrium applies, (2) the effect of surface charge caused by the formation of the ternary carbonates surface species is negligible, (3) the composition of the recharge water from the river can be approximated by the background groundwater composition, and (4) the redox conditions were generally oxic, so that redox reactions could be ignored. The first two

assumptions are tested in separate simulations below. The assumption that the recharge water has the same composition as the background water is supported by observations at well DM-1, which is ~10 m from the river but has pH and alkalinity values that are similar to the values at well DOE-547 (Section 3). The assumption that redox reactions are not important is based on the existing high dissolved U(VI) concentrations (Section 3) and the N_2-headspace extraction results of freshly collected sediments that suggested that no U(IV) was on the sediment surfaces (see Section 6).

9.3 Effect of Variable Chemical Conditions on U(VI) Adsorption and Transport

U(VI) K_d values were computed from the observed geochemical conditions in the Naturita alluvial aquifer and the SCM developed for the NABS sample. Model-predicted K_d values were computed using the 469 groundwater analyses (Section 3) using a temperature of 25ºC, which approximates conditions in the laboratory for which the U(VI) adsorption data were collected. Figure 9.1 shows that the computed K_d values have an average of 3.96 mL/g and range from 0.29 to 22 mL/g. A normal distribution based on the observed mean and standard deviation of the K_d values overpredicts the K_d values at the high and low ends of the range and underpredicts the K_d values in the center of the distribution (Fig. 9.1). The bimodal model-predicted K_d distribution results because the K_d values for background wells are statistically different from the K_d values for wells in U-contaminated region. The smallest K_d values occurred in groundwaters that had high alkalinity and U(VI), such as well NAT-26, and the largest K_d values occurred in upgradient wells that had low alkalinity and U(VI) concentrations.

Observed U(VI) and alkalinity are significantly correlated in the field, which makes it difficult to evaluate which of these parameters is most significant in determining the mobility of U(VI). To make this assessment, one-dimensional transport simulations were conducted where long pulses of a U(VI)-bearing solution displaced water that had an average pH and background alkalinity (4.8 meq/L) and a low U(VI) concentration of 10^{-9}M. The injected high U(VI) solution used average values for two parameters (e.g., pH and alkalinity) and the observed range of values for the third parameter (e.g., U(VI) concentration). For each parameter, the variable concentration was set equal to: (1) the minimum, (2) the value at the 2.5th percentile, (3) the value at the 17th percentile, (4) the mean, (5) the value at the 83rd percentile, (6) the value at the 97.5th percentile and (7) the maximum value (Table 9.2). Simulated breakthrough between the 17th and 83rd percentiles accounts for 1 standard deviation of the parameter variability and simulations between the 2.5th and 97.5th percentiles accounts for 95% of the parameter variability.

Figure 9.2a shows the breakthrough of a U(VI) pulse (3.04 μM) for pH values that ranged from 6.54 to 7.71. For the complete range of pH values, the simulated U(VI) breakthrough occurred between 2 and 4.5 pore volumes. Faster rates of migration were associated with higher pH values, consistent with increased concentration of the aqueous uranyl-tricarbonato complex, $UO_2(CO_3)_3^{4-}$. Figure 9.2b shows the breakthrough of a U(VI) pulse for U(VI) concentrations that ranged from 0.084 to 21.8 μM. These breakthrough curves cluster into two groups. The first cluster breaks through between 2.8 and 3.5 pore volumes and is associated with U(VI) concentrations equal to or greater than the mean U(VI) concentration (3.04 μM). The second cluster breaks through at approximately 5.2 pore volumes and is associated with U(VI) concentrations of 0.16 μM and smaller. The larger retardation at lower U(VI) concentrations occurs because the U(VI) adsorption isotherm on NABS sediments is non-linear (see Section 5). Under field conditions at high U(VI) concentrations, the very strong sites are nearly completely occupied, and consequently, the simulated U(VI) migration is controlled by adsorption on the strong and weak sites.

Figure 9.2c shows that the observed variability of alkalinity has the largest effect on U(VI) front

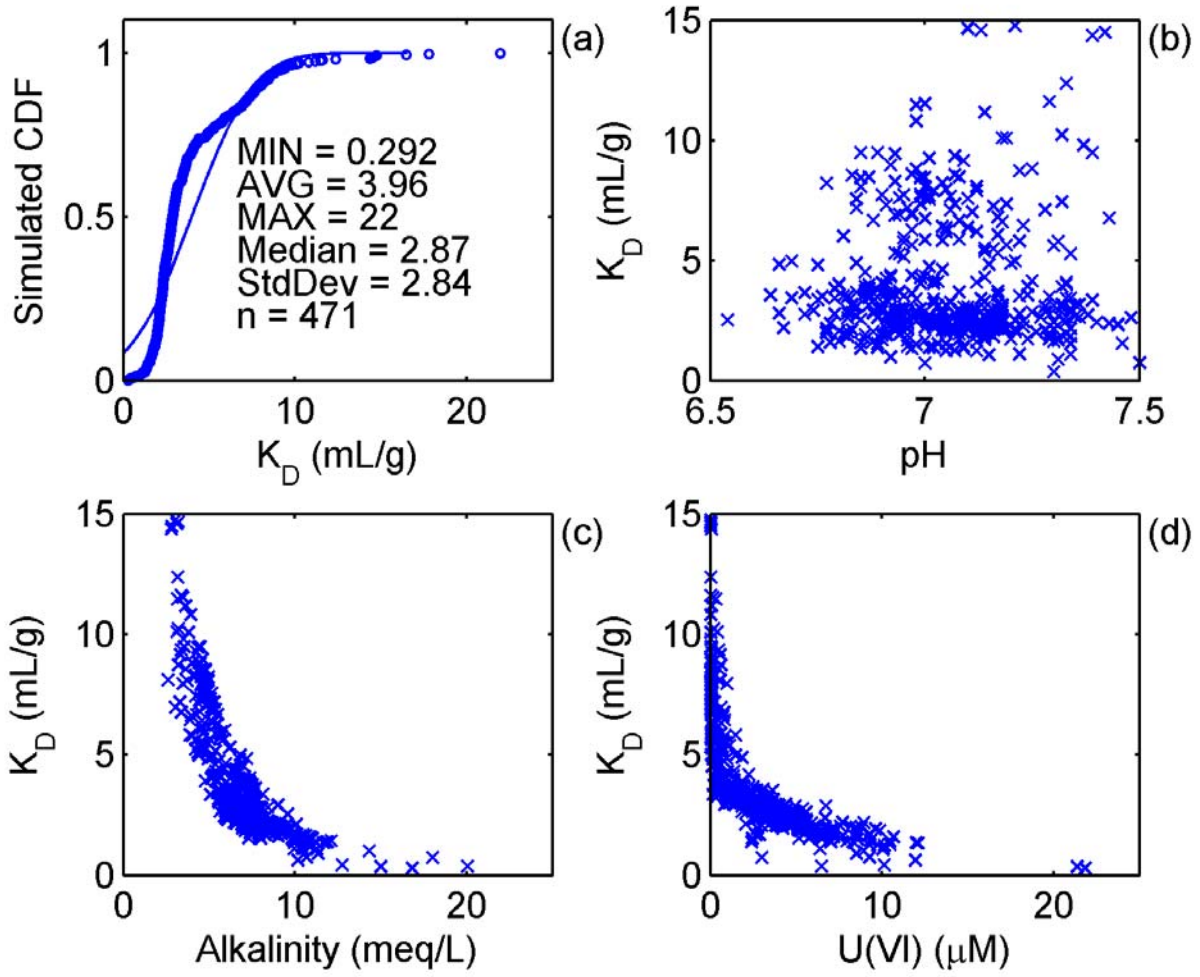

Figure 9.1. Simulated K_d values for Naturita groundwater using the Generalized Composite SCM developed from laboratory experiments with the NABS sample (Section 5). Plots illustrate (a) simulated cumulative distribution of K_d values, and (b-d) model K_d values plotted versus pH, alkalinity, and U(VI) concentration.

migration. The simulation with the maximum alkalinity had a breakthrough at 1.5 pore volumes and the simulation with the minimum alkalinity had a breakthrough at 13 pore volumes. The simulations show that U(VI) transport is particularly sensitive to alkalinity at low alkalinity values. For example, the average background alkalinity is 4.8 meq/L, which is close to the alkalinity at the 17th percentile of 4.77 meq/L. Breakthrough at this latter alkalinity occurred at 5.6 pore volumes. This is less than half the time required for a U(VI) pulse in waters with 2.5 meq/L alkalinity. This suggests that U(VI) transport simulations for the Naturita site may be sensitive to the alkalinity value assumed for the background water. Overall, the variability of alkalinity at the site had a larger effect on the simulated U(VI) migration than either U(VI) concentration or pH.

9.4 Field Transport Modeling

Modeling the field scale transport of U(VI) at the Naturita site focused on matching the historical observations. One objective of the history-matching simulations was to evaluate if the existing distribution of U(VI) at the Naturita site could be reproduced with a reactive transport model that used the SCM determined

Table 9.2 Summary of observed U(VI), pH and alkalinity in Naturita groundwater, 1986-2001

percentile	pH	Dissolved U(VI)	Alkalinity	K_d
		μM	meq/L	mL/g
Minimum	6.54	0.0084	2.47	0.29
2.5	6.75	0.0303	3.21	1.11
17	6.90	0.16	4.77	2.04
Median	7.06	2.78	6.79	2.87
83	7.23	5.25	8.11	6.67
97.5	7.48	9.87	11.20	11.5
Maximum	7.71	21.80	18.00	22.0
Average	7.07	3.07	6.88	3.96
Standard deviation	0.19	2.92	2.29	2.84
Number of data points	469	469	469	469

for the NABS sample to calculate U(VI) adsorption.

9.4.1 Description of Source Term

A constant, mass-loading source was used (Zheng and Wang, 1999). For this source, a constant flux of solute was added to the transport model but there are no fluid sources that would affect groundwater flow. The upgradient extent of the source term was assumed to be at well NAT-30, which coincides with the upstream extent of the former mill yard (Section 3) and currently has U(VI) concentrations that are 35% greater than the average value at the upgradient wells NAT-20, -21, -22 and DOE-547. The downstream extent of the source was assumed to coincide with the end of the former tailings pile near well NAT-10. The duration of the sources could have been (1) as long as U was processed at the site (24 years), (2) as long as U tailings were present at the site (38 years), or (3) as long as contaminated soils were present at the site (58 years). Simulations of Cl transport required a source of at least 38 years (Section 3), and therefore a U(VI) source with a duration of either 38 or 58 years was considered.

9.4.2 Model Calibration

The reactive transport model was calibrated to the existing site data using UCODE (Poeter and Hill, 1998) by varying the source strength. Two-dimensional reactive transport simulations were conducted, and simulated dissolved U(VI) concentrations and alkalinity values at selected monitoring wells were compared with the observed values. Field data were used from the same locations used in calibrating the flow and transport model to Cl transport (see Section 3). These locations are roughly along a flow path that was as far from the river as was practical. This was done to minimize the effect of dilution with river water on the dissolved U(VI) concentrations and alkalinity.

The calibration estimated the U(VI) and alkalinity loading rates that gave a best fit to the observed values. The observed and simulated concentrations were scaled by the recent maximum observed concentrations of U(VI) (10 μM) and alkalinity (12.1 meq/L), so that each type of data was weighted nearly equally. The calibration did not vary the SCM parameters or the hydraulic conductivity (K_X), which were determined independently. A single source-loading rate for the entire source area was used in the simulations. In some simulations, two separate source terms were included: the first was for the mill yard and the second was for the tailings area. However, the fit for the two source

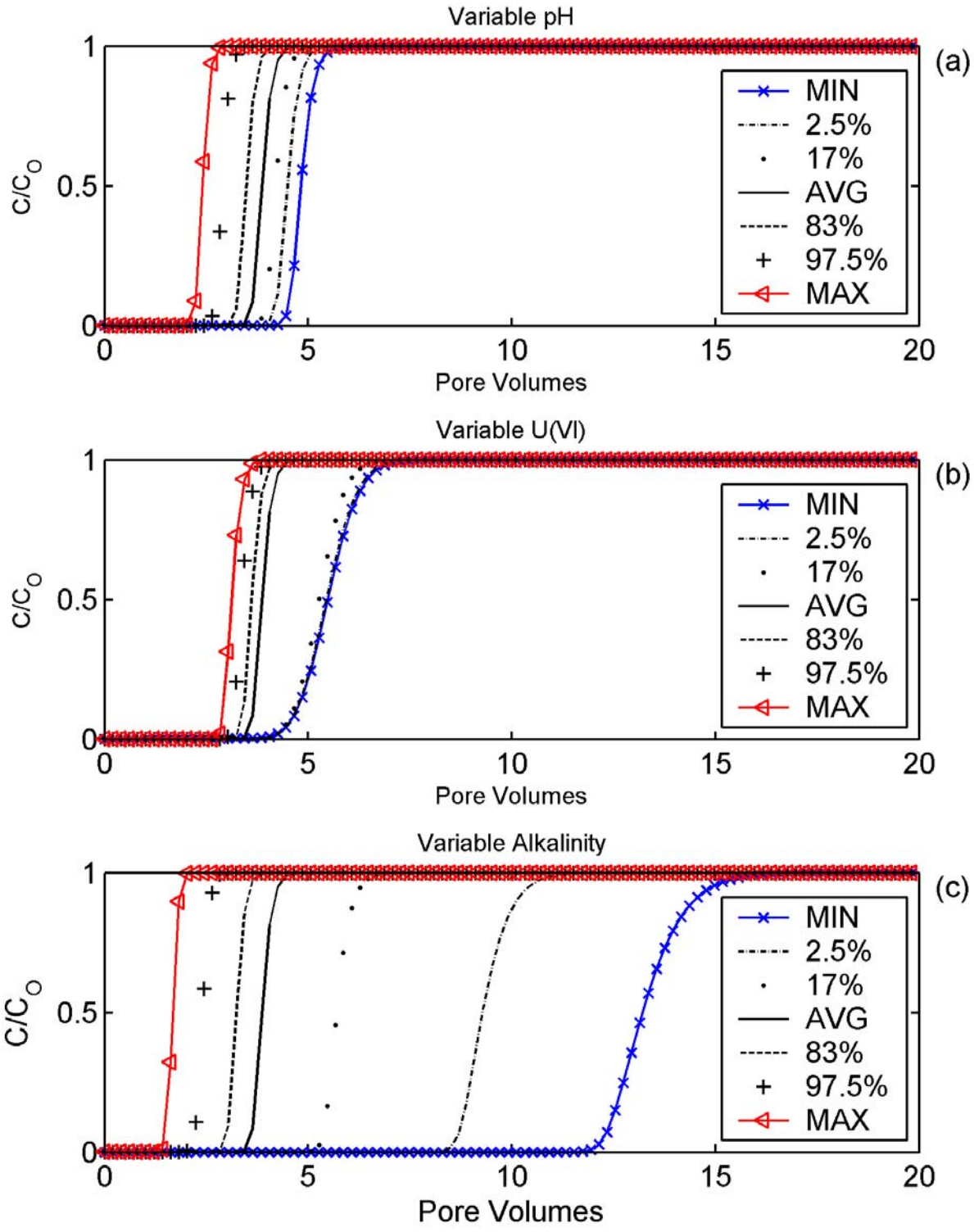

Figure 9.2. Simulated breakthrough created by a step change in inlet boundary conditions. The boundary conditions were (a) variable pH , average U(VI) concentration and average alkalinity, (b) average pH , variable U(VI) concentration, and average alkalinity, and (c) average pH , average U(VI) concentration, and variable alkalinity. See Table 9.2 for specific concentration values.

terms was not significantly better (results not shown) and therefore, only the single source was considered below.

Figure 9.3 illustrates the simulated and observed breakthrough curves for U(VI) and alkalinity for each of the calibration wells. For each well, there was good agreement between the simulated and observed alkalinity values. The largest difference between the model and observed data occurred for well DOE-656, which had a single measured alkalinity of 16 meq/L and a simulated value of 9.5 meq/L. For all other wells, the agreement between the simulated and measured alkalinity values was better, with the average absolute difference being 2.8 meq/L. The fit to the dissolved U(VI) data is also generally very good, with the average absolute difference being 2 μM. The largest, consistent difference between the simulated and observed U(VI) concentrations was for well DOE-506, which was located at the downstream border of the mill yard. Possibly U(VI) was high at this location because of a more highly concentrated source in the mill yard.

Figure 9.4 shows a series of two-dimensional images that summarizes the simulated distributions of U(VI), alkalinity and pH. The dissolved U(VI) and alkalinity plumes generally match the observed spatial distribution (Fig. 9.5). The simulated pH was practically constant because of the buffering from calcite. As in the case of the breakthrough curves, there is generally a good match to the observed data. The most significant differences occurred primarily along highway 141 at the west border of the aquifer (see Fig. 3.1). In the middle of the aquifer, near well NAT-10 but closer to the highway, the simulated concentrations near the highway are higher than the observed values. In contrast, downgradient of well NAT-25 observed values are higher near the highway than the simulated values. In both cases however, the observed values shown are the result of kriging calculations that used concentrations at the observation wells. There are no data close enough to the highway to support the kriging results in either location. The goodness of the fit is best evaluated from Figure 9.3, although Figure 9.5 does give an overall picture of agreement between the model simulations and the observations.

Figure 9.5 also shows a subtle difference between the simulated alkalinity and dissolved U(VI) plumes near the highway downgradient of well NAT-26. In the case of alkalinity, the simulated plume is adjacent to the highway and extends all the way to the river. In contrast, for U(VI), the plume extends onto the Maupin property as a long, thin lobe with a clear region with low U(VI) concentrations adjacent to the highway. This difference results because U(VI) is retarded relative to alkalinity. The velocities are generally lower adjacent to the highway, and it takes a longer time for the plume near the highway to migrate to the San Miguel River.

The distributions of the individual surface species shown in Figure 9.4 illustrate that the ternary surface carbonate complex, $>SOUO_2CO_3^-$, is the predominant U(VI) surface species in most of the aquifer. In the middle of the aquifer, the $>SOUO_2CO_3^-$ is at concentrations equivalent to >10 μM and accounts for approximately 80% of the adsorbed U(VI). However, the plume shape for $>SOUO_2CO_3^-$ does not exactly match that for dissolved U(VI), and the region of high $>SOUO_2CO_3^-$ is located upgradient of the high dissolved U(VI). In the extreme upgradient and downgradient zones of the aquifer, $>SOUO_2CO_3^-$ is still the most abundant U(VI) surface species, but in these regions it accounts for roughly 46 % of adsorbed U(VI). Interestingly, the two U surface complexes involving the very strong sites, $>SSOUO_2OH$ and $>SSOUO_2CO_3^-$, have maximum concentrations at different locations. The maximum concentration of $>SSOUO_2OH$ occurs in upgradient locations where alkalinity values ranges from 4.8 to 7.4 meq/L, whereas the $>SSOUO_2CO_3^-$ maximum occurs downgradient of the peak $>SSOUO_2OH$ concentration and in areas where both the dissolved U(VI) concentration and alkalinity are relatively high.

Figure 9.6 also shows K_d values computed from the simulated total aqueous and adsorbed U(VI) concentrations. The K_d map clearly illustrates

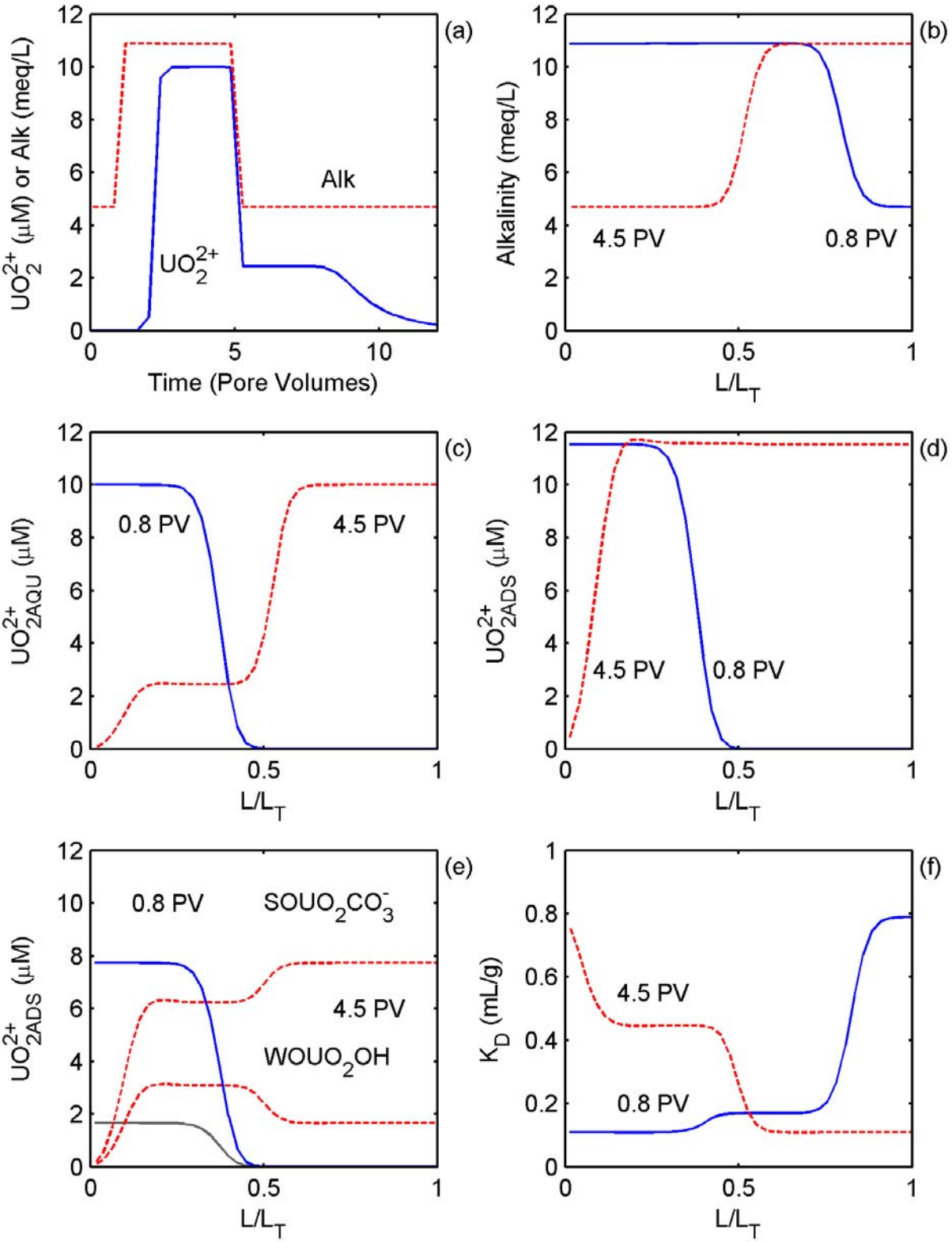

Figure 9.3. Dissolved U(VI) and alkalinity breakthrough curves and concentration profiles for a 4 pore volume pulse of 10 μM U(VI) and 11 meq/L alkalinity. Curves are shown for elapsed times of 0.8 and 4.5 pore volumes.

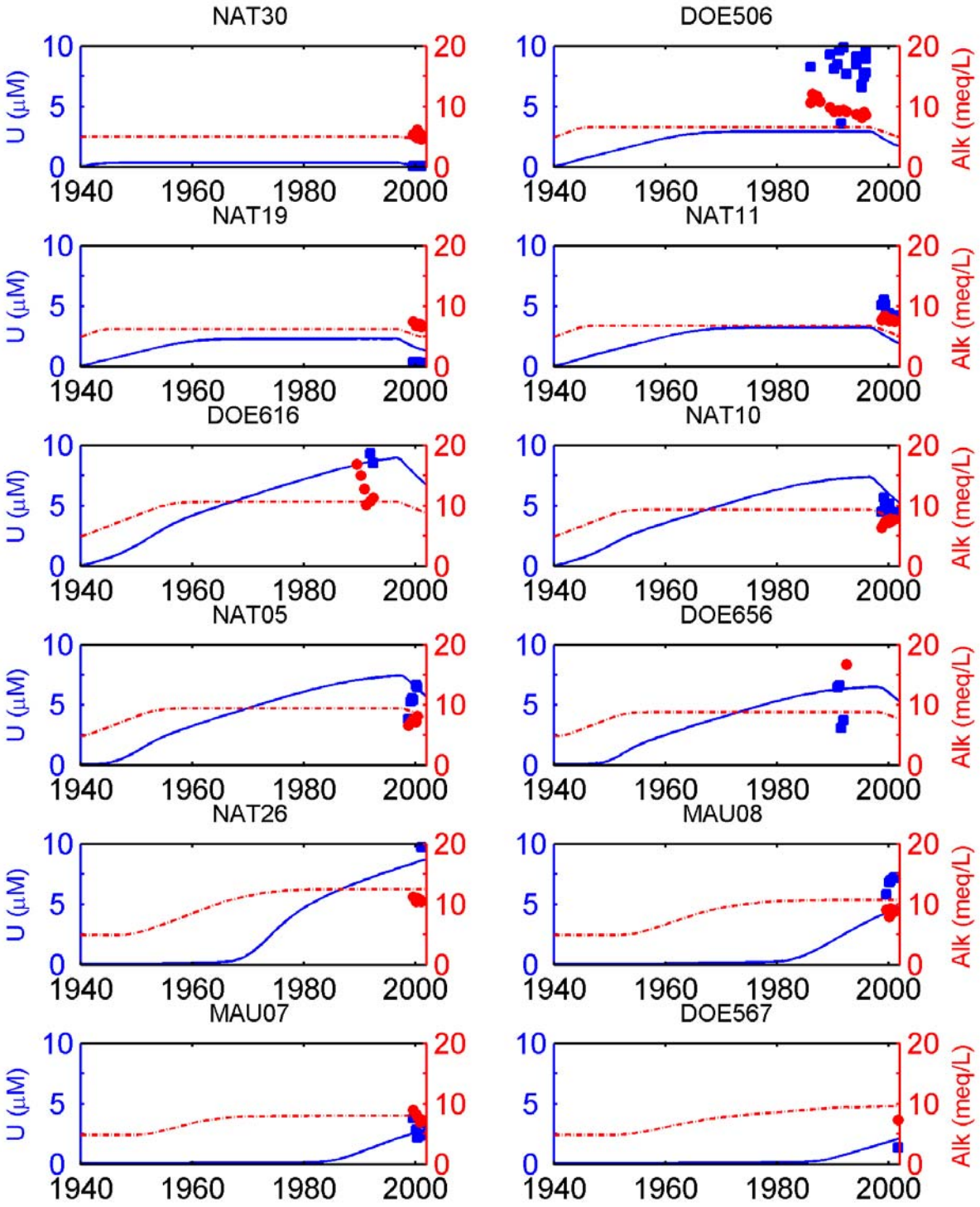

Figure 9.4. UCODE calibration results for uniformly distributed mass loading source. Each subplot shows the observed dissolved U(VI) (□), simulated dissolved U(VI) (—), observed alkalinity (○) and simulated alkalinity (- • -).

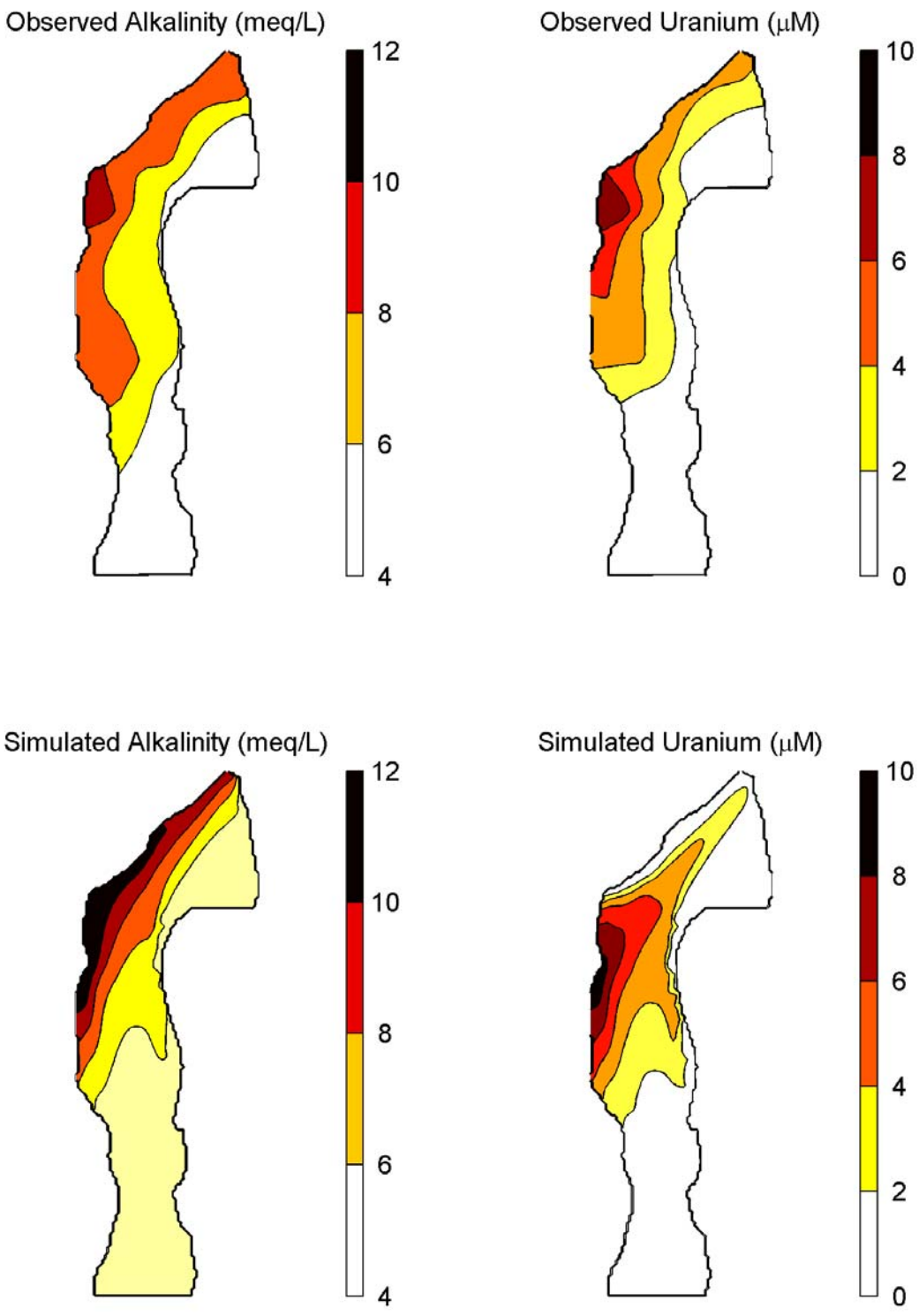

Figure 9.5. Comparison of observed and simulated distributions of dissolved U(VI) concentration and alkalinity in 1999.

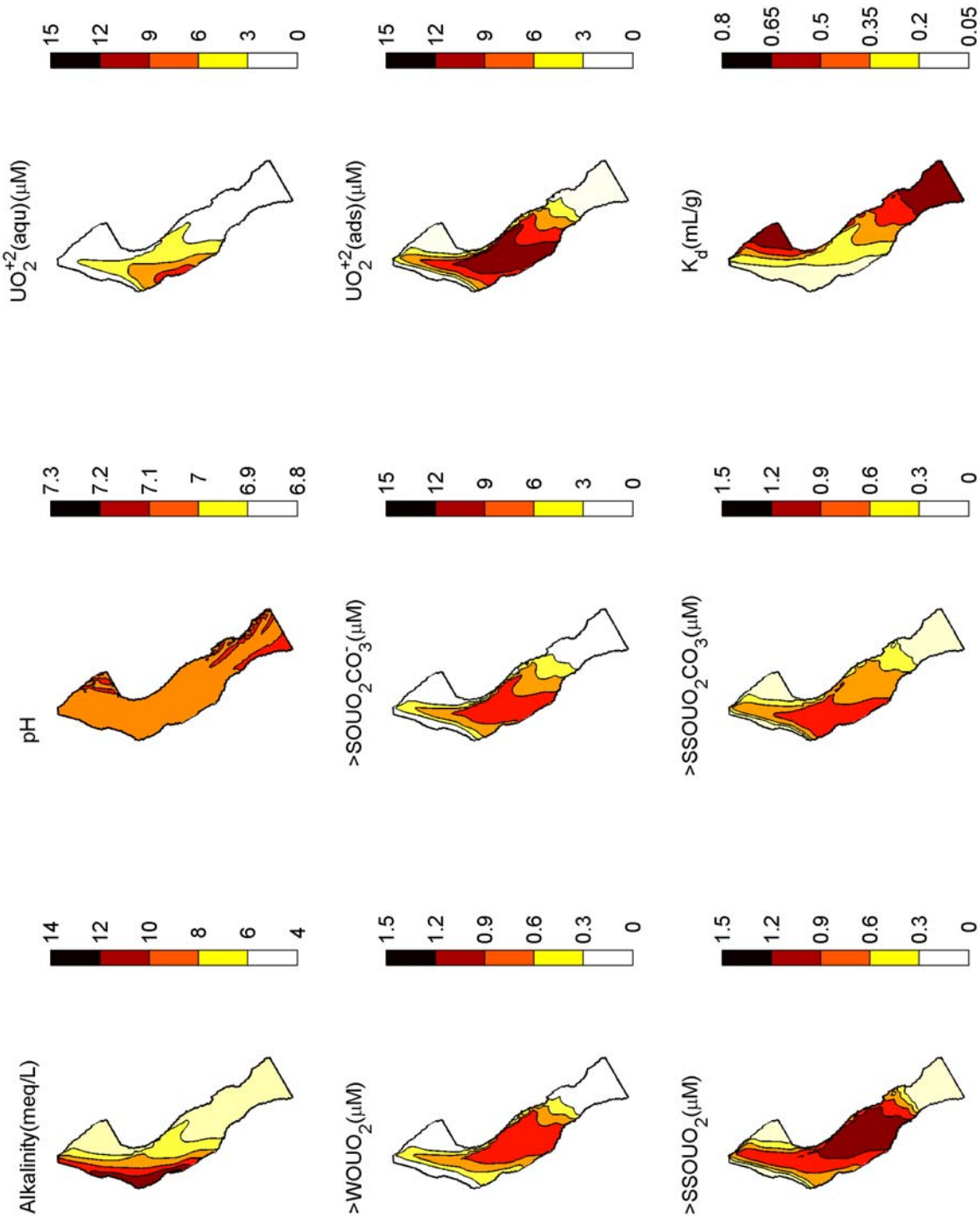

Figure 9.6. Simulated spatial distribution of dissolved U(VI) concentration, pH, alkalinity, surface species, and K_d values.

that the peak U(VI) concentration is migrating with the smallest K_d values and the smaller concentrations migrate with K_d values that are nearly an order of magnitude higher than the minimum K_d. This spatial distribution is particularly important when compared with the distribution of K_d values shown in Figure 9.1. K_d distributions are sometimes used in performance assessment calculations. Such models should recognize that not only variable chemical conditions cause a range of effective K_d values to be observed, but also that the spatial distribution of K_d values within that range is not likely to be a random distribution. In plumes with chemical gradients, the spatial distribution of K_d values can be quite complex and be characterized by significant spatial character.

9.5 Sensitivity Analysis

An analysis was conducted to illustrate the sensitivity of the model simulation to the SCM parameters only, and then subsequently to illustrate the sensitivity of the model to K_X and the initial and boundary conditions. The primary goal of the sensitivity analysis was to determine which of the model input parameters is most important in determining the simulated U(VI) concentrations.

9.5.1 Sensitivity to Surface Reaction Parameters

First order sensitivity analyses were calculated for the simulated U(VI) concentrations in the entire aquifer. The scaled sensitivities (Poeter and Hill, 1998) were defined by:

$$SS_i = \frac{\partial Y}{\partial b_i} b_i \qquad \textbf{(9.1)}$$

where SS_i is the scaled sensitivity, Y is the simulated quantity, and b_i is the i'th parameter value. Equation 9.1 was approximated by first-order finite differences:

$$SS_i \approx \frac{C_{b+\Delta b_i} - C_b}{\Delta b_i} b_i \qquad \textbf{(9.2)}$$

where C is the simulated U(VI) concentration. For consistency, the parameters were perturbed by 0.1 log units ($\Delta b_i \approx 0.26 b_i$), and in this case, the SS_i values are proportional to the differences in simulated U(VI) concentrations.

Sometimes in simple cases it is possible to evaluate analytically the derivatives in order to compute the scaled sensitivities. Because an analytical evaluation is not available for the reactive transport simulation, it is useful to consider a simpler system. A single-site, single-reaction adsorption model in a batch system is described by the reaction,

$$>SOH + UO_2^{+2} + H_2O = >SOUO_2OH + 2H^+ \qquad \textbf{(9.3)}$$

and the mass action expression,

$$K = \frac{(>SOUO_2OH)(H^+)^2}{(>SOH)(UO_2^{+2})} \qquad \textbf{(9.4)}$$

The total site concentration is defined by,

$$S_T = >SOH + >SOUO_2OH \qquad \textbf{(9.5)}$$

Combining Equations 9.4 and 9.5 with the assumption that $>SOUO_2OH << S_T$ gives:

$$>SOUO_2OH = KS_T \frac{UO_2^{+2}}{(H^+)^2} \qquad \textbf{(9.6)}$$

The scaled sensitivity (Eq. 9.1) of the adsorbed U(VI) concentration to the SCM model parameters, K and S_T, are both equal to:

$$SS = KS_T \frac{UO_2^{+2}}{(H^+)^2} \qquad \textbf{(9.7)}$$

Equation 9.7 shows that the scaled sensitivity of the adsorbed U(VI) is equally sensitive to K and S_T if the surface coverage is low. It also illustrates that the K and S_T values should be highly covariant in batch systems, and these scaled sensitivities may also be covariant in a transport model.

Figures 9.7a and b illustrate the scaled sensitivities of the simulated U(VI)

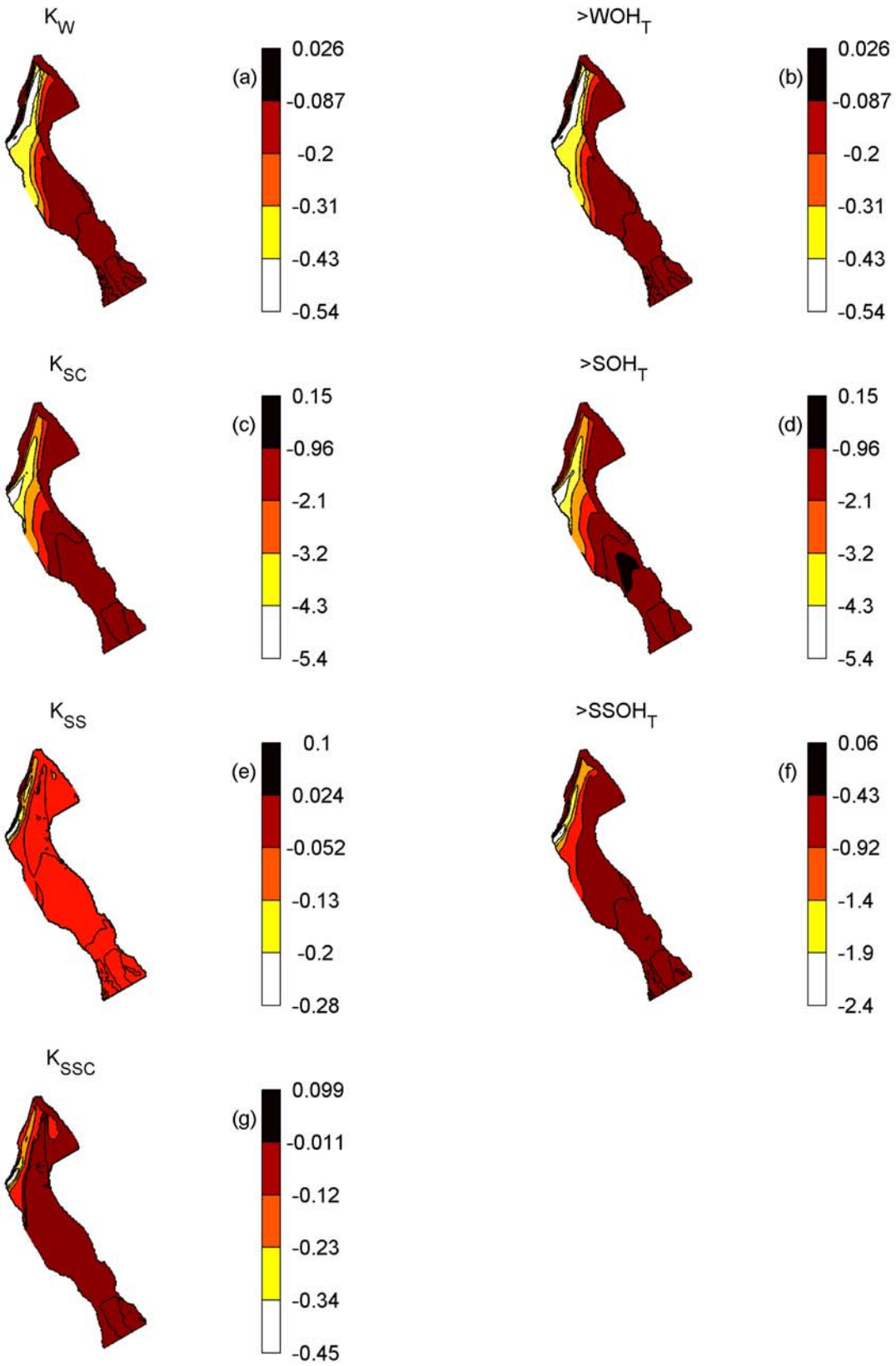

Figure 9.7. Scaled sensitivity plots for surface complexation model parameters.

concentration to the weak site reaction parameters, K_W and WOH_T, after 60 years of transport. The sensitivities shown in the two figures are essentially identical, as was suggested by the simplified model discussed above. The identical behavior results in part because the maximum coverage of the weak sites is only 0.005%, and therefore the approximation that $>WOUO_2OH$ is much less than >WOH is met. The sensitivity maps show that the scaled sensitivity values are near zero in the background areas and are at an absolute maximum at the leading edge of the U(VI) plume. The values for the weak site parameters range from approximately 0 to -0.54 μM. The general trend of negative sensitivity values results because there is an inverse relation between U(VI) transport and both K_W and $>WOH_T$; an increase in either value decreases U(VI) mobility. Figures 9.7c and d show analogous results for the strong site reaction parameters, K_S and SOH_T. Again, the two maps are nearly identical and in this instance the maximum surface coverage is 3.2%. The maps of the sensitivities show maximum absolute values of approximately 5.4 μM, which is ten times greater than the weak site values. The greater sensitivity occurs because $>SOUO_2CO_3^-$ is the dominant surface species.

The shapes of the sensitivity maps are different for the weak and strong site parameters. The maximum absolute scaled sensitivity for the strong site occurs near well NAT-26, where both dissolved U(VI) and alkalinity are high. This location is upgradient from the location of the weak site sensitivity maximum (the U(VI) plume leading edge). The strong site maximum sensitivity occurs where both dissolved U(VI) and alkalinity are high because both are important in the formation of the ternary $>SOUO_2CO_3^-$ complex.

In contrast, the scaled sensitivities for the very strong reaction parameters are not identical (Figs. 9.7e-g). This results because there is competition on the very strong sites for the formation of $>SSOUO_2OH$ and $>SSOUO_2CO_3^-$, and because the very strong sites are over 50% occupied by U(VI) where the U(VI) concentration is large. Taken together, Figure 9.7 illustrates that U(VI) transport is most sensitive to the strong site adsorption parameters, but that simulation of the leading edge of the plume is also sensitive to the weak and very strong sites.

9.5.2 Sensitivity to Hydrogeochemical Parameters

Sensitivity calculations were also performed to investigate the sensitivity of the transport simulations to hydraulic conductivity and the concentrations of solutes in the source water and upgradient background waters (Fig. 9.8). The simulated U(VI) concentrations were most sensitive to K_X. The sensitivity to K_X is positive in downgradient areas and negative in the upgradient areas. This trend results because higher K_X values give higher velocities, and therefore higher U(VI) concentrations in the downgradient areas. Similarly, higher velocities flush U(VI) faster from upgradient areas, creating the negative sensitivities.

The sensitivity values for the background alkalinity, U(VI) and pH varied widely. The sensitivity to the background alkalinity was near zero in most of the aquifer, but relatively large values of 12 μM were found near well NAT-26. This coincides with the highest dissolved U(VI) concentrations and suggests that the advancement of the front is sensitive to the initial alkalinity in the aquifer. The simulated U(VI) concentrations are insensitive to the background U(VI) concentration because background U(VI) is so small in comparison to the source U(VI) concentration. The main effect of the elevated background U(VI) is that more of the very strong sites are initially occupied, and therefore the simulations exhibit less tailing of the plume because fewer very strong sorption sites are available. The simulations were moderately sensitive to the background pH values. The largest sensitivity was associated with the leading edge of the dissolved U(VI) plume.

Sensitivity calculations were also conducted for the U(VI) and alkalinity concentrations in the source term (Fig. 9.8e and f). The model is

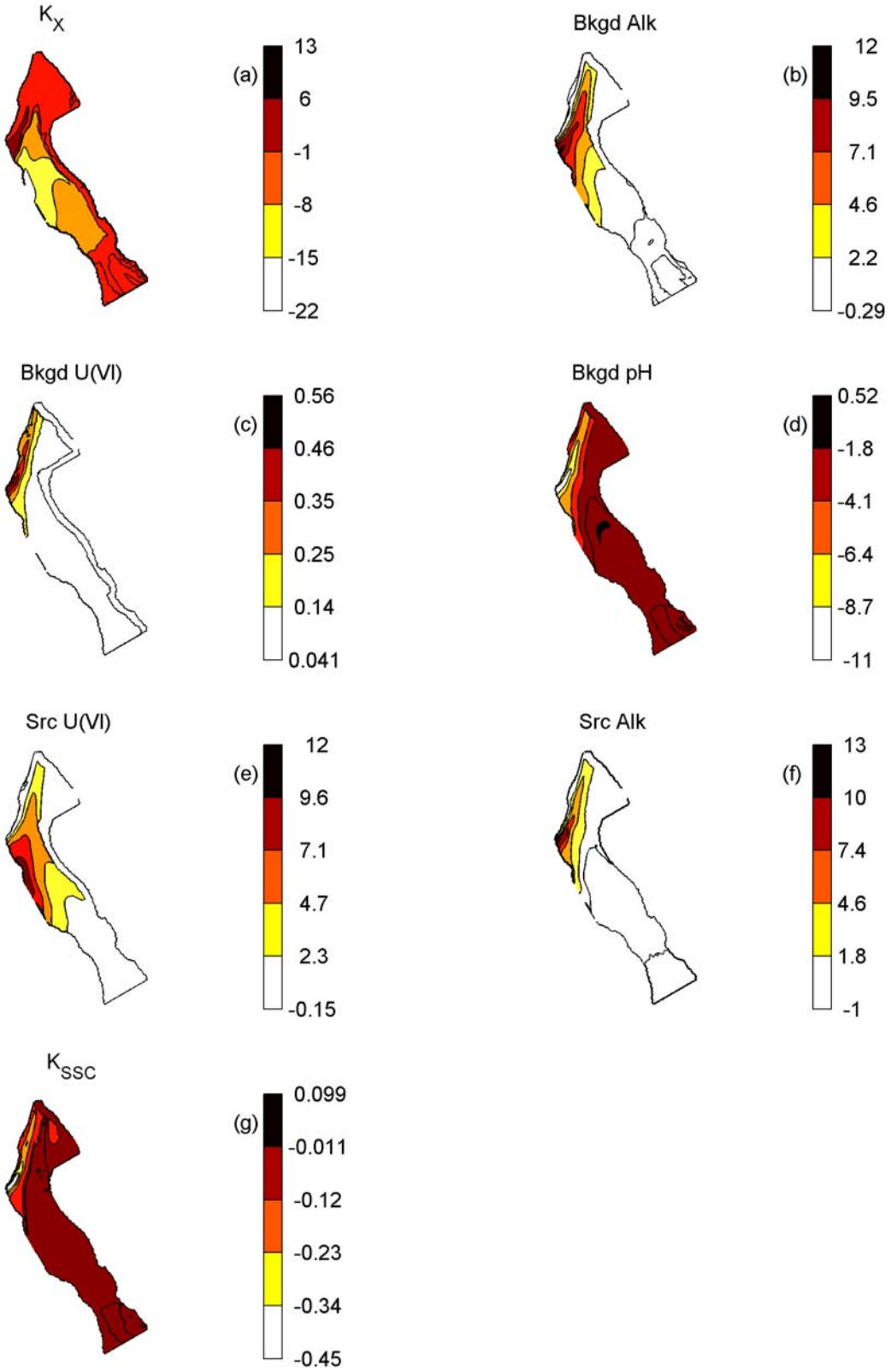

Figure 9.8. Scaled sensitivity plots for hydraulic conductivity (K_x), background U(VI) concentration, alkalinity, pH and source U(VI) concentration and alkalinity.

approximately equally sensitive to each of these two calibration parameters. The sensitivity maps for the two species generally reflect the simulated dissolved concentrations, as would be expected from increasing the source strength.

Figure 9.9 shows a summary of the sensitivity calculations. For each parameter included in the sensitivity analysis, the sum of the absolute scaled sensitivity is illustrated. This figure shows that the model is most sensitive to K_X. It is useful to compare this sensitivity value with that computed for the SCM model parameters. Because the parameters for each of the site types are covariant, the K_X values are compared with the sum of the sensitivity of $>WOH_T$, $>SOH_T$ and $>SSOH_T$ (equal to $2 \cdot 10^{-4}$ M), which is about 40% of the K_X value. An important aspect of this comparison is that U(VI) is only moderately adsorbed within the Naturita alluvial aquifer, largely because of aqueous carbonate complexation.

The simulated U(VI) concentrations were relatively insensitive to the weak site SCM parameters. However, as discussed above, these variables are important in the leading edge of the plume. Therefore, the time required for U(VI) to reach the San Miguel River would be sensitive to the weak site SCM parameters.

9.6 Conceptual Model Evaluation

Simulations were conducted to evaluate the significance of two assumptions made in formulating the conceptual reactive transport model:(1) the assumption that transport could be simulated using an average ionic strength, (2) the assumption of local chemical equilibrium, (3) the assumption of a non-electrostatic adsorption model, and (4) the assumption that there were no ion exchange reactions.

9.6.1 Effect of Constant Ionic Strength

The simplified geochemical model assumes that the speciation of U(VI) is dominated by the formation of carbonate complexes. For simplicity and numerical efficiency, the conceptual model did not describe the transport of the major ions Na^+, Cl^- and SO_4^{-2}, which vary spatially. This assumption has two consequences. First, the formation of soluble U(VI) chloride and U(VI) sulfate complexes are not considered. Second, the effects of the major ions on ionic strength and therefore U(VI) speciation reactions was not considered. The significance of ignoring the major ions was addressed by computing K_d values using (1) the simplified geochemical model that considered pH, alkalinity, an average ionic strength of 0.018M and assumed equilibrium with calcite and (2) a complete geochemical model that included all of the species summarized in Table A.1 and used a variable ionic strength for each sample. The K_d values computed from the two approaches are illustrated in Figure 9.10. On average, the simplified model gives Kd values that are 20% larger than the complete geochemical model. The simplified model also introduces a slight bias in that a small K_d values, the simplified model gives larger K_d values than the complete geochemical model. In general, however, the difference between the two approaches is small compared to range of K_d values at the site.

9.6.2 Effect of Non-equilibrium Adsorption

Adsorption of U(VI) by the NABS sample in batch adsorption studies required approximately 3 days to reach steady-state aqueous U(VI) concentrations (see Section 5). Transport simulations were conducted to evaluate if this time scale for adsorption reaction kinetics might produce significant deviations from local equilibrium in the field scale simulations. Slow sorption kinetics could be a particular problem downgradient of well NAT-25, where the groundwater velocities are about 2 times faster than the velocities at the upgradient well NAT-06.

The rate processes included in the transport simulations were based on the batch laboratory kinetic observations (Section 5). An empirical approach to simulate the effect of slow sorption kinetics is to use 'mass action kinetics'. In this approach, the rate of the reaction is based on the

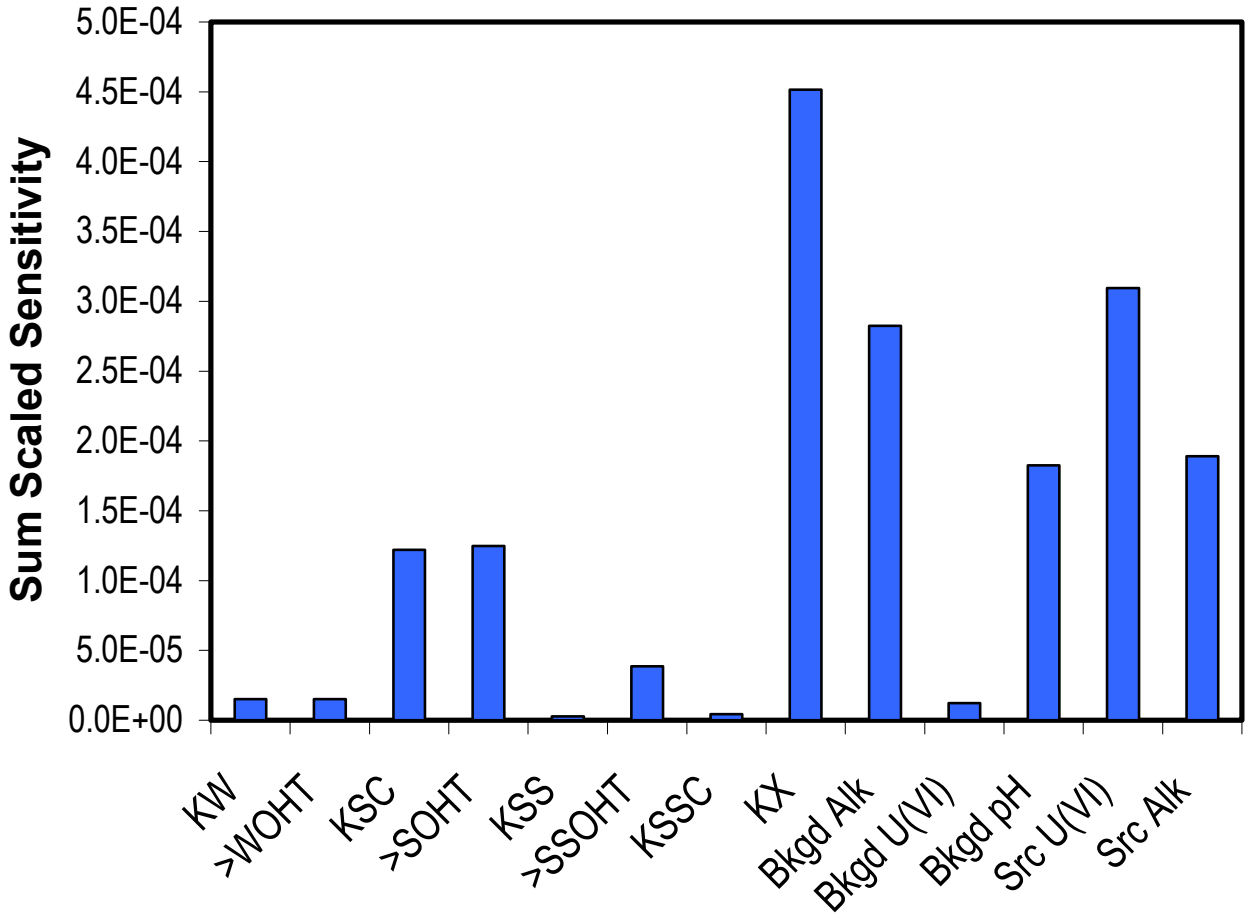

Figure 9.9. Summary of sensitivity calculations.

stoichiometry of the adsorption reaction. For example, if the adsorption reaction is written as:

$$UO_2^{+2} + >WOH + H_2O \underset{k_r}{\overset{k_f}{\rightleftharpoons}} >WOHUO_2OH + 2H^+ \qquad \textbf{(9.8)}$$

then the rate law is written as:

$$\frac{\partial(>WOHUO_2OH)}{\partial t} = k_f(>WOHUOOH)(H^+)^2 - k_r(>WOH)(UO_2^{+2}) \qquad \textbf{(9.9)}$$

where k_f and k_r are rate constants.

In order to maintain consistency with the SCM, the rate constants were related to the equilibrium constant (K_{EQ}) by Equation 9.10:

$$K_{EQ} = \frac{k_f}{k_r} \qquad \textbf{(9.10)}$$

Alternatively, the adsorption reaction can be written in terms of the abundant aqueous $UO_2(CO_3)_2^{-2}$ species, as shown in Equation 9.11:

$$UO_2(CO_3)_2^{-2} + >WOH + H_2O \underset{k_r}{\overset{k_f}{\rightleftharpoons}} >WOHUO_2OH + 2H^+ + 2CO_3^{-2} \quad \textbf{(9.11)}$$

A complete set of rate expressions developed using UO_2^{+2} ion as the reactant in the adsorption equations is referred to as Model 1 below, and a complete set of rate expressions developed using the $UO_2CO_3^{-2}$ ion as the reactant is referred to as Model 2 and these are summarized in Table 9.1. The values of the rate constants in Table 9.1 were calibrated to batch data collected at pH 7.9 and at atmospheric partial pressure of CO_2 (data from Section 5). The two stoichiometric formulations listed in Table 9.1 were used because the two kinetic models are affected differently by variable chemical conditions.

A comparison of simulations obtained using the two approaches is shown for wells NAT-26 and MAU-08, which are located at the beginning and in the middle of the region where groundwater velocities are relatively high. The two rate models agree nearly exactly with the U(VI) concentrations simulated with the local equilibrium assumption (Fig. 9.11). Most of the differences probably result from activity effects, which are not accounted for in the rate laws. The small kinetic effects illustrated in Figure 9.11 result because the higher concentration of adsorption sites increases the adsorption rate. Kinetics could be important if mass transfer limitations are important in the field or if the adsorption reactions proceed by some other mechanism that gives slower rates for field conditions. The agreement between the rate-controlled and equilibrium simulations does illustrate, however, that it is possible to have batch reaction rates that require 3 days to attain equilibrium and still use an equilibrium-based transport model for field-scale transport simulations for the Naturita field site.

Appendix D describes how the forward rate constants were estimated. It is also demonstrated in Appendix D that the two models give equivalent simulations for batch kinetic experiments at pH 7.9 and at atmospheric partial pressure of CO_2, but application of the models to other chemical conditions gives batch simulations that differ between the two models.

9.6.3 Effect of Surface Charge

Adsorption reactions generally result in the accumulation of charge at mineral/water interfaces (Davis and Kent, 1990). The use of a non-electrostatic Generalized Composite SCM simplifies the adsorption model by neglecting the accumulation of counter ion charge in the diffuse layer that maintains the electroneutrality of the interface. If the surface charge is large enough, errors in major ion aqueous chemistry could result during the simulations. For example, adsorption of a ternary U(VI)-carbonate species causes immobilization of some carbonate ions, while all Ca^{+2} is transported. This causes some calcite to dissolve in the simulations, which could affect aqueous U(VI) speciation. In reality, some Ca^{+2} would likely be immobilized in the diffuse layer as a counter ion, and this would reduce calcite dissolution.

One of the simplifying assumptions of the non-electrostatic SCM approach is that the electrical double layer is not considered in the mass law equations, and therefore the properties of the diffuse layer do not need to be defined. Therefore, direct approaches of simulating counter ions in the diffuse layer by integrating the charge-potential versus distance equations, as is done in PHREEQC (Parkhurst and Appelo, 1999), are not possible. Instead, adsorbed surface charge can be empirically balanced by stoichiometrically removing counterions from solution to exactly balance the surface charge, such that all surface species are uncharged. This can be expressed as:

$$\sum_{j=1}^{N_S} z_j^s S_j + \sum_{i=1}^{N_A} z_i C_i^e = 0 \quad \textbf{(9.12)}$$

where N_S is the number of surface species, z_j^s is the charge of the j^{th} surface species, S_j is the

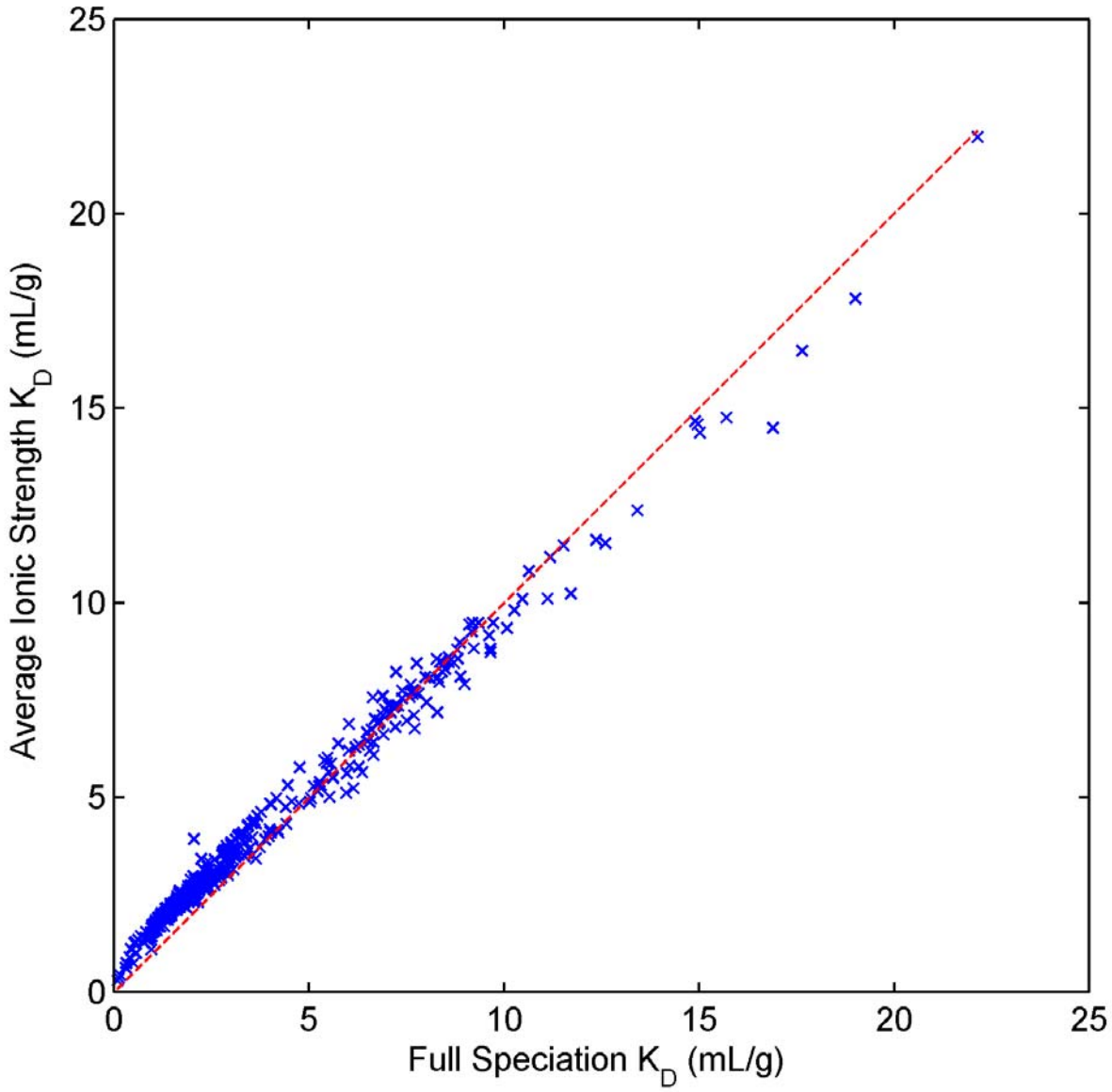

Figure 9.10 Comparison of K_d values computed using a complete measured water analysis, including variable ionic strength, with K_d values computed from observed pH, alkalinity and U(VI) concentrations at an average ionic strength.

concentration of the j'th surface species, N_A is the number of aqueous species, z_i is the charge of the i'th species, and C_i^e is the surface excess concentration of the i'th species. The excess concentration of each ion is given by:

$$C_i^e = f\delta_i z_i C_i \qquad \textbf{(9.13)}$$

where f is a proportionality constant that applies to all ions and δ_i is 1 if the charge z_i is opposite that of the surface charge and is 0 otherwise. The approach of using the charge to weight the immobilized concentrations is empirical; it comes from electrostatic considerations even though a non-electrostatic model was used. Equation 9.13 can be substituted into Equation 9.12 and rearranged to yield:

$$f = \frac{\sum_{j=1}^{N_S} z_j^s S_j}{\sum_{i=1}^{N_A} \delta_i z_i^2 C_i} \qquad \textbf{(9.14)}$$

Given this definition of f, the immobilized surface excess is readily calculated from Equation 9.13. The combination of equations 9.11-9.14, together with mass balance equations modified to account for immobilized counter ions, was used to test the sensitivity of model simulations to the development of surface charge.

Simulations were conducted based on the assumption that the major ions, Ca^{+2}, Na^{+} and Mg^{+2}, were immobilized within the diffuse layer to neutralize the surface charge of adsorbed U(VI) species. The simulations are summarized in Table 9.3. Simulated breakthrough curves for cases 1 and 2 are illustrated in Figure 9.12, and the results are compared with a simulation where no counter ions were included. The simulations show that the three models agree very closely.

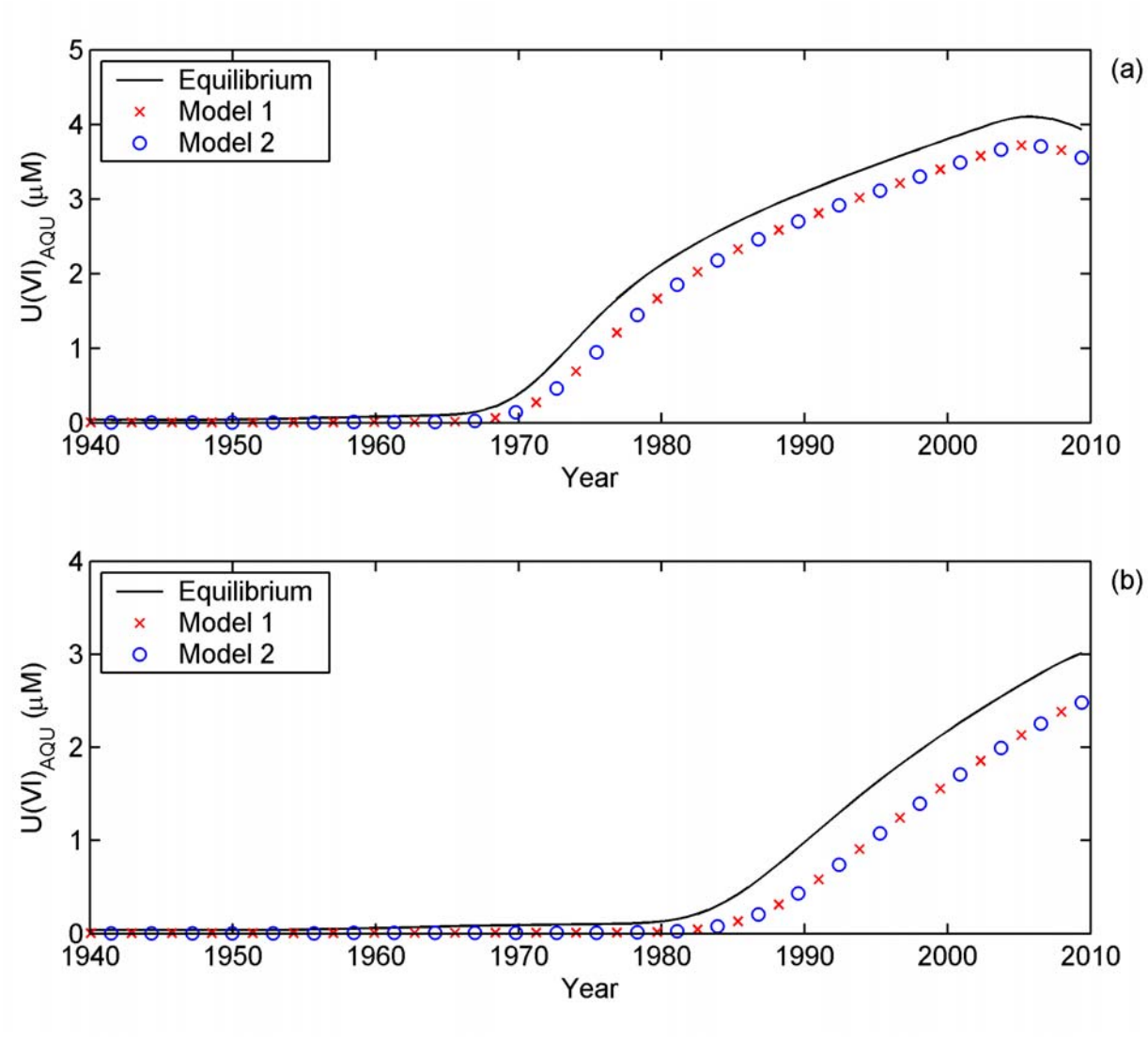

Figure 9.11. Comparison of equilibrium-controlled and rate-controlled simulated breakthrough curves for U(VI) at (a) well NAT26 and (b) well MAU08.

Table 9.3. Conditions considered in surface charge solute transport simulations

Case	Counter Ion	Solubility Control	Comment
1	Ca^{+2}	Calcite	
2	Ca^{+2}, Na^{+}	Calcite	Na^{+} introduced with Cl^{-} source
3	Ca^{+2}, Na^{+}, Mg^{+2}	Calcite, Dolomite	

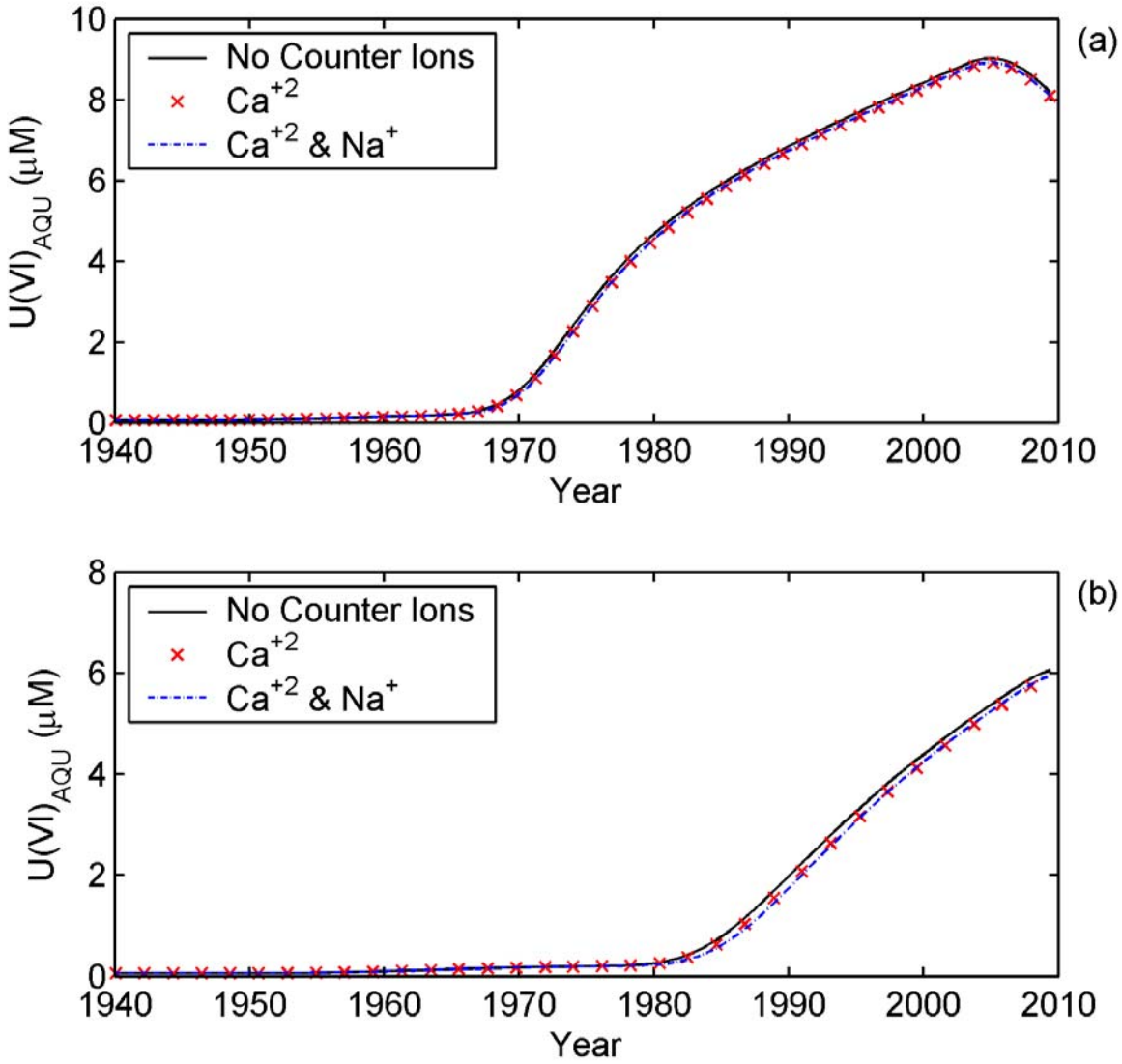

Figure 9.12. Simulated U(VI) breakthrough curves comparing the effect of the counter ion immobilized from solution. Simulations are for (a) well NAT26 and (b) well MAU08.

The simulations for both cases 1 and 2 resulted in dissolved U(VI) concentrations that were only 2% smaller than those simulated with no counter ions. The simulations for case 3 that include Mg^{+2} as a counter ion are not shown, but these gave similar results to those observed for cases 1 and 2. These simulations show that neglecting the development of surface charge caused by the formation of charged U(VI) surface species does not introduce significant errors into the transport simulations for the Naturita alluvial aquifer. The significance of the assumption could be greater at other sites with different groundwater compositions.

9.6.4 Effect of Cation Exchange Reactions

U(VI) adsorption and transport is strongly affected by alkalinity, and therefore processes that can affect alkalinity could affect U(VI) transport. Ion exchange reactions are one of the potential processes that can modify alkalinity, given that the waters are at or nearly at equilibrium with respect to calcite (see Section 3). One driving process for a change in alkalinity is that Na^+ introduced into the groundwater from the salt roasting process could displace Ca^{+2} from an ion exchanger, such as a clay mineral (X), e.g.,

$$Na^+ + ½\ CaX_2 = NaX\ + ½\ Ca^{+2} \qquad \textbf{(9.15)}$$

The calcium can precipitate as calcite to decrease the alkalinity and pH, e.g.,

$$Ca^{+2} + HCO_3^- = CaCO_3 + H^+ \qquad \textbf{(9.16)}$$

and U(VI) transport is affected by the combined effects of lower alkalinity and pH. If the Na^+ source is removed, the reverse process presumably occurs.

To test the significance of this process, simulations were conducted that include the Ca/Na ion exchange reaction (Eq. 9.15). The Gaines-Thomas approach was used to model the ion exchange reaction and the equilibrium constant was taken from Appelo and Postma (1993). Because the cation exchange capacity (CEC) of the NABS sample was not determined, a range of values equal to 1 meq/L, 3 meq/L, and 10 meq/L was considered.

Simulation results are shown in Figure 9.13 as breakthrough curves at well NAT-26. The simulations for the CEC equal to 1 meq/L agreed very closely with simulations that did not consider ion exchange reactions (simulations not shown). At 3 meq/L, the start of the U(VI) breakthrough was slightly delayed, and the peak U(VI) breakthrough in 2008 was approximately 10% larger than the 1 meq/L case. A similar trend was observed for the 10 meq/L case, but the start of the breakthrough was delayed more and the peak concentration was 60% higher than the case with no ion exchange. The plots of Ca^{2+}, pH and alkalinity all agree with the trend expected from ion exchange of Na^+ for Ca^{2+} and the precipitation of calcite.

Although the ion exchange capacity was not known, the field observations suggest that the effective CEC is less than 10 meq/L. First, the simulations with a CEC of 10 meq/L showed pH values that ranged between 6.5 and 7.4, and the highest pH values were present at the leading edge of the plume and the lowest pH values were at the trailing edge of the plume. In contrast, the field data do not illustrate such a trend in pH. Second, the simulations suggest that a peak of high Ca^{+2} would have passed through the system around 1960. No evidence for this peak was observed in the earliest samples taken in 1984, although it is possible that the peak was missed in the early sampling. Simulations that included Mg^{+2} as an exchanging ion gave qualitatively similar results, although the amplitudes of the changes in dissolved U(VI), Ca, pH and alkalinity were smaller. The simulations did not include pH-buffering reactions by the solid surfaces, which are likely to have a significant impact of pH excursions. The pH-buffering reactions would probably further dampen the changes in dissolved U(VI) concentrations. Nevertheless, ion exchange reactions may play an important role in modifying U(VI) transport in some systems, even if U(VI) does not directly adsorb to the ion exchanger.

9.7 Conclusions

Adsorption and reactive transport of U(VI) is affected by variable chemical conditions. One likely important type of chemical variability within the Naturita alluvial aquifer is that resulting from variable alkalinity, which in freshwaters is primarily accounted for by HCO_3^- and CO_3^{-2} anions. Variable alkalinity concentration is particularly important for U(VI) mobility because U(VI) forms both aqueous and sorbed complexes with the carbonate anions. For the Naturita conditions, the observed alkalinity was more important than either

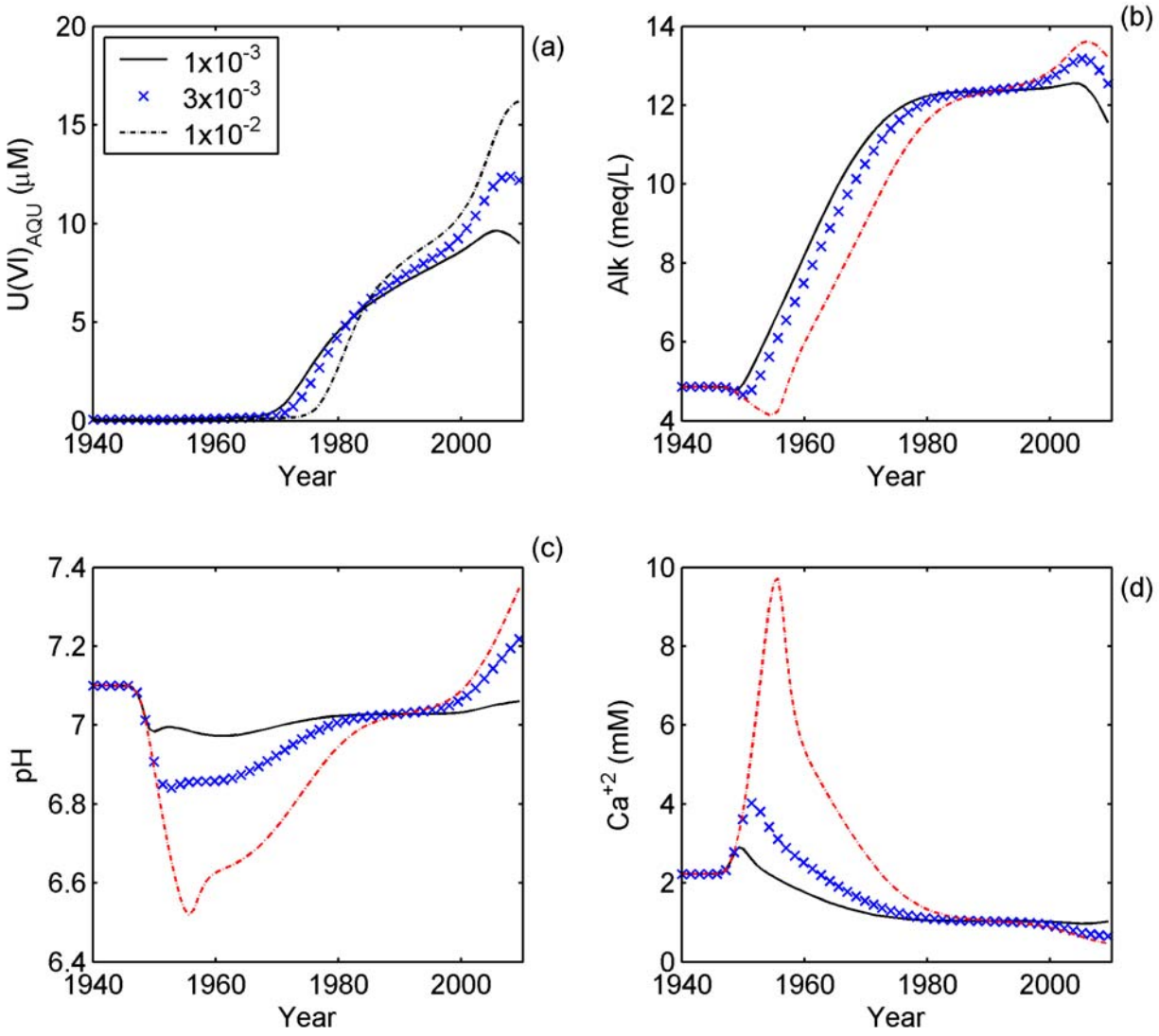

Figure 9.13. Effect of ion exchange reactions on U(VI) breakthrough for various cation exchange capacities.

variable pH or U(VI) concentration in influencing U(VI) mobility.

K_d values calculated for the groundwater analyses and the SCM developed in Section 5 ranged from 0.12 to 9.1 mL/g, and the values were bimodally distributed. Low K_d values were associated with portions of the plume containing high concentrations of dissolved U(VI) and alkalinity. Higher K_d values were associated with low concentrations of dissolved U(VI) and alkalinity. Performance assessment modelers must recognize not only that variable chemical conditions can cause a range of effective K_d values to be observed, but also that the spatial distribution of K_d values within that range is not likely to be a random function or a normal distribution. In plumes with chemical gradients, the spatial distribution of K_d values can be quite complex and be characterized by significant spatial character.

A two-dimensional reactive transport model was calibrated to the observed distribution of dissolved U(VI) in the field. The model was based on an independently calibrated flow

model and an independently calibrated SCM for U(VI) sorption. The transport model was calibrated to the field data using well water analyses from samples collected between 1984 and 2001. The model was calibrated by applying a single constant mass loading rate over the area that was occupied by the former mill and tailings pile. The source added U(VI) and alkalinity to the groundwater. With this simple source term, the observed U(VI) and alkalinity in 12 wells was reproduced satisfactorily by the model simulations. K_d values were calculated from the simulated concentrations. A comparison of these K_d values with the U(VI) concentrations showed that the largest U(VI) concentrations were transported with the smallest K_d values.

A sensitivity analysis illustrated that for the weak and strong surface sites in the SCM, the simulations were equally sensitive to the site concentrations or equilibrium constants. It was shown that this is expected if the surface coverage is small, because it is the product of these two quantities that determines the amount of U(VI) sorption. Overall, the simulated U(VI) concentrations were most sensitive to hydraulic conductivity. The sensitivity to the entire SCM was approximately 45% of the sensitivity to the hydraulic conductivity.

Several simplifying model assumptions were also examined. The simplified geochemical model that assumed equilibrium with calcite and an average ionic strength for the groundwater resulted in K_d values that were on average within 20% of the K_d values calculated from a complete aqueous speciation model. The assumption of local chemical equilibrium was tested by including reaction rates that were estimated from batch kinetic data. Although the batch experiments showed that approximately 3 days was required to reach steady-state aqueous U(VI) concentrations, the transport simulations using the rate-controlled model agreed well with the local equilibrium approximation. The assumption that the surface charge resulting from a charged surface species could be neglected was also investigated. Simulations that balanced the adsorbed charge by removing a cation from solution were nearly identical to the simulation results that did not consider the surface charge.

The reactive transport model that includes the Generalized Composite SCM (see Section 5) is a useful tool for simulating the transport of U(VI) at the field scale with chemically variable conditions. This modeling approach is a compromise modeling approach between the simple constant K_d approach and the most complex of SCM modeling approaches that attempt to account for sorption on each of the many minerals present in most sediments and possibly the electrical double layer properties of each mineral phase. The Generalized Composite modeling approach is based on the premise that the surface chemistry of mineral grains is dominated by coatings, and as a consequence, adsorption can be described with a relatively small set of reactions and mass action expressions. The Generalized Composite modeling approach can be easily applied, and it does not require a burdensome program of data collection. The model is capable of accounting for the effects of variable chemical conditions on U(VI) adsorption and transport. In the Naturita case, the most important variable chemical condition was the alkalinity, but at other sites, pH or the concentrations of other complexing ligands could be important.

10 COMPARISON OF APPROACHES FOR SIMULATING THE REACTIVE TRANSPORT OF U(VI) IN GROUNDWATER

10.1. Introduction

Simulations of the reactive transport of U(VI) in groundwater are an important step in evaluating the future risk associated with U(VI) contaminated groundwater. Reactive transport models couple the effects of groundwater transport with the effects of groundwater geochemistry and thus provide a critical linkage between groundwater transport and geochemical reactions. For U(VI), which is relatively soluble in oxic waters, the migration can be controlled by adsorption to subsurface sediments. The purpose of this section is to compare simulation results obtained using both the single K_d approach and the semi-empirical SCM approach for simulating adsorption in solute transport simulations. Model simulations were conducted using the distribution of U(VI) concentrations in groundwater observed in 2000 as the initial condition and transport was simulated for a period of 200 years or more. In addition, simulations are presented that compare the uncertainty of selected predicted values associated with different adsorption models.

10.2. Comparison of Approaches for Describing U(VI) Adsorption

This section compares the constant-K_d and the semi-empirical SCM approach for describing adsorption by Naturita sediments and also summarizes how parameters for the two approaches could be estimated.

For the constant-K_d approach, K_d values were obtained from (1) a screening level distribution of K_d values, (2), site-specific K_d values, and (3) K_d values generated from the semi-empirical SCM (Section 5, the version that did not consider the aqueous species, $CaUO_2(CO_3)_3^{2-}$ and $Ca_2UO_2(CO_3)_3^0$(aq), coupled with the observed variable chemical conditions (Sections 3 and 9). Simulations were also conducted with a coupled reactive transport model using the site-specific, semi-empirical SCM that was calibrated with laboratory measurements (Section 5). Each of these 4 approaches are described in greater detail below with a particular emphasis on how each of these approaches was used for the Naturita site.

The application of K_d values at the Naturita site needs to account for the large fraction of cobbles in the aquifer. This was done by assuming that the <3 mm fraction accounts for all of the sorption capacity of the aquifer. Under these assumptions, the gravel corrected K_d values are given by (Kaplan et al., 2000):

$$K_{dc} = (1\text{-}f)K_d(<3\text{ mm}) \qquad \textbf{(10-1)}$$

where K_{dc} is a gravel-corrected K_d value, f is the fraction of gravel and cobbles, and K_d(<3 mm) is the K_d of the less than 3mm fraction of the sediment. In Section 5 it was estimated that the cobbles and gravels accounted for 85% of the aquifer sediments. Consequently, the gravel-corrected K_d values equal 0.15 times the K_d values for the NABS sample.

Often in groundwater studies, the rate of movement of a contaminant plume is described by a retardation factor (R_f) which is define as ratio of the velocity of a nonreactive contaminant to that of reactive contaminants. The R_f is related to the K_d value by

$$R_f = 1 + \frac{\rho_b}{\theta} K_d \qquad \textbf{(10-2)}$$

where ρ_b is the bulk density and θ is the effective porosity.

10.2.1 Reactive Transport Coupled with a Surface Complexation Model

Section 5 presented a semi-empirical SCM to describe U(VI) adsorption by the NABS sample. The SCM was used in a reactive transport model so that the effects of variable chemical conditions could be simulated. Simulations were performed using RATEQ (Curtis, 2003), which couples reactive transport to MODFLOW

and MT3DMS. An advantage of the reactive transport model is that the spatial structure of the variable K_d values (Section 9) is honored. In addition, the spatial structure varies temporally in simulations in response to the transport and reactive processes.

10.2.2 Handbook K_d Values

Krupka et al. (1999) summarized measured U(VI) K_d values determined in single mineral studies and in soil/sediment studies. Solution pH and alkalinity were identified as key variables that determine K_d values. However, even with this understanding, K_d values in a graphical summary at pH 7 ranged from 63 to 630,000 mL/g. In addition, it is important to note that this range was based on experimental values determined under atmospheric pCO_2. At higher pCO_2 values, which are typical of the soil environment, smaller K_d values would be expected. The measured K_d values for the Naturita field conditions described in Section 6 were all smaller than the range described above, probably because the pCO_2 values in the field are significantly above atmospheric values.

The US NRC code DandD (MacFadden et al., 2001) is intended to perform screening analyses of dose associated with exposure to radionuclides including U. This code contains a default distribution of K_d values for U(VI); the default distribution is a log normal distribution with a mean log K_d value of approximately 2.1 log units and a standard deviation of 1.4 log units. It is recognized in the screening level calculations that there is considerable uncertainty associated with the K_d value for any particular site and therefore most screening level applications involve sampling the entire distribution of K_d values. In the simulations presented below, the default distribution of K_d values for the DandD code was used to demonstrate the full range of values that could be encountered in a screening study. The screening level distribution, which is shown in Figure 10.1, has K_d values that range from 0.1 to 100,000 mL/g. This distribution was not corrected for the presence of gravels and cobbles in the aquifer because it was assumed that the wide distribution of K_d values in the screening level distribution accounted for the presence of these weakly or nonsorbing large particles. Moreover, screening level calculations would presumably be performed without any site characterization, and therefore it would not be known what the fraction of cobbles and gravels would be in the aquifer.

10.2.3 Site-Specific K_d Values

K_d values were measured on contaminated sediment samples collected at the site and on the Naturita aquifer background sediment (NABS) sample (Section 6). The contaminated and background sediments were each collected from a different location and the groundwater at the different locations had variable U(VI) concentration, alkalinity, and pH. Field K_d values were calculated from the observed total U(VI) concentrations in groundwater and from the amount of "labile" U(VI) associated with the sediment samples. The sediment-associated labile U(VI) was estimated by both an isotopic exchange approach and by extraction of U(VI) with a pH 9.45, 20 meq/L carbonate solution (Section 6). The two methods gave nearly identical results. The K_d values calculated from the isotopic exchange results were used as the site-specific values. It is possible that K_d values for two samples from wells MAU-03 and MAU-04 could have been influenced by reducing conditions. Nevertheless, the K_d values measured on MAU-03 and MAU-04 sediments were used together with all other K_d values determined by isotopic exchange in the following analysis.

The K_d values determined by the isotopic exchange method for all of the samples ranged from 0.51 mL/g to 36.9 mL/g and had a mean value of 7.92 mL/g. These K_d values are illustrated in Figure 10.1 which shows minimum and maximum K_d values as well as K_d values at each tenth percentile. In using these K_d values in the transport model, the K_d values were first corrected for the presence of gravels and cobbles using Equation 10-1. The site-specific determinations decreased the range in K_d values from a factor of 10^6 for the screening level K_d values to a factor of 72 for the measured values.

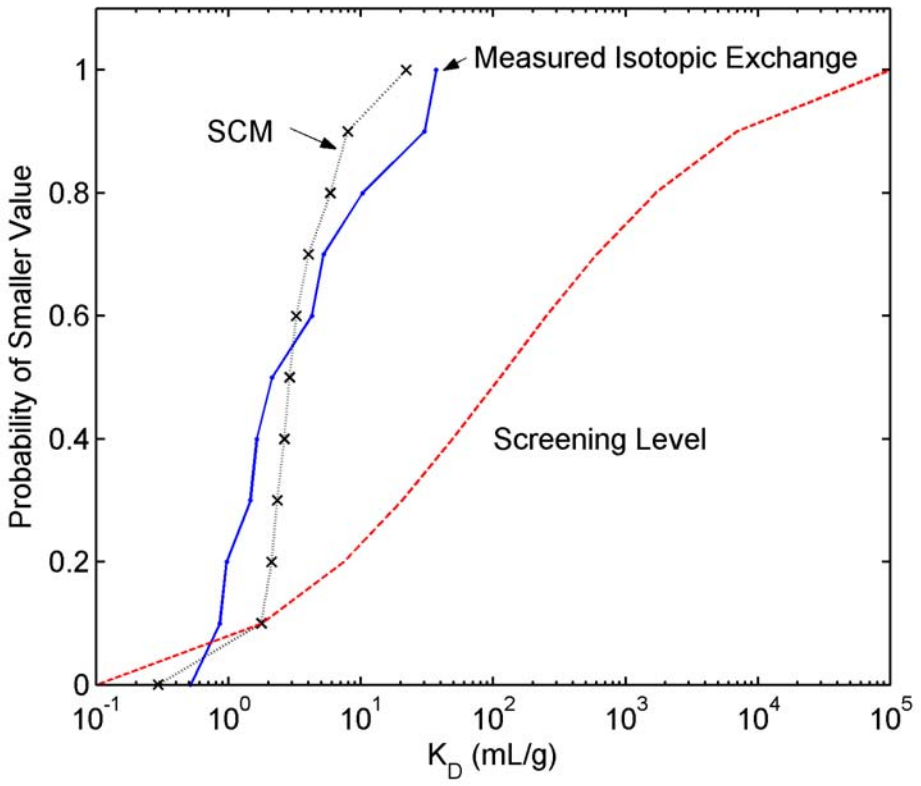

Figure 10.1. K_d distributions based on the screening level K_d values, measured isotopic exchange values for the <3 mm particle size of the NABS sample, and SCM-predicted K_d values for the < 3 mm particle size.

10.2.4 Model-Generated K_d Values

The distribution of K_d values determined from the isotopic exchange results is limited in part by the locations where contaminated sediments were collected. In particular, no sediment samples were collected during the installation of either well NAT-26 or NAT-25, which have historically had the largest alkalinity values. These large alkalinity values are consistent with the smallest K_d values for the site (Section 9). An approach for accounting for the limitation imposed by having sediment extraction results at only some well locations is to compute model-generated K_d values at all sampling wells. Thus, K_d values were calculated from a combination of (1) the semi-empirical SCM, (2) the observed values of pH, alkalinity and U(VI) concentration, and (3) an average surface area of 12.4 m^2/g of the < 3 mm fraction. This value for the specific surface area is the average of all surface area determinations on sediments collected at the Naturita site (Section 6). The simulated distribution is illustrated in Figure 10.1. The K_d values computed from the SCM ranged from 0.29 mL/g to 22 mL/g. The minimum K_d of 0.29 mL/g is smaller than the values measured by isotopic exchange; the smaller calculated value results from the combination of high alkalinity and high U(VI) concentrations at well NAT-26. The maximum model K_d is also smaller than the measured K_d values. This could result because the K_d values at MAU03 and MAU04 are anomalously high (Section 6). As in the case of the measured K_d values, the model-generated K_d values ranged by nearly two orders of magnitude. The model-generated K_d values were adjusted for the presence of gravels and cobbles using equation 10-1.

10.3 U(VI) Transport Predictions

Two-dimensional reactive transport simulations were conducted to illustrate the key differences that result when adsorption is simulated using the K_d approach versus the SCM approach. The simulations used the existing U(VI) plume concentrations (Figure 10.2a) as the initial conditions. The reactive transport simulations that used the SCM also used the observed alkalinity (Figure 10.2b) together with a constant pH of 7.1. Figure 10.2c illustrates the initial adsorbed U(VI) concentration computed from the SCM and the observed geochemical data. The peak adsorbed concentration is located at well NAT-26, and there is region upgradient of well NAT-26 that has predicted adsorbed U(VI) concentrations that remain high even though the dissolved U(VI) concentrations decrease. Figure 10.2d shows the R_f values computed from the observed dissolved U(VI) concentration and the simulated adsorbed U(VI) concentrations. The simulated log R_f values have minimum values of 0.18 log units ($R_f = 1.5$) to maximum values of 1.2 ($R_f = 16$), and the distribution of these values generally reflects the distribution of the observed alkalinity.

The simulations that used the constant-K_d approach used gravel and cobble corrected K_d values of 0.08 mL/g, 0.14 mL/g and 1.5 mL/g. The K_d of 0.08 mL/g is the minimum K_d observed in the isotopic exchange experiments (Section 6). In addition, this K_d value nearly equals the K_d simulated from the recent conditions at well NAT-26, which has the highest alkalinity values. This K_d value is particularly important because the results in Section 9 demonstrated that the largest U(VI) concentrations were associated spatially with the largest alkalinity values, and therefore, the smallest K_d values.

The K_d value of 0.14 mL/g was chosen for illustrative purposes. It equals the K_d of the 15th percentile of the isotopic exchange values after correction for gravel and cobbles. (i.e., only an estimated 15% of the isotopic exchange values were smaller that 0.15 mL/g). The value of 1.5 mL/g was selected because this value equals the value of the 85th percentile of the isotopic exchange values. The K_d values of 0.08 mL/g, 0.14 mL/g and 1.5 mL/g correspond to retardation factors of 1.7, 2.3, and 23, respectively.

10.3.1 Multicomponent Reactive Transport Predictions

Figure 10.3 shows the predicted evolution of the dissolved U(VI) and alkalinity plumes after 20 and 60 years of transport. In addition, the log of R_f values are also shown. After 20 years of transport, both the U(VI) and alkalinity plumes have high concentrations that are similar in value to the initial conditions, and the higher concentrations are still present adjacent to the western side of the aquifer. The R_f values, which were initially relatively constant over most of the aquifer, show considerably more spatial variability. In particular, the log of R_f values range from approximately 0.2 ($R_f \sim 1.5$) in regions where the U(VI) and alkalinity values are largest to approximately 1.0 ($R_f \sim 10$) in the upgradient areas. The R_f value of 1.5 corresponds to a K_d value of 0.065, and the R_f of 10 corresponds to a K_d value of 1.0 mL/g. After 60 years of transport, the simulated alkalinity has nearly reached background values, but a U(VI) plume with concentrations from 1 to 3 μM remains along the western side of the aquifer. The log R_f values after 60 years are almost all in the range of 0.7–1.1 (R_f = 5.5-12.5) which corresponds to K_d values of 0.44 to 1.3 mL/g. Over the 60 years of transport, the R_f values ranged from nearly uniform values equal to approximately 1.5 to nearly uniform values equal to approximately 10, but at the intermediate time scale, the simulations show significant spatial character.

10.3.2 Comparison of Two-Dimensional Simulated Plumes

Predicted U(VI) concentrations are illustrated for simulations obtained using the three K_d values and the SCM model after 20 and 60 years of transport in Figure 10.4. The SCM simulations show that after 20 years of transport, high U(VI) concentrations still exist near well

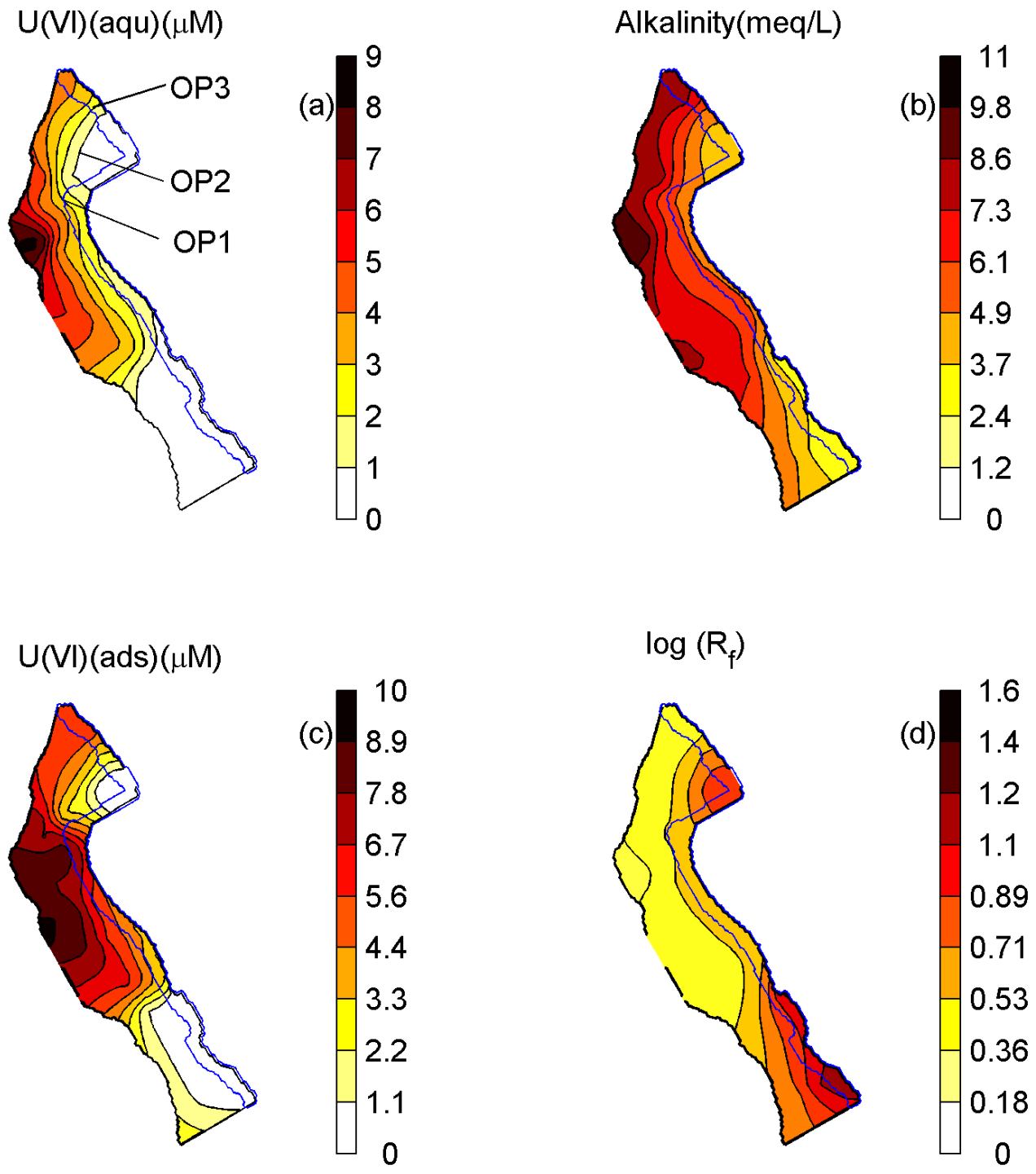

Figure 10.2 Observed distributions of U(VI) concentration, alkalinity and SCM-predicted K_d values in September 1999. The K_d values were computed from the SCM using the observed U(VI) concentrations, alkalinity, a pH of 7.1, and an average surface area of 12.4 m^2/g for the aquifer sediments.

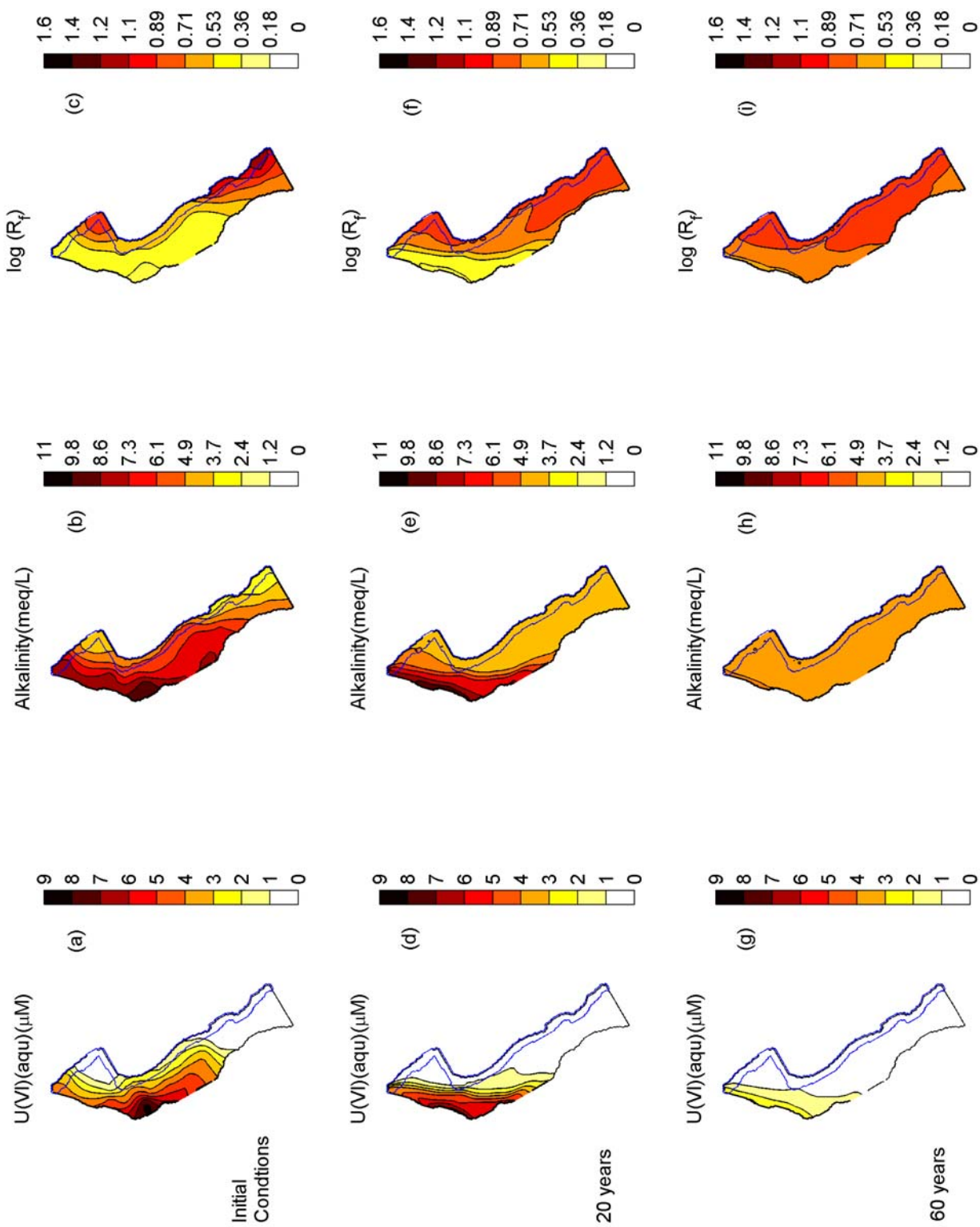

Figure 10.3 U(VI) concentrations, alkalinity, and log R_f values at September 1999 (initial conditions), at 20 years of simulated reactive transport, and at 60 years of simulated reactive transport.

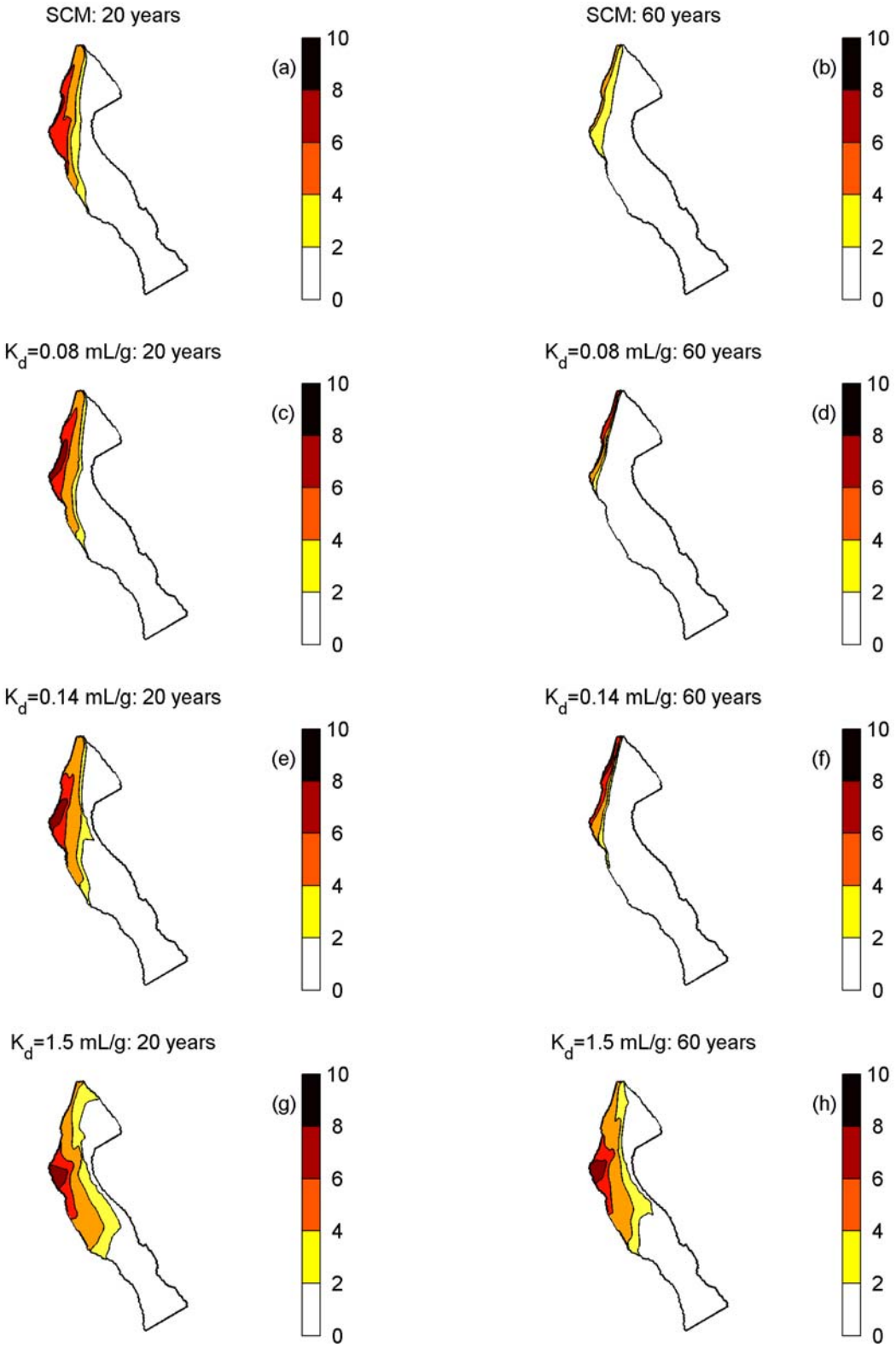

Figure 10.4. Simulated U(VI) concentrations after 20 and 60 years of transport, with U(VI) adsorption predicted by the SCM or constant-K_d values of 0.08, 0.14, and 1.5 mL/g.

NAT-26. In addition, the U(VI) concentrations near the river are predicted to decrease as a result of recharge of the aquifer from the San Miguel River. After 60 years, the effect of transport on peak U(VI) concentrations is more pronounced. The peak concentrations of approximately 1-3 μM are confined to a narrow plume adjacent to the highway along the western edge of the aquifer, and most of the U(VI) has been flushed into the San Miguel River.

The constant-K_d simulation with a K_d value of 0.08 mL/g shows results that are similar to the results predicted with the SCM after 20 years of transport. The shape of the U(VI) plume after 20 years generally agrees in the two simulations, suggesting a similar extent of transport. The constant-K_d approach predicts slightly higher concentrations downgradient of well NAT-26 relative to the SCM approach.

After 60 years of transport, the U(VI) plume simulated with a K_d value of 0.08 mL/g is considerably smaller than that predicted by the SCM modeling approach. The smaller plume is probably the result of a of two factors. First, in the SCM simulations, the lower concentrations of U(VI) and alkalinity result in larger K_d values, and therefore the plume in the SCM simulations migrates more slowly with increasing time. Second, the mass of U(VI) considered in the two simulations is different because the initial adsorbed U(VI) is computed from the dissolved U(VI) concentrations. This factor is discussed further below.

The simulation with a constant-K_d value of 0.14 mL/g ($R_f = 2.3$) gave a larger U(VI) plume after 20 years of transport in comparison to the SCM prediction, but after 60 years, the plumes have generally similar characteristics. Thus, the constant-K_d simulations using a K_d value of 0.08 mL/g generally agree with the SCM predictions after 20 years of transport, whereas the constant-K_d simulations using a K_d value of 0.14 mL/g generally agree with the SCM predictions after 60 years. This result occurs because the SCM approach predicts increasing adsorption as the U(VI) concentrations and alkalinity values decrease with time.

The predicted U(VI) plumes with the constant-K_d of 1.5 mL/g did not change significantly over the 60 years of simulation because of extensive retardation.

10.3.3 Comparsion of U(VI) Breakthrough at Selected Locations

Simulated breakthrough curves were recorded at 3 locations, (OP1, OP2, and OP3) shown on Figure 10.2a. Predicted breakthrough curves for constant-K_d values of 0.08, 0.14 and 1.5 mL/g and for simulations using the semi-empirical SCM are illustrated in Figure 10.5. The simulated peak concentrations were nearly identical in the three constant-K_d simulations. This occurs because, in each case, the initial plume (Figure 10.2a) is eventually transported to the observation well. However, in the SCM predictions, the peak concentrations were between 0 and 20% smaller than in the constant-K_d simulations. The differences exist because alkalinity also varies in the simulations to varying degrees at the different wells. Simulations obtained using the constant-K_d values equal to 0.08 and 0.14 mL/g gave peak shapes that generally agreed with the SCM predictions during the first 30 to 40 years of transport. However, with increasing time, the SCM simulation gave significant tails that were considerably larger on a relative scale than the tails predicted with constant-K_d values of 0.08 and 0.14 mL/g. The tailing that is simulated with the SCM is caused by the three types of adsorption sites (Section 5), and because the alkalinity at the observation wells decreases with time (Fig. 10.4).

Simulations with a constant-K_d value of 1.5 mL/g ($R_f = 14$) gave significantly different results from the other simulations because there was negligible U(VI) transport in 60 years. The breakthrough simulated in this latter case occurs significantly after breakthrough simulated with the other K_d values or the SCM.

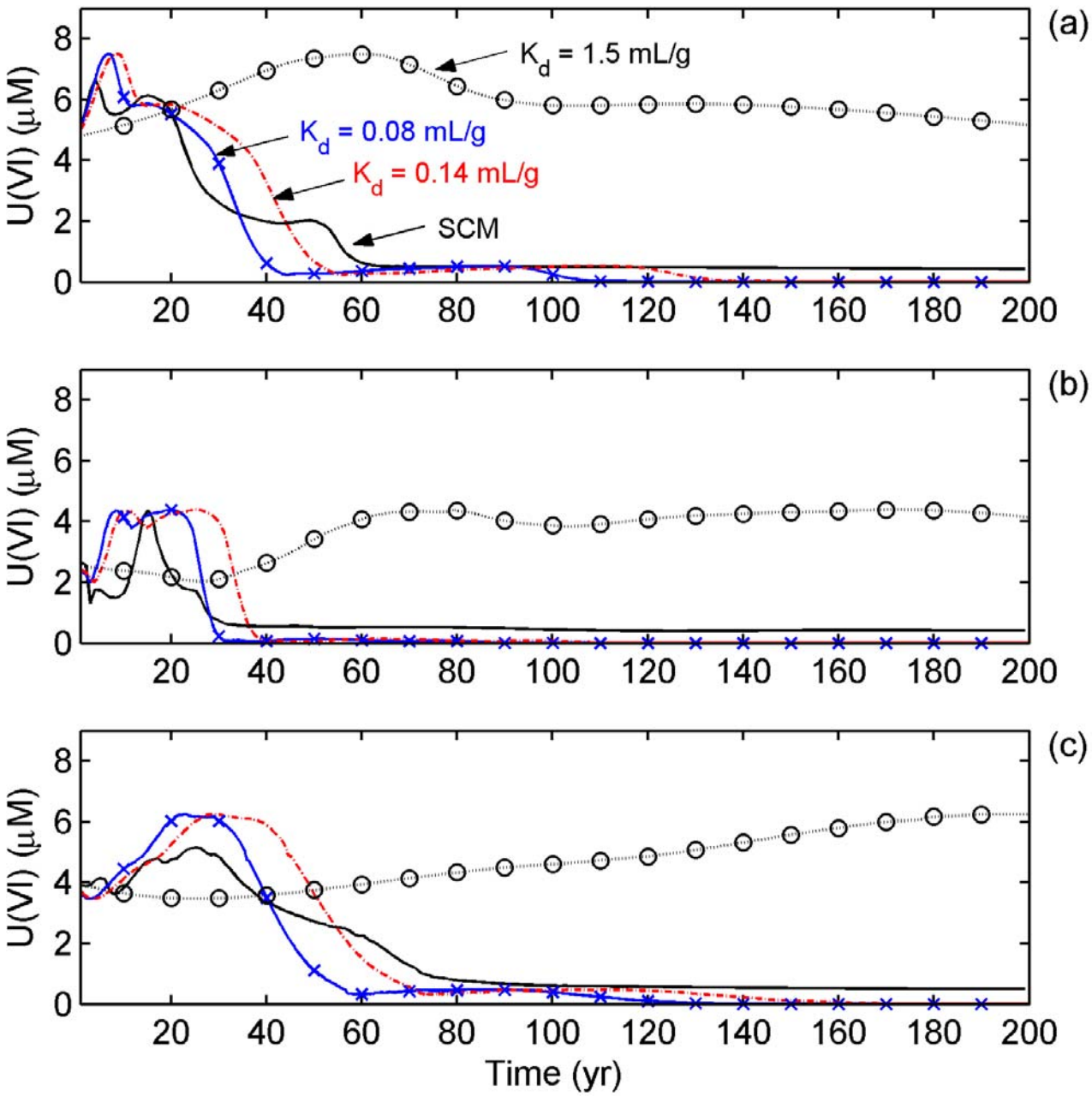

Figure 10.5 Simulated U(VI) breakthrough curves computed using the semi-empirical SCM and constant-K_d values of 0.08 mL/g, 0.13 mL/g, and 1.5 mL/g. Curves are shown for breakthrough at points a) OP1, b) OP2, and c) OP3 (see Fig. 10.2a).

10.3.4 Comparison of U(VI) Mass Discharge to the San Miguel River

A second important difference between the constant-K_d and the SCM simulations is that the total mass of U(VI), defined as the sum of the dissolved U(VI) and the adsorbed U(VI), is different in the two simulations. In all cases, the same initial dissolved U(VI) concentration was used (Figure 10.2a). However, the initial adsorbed U(VI) was computed from the dissolved U(VI) concentration and the adsorption model. In simulations that had K_d values of 0.08, 0.14 and 1.5 mL/g, the total U(VI) mass increased linearly with the K_d value.

Simulated dissolved mass of U(VI) is shown in Figure 10.6 for constant-K_d values of 0.08 mL/g, 0.14 mL/g, 1.5 mL/g and the SCM. Initially, all four cases had the same mass of dissolved U(VI) in the aquifer. For K_d values of 0.08 and 0.14 mL/g, the total dissolved mass decreased to near zero after approximately 150 years. The total dissolved U(VI) mass predicted using the SCM was similar to that observed for the two small K_d values in the first 30 years of transport. Subsequently, the dissolved U(VI) mass predicted with the SCM showed a very long tail that decreased very slowly. This long tail results because of the presence of the strong and very strong adsorption sites (Section 5). The total dissolved mass predicted using a constant-K_d value of 1.5 mL/g decreased very slowly, because of the extensive retardation at this larger K_d value.

The total mass (aqueous plus adsorbed) of U(VI) in the aquifer is shown in Figure 10.6b. The total mass predicted using the constant-K_d values of 0.08 mL/g and 0.13 mL/g were initially about half of the mass simulated using the SCM. The initial total mass predicted using a K_d value of 1.5 mL/g was about 2 times larger than the mass simulated using the SCM. Simulations with even larger K_d values, such as the largest K_d values from either the isotopic exchange or model-generated K_d distributions or most of the screening level K_d values, would significantly overestimate the total mass of U(VI) in the aquifer.

10.4. Variability of Sorption Parameters

K_d values are lumped parameters for describing adsorption. The lumped parameters account for the effects of natural heterogeneities of the aquifer sediments as well as the effects of variable chemical conditions. In some poorly controlled studies, K_d values may have been affected by precipitation and/or redox reactions. Because K_d values are lumped parameters, there is no simple way of accounting for the individual processes that affect the K_d value. In contrast to the constant-K_d approach, the SCM approach provides a framework that can be used to account for effects of SCM model parameter variability and/or geochemical variability on the predicted U(VI) transport. Specifically, with the SCM approach, it is possible to conduct sensitivity and uncertainty simulations that evaluate the effects of parameter uncertainty and geochemical variability on simulation results.

10.4.1. Variability of K_d Values

The variability in K_d values is generally represented by probability distributions such as those illustrated in Figure 10.1. Simulations are often conducted by repeatedly sampling this probability distribution to evaluate how predicted concentrations depend on the assumed variability in K_d values. In the simulations below, calculations were performed using the distribution of K_d values shown in Figure 10.1. These simulations included the minimum and maximum K_d values and K_d values at each tenth percentile. The calculations were performed using this relatively small set of K_d values because the intent was to consider only the variability introduced from the different adsorption models. Because of the linearity of the K_d simulations, and because only the K_d values were varied, the calculations with this small set of K_d values were adequate for representing the effects of K_d variability on predicted U(VI) concentrations.

10.4.2 Variability of SCM Model Parameters

In contrast to the constant-K_d approach, the semi-empirical SCM adsorption modeling approach provides an efficient means of synthesizing various experimentally accessible and disparate data. These kinds of data include the solution composition (e.g., pH, alkalinity and U(VI) concentration), the SCM parameters, including the equilibrium constants and the fractions of various reactive sites, and finally, the total amount of reactive sites, which is assumed to be proportional to the specific surface area of the sediments. One approach for

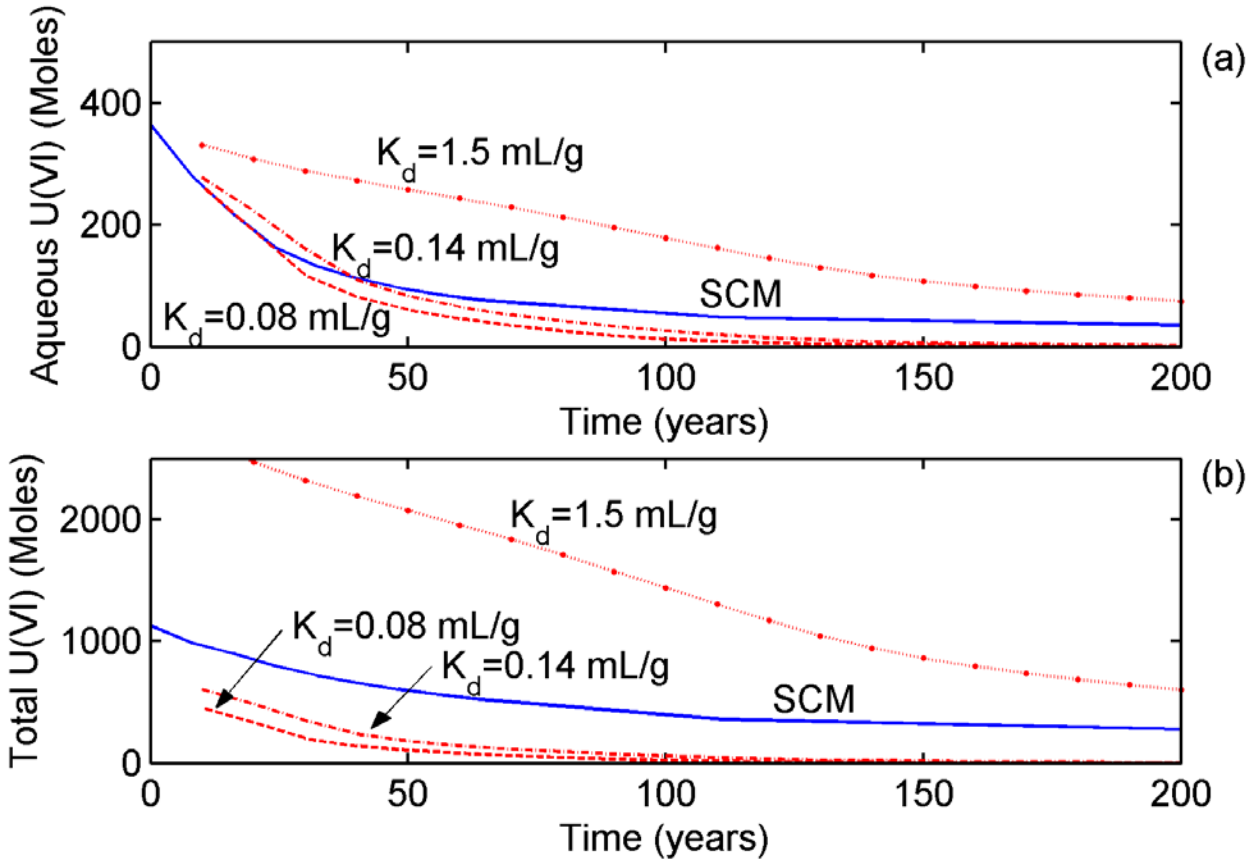

Figure 10.6 Predicted dissolved and total mass of U(VI) in the Naturita aquifer determined using constant-K_d values of 0.08 mL/g, 0.14 mL/g and 1.5 mL/g, and the semi-empirical SCM.

evaluating all of these parameter values is to conduct Monte Carlo simulations where each input parameter value is varied randomly.

Two-dimensional reactive transport simulations were conducted to evaluate the effect of SCM parameter variability on U(VI) transport by conducting Monte Carlo simulations. Parameter values were generated using the Latin Hypercube Sampling (LHS) approach using the LHS code (Iman and Shortencarier, 1984). In this approach, for N Monte Carlo simulations, each parameter is partitioned into N intervals of equal probability. Parameter sets are then formed by selecting one parameter for a given interval and pairing this parameter with other parameters from different intervals. Simulations are then performed for each of the N sets of parameters. The purpose of the LHS approach is to reduce the total number of calculations required for the Monte Carlo simulations.

The SCM parameter values were generated using the LHS code assuming that each of the parameters was independent of all other parameters. The SCM model parameters that were varied are listed in Table 10.1. The four log K values were each varied over 2 orders of magnitude, and it was assumed that each value was described by a uniform probability distribution. For each log K, the distribution was centered on the log K value determined by fitting batch adsorption data (Section 5). The fractions of the strong sites and very strong sites were each varied over 1 order of magnitude. With this range, the concentration of the strong sites was always larger than the concentration of the very strong sites. The fraction of weak sites was computed by subtracting the fractions of the strong and very strong sites from the total site density. Finally, the surface area was assumed to be described by a normal distribution, based on all of surface areas measured for the

Table 10.1 Summary of parameter distributions used for the SCM uncertainty analysis.

Parameter Description	Symbol	Distribution Type	Distribution Values	Comment on Values
Weak site log K	Log K_W	Uniform	-7.74 to -5.74	Range
Strong site log K	Log K_{SC}	Uniform	-9.00 to -7.00	Range
Very strong site log K	Log K_{SS}	Uniform	-3.06 to -1.06	Range
Very strong site ternary log K	Log K_{SSC}	Uniform	-7.36 to -5.36	Range
Fraction of strong site	Log f_s	Uniform	-2.42 to -1.42	Range
Fraction of very strong sites	Log f_{ss}	Uniform	-3.50 to -2.50	Range
Specific surface area	S_T	Normal	12.4±3.8	Mean and standard deviation

Naturita sediments (Section 6). A total of 225 sets of parameters were generated using the LHS code. This number of parameters is somewhat small for the LHS approach, but the number of calculations was limited by computing resources.

In Section 9 it was shown that the SCM model parameters were highly covariant, but the SCM parameters generated by the LHS code were independent. The covariance was most readily observed for the pairs of parameters such as the equilibrium constant of the strong site (K_S) and the total concentration of strong sites (>SOH_T). Similarly, the values of K_W and >WOH_T were also covariant. In addition, it is probable that all of the parameters are covariant to varying degrees. The covariance is difficult to quantify given the nonlinearity of the aqueous solution and surface speciation calculations. Thus, although the LHS code can account for covariance among parameters, the description of this covariance is difficult to define and likely varies with solution composition. However, it is important that this covariance be considered, because failure to account for the covariance can yield simulation results that are inconsistent with observations. For example, if a parameter set has values of both K_S and >SOH_T that are 10 times larger than the mean value, the simulated adsorption would be nearly 100 times larger than that simulated with the mean values.

To account for the covariance, parameters sets that gave model K_d values that were either too small or too large were rejected. The rejection criterion was based on comparing simulated K_d values with the K_d values measured by isotopic exchange at 17 different locations (see Section 6). For the comparison, the measured surface areas of each of the sediment samples was used in the calculations (Section 6). The semi-empirical SCM model (Section 5) gave predicted K_d values that agreed with observed K_d values within a factor of approximately 3 (Sections 6 and 7). The LHS parameter values were accepted if the predicted and observed K_d values agreed within an average factor of 4 for a particular set of parameters; otherwise, the parameter values were rejected. It was found that 113 sets of parameters met the acceptance criterion. Reactive transport simulations were then conducted with each of those parameter sets. The factor of 4 used in the rejection step was selected arbitrarily, but was guided by the agreement between the SCM and the isotopic exchange values.

10.4.3 Comparison of Results

Simulated breakthrough curves at well OP3 obtained using the three K_d distributions shown in Figure 10.1 and the reactive transport simulations are shown in Figure 10.7. The simulations with the isotopic exchange K_d values showed the expected trend of longer breakthrough times with increasing K_d value.

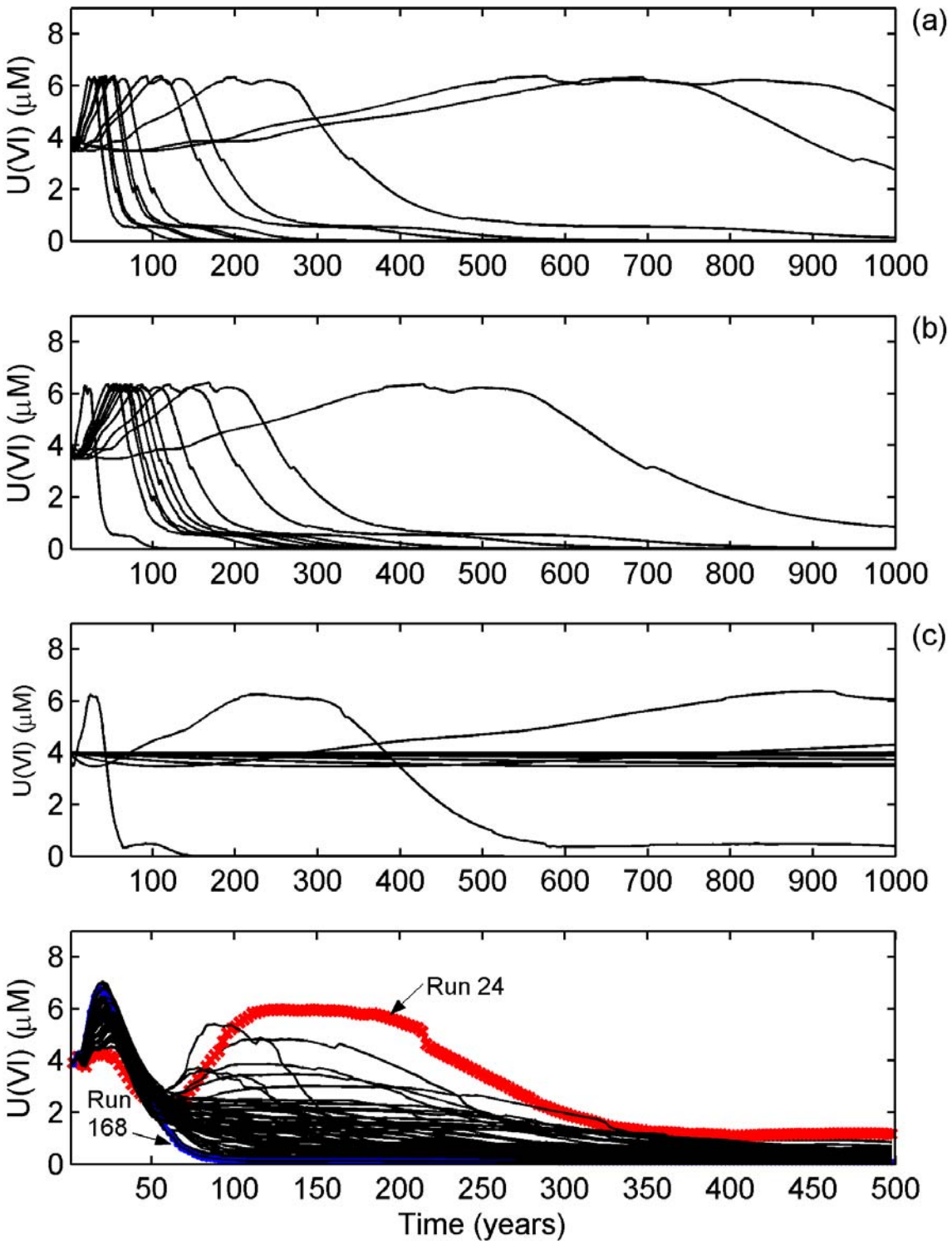

Figure 10.7. Comparison of predicted breakthrough of U(VI) at well OP3. Simulations are shown for: (a) the isotopic exchange K_d values, (b) SCM-generated K_d values, (c) screening-level K_d values, and (d) Monte Carlo simulations using the reactive transport model coupled with the SCM. Note the difference in scale for Figure 10.7d.

For each breakthrough curve, the U(VI) concentration initially increased to 7.5 μM, then dropped to 6 μM, followed by a more gradual decrease to 0.4 μM. The concentration then increased slowly to 0.6 μM, and eventually decreases to background concentrations. Each of these features in the breakthrough curves results from the U(VI) concentrations in the initial conditions. The main effect of the different K_d values is that the time required for each of these changes increases with increasing K_d value. For all of the isotopic exchange breakthrough curves, the peak concentration is nearly independent of the K_d value. However, the time of the peak arrival increases linearly with the K_d value; the arrival times increase from approximately 40 years for a gravel-corrected K_d value of 0.08 mL/g to 900 years for a gravel corrected K_d of 5.54 mL/g.

The results obtained with the SCM-generated K_d distribution are very similar to the results obtained with the isotopic exchange K_d values. The main difference is that the breakthrough curves for the largest SCM-K_d values eluted earlier than the corresponding isotopic exchange K_d value. For the smallest K_d values, there was practically no difference between the modeling approaches because adsorption, and therefore retardation, was small.

The results for the screening-level K_d values show a very broad range of breakthrough behavior. In seven out of eleven simulations, the simulated peak eluted after 1000 years. However, two of the simulations had peak concentrations that occurred between 40 and 200 years, which was similar to the range obtained with the isotopic exchange K_d values. Although the results with the screening-level K_d distribution covered a wide spectrum, the screening-level calculations were adequate in one sense, in that some of the simulations were similar to those obtained using the isotopic exchange K_d distribution.

The Monte Carlo simulations with the reactive transport model using the SCM gave results that were significantly different from the isotopic exchange K_d distribution or the SCM model-generated K_d distribution. Of the 225 Monte Carlo simulations, 63 yielded K_d values that agreed with the measured isotopic exchange values within a factor of 3. Predicted breakthrough curves for each of these 63 simulations are shown in Figure 10.7d. For the first 40 years, the predictions are very tightly grouped with a peak that occurs after approximately 20 years at a U(VI) concentration between 6 and 8 μM. After 40 years, the results show a considerable amount of tailing, as described in Section 10.3.2. In addition, there is a significant amount of variability that occurs between the various predictions. Some of the simulations reach concentrations that are less than 0.5 μM after approximately 80 years, while other simulations have long tails that slowly decrease the U(VI) concentration to approximately 1 μM after 200 years. Finally, several simulations show complex behavior, where the U(VI) concentration decreases after approximately 80 years, but then increases to concentrations exceeding 4 μM, as shown for RUN 24 in Figure 10.7.d.

A qualitative analysis of the cause of the significant tailing in some of the simulations suggests that this tailing was caused by sets of parameters with relatively large equilibrium constants for the strong and very strong sites and site concentrations that were relatively small. Kohler et al. (1996) observed that the simulations that had a small fraction of strong sites and large equilibrium constants also created a large amount of tailing. The parameters used in runs 24 and 168 are listed in Table 10.2 together with the mean values. The table shows that the most significant difference occurs for the strong site parameters. For run 168, that showed the least amount of tailing, the equilibrium constant was relatively weak, and the number of strong sites was large relative to the mean value. Thus, the strong site characteristics for run 168 were more like the weak site than the mean values of the strong site. The similarity between the weak and strong sites results in a more linear isotherm, and therefore less tailing. Conversely, the parameter values for run 24 show that the equilibrium constant is stronger than the mean value and the strong site

Table 10.2. SCM parameters for selected simulations

	Log Equilibrium Constant				Surface Site Concentration (Mole/L)		
	K_W	K_{SC}	K_{SS}	K_{SSC}	$>WOH_T$	$>SOH_T$	$>SSOH_T$
RUN 24	**-6.20**	**-7.26**	**-1.79**	**-5.52**	$2.03 \cdot 10^{-2}$	$1.03 \cdot 10^{-4}$	$9.78 \cdot 10^{-7}$
MEAN	**-6.74**	**-8.00**	**-2.062**	**-6.360**	$2.81 \cdot 10^{-2}$	$3.42 \cdot 10^{-4}$	$2.85 \cdot 10^{-6}$
RUN 168	**-6.85**	**-8.76**	**-2.77**	**-5.44**	$3.02 \cdot 10^{-2}$	$1.24 \cdot 10^{-3}$	$8.65 \cdot 10^{-6}$

concentration is much smaller than the mean values. These differences in the strong site characteristics cause a more nonlinear isotherm and more tailing in simulations. The U(VI) concentration increases after 80 years for run 24 because of increases in the alkalinity and the increased nonlinearity of the isotherm.

The results shown in Figure 10.7d are also probably strongly influence by the criteria used to reject some of the parameter sets. For example, the parameters for runs 24 and 168 may have given an adequate fit to the isotopic exchange data, but it is possible that one or both sets would have given a poor description of the batch U(VI) adsorption data (Section 5).

10.5 SUMMARY

Future transport of U(VI) at the Naturita site was simulated using the constant-K_d approach and semi-empirical SCM approach. The U(VI) K_d values used in the predictions were selected from values measured on contaminated Naturita sediments by isotopic exchange and values computed from an SCM developed from U(VI) adsorption experiments with uncontaminated Naturita sediments. In addition, U(VI) K_d values were used from a screening level distribution. Reactive transport simulations were conducted using the SCM developed in Section 5 together with the observed geochemical data. The relative level of agreement among the various transport predictions depended on which observation was used for comparison. For example, the maximum concentration of U(VI) at observation wells located downgradient of the existing U(VI) plume generally agreed within a factor of 2. This good level of agreement in most of the predictions resulted from the fact that the existing plume passed by the selected observation points during the 1000-year simulations. In addition, the existing plume is currently discharging to the San Miguel River at concentrations of 3 to 4 μM dissolved U(VI), and the peak concentrations in the existing plume are 9 μM. Therefore, the concentrations in the downgradient wells are not likely to increase by more than a factor of 3 unless alkalinity increases in the aquifer for some reason.

Significant differences among the transport predictions were observed when the times required to reach the peak concentrations were compared. For two site-specific K_d distributions used in the modeling, the time elapsed to reach the peak dissolved U(VI) concentration ranged from 22 to 700 years. In contrast, in the predictions with the SCM modeling approach, the time elapsed to reach the peak dissolved U(VI) concentration was between 18 and 30 years in 92% of the simulations. The remaining 8% of the simulations predicted that the elapsed time to peak concentrations was between 80 and 170 years. This relatively narrow range for the SCM simulations resulted in part because it was possible to reject some of the Monte Carlo simulations because the parameter sets yielded calculated K_d values that did not agree with the K_d values measured by isotopic exchange. It is possible that an even narrower range of values would have been observed if the rejection criterion was based on a comparison between calculated K_d values and U(VI) batch adsorption data.

A second difference between the constant-K_d and SCM modeling approach results was that the SCM approach predicted a greater degree of tailing in downgradient U(VI) breakthrough curves. As noted by Bethke and Brady (2000),

the tailing could significantly impact the time required for a contaminated site to reach background concentrations by natural groundwater flushing or engineered remediation cleanup alternatives. Predictions that used small U(VI) K_d values (0.04 to 0.14 mL/g) yielded dissolved U(VI) breakthrough curves that matched SCM simulations for short times but did not reproduce the long tails simulated by the SCM modeling approach. In addition, the predictions with small K_d values yielded a total mass of U(VI) in the aquifer that was approximately half of the mass simulated with the SCM approach. Predictions with larger U(VI) K_d values resulted in higher dissolved U(VI) concentrations at longer times but did not give a good match to the SCM predictions at early times. In addition, these simulations yielded a total mass of U(VI) in the aquifer that was significantly larger than that obtained with the SCM approach. Even when U(VI) K_d values are generated using the same SCM as in the reactive transport model, differences between the constant-K_d and SCM transport simulations were observed. These differences resulted because the U(VI) K_d values in the SCM approach vary spatially and temporally as the U(VI) and alkalinity plumes migrate with groundwater flow.

The SCM approach has an advantage for transport modeling in that effects of model parameter variability and geochemical variability on U(VI) transport predictions can be evaluated. Specifically, with the SCM approach, it is possible to conduct sensitivity and uncertainty simulations that evaluate the effects of adsorption parameter uncertainty and geochemical variability on predicted results.

11 EXAMPLE DOSE ASSESSMENT CALCULATIONS FOR THE NATURITA FIELD SITE

11.1 Introduction

The purpose of this section is to demonstrate the application of reactive-transport models as a potential component of dose-assessment (or performance-assessment) analyses as part of the license-termination process. Dose assessment is part of a potentially iterative process described by the U. S. Nuclear Regulatory Commission (USNRC) in NUREG-1549 (USNRC, 1998) involving a number of steps to converge on decisions regarding a site. A decision framework that portrays steps in the process is shown in Figure 11.1 (USNRC, 1998). Some of these steps may result in evolving models of the site and processes existing or hypothesized for the site.

Ground water of the shallow alluvial aquifer in the vicinity of the Naturita UMTRA site is neither a current or projected source of drinking water (CDPHE, 2002). The selected mechanism for the remediation of contaminated ground water at the site is natural flushing during which the ground water quality is being monitored. Nevertheless, the doses associated with consuming the groundwater on the site were computed for illustrative purposes.

This exercise in dose-assessment modeling of the exposures to contaminated ground water was conducted for this site to compare and contrast a number of different approaches that may be appropriate for similar sites. Each of the approaches relied on the DandD version 2.1.0 software (hereafter referred to as simply DandD) that USNRC has developed to evaluate compliance with the dose criterion of the License-Termination Rule, 10CFR Part 20 (McFadden et al., 2001). An option provided in the DandD code allows an analyst to calculate the dose from exposure to known time-dependent soil and ground-water contamination. For the analyses of this site, soil contamination is no longer present and was entered as zero in the input to the DandD code.

Prior to calculating the doses, uranium (U)-concentration time series must be configured to conform to the electronic-file format required by the DandD software (McFadden et al., 2001). For the purposes of estimating dose from U contamination at the site, a consistent assumption is that the U(VI) observed in the ground water consists of the isotopes U-234, U-235, and U-238 in proportions associated with natural U. Time series of activities for these isotopes were calculated from these proportions and the U(VI) concentration time series. The decay chains for each of the isotopes were not included in the dose calculations. The U(VI) concentration used in the dose calculations was obtained from: (1) the observed existing distribution of dissolved U(VI) in the aquifer, (2) solute transport simulations where adsorption is described by a constant U(VI) K_d value, and (3) solute transport simulations where adsorption is described by the surface complexation model (SCM) developed in Section 5.

11.2 Solute Transport Simulation Approach

While the residential farmer scenario is one of the general exposure scenarios modeled as part of the license-termination process, wells in the alluvial aquifer at the Naturita site cannot be pumped at the rate needed to support the irrigation-water needs of this scenario because the site's thin alluvial aquifer would become dewatered. However, wells pumping from the alluvial aquifer would be able to provide sufficient volume to the meet the domestic-water needs of a typical household. The exposure scenario that will be evaluated by the DandD code is a typical drinking-water scenario in which ground water is used for domestic purposes, including meeting household drinking water needs.

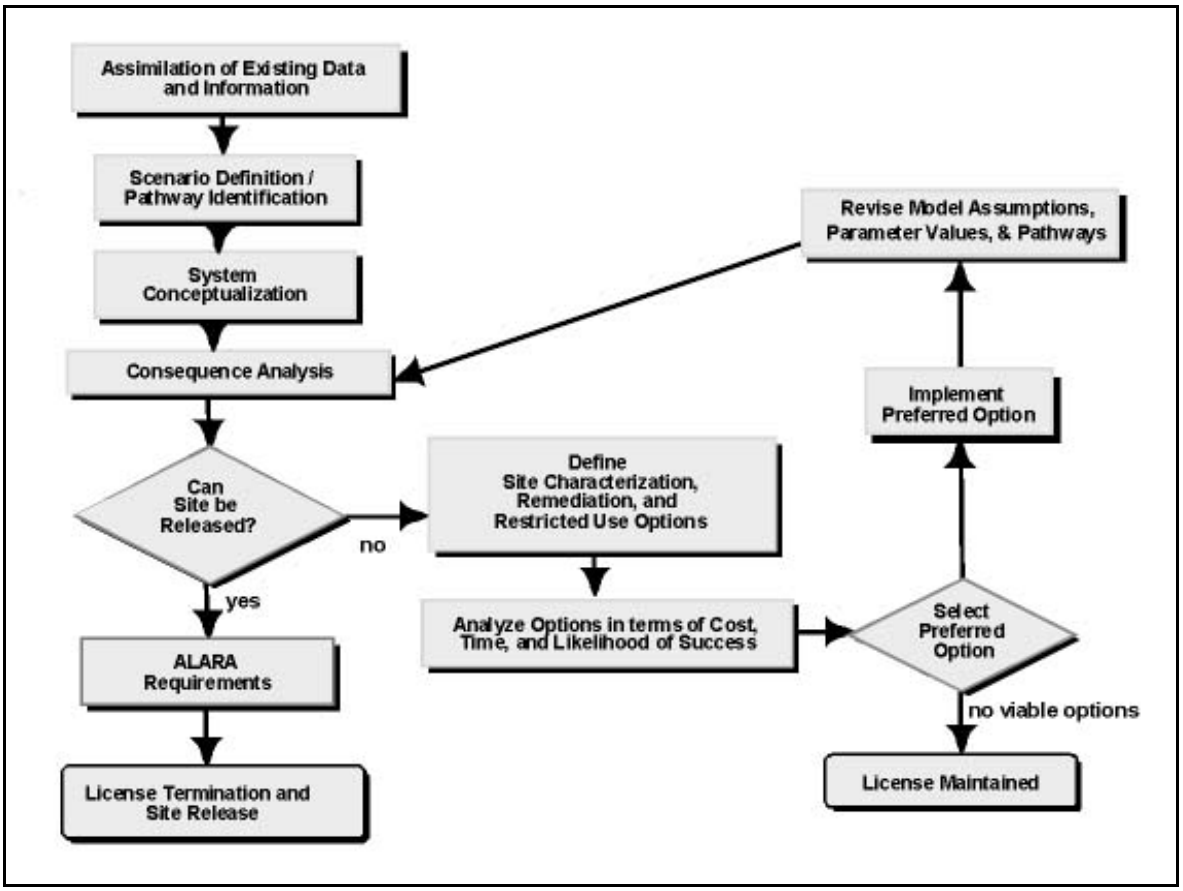

Figure 11.1. USNRC decontamination and decommissioning decision framework.

11.2.1 Flow and transport model

The flow and transport model used for the dose calculations is described in Section 3. The steady state MODFLOW flow model was used with a uniform hydraulic conductivity of $1.59 \cdot 10^{-4}$ m/s. MT3DMS (Zheng and Wang, 1998) was used for solute transport simulations based on a constant U(VI) K_d value. RATEQ (Curtis, 2003) was used for coupled reactive solute transport simulations that modeled sorption reactions using the SCM.

The existing U(VI) concentrations (Fig. 11.2a) were used as the initial condition. Simulations with RATEQ also used the existing distribution of alkalinity shown in Figure 11.2b and a constant pH equal to 7.1. U(VI) concentrations used in the dose calculations were those observed at the two wells shown in Figure 11.2 which are described as the onsite and the offsite wells. The onsite well is roughly midway between wells MAU-07 and MAU-08 and the offsite well is midway between wells NAT-24 and NAT-25. In some of the simulations it was assumed that the offsite well was pumped at $3.28 \cdot 10^{-5}$ m^3/s (100 ft^3/d) and the onsite well was pumped at $9.83 \cdot 10^{-5}$ m^3/s (300 ft^3/d).

Figure 11.2 also shows MODPATH (Pollock, 1994) flow path lines back-tracked from the onsite and offsite wells for the case with no pumping. The flow paths from both the onsite and offsite wells intersect locations where U(VI) concentrations vary spatially in a complex way: upstream of the onsite well, the U(VI) concentration increases, decreases, increases again, and then finally decreases to background values as shown in Figure 11.3. The alkalinity shows a similar profile except that there is an additional peak present approximately 150 m upgradient of the offsite well. The U(VI) and

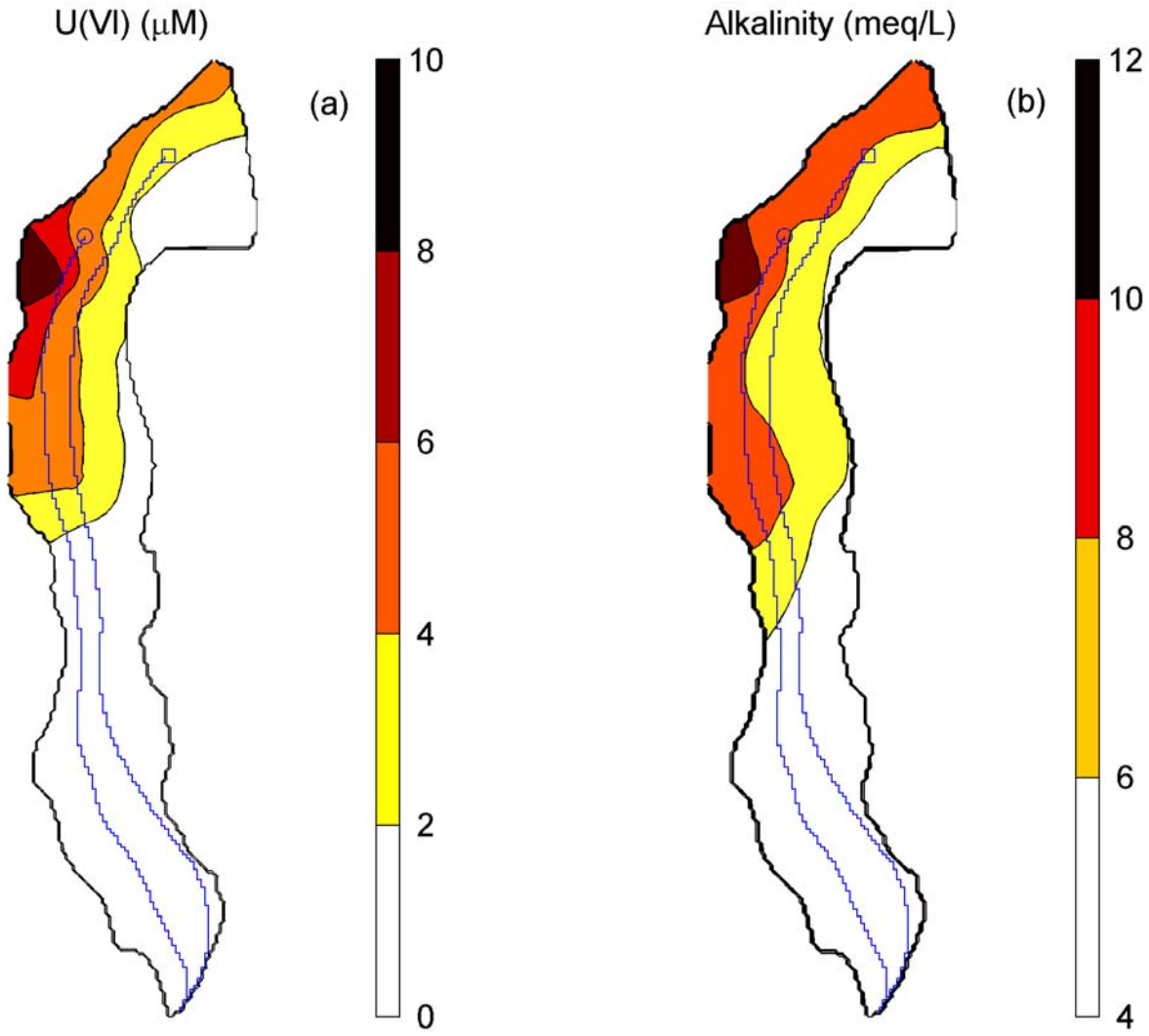

Figure 11.2. Existing distribution of U(VI) concentration and alkalinity in the Naturita alluvial aquifer. Also shown are the locations of the onsite well (□), the offsite well (○), and the groundwater flow path backtracked from the two wells.

alkalinity concentrations show similar trends for the onsite well, although the amplitudes of the spatial fluctuations are damped. The non-smooth appearance of the concentration profiles results from kriging the observed data and because the flow path lines are oblique to the numerical grid. For the single K_d value simulations, the breakthrough at both wells is impacted by the initial conditions shown in Figure 11.3. For the multicomponent reactive transport simulations, the distribution of alkalinity imparts additional complexity into the simulated breakthrough.

11.2.2 Sorption parameters

Each contaminant-transport approach consisted of a series of two-dimensional flow and transport analyses using both the MT3DMS transport code and the RATEQ reactive transport code to calculate U(VI) concentrations at both wells. We chose MT3DMS to represent the traditional approach to contaminant transport simulation, by assuming that sorption reactions could be represented by a linear sorption isotherm, which is equivalent to a constant K_d value for U(VI) sorption. RATEQ uses MT3DMS for solute transport simulation but

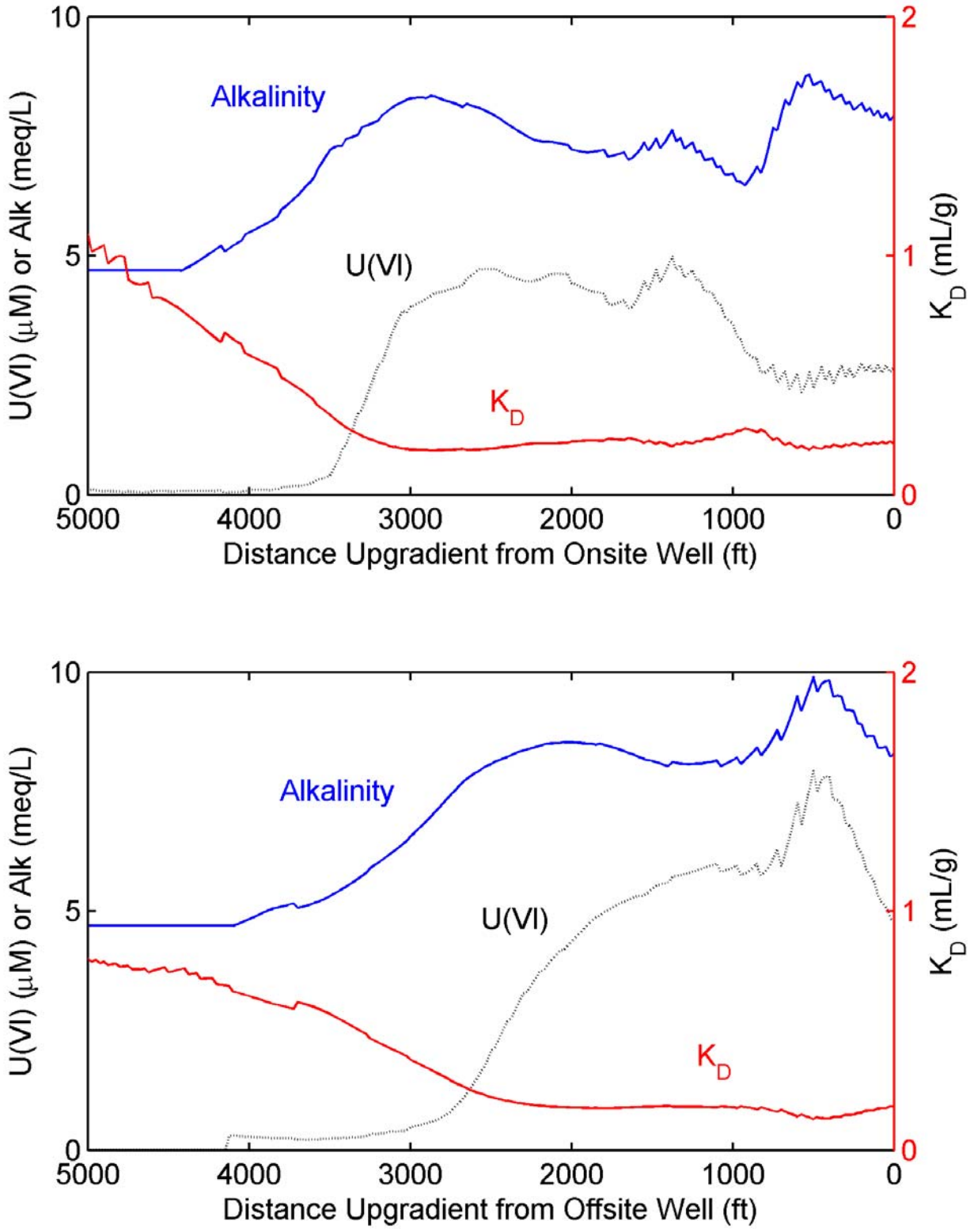

Figure 11.3. Initial U(VI) concentration and alkalinity values on flow paths upgradient of the onsite and offsite wells.

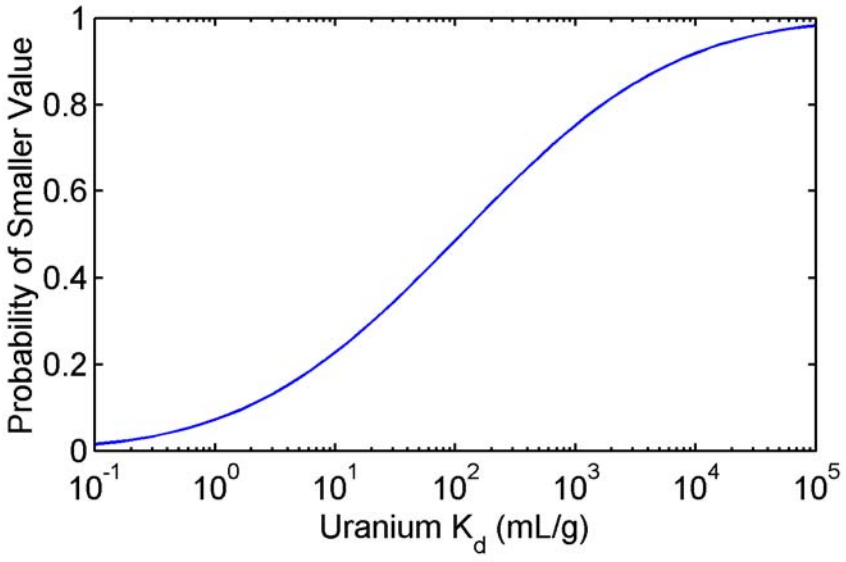

Figure 11.4. Default screening distribution for uranium(VI) K_d values from the DandD code.

solves the coupled geochemical reactions by operator splitting.

To represent the uncertainty in the value of K_d, a distribution of values was selected. Assuming no site-specific information, the distribution was taken from the default screening-analysis distribution in the DandD software (Fig. 11.4). This distribution ranges from near zero to 400,000 mL/g. For screening analyses under 10CFR Part 20 that require very limited site-specific data, the USNRC recommends compliance with regulatory limits for the 90th percentile of the results of uncertainty analyses in NUREG-1757 (Vol. 2, Draft Report). Because the largest U(VI) concentrations are located upgradient of the two wells, and therefore must be transported to the receptor, it is reasonable to assume that any dependency of dose to the U(VI) K_d value may be characterized as an inverse relationship. Therefore, the respective 90th percentile value for U(VI) K_d from the screening DandD distribution given in Figure 11.4 is about 2 mL/g.

Site-specific U(VI) K_d value measurements derived from testing the NABS sample in the presence of atmospheric CO_2 (and corrected for the large percentage of cobbles in the alluvial aquifer) range from slightly less than 1 mL/g to slightly over 5 mL/g, with a mean value of about 2.7 mL/g (The K_d values in Section 5 are before the cobble correction). The U(VI) K_d values determined in the presence of air were chosen for analysis for illustrative purposes. Although U(VI) sorption is sensitive to the partial pressure of CO_2 (Section 5) and the aquifer has partial pressures that range from 0.005 to 0.1 atm (Section 3), the K_d values determined in air were used because we assumed that this approach could be used in practice (USEPA, 1999). For analyses using site-specific data, we evaluated compliance by comparing the mean value of the dose from the uncertainty analyses with the regulatory limit.

Sorption parameters for the RATEQ simulations were derived from the reactions described in Section 5 and the adsorption site densities for the field application that are described in Section 9. The simulation used the distributions of dissolved U(VI) and alkalinity observed in 1999 shown in Figure 11.2 as initial conditions. The initial conditions also assumed a uniform pH equal to 7 and the presence of excess calcite that was in equilibrium with the groundwater. U(VI) K_d values computed from the initial conditions are shown in Figure 11.3 for the flow paths back

tracked from the onsite and offsite wells. The U(VI) K_d values predicted by the SCM range from 0.15 to 1.0 mL/g, and the values are generally inversely proportional to the alkalinity. As in previous sections, the version of the SCM (Section 5) that did not consider the aqueous species, $CaUO_2(CO_3)_3^{2-}$ and $Ca_2UO_2(CO_3)_3^0(aq)$, was used here.

11.2.3 Retardation Factors

The retardation factors, defined as the ratio of U(VI) migration velocity to the velocity of a non-reactive solute, were computed from:

$$R_f = 1 + \frac{\rho_b}{\theta} K_d$$

where ρ_b is the bulk density and θ is the effective porosity. The bulk density is estimated to be 1.8 g/mL, and the effective porosity was assumed to equal 0.2 (see Section 10).

With these values, a U(VI) K_d value of 2 mL/g corresponds to an R_f of 19 and a K_d value of 2.7 corresponds to an R_f of 25. For the SCM-predicted values, the R_f values range from 2.8 to 10. These calculations show that U(VI) breakthrough for the constant-K_d based simulation should require significantly longer time compared to the simulations where U(VI) sorption was modeled with the SCM.

11.3 Dose Calculations

Hypothetical exposures were estimated for three related modeling approaches. The simplest approach is that an estimate of exposure to contamination in ground water can be approximated by the current peak-observed concentration in the contamination plume that exists at the site. In contrast to this approach, the remaining approaches relied on approximations of contaminant transport over the site to predict the evolution of the existing ground-water contamination and interception by domestic wells. These transport approaches used (1) the default K_d values from DandD, (2) K_d values from site-specific measurements, and (3) sorbed U(VI) concentrations predicted by the SCM (Section 5).

11.3.1 Existing Conditions

The most simplistic dose estimate was based on the maximum initial U(VI) concentration for the existing plume at the site. This concentration was used as input to the DandD code. The maximum observed U(VI) concentration is approximately $9 \cdot 10^{-6}$ M; inserting that value as the known ground-water concentration results in a hypothetical drinking-water dose from DandD of about 180 mrem/year. This exposure is conservative for the Naturita site providing that background geochemical conditions remain constant. If the geochemical conditions changed significantly in a manner to decrease U(VI) adsorption, the U(VI) concentration could increase.

11.3.2 Transport Simulated with Constant K_d values for U(VI) Sorption

The hypothetical premise of the contaminant-transport approaches is the presence of two wells pumping sufficient water to serve the domestic water needs of a household. The wells are located such that one is onsite and the other is located offsite; both wells draw from the alluvial aquifer and are located so that eventually the existing contaminant plume will pass through them.

U(VI) K_d values selected from the default screening distribution in DandD were used to examine the sensitivity of dose with respect to K_d. The selected U(VI) K_d values are given in the first column of Table 11.1, and the corresponding doses calculated from the MT3DMS simulations followed by the DandD calculations are shown in the adjacent columns for the onsite and offsite wells. Results are presented for the case where simultaneous pumping at the offsite and onsite wells is included, and for comparison, the case where no pumping is considered. Results from both approaches are given in Table 11.1 and discriminated by the presence or absence of a **T** in the second column. Analyses with the **T** mark are those in which the well withdrawals were explicitly simulated and impact the site ground-water flow field.

Table 11.1 Summary of Results of Hypothetical Exposure Analyses

Sorption Model	Pumped Wells[1]	Offsite Well		Onsite Well	
		Drinking Water Dose (mrem/year)	Time of Peak Dose (years)	Drinking Water Dose (mrem/year)	Time of Peak Dose (years)
Existing plume maximum concentration	n/a	180	N/a	180	n/a
K_d =0	✓	145	3	59	4
		151	4	90	5
K_d =1 mL/g	✓	134	28	51	0
		150	41	88	115
K_d =2 mL/g	✓	135	56	51	1
		150	78	91	96
K_d =2.7 mL/g	✓	135	74	51	1
		150	102	88	292
K_d =3 mL/g	✓	135	82	51	1
		150	112	88	323
K_d =10 mL/g	✓	135	268	51	3
		150	365	87	484
K_d =12 mL/g	✓	135	319	51	3
		150	437	87	581
K_d =15 mL/g	✓	135	400	51	4
		150	545	87	724
K_d =25 mL/g	✓	135	666	51	6
		149	900	85	1000
K_d =50 mL/g	✓	131	1000	51	10
		129	1000	52	0
K_d =100 mL/g	✓	115	1000	51	10
		109	1000	52	0
K_d =500 mL/g	✓	100	1000	52	10
		98	1000	52	0
K_d =1000 mL/g	✓	98	1000	52	10
		96	1000	52	0
K_d =5000 mL/g	✓	96	1000	52	10
		95	0	52	0
RATEQ	✓	137	3	73	12
		142	4	106	13

[1]If marked with a **T**, the offsite and onsite wells were pumped as described in the text.

At the offsite well, sensitivity of the calculated doses to U(VI) K_d value for both the pumped and unpumped cases appears primarily near the time of the peak concentration for all but the highest values of K_d. At the higher K_d values, the peak does not arrive at the well during the simulation period. Otherwise, that part of the existing plume with the peak U(VI) concentration eventually migrates to the offsite well, and the U(VI) concentration, and therefore dose, is not significantly affected by dispersion. The doses calculated for the pumped cases are generally 2 to 10% smaller than the doses calculated with no pumping. The decrease in dose is caused by the radially convergent flow that develops at the pumped well. The radial flow captures water from the east side of the aquifer where the U(VI) concentrations are lower. Thus, the doses calculated with pumping are decreased by dilution.

At the onsite well, the dependence of simulated doses on U(VI) K_d values and pumping is slightly more complex than at the offsite well. The doses computed with no pumping generally follow the same trend as observed for the analogous calculations at the offsite well. The dose does not depend strongly on U(VI) K_d for values less than 50 mL/g. In these simulations, that part of the plume with the peak in U(VI) concentration is eventually transported to the onsite well. For larger U(VI) K_d values, the part of the plume with the peak in U(VI) dose not reach the onsite well within 1000 years, and in this case, the dose is determined by the initial conditions at the well.

With pumping, the calculated doses are approximately 35% smaller than for the unpumped case, and the maximum dose occurs in 10 years or less. The decrease in dose results from dilution of the water with high U(VI) concentrations with water from the east side of the aquifer, which has lower dissolved U(VI) concentrations.

11.3.3 Reactive Transport Simulated with the SCM for U(VI) Sorption

Table 11.1 lists the doses computed from the reactive transport simulations that used the SCM approach for modeling U(VI) sorption. At the offsite well, the computed doses and time to maximum dose do not differ significantly from the doses computed for assumed K_d values of 0 and 1 mL/g. This agreement is consistent with the K_d values computed from the SCM that range from 0.15 to 1.0 mL/g (Fig. 11.3). For the onsite well, significant differences between the SCM simulations and the constant-K_d simulations were obtained for both the pumped and unpumped cases. In the pumped cases, the maximum dose in the constant-K_d simulations equaled 59 mrem/year for a U(VI) K_d value equal to zero and equaled 51 mrem/year in all other cases. In contrast, the maximum dose computed in simulations using the SCM for U(VI) sorption was 73 mrem/year.

Similarly, the dose computed in the unpumped case using the SCM was 106 mrem/year, whereas the maximum doses computed using a constant-K_d ranged from 52 mrem/year for large U(VI) K_d values to approximately 90 for small K_d values. The reasons for these differences are discussed below.

11.4 Comparison of U(VI) Transport Simulation Approaches

Figure 11.5 shows a portion of the dose time series for 3 significant analyses; the reactive-transport results from RATEQ, the MT3DMS 90^{th}-percentile U(VI) K_d value screening analysis, and the MT3DMS mean site-specific, constant K_d analysis with no pumping. Note that the time to the peak dose for the screening analysis is conservative (smaller) relative to timing of the peak dose for the site-specific constant-K_d analysis. The peak dose at approximately 100 years and the tail that extends beyond 1000 years is a consequence of the initial distribution of U(VI) shown in Figure 11.2. Simulations using the SCM gave peak U(VI) doses that were similar to the values obtained from the constant-K_d simulations, but the time required for the peak was only 3 years. A relatively long tail persists at least until 200 years, when the simulation was terminated. Figure 11.6, which shows the offsite results with pumping, has results similar to those shown in

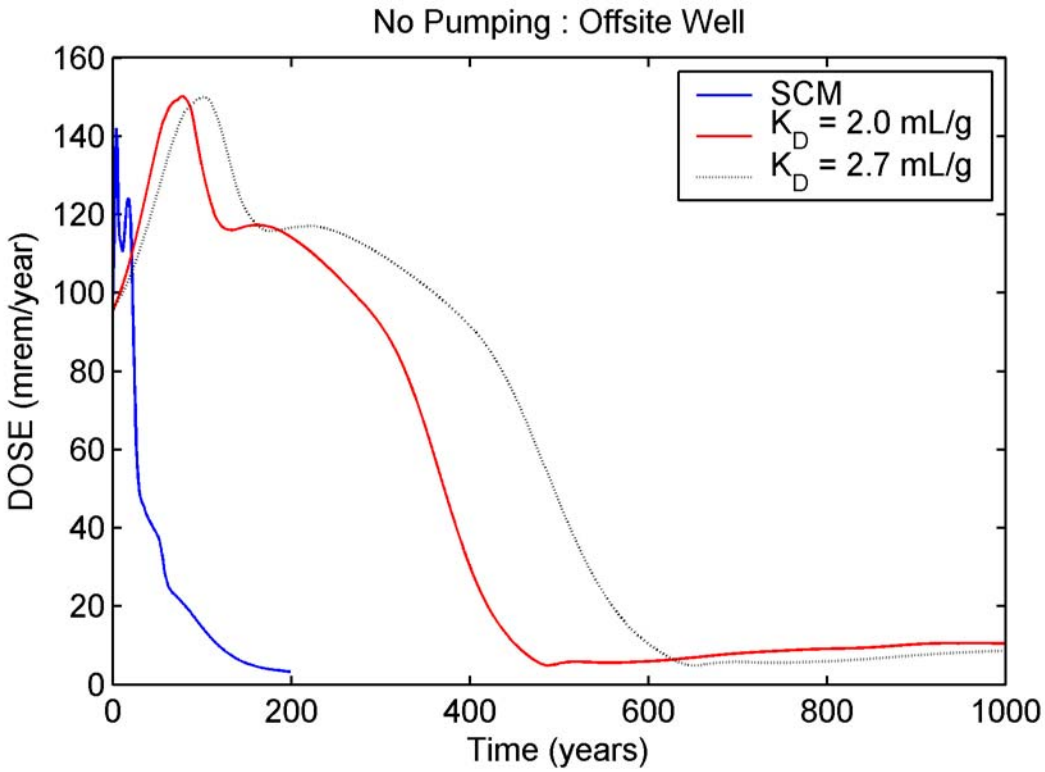

Figure 11.5. Offsite unpumped-well results; RATEQ & MT3DMS for selected U(VI) K_d values.

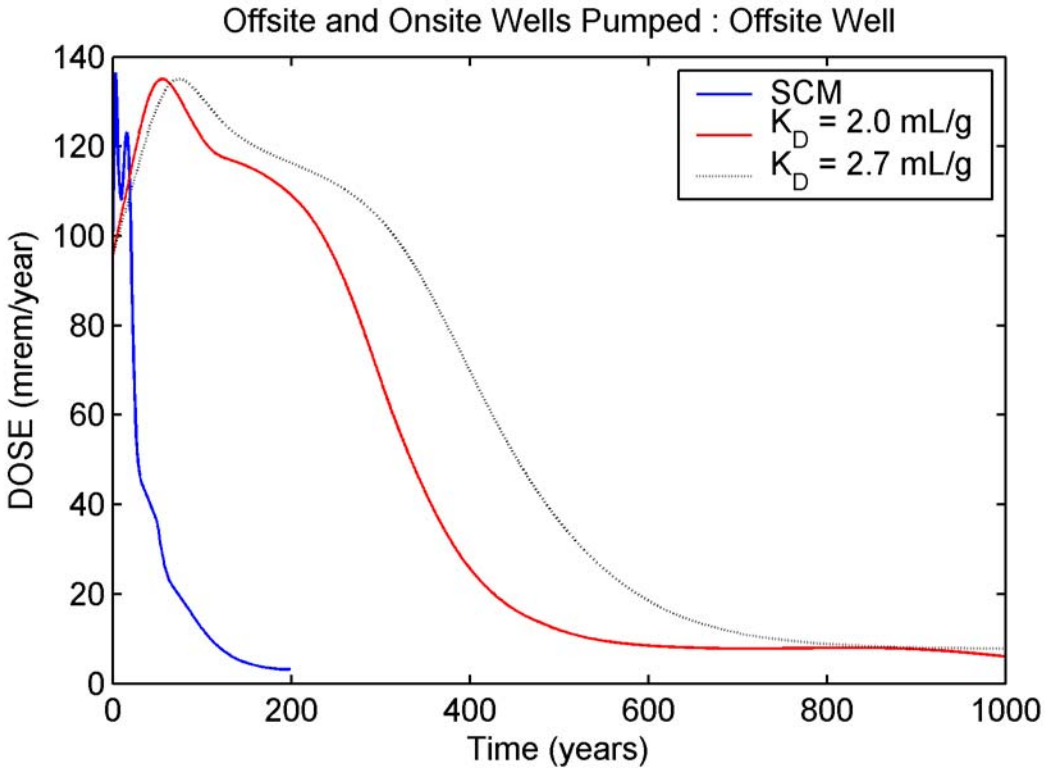

Figure 11.6 Offsite pumped-well results; RATEQ & MT3DMS for selected U(VI) K_d values.

Figure 11.5, except that the doses are approximately 10% smaller because of the dilution that results when the wells are pumped.

The area under the breakthrough curves, which is a measure of the mass of U(VI) that passes a particular sampling point, is smallest in the case of the RATEQ simulation, and increases with increasing U(VI) K_d value. This difference results because the initial adsorbed U(VI) was computed by the three different adsorption models using the same initial dissolved U(VI) concentrations. Because the SCM predictions for U(VI) sorption are consistent with U(VI) K_d values that ranged from approximately 0.15 to 1.0 mg/L, the total U(VI) mass in the RATEQ simulations was less than half of the mass in the constant-K_d simulations.

Figure 11.7 shows the doses simulated from the 3 methods at the onsite well for the case of no pumping. In this case, the dose simulated using the SCM predictions is 106 mrem/year, whereas the peak doses for the constant-K_d methods both equal 91 mrem/year. In the pumped case shown in Figure 11.8, the spread between the SCM simulations and the constant-K_d simulations is larger; the maximum dose computed using the SCM is 74 mrem/year and the maximum dose from the constant-K_d simulations is 51 mrem/year. The simulated doses for the pumped cases are smaller because of dilution by water from area east of the onsite well.

An interesting difference between the doses simulated for the onsite well with and without pumping is that the peak dose computed using the SCM is larger than that computed from the constant-K_d simulation, and the difference increases with pumping. The reasons for this are complex but are related to the effects of variable chemical conditions, especially variable alkalinity. Figure 11.9 shows simulated breakthrough curves for U(VI), alkalinity and sorbed U(VI). The curves show that with pumping, the alkalinity and dissolved U(VI) concentration decrease, but sorbed U(VI) is relatively insensitive to pumping. Eventually, the broad pulse of high alkalinity shown in Figure 11.2 reaches the onsite well and this causes most of the U(VI) to be desorbed. Consequently, the maximum simulated dose is larger than that computed from the constant K_d model, even for the case of no retardation (K_d=0; Table 11.1).

11.5 Summary

The dose calculations presented in this section have demonstrated a variety of approaches to dose assessment from existing ground-water contamination. In the process of completing these analyses, we have also demonstrated the linkage of traditional contaminant-transport models and reactive-contaminant-transport models to models for dose assessment. These analyses have exhibited both expected behavior and some unexpected behavior. The dose calculated at the offsite well generally showed that the dose was relatively insensitive to the modeling approach and to the U(VI) K_d value selected, providing the K_d value was small enough that the part of the plume with high dissolved U(VI) concentrations upgradient of the offsite well were transported to the well during the 1000 year simulation. The pumped and unpumped cases agreed well because the offsite well is on a flowpath line that passes near the part of the existing dissolved U(VI) plume with the highest concentrations.

For the onsite well, the dose calculated was sensitive to the amount of pumping because of dilution. In addition, the dose calculated using the SCM to predict sorbed U(VI) was larger than that obtained with the constant- K_d model, regardless of the U(VI) K_d value, because of the effects of variable alkalinity. Thus, these simulations illustrate that the constant-K_d model may not always be the most conservative approach to simulating dose.

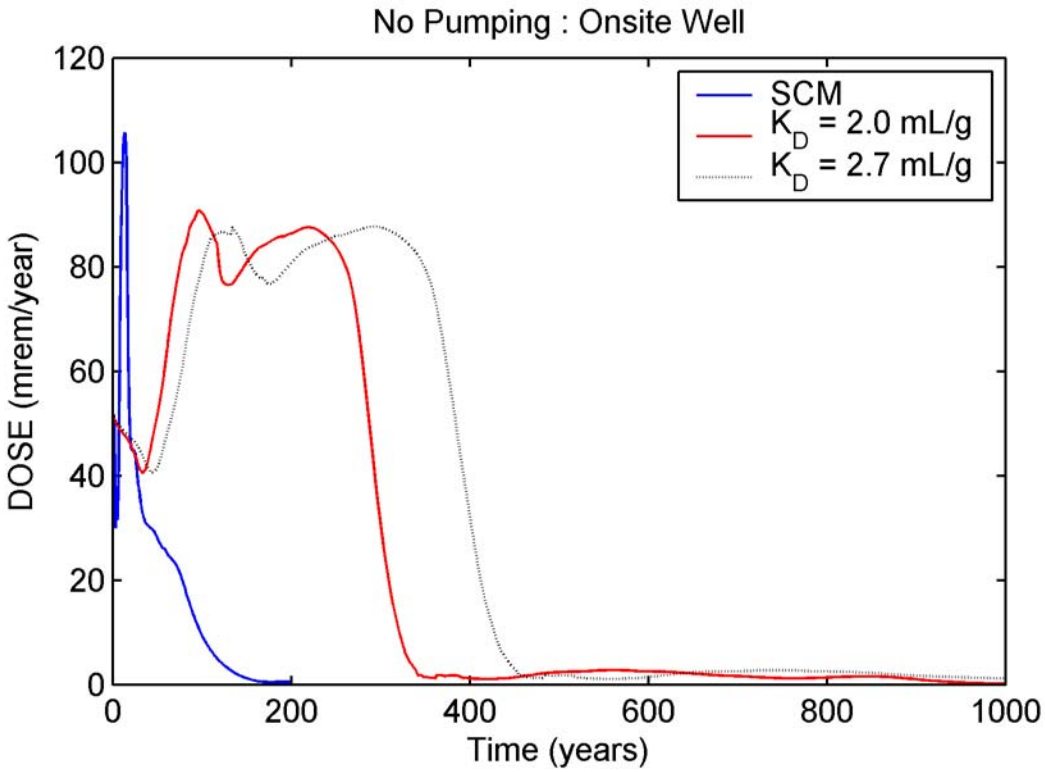

Figure 11.7. Onsite unpumped-well results; RATEQ & MT3DMS for selected U(VI) K_d values.

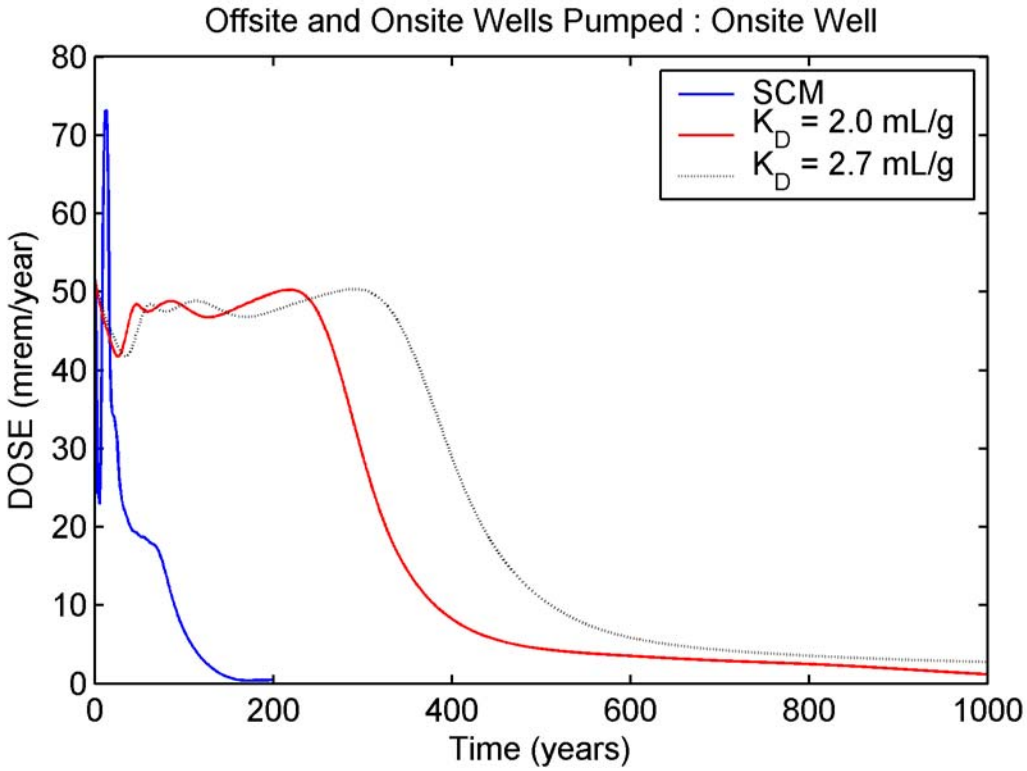

Figure 11.8 Onsite pumped-well results; RATEQ & MT3DMS for selected U(VI) K_d values.

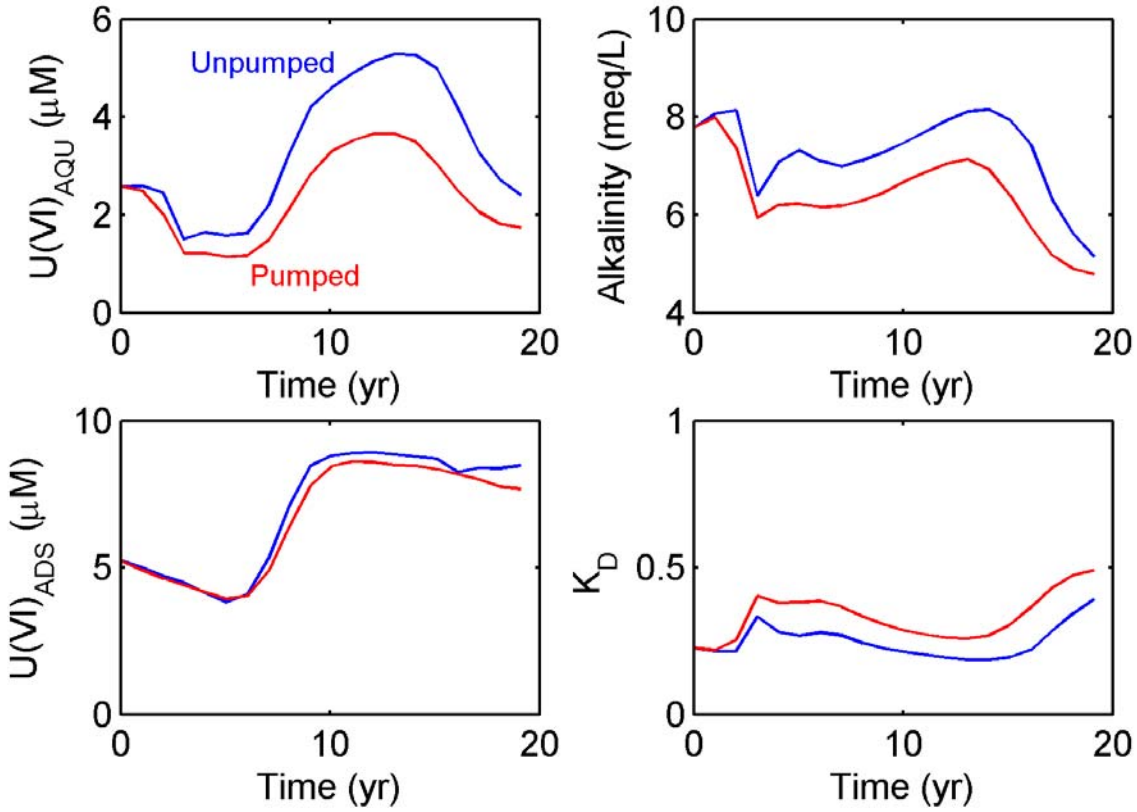

Figure 11.9. Simulated U(VI) and alkalinity breakthrough curves at the onsite well and calculated adsorbed U(VI) and U(VI) K_d values in the aquifer at the onsite well location.

12 CONCLUDING REMARKS AND SUMMARY

Prior to this investigation, the Generalized Composite (GC) modeling approach to surface complexation model development had only been tested at the field scale in one other study (Kent et al., 2000). The objective of the current study was to demonstrate the GC modeling approach at the field scale for a sorbing radionuclide with complex aqueous chemistry. The Naturita UMTRA site was chosen for study, because it had a well-developed and definable U(VI) plume in the shallow alluvial aquifer and had spatially variant chemical conditions (alkalinity) that we believed would be important in influencing U(VI) transport and retardation. It is not unusual at field sites contaminated by point sources to find other co-solutes that form plumes, in addition to the radionuclides or metal contaminants of interest. In the Naturita case, the acids and bases used in dissolving uranium from crushed ore reacted with calcite in the vadose zone sediments at the site to produce a significant alkalinity plume associated with the dissolved U(VI) (see Section 3).

It is known from studies of pure mineral phases that the dissolved carbonate concentration and pH are significant aqueous chemical variables that influence the adsorption of U(VI) (Waite et al., 1994; Hsi and Langmuir, 1985; Davis, 2001). As expected, adsorption of U(VI) by the Naturita sediments was strongly influenced by the carbonate concentration (Sections 5, 6, and 7). In the Naturita aquifer, carbonate species are the only groundwater solutes that contribute to the field-measured alkalinity, and therefore, the alkalinity is directly related to the carbonate concentrations. Under conditions typical of the groundwater at the field site in Naturita (pCO_2 of 2-6%, pH 7), the K_d value for U(VI) adsorption was much smaller (about ¾ to one order of magnitude) than was measured in batch experiments equilibrated with air. This illustrates the importance of pCO_2 in experiments designed to determine K_d values; most K_d values in the literature have been determined in equilibrium with respect to or at least exposure to air (USEPA, 1999). It also illustrates how major co-solutes emanating from radionuclide or other contaminant source areas can create spatially variant chemical conditions that affect the K_d values for radionuclide adsorption.

In the literature, at least three types of adsorption modeling approaches can be distinguished: 1) empirical partitioning relationships (Davis and Kent, 1990), 2) thermodynamic surface speciation models that describe the molecular details of chemical species formation at mineral surfaces (Hiemstra and van Riemsdijk, 1999; Sahai and Sverjensky, 1997), and 3) semi-empirical site-binding models that utilize concepts from the first two model types (Davis et al., 2002; Borkovec et al., 1998; Davis et al., 1998).

In the first approach, empirical relationships such as K_d values, sorption isotherms, and partitioning equations are used to predict adsorption as a function of aqueous concentration variables (Davis and Kent, 1990). K_d values are defined as:

$$K_d = RN_{ads} / RN_{aq}$$

where RN_{ads} refers to the quantity of radionuclide sorbed and RN_{aq} refers to the dissolved concentration of the same radionuclide. The relationship implies that a constant ratio is obtained between these two quantities, as in a linear isotherm.

There are many types of non-linear adsorption isotherms. The most common, the Langmuir isotherm can be represented as (Davis and Kent, 1990):

$$K_L = RN_{ads} / (RN_{aq})(\Gamma_{free})$$

where K_L is a constant and Γ_{free} refers to the quantity (or concentration) of available surface sites. The Langmuir isotherm accounts for the decrease in K_d values that occurs as an adsorbing surface becomes partially saturated with adsorbed species (Davis and Kent, 1990). The relationship is usually determined for a

specific set of constant chemical and physical conditions while a radionuclide concentration is varied.

K_d values for radionuclides have been determined experimentally on a wide variety of geological solids (Altmann et al., 2001; USEPA, 1999), and the variability of K_d values with chemical conditions has been the subject of several studies (Waite et al., 1994; Davis et al., 2002; USEPA, 1999; Pabalan et al., 1998; Altmann et al, 2001; Turner and Sassman, 1996; Prikryl et al., 2001; Barnett et al., 2002). For example, it has been shown that K_d values for adsorption of U(VI) on sediments and pure mineral phases may vary by more than 8 orders of magnitude over a wide range of chemical conditions in which U(VI) aqueous speciation changes significantly (e.g., pH 4-10) (USEPA, 1999, and also see Fig. 5.1). However, even when the range of chemical conditions is constrained to the narrower range of conditions within the Naturita alluvial aquifer (Section 3), K_d values for U(VI) sorption varied by nearly 2 orders of magnitude (Section 5). This is in agreement with other reports that show that K_d values are highly sensitive to chemical conditions (Davis et al., 2002; Bethke and Brady, 2000; Kent et al., 2000; Davis, 2001).

For the Naturita aquifer conditions, alkalinity was more important than either variable pH or U(VI) concentration in influencing U(VI) mobility. K_d values ranged from 0.29 to 22 mL/g when calculated for all Naturita groundwater analyses using the surface complexation model (SCM) developed in Section 5. Low K_d values were associated with portions of the plume containing high concentrations of dissolved U(VI) and alkalinity. Higher K_d values were associated with low concentrations of dissolved U(VI) and alkalinity.

For the second and third approaches, surface complexation models (SCM) use mass action laws analogous to aqueous phase reactions to describe adsorption (Davis, 2001; Davis and Kent, 1990) as a function of aqueous chemical conditions, thus taking into account changes in chemical speciation, competitive adsorption, and other multi-solute interactive chemical effects. The possible advantages of applying the surface complexation concept to describe radionuclide sorption in nuclear waste performance assessment (PA) include the following factors:

1) the modeling approach provides a thermodynamic framework to describe adsorption reactions of radionuclides,

2) the stability constants for the adsorption reactions can be included as part of an overall network of chemical reactions in geochemical equilibrium or coupled reactive transport models, and thus coupled with thermodynamic databases for radionuclide aqueous speciation and solubilities, such as the NEA thermodynamic database (Grenthe et al., 1992),

3) the modeling approach allows predictive calculations for a range of chemical conditions without adjustment of the values of the model parameters, as chemical conditions are varied in space or time, unlike the condition-dependent empirical relationships,

4) the modeling approach can be included efficiently in transport simulations (or PA scenarios) in which there are chemical gradients in space or time.

The thermodynamic surface speciation and GC modeling approaches represent two extremes of surface complexation modeling (Davis et al., 1998). Table 12.1 compares the modeling approaches and their data requirements. In thermodynamic surface speciation models (Weerasoriya et al., 2001; Hiemstra and van Riemsdijk, 1999), the surface species postulated must be supported with spectroscopic evidence (e.g., Bargar et al., 2000, 1999). Thermodynamic surface speciation models typically include electrical double layer terms in the mass law equations, and hence, adsorption predictions with these models are sensitive to the double layer parameters, as was shown for U(VI) adsorption on hematite in Section 5 of this report.

The sensitivity to electrostatic terms illustrates a significant practical problem in extending thermodynamic surface speciation models directly to simulate radionuclide adsorption on complex mineral assemblages in the environment. Mineral surfaces in the

Table 12.1. Characteristics of Surface Complexation Modeling Approaches for Environmental Adsorbents

	Thermodynamic Surface Speciation Modeling[1]	Semi-Empirical (GC) Modeling
A	**Adsorption is predicted from thermodynamic constants and known (confirmed) surface species**	**Adsorption data are simulated (fit) using site-specific adsorbent samples, using chemically plausible surface reactions**
B	**Surface sites are unique and defined for each specific mineral phase present in environmental samples**	**Generic surface sites are assumed, with average chemical characteristics**
C	**Surface site densities are quantified by detailed characterization of the surface of environmental samples**	**Surface site densities are quantified by the measurement of specific surface area or by fitting adsorption data of environmental samples**
D	**Apparent stability constants and reaction stoichiometries are obtained from studies of adsorption by reference mineral phases present in environmental samples**	**Apparent stability constants and reaction stoichiometries are fit to experimental adsorption data for environmental samples**
E	**Overall adsorption is predicted by the sum of adsorption calculated for each specific mineral phase present in environmental samples**	**Numbers of surface site types and chemical reactions are increased as necessary to achieve good model simulations and to meet modeling objectives**

[1] Thermodynamic surface speciation models that are developed by predicting adsorption as the sum of contributions from individual mineral phases are called Component Additivity models (Davis et al., 2002; Sanpawanitchakit, 2002; Davis et al., 1998; Honeyman, 1984). Characteristics D and E for thermodynamic surface speciation modeling in Table 12.1 apply to the Component Additivity modeling approach.

environment are typically coated with poorly crystalline secondary mineral coatings, as was shown for the Naturita alluvial sediments in this report, as well as in Jove-Colon et al. (2003) and Sanpawanitchakit (2002). The coatings make it extremely difficult to assess the electrostatic contribution to the free energy of adsorption quantitatively. In the literature one finds the frequently made assumption (e.g., Barnett et al., 2002; Arnold et al., 2001) that the electrical double layer properties of pure mineral phases studied in the laboratory are the same in a mineral assemblage in the environment. It seems highly unlikely that this assumption is valid given the fact that coatings of various materials on mineral surfaces are very prevalent in soils and sediments. In addition to the fact that coatings drastically change the electrical double layer at surfaces, the Component Additivity modeling approach is difficult to apply because the site densities of the mineral and organic phases in the coatings that are contributing to radionuclide adsorption are unknown (Davis et al., 2002; Sanpawanitchakit, 2002).

Thus, the challenge in applying the surface complexation concept in the environment is to simplify the adsorption model, such that predicted adsorption is still calculated with mass laws that are coupled with aqueous speciation, while lumping parameters that are difficult to characterize in the environment in with other parameters. This modeling approach can be

achieved with the semi-empirical, site-binding (GC) modeling approach used in this report and elsewhere (Davis et al., 2002; Borkovec et al., 1998; Davis et al., 1998).

While a thermodynamic surface speciation model must be validated with spectroscopic evidence and other detailed data to confirm surface speciation and electrical double layer properties (Hiemstra and van Riemsdijk, 1999), the GC modeling approach is more easily applied and less experimental data need to be collected. The range of applicability of a GC model with respect to chemical variation is determined by the type and amount of experimental data collected. GC model parameters are calibrated by fitting a simple surface speciation model such that the major features of radionuclide adsorption are simulated as chemical conditions are varied over field-relevant ranges (Davis et al., 1998). With only two surface species, a GC model without electrical double layer terms was able to simulate K_d values accurately for U(VI) adsorption on the Naturita aquifer sediments as a function of pH and pCO_2, and U(VI) concentration (see Section 5).

An important limitation of the GC approach is that adsorption predictions should not be extrapolated to conditions outside of the range for which data were collected for model calibration. However, a GC model can be used for predictive calculations that interpolate within the range of chemical conditions studied. This was demonstrated in this report for U(VI) adsorption on Naturita sediments in Sections 6-11.

While the GC modeling approach has not been widely used to date, we believe it is a practical approach in terms of data collection needs and the capability to predict radionuclide distributions over a range of chemical conditions at field sites (Section 5, and Davis et al., 2002; Kent et al., 2000; Davis et al., 1998). The GC modeling approach is also an important compromise between the simple constant K_d approach and the most complex SCM, the thermodynamic surface speciation models (Hiemstra and van Riemsdijk, 1999). In order to be applied by solute transport modelers and within PA applications, the complexity of the adsorption model needs to be balanced with the goal of using the simplest model possible that is consistent with observed data. Historically, solute transport modelers have lacked the necessary expertise to apply the SCM modeling approach and many have believed that the SCM approach is too complex to be applied. While it is true that the thermodynamic surface speciation models are currently difficult to apply, it has been demonstrated in this study (Sections 9-11) that the GC modeling approach can be easily applied to simulations of radionuclide transport at the field scale.

In addition to the common experimental technique of batch adsorption studies, methods were investigated in this study to estimate K_d values in the field. Such methods are needed in order to: 1) validate GC-SCM parameters or K_d values for transport simulations and PA, and 2) constrain initial conditions for adsorbed radionuclides as part of transport simulations for previously contaminated sites. We showed that isotopic exchange and desorption extraction methods can be an important part of a field characterization and modeling program (Section 6). Experimental determinations of sorbed U(VI) in the contaminated portion of the Naturita alluvial aquifer (Section 6) build confidence in the GC model developed from laboratory experiments with uncontaminated sediments (Section 5). The results also increase the credibility of the initial conditions used in simulating U(VI) transport in the aquifer (Sections 9 -11).

Another approach used in this study to validate the GC modeling approach was the determination of *in-situ* K_d values by suspending uncontaminated Naturita sediments in wells with U-contaminated groundwater for periods of time ranging from 3-15 months (Section 7). *In-situ* (field) K_d values were calculated from groundwater measurements of dissolved U(VI) and U extracted from the suspended sediment samples. The *in-situ* K_d values in 17 wells ranged from 0.5 to 12 mL/g, and the K_d values decreased with increasing groundwater alkalinity. The *in-situ* K_d values were compared

with K_d values predicted by the GC model, and there was close agreement between the model-predicted and measured *in-situ* K_d values. Column experiments were conducted to investigate the effects of variable chemical conditions on U(VI) transport through columns packed with Naturita sediments (Section 8). The results showed that U(VI) retardation was significantly affected by variable chemical conditions; especially variable alkalinity and pH. The observed variations in U(VI) retardation were predicted reasonably well by a transport model that included the GC model and assumed local chemical equilibrium. The transport predictions were made without adjusting any SCM model parameters. The U(VI) transport model predictions suggest that alkalinity is the most important chemical variable in the Naturita alluvial aquifer with respect to U(VI) mobility.

Transport simulations conducted for the field scale demonstrated the importance of using the SCM rather than a constant-K_d modeling approach, to describe U(VI) adsorption (Sections 9 and 10). A two-dimensional reactive transport model was calibrated to the observed distribution of dissolved U(VI) in the Naturita alluvial aquifer. The model was based on an independently calibrated flow model and the independently calibrated GC model for U(VI) adsorption (Section 5). The transport model was calibrated to the observed concentrations of solutes in groundwater samples collected between 1984 and 2001. The model was calibrated by applying a single constant mass loading rate over the area that was occupied by the former mill and tailings pile. The source added U(VI) and alkalinity to the groundwater. K_d values were calculated from the simulated concentrations. A comparison of the spatial trends in the predicted K_d values and U(VI) concentrations showed that the regions of the plume with the greatest U(VI) concentrations had the smallest predicted K_d values.

Several simplifying model assumptions in the conceptual model for U(VI) adsorption were examined. We tested the assumption of local chemical equilibrium by comparing with transport simulations that used a rate-controlled model with reaction rates estimated from batch kinetic data. U(VI) batch adsorption experiments showed that approximately 3 days were required to reach steady-state dissolved U(VI) concentrations (Section 5). Transport simulations with the rate-controlled adsorption model agreed well with those that used the local chemical equilibrium approximation.

The GC model for U(VI) adsorption by the Naturita sediments did not correct the mass laws with terms that estimate electrostatic attraction or repulsion of surface species by average surface charge (Section 5). The sensitivity of the U(VI) transport simulations to the use of the non-electrostatic adsorption model was investigated with additional simulations that balanced the adsorbed charge by removing a cation from solution. The simulations showed that predicted U(VI) transport was nearly identical, regardless of whether the surface charge was or was not explicitly considered.

Although the GC modeling approach is semi-empirical, it can be constrained to consider plausible surface species that are supported by ancillary spectroscopic studies, e.g. the ternary surface-uranyl-carbonate complex (see Section 5). However, one limitation of the GC approach is that the mass action equations and associated stability constants are valid only for site-specific materials; a database that is transferable to other mineral assemblages is not expected. However, the GC approach is preferable to completely empirical approaches, such as the constant K_d model or adsorption isotherms, because the important linkage between surface and aqueous species (and associated thermodynamic data) is retained in the modeling through the coupling of mass action equations (Sections 9 and 10).

A major conclusion from the transport simulations was that PA modelers must recognize not only that variable chemical conditions can cause a range of effective K_d values to be observed, but also that the spatial distribution of K_d values within that range is not likely to be a random function or a normal distribution. In plumes with chemical gradients, the spatial distribution of K_d values can be quite complex and be characterized by significant spatial character.

Dose calculations presented in Section 11 demonstrate a variety of approaches to dose assessment from existing ground-water contamination by radionuclides. In addition, the linkage of traditional contaminant-transport models and reactive-contaminant-transport models to models for dose assessment was investigated. The analyses exhibited both expected and unexpected behavior. The dose calculated at a hypothetical offsite well at the Naturita site generally showed that the dose was relatively insensitive to whether the GC model or constant-K_d modeling approach was used, or even to the U(VI) K_d value selected, providing the K_d value was small enough that the portion of the plume with high dissolved U(VI) concentrations upgradient of the offsite well was transported to the well during the 1000 year simulation.

For a hypothetical onsite Naturita well, the dose calculated using the GC model to predict sorbed U(VI) was larger than that obtained with the constant-K_d model because of the effects of variable alkalinity in the Naturita aquifer. The latter simulations illustrated that the constant-K_d model may not always be the most conservative approach to simulating dose.

Our current understanding and models for adsorption are well advanced at the molecular scale (Bargar et al., 2000; Sylwester et al., 2000), but our understanding and models become increasingly uncertain as the physical scale increases. The observed adsorption of U(VI) by the aquifer sediments is ultimately controlled by sorptive phases with dimensions on the order of tens of nanometers. This inherent heterogeneity of environmental samples makes application of the thermodynamic surface speciation models difficult at present, even at the microscale level. However, in the authors' opinion, the current operational paradigm that employs constant-K_d values for individual radionuclides introduces more uncertainty than is necessary in our predictions of radionuclide retardation during transport. This uncertainty could be reduced in the future with the use of the site-binding (GC-SCM) models (see Sections 9-11). To reduce the uncertainty, more emphasis needs to be placed on site-specific characterization of natural mineral assemblages that are expected to be encountered along major flowpaths away from disposal sites or other source areas. Data collection for such studies should be focused on those radionuclides that are expected to be important contributors of dose in the far-field regime. From a practical point of view, a limiting factor in applying any type of SCM is the knowledge of the spatial and temporal variation in aqueous chemical conditions and mineral surfaces exposed along flow paths in PA scenarios.

Appendix A: Summary of Geochemical Data for the Naturita UMTRA site

A.1 Introduction

This appendix summarizes the geochemical data collected at the Naturita UMTRA site. The data include results determined prior to this project by the Department of Energy (DOE) on samples from wells DOE-505, DOE-506, DOE-538, DOE-546, DOE-547, DOE-548, DOE-549, DOE-567, DOE-616, DOE-619, DOE-630, DOE-632 and DOE-637 between 1986 and 1997. The data also include results determined by the U. S. Geological Survey (USGS) on samples from wells DOE-547, DOE-548, all NAT wells, all MAU wells, and well DM-1. In addition to summarizing the raw analytical data, the appendix also summarizes the results of speciation calculations that were conducted using the groundwater analyses to investigate the saturation state of various mineral phases, the redox state of uranium (U), and the distribution of U(VI) species in Naturita groundwaters.

A.2 Observed Data

A.2.1 Groundwater Sampling Procedures

Before samples were collected, about three casing volumes of water were purged from each well with a peristaltic pump. 5.1 cm (2 inch) diameter wells were purged and sampled through dedicated 1.3 cm (0.5 inch) diameter polyvinyl chloride tubes with a 15.2 cm screen on the bottom. These tubes were set in the casing to sample 76 cm from the bottom of the well where possible (the depth at the middle of the screened interval). 1.3 cm diameter wells were connected directly to the pump tubing, and samples from these wells were collected from the 15.2 cm screened interval at the bottom of the well casing. All purging and sampling was done through a peristaltic pump using low-diffusion Norprene tubing. All field measurements (pH, specific conductance, redox potential, water temperature, and dissolved oxygen) were monitored continuously during purging with a flow-through chamber attached to a Hydrolab Mini-Sonde Water Quality Multi-probe. After purging was completed, water samples for anion analysis were filtered on site using a 0.45 μm capsule filter and collected in field-rinsed polyethylene bottles. Samples for cation analysis were also filtered on site and collected in acid-rinsed polyethylene bottles. After collection, these samples were preserved with ultra-pure concentrated nitric acid. Dissolved ferrous iron (Fe(II)) was measured colormetrically in the field using a Chemetrics photometer. Alkalinity in filtered (0.45 μm) water samples was measured on site with a Hach digital titrator and 1.6N sulfuric acid.

A.2.2 Analytical Analysis Procedures

Dissolved U concentrations were measured by kinetic phosphorescence analysis (KPA). Dissolved Al, As, B, Ba, Br, Ca, Cd, Co, Cr, Cu, Fe, Li, Mg, Mn, Mo, Na, Ni, P, Pb, Se, Si, Sr, V, and Zn concentrations were measured by inductively coupled plasma optical emission spectrometry (ICP-OES). The K concentration was measured by direct air-acetylene flame atomic absorption spectrometry. Chloride, nitrate, and sulfate concentrations were measured by ion chromatography.

A.2.3 Groundwater and Surface Water Results

DOE collected 124 groundwater samples between January 1986 and September 1997 at the wells DOE-505 through DOE-637. Nine of the groundwater samples had charge balance errors greater than 15% and these data were not considered further. USGS collected 365 groundwater samples between November 1998 and September 2001 at the wells DOE-547, DOE-548, all NAT wells, all MAU wells, and well DM-1. Six of these groundwater samples had charge balance errors greater than 15% and these data were not considered further. In both datasets, some of the minor species were not analyzed in each sample. These species include NO_3, Fe, and Mn.

Twenty five grab surface water samples were collected from the San Miguel River between 1998 and 2001 and all samples had charge balance errors less than 15%.

A summary of the analytical results for the DOE data, the USGS groundwater data, the pooled DOE and USGS data, and the USGS surface water data is listed in Tables A.1 and A.2. The table shows the minimum, maximum, average, standard deviation, and median concentration for 15 different parameters. Generally, these statistical parameters for the DOE and USGS groundwater samples agree. The pooled data form the basis for assessing the influence of the variable chemical composition of groundwater on simulated K_d values that are presented in Section 9. The distributions of dissolved U(VI), pH and alkalinity are shown in the quantile plots in Figure A.1. These plots provide a view of the range and distribution of both the USGS and DOE data. For each of the species, the distribution of the data from the DOE dataset is more asymmetric than the USGS data. This probably results from the sparse spatial distribution of the original DOE wells. In most cases, the means of the two data sets agree fairly closely, and because of this close agreement, the two data sets were pooled for the purposes of examining the effects of variable chemical conditions on computed K_d values.

A.3 Aqueous Speciation Calculations

Speciation calculations were performed on each of the 474 groundwater samples. The calculations included the effects of temperature on the speciation reactions even though enthalpy data were not available for all of the species. This was a particular problem for the solid U phases. The results of calculations are summarized below.

A.3.1 CO_2(g)

The partial pressure of CO_2 (pCO_2) that would be in equilibrium with the groundwater sample was computed with the speciation model and the results are show in Figure A.2. The figure shows the simulated pCO_2 versus the distance in feet from well DM-1. Because the aquifer is long relative to the width, a one-dimensional plot is a simple way of illustrating the spatial variability for computed values for each of the sampling rounds. The pCO_2 values ranged from 0.0024 to 0.14 atm, had a mean value of 0.032 atm and a median value of 0.028 atm.

A.3.2 Saturation Indices

Figure A.2 shows that the groundwaters are nearly saturated with respect to calcite, slightly undersaturated with respect to gypsum and slightly oversaturated with respect to quartz.

Figure A.3 shows the U(VI) phases schoepite and soddyite are below saturation for all analyses. In contrast, carnotite and tyuyamunite are supersaturated in the area between approximately 520 and 1070 m feet from well DM-1. As discussed in Section 3, although the waters are supersaturated with respect to these phases, detailed characterization of sediments from NAT06 (Jove-Colon et al., 2003) did not identify either carnotite or tyuyamunite. Figure A.4 shows computed saturation indices of four U(IV) phases; uraninite, am-UO_2, U_3O_8 and $USiO_4$. The calculations assumed that the Fe(III)/Fe(II) redox couple was at equilibrium, and that the Fe(III) activity was controlled by the solubility of ferrihydrite. Each of the U(IV) phases is below saturation, with uraninite being the closest to saturation. In contrast, Figure A.5 shows the saturation indices for the same phases, except in this case the Fe(III) activity was assumed to be controlled by the solubility of goethite. In this instance, all of the U(IV) phases are supersaturated over most of the aquifer.

A.3.3 Aqueous Uranium Speciation

As discussed in Section 2, U(VI) speciation in solution is complex and depends on pH, pCO_2, and the total dissolved U(VI) concentration. Section 2 summarized reactions that included a total of 25 different U(VI) species in solution. The results of the speciation calculations established that the U(VI) – carbonate complexes, $UO_2(CO_3)_2^{-2}$ and $UO_2(CO_2)_3^{-4}$, were

Table A.1 Summary of geochemical data for Naturita groundwater samples

Summary of USGS Groundwater Data															
	U	pH	Alkalinity	Ca	Mg	Na	K	Cl	SO_4	Fe	DO	Sr	Mn	V	NO_3
	μM	su	meq/L	mM	mM	mM	mM	mM	mM	mM	μM	mM	mM	mM	μM
Minimum	0.01	6.54	2.48	1.37	0.60	0.79	0.04	0.00	1.03	0.00	1.56	0.01	0.00	0.00	0.32
Maximum	10.46	7.53	11.92	12.28	5.97	50.89	1.03	17.83	20.10	0.10	125.00	0.07	0.12	0.15	57.42
Average	2.93	7.07	6.79	5.24	2.33	8.96	0.26	2.04	7.43	0.01	10.76	0.03	0.02	0.03	3.62
Standard deviation	2.25	0.17	1.59	1.33	0.83	7.33	0.16	2.60	3.39	0.01	13.30	0.01	0.02	0.03	7.72
Median	2.87	7.07	7.06	5.39	2.38	7.83	0.25	1.40	7.52	0.00	7.19	0.03	0.02	0.00	1.85
Sample number	359	359	359	359	359	359	359	359	359	359	348	359	359	359	106
Summary of DOE Groundwater Data															
Minimum	0.01	6.64	2.60	1.67	0.60	1.22	0.02	0.06	1.54	0.00	2.19	0.01	0.00	0.00	1.00
Maximum	21.85	7.71	23.04	9.38	4.90	46.98	1.23	24.14	15.10	0.05	26.88	0.08	0.14	0.20	725.81
Average	3.50	7.04	7.17	4.54	1.92	8.09	0.22	2.05	6.06	0.00	12.02	0.02	0.02	0.03	120.06
Standard deviation	4.42	0.23	3.71	1.64	0.95	9.67	0.24	4.03	3.27	0.01	7.80	0.01	0.02	0.05	133.98
median	1.48	7.00	6.32	4.14	1.67	4.18	0.14	0.53	5.14	0.00	12.50	0.02	0.01	0.01	60.24
Sample number	113	115	115	115	115	115	115	115	115	60	17	88	115	113	42
Summary of Pooled Groundwater Data															
Minimum	0.01	6.54	2.48	1.37	0.60	0.79	0.02	0.00	1.03	0.00	1.56	0.01	0.00	0.00	0.32
Maximum	21.85	7.71	23.04	12.28	5.97	50.89	1.23	24.14	20.10	0.10	125.00	0.08	0.14	0.20	725.81
Average	3.07	7.07	6.88	5.07	2.23	8.74	0.25	2.04	7.10	0.01	10.82	0.03	0.02	0.03	36.66
Standard Deviation	2.92	0.19	2.29	1.44	0.87	7.96	0.18	3.00	3.41	0.01	13.09	0.01	0.02	0.04	88.45
Median	2.78	7.05	6.88	5.24	2.27	7.00	0.22	1.24	7.13	0.00	7.50	0.03	0.02	0.00	3.23
Sample number	472	474	474	474	474	474	474	474	474	419	365	447	474	472	148

Table A.2 Summary of geochemical data for Naturita surface water samples

Summary of Surface Water Data															
	U	pH	Alkalinity	Ca	Mg	Na	K	Cl	SO_4	Fe	DO	Sr	Mn	V	NO_3
	μM	su	meq/L	mM	mM	mM	mM	mM	mM	mM	μM	mM	mM	mM	μM
Minimum	0.003	7.73	1.16	0.90	0.20	0.18	0.02	0.03	0.67	0.00	62.50	0.00	0.00	0.00	0.32
Maximum	0.02	8.66	3.52	4.02	2.44	2.46	0.10	0.32	5.76	0.00	496.88	0.04	0.00	0.00	1.77
Average	0.01	8.35	2.26	2.01	0.99	1.00	0.05	0.16	2.28	0.00	298.83	0.01	0.00	0.00	0.66
Standard Deviation	0.006	0.25	2.26	1.00	0.75	0.79	0.03	0.10	1.70	0.00	97.32	0.89	0.00	0.00	0.45
Median	0.009	8.41	2.3	1.91	0.88	0.88	0.04	0.13	1.80	0.00	252.2	0.95	0.00	0.00	0.48
Sample number	25	25	25	25	25	25	25	25	25	25	25	25	25	25	19

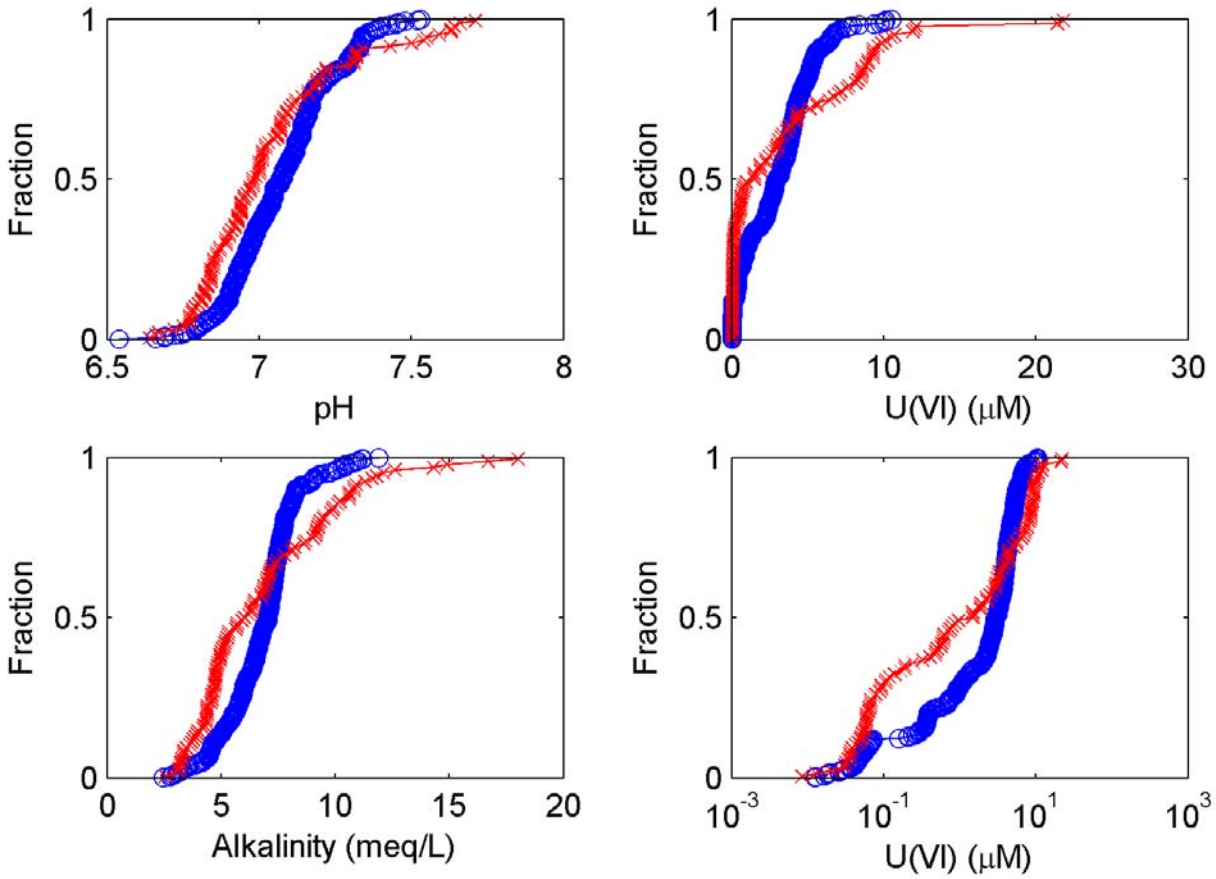

Figure A.1. Quantile plots of pH, alkalinity and U. Results from the USGS database are shown as O and results from the DOE database are shown as X.

the two dominant species in solution in all of the Naturita groundwaters. This is illustrated in Figure A.6, which shows the fraction of total dissolved U(VI) in solution that is accounted for by the two species, $UO_2(CO_3)_2^{-2}$ and $UO_2(CO_2)_3^{-4}$. These fractions are plotted versus distance from well DM-1, the most upgradient well at the site. Because of the long thin shape of the aquifer, this plot gives an approximate representation of the spatial distribution in the aquifer. The figure illustrates that either species could be the dominant species at a given location. In addition, the figure illustrates the sum of the fractions of the two species, $UO_2(CO_3)_2^{-2}$ and $UO_2(CO_2)_3^{-4}$. In all cases the sum of the two species accounted for greater than 96% of the total dissolved U(VI).

A.4 Spatial Distributions

Figure A.7 illustrates the spatial distribution for 15 species based on observations made in September, 1999.

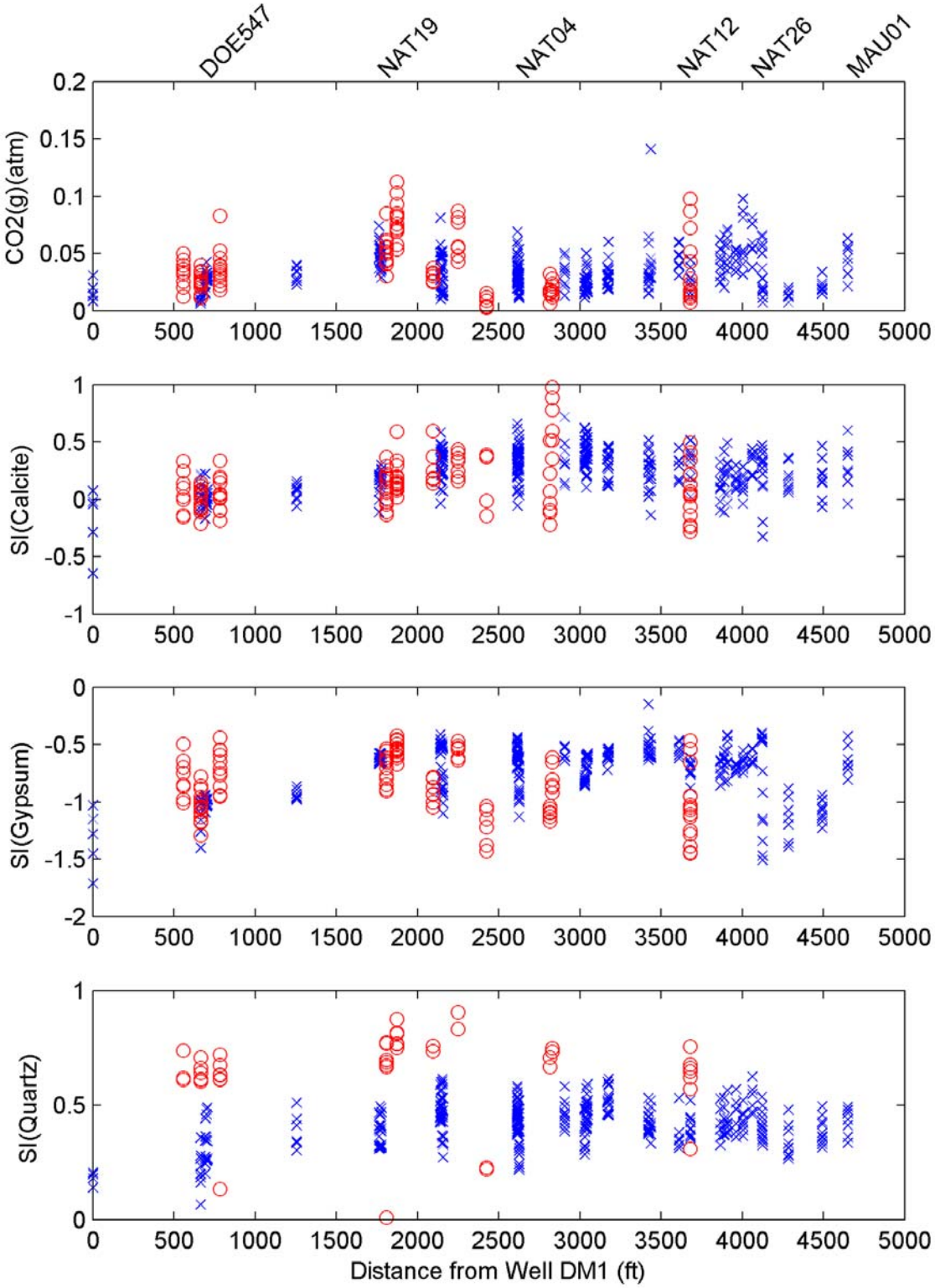

Figure A.2. Speciation calculation results for Naturita groundwaters. Results from the USGS database are shown as X and results from the DOE database are shown as O.

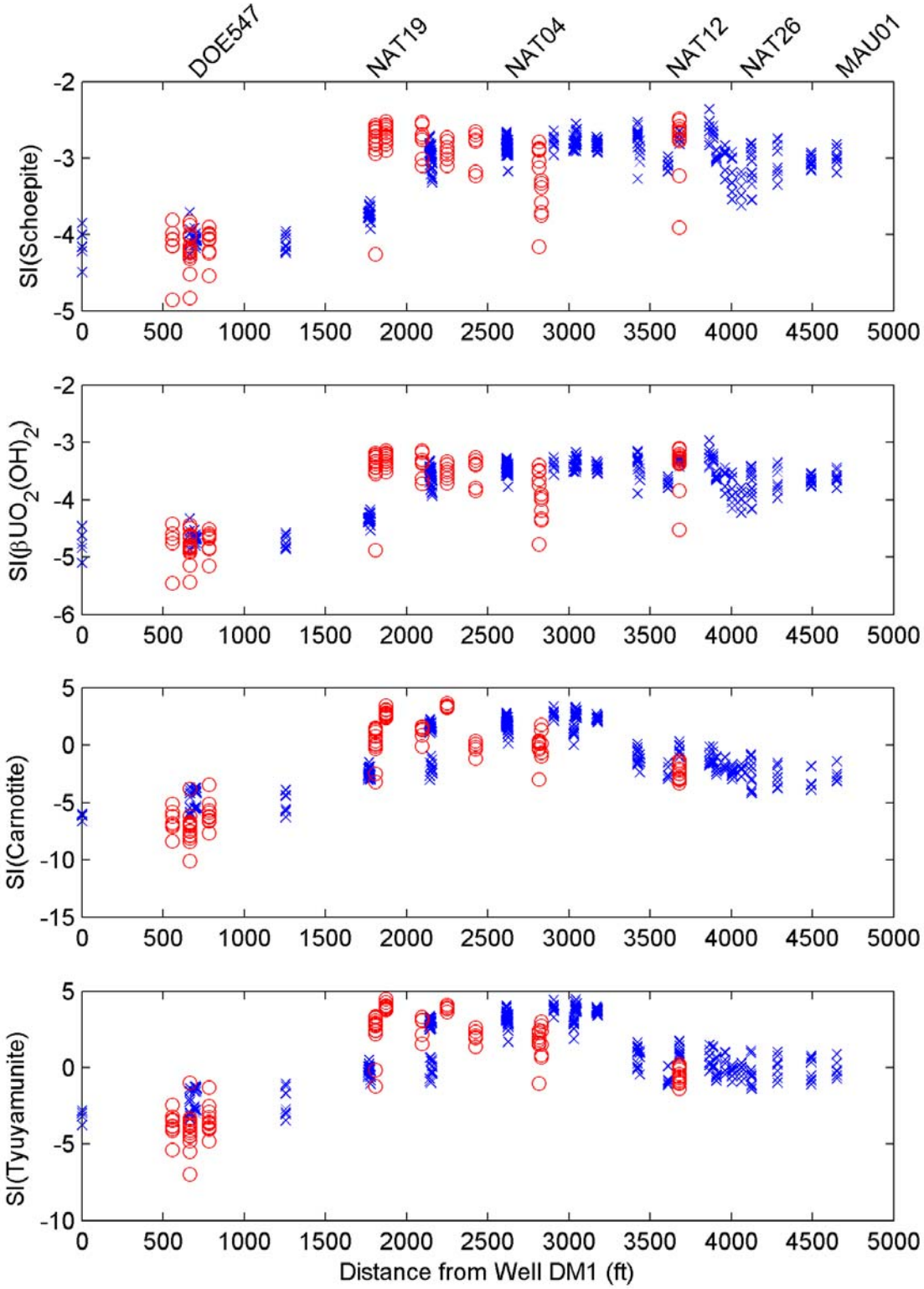

Figure A.3. Saturation Indices for selected U(VI) phases for Naturita groundwaters. Results from the USGS database are shown as X and results from the DOE database are shown as O.

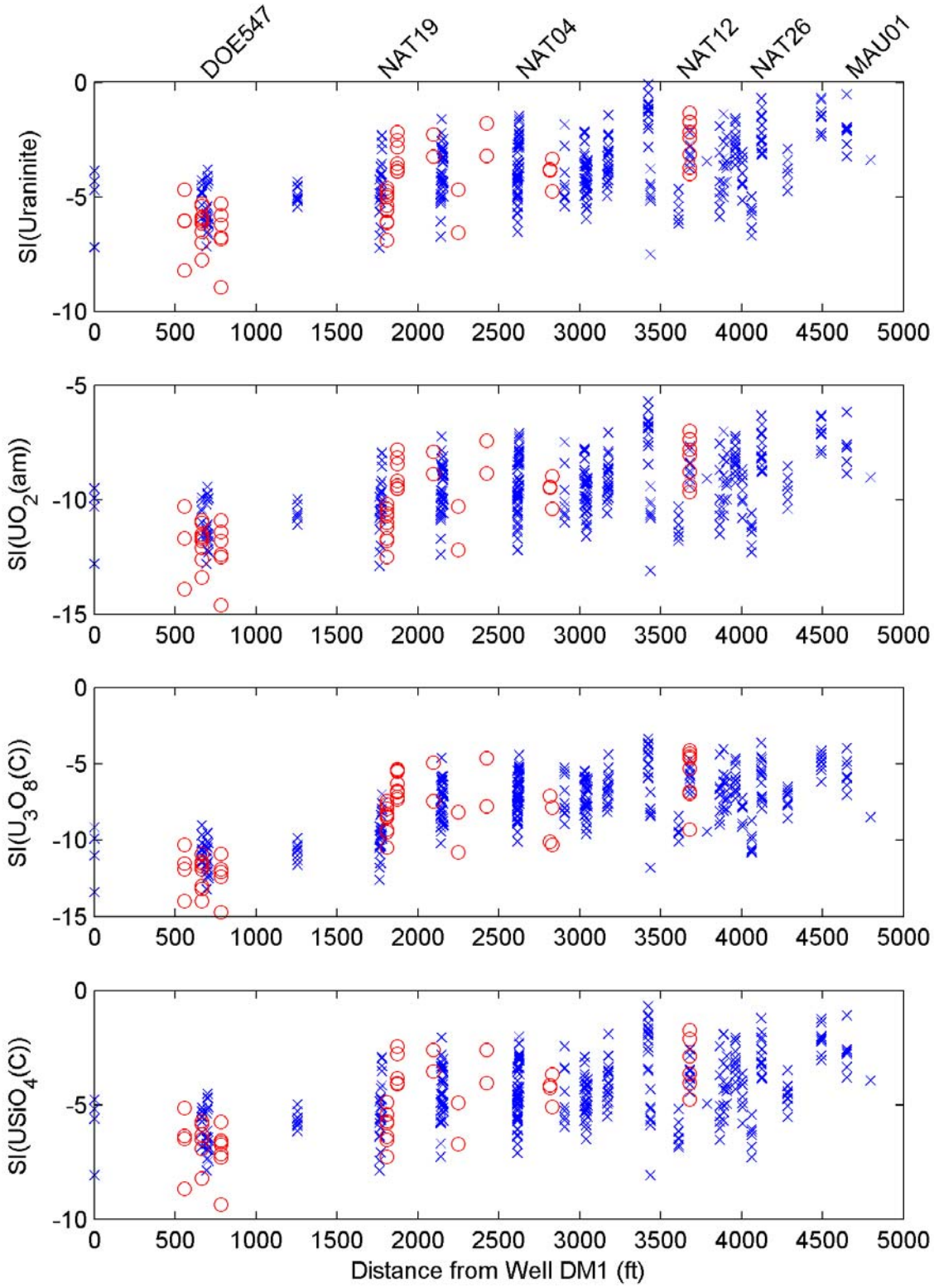

Figure A.4. Saturation Indices for selected U(IV) phases for Naturita groundwaters. Calculations assumed Fe(III) activity was controlled by ferrihydrite. Results from the USGS database are shown as X and results from the DOE database are shown as O.

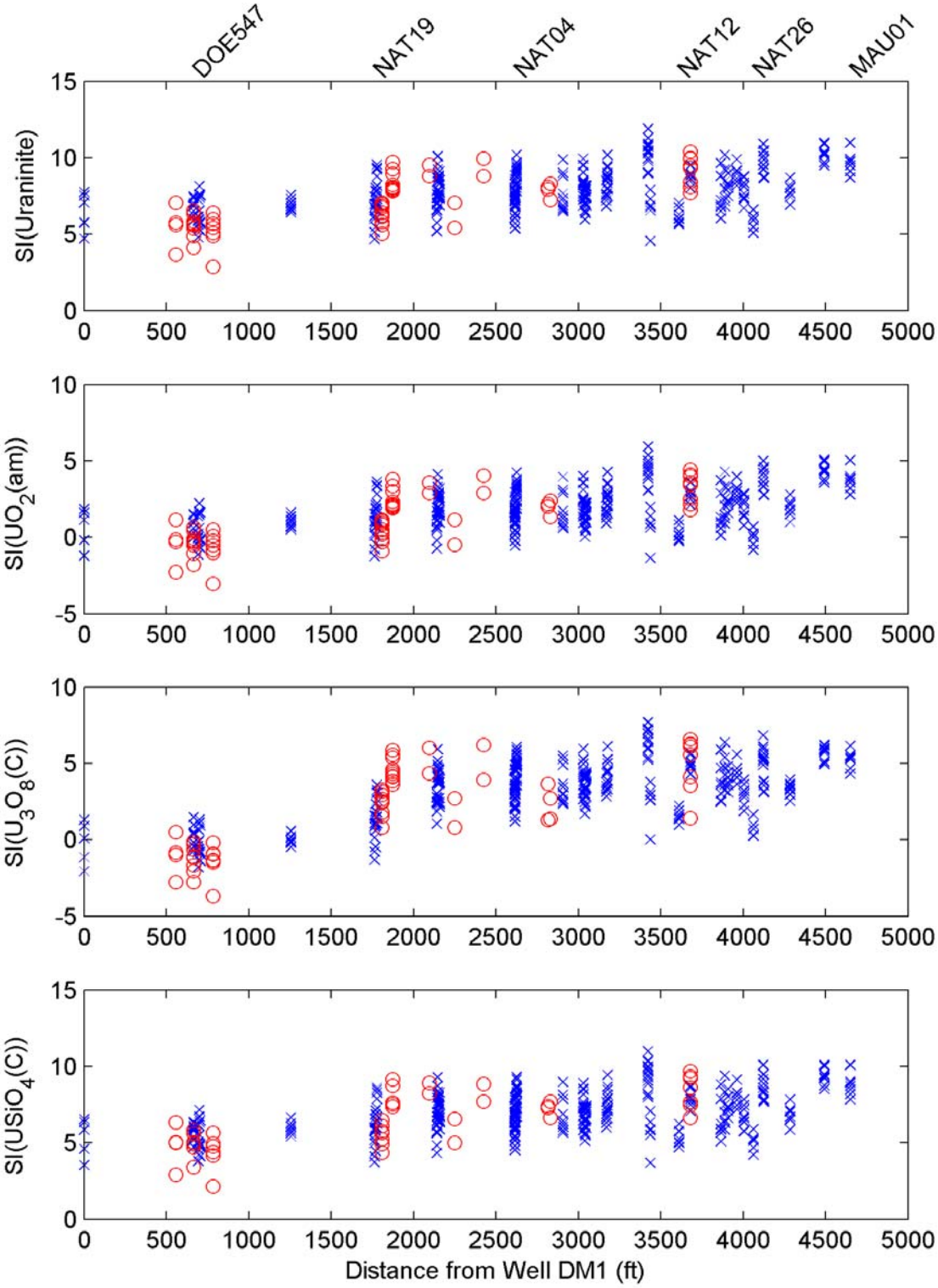

Figure A.5. Saturation Indices for selected U(IV) phases for Naturita groundwaters. Calculations assumed Fe(III) activity was controlled by goethite. Results from the USGS database are shown as X and results from the DOE database are shown as O.

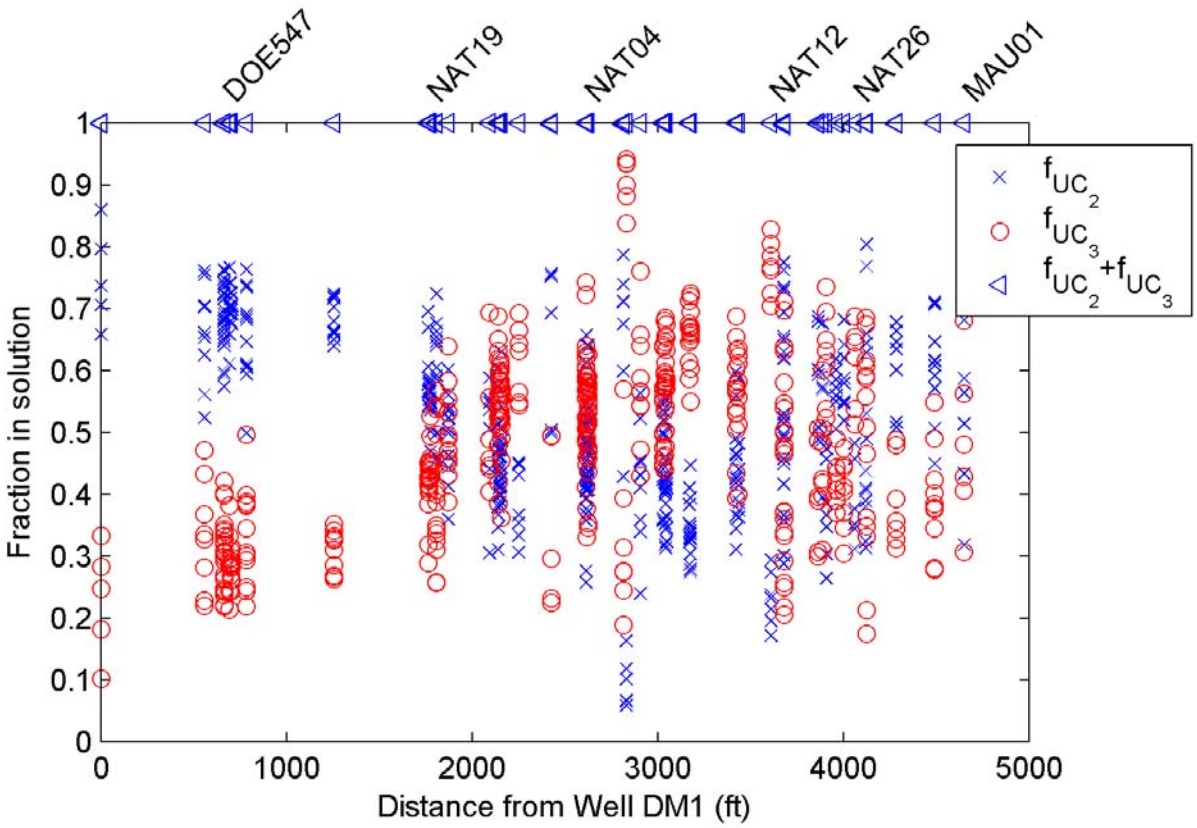

Figure A.6. Computed fraction of total dissolved U(VI) present as $UO_2(CO_3)_2^{-2}$ (denoted by f_{UC2}) and $UO_2(CO_2)_3^{-4}$ (denoted by f_{UC3}). Also shown is the sum of only the $UO_2(CO_3)_2^{-2}$ and $UO_2(CO_2)_3^{-4}$ species. Results from the USGS database are shown as X and results from the DOE database are shown as O.

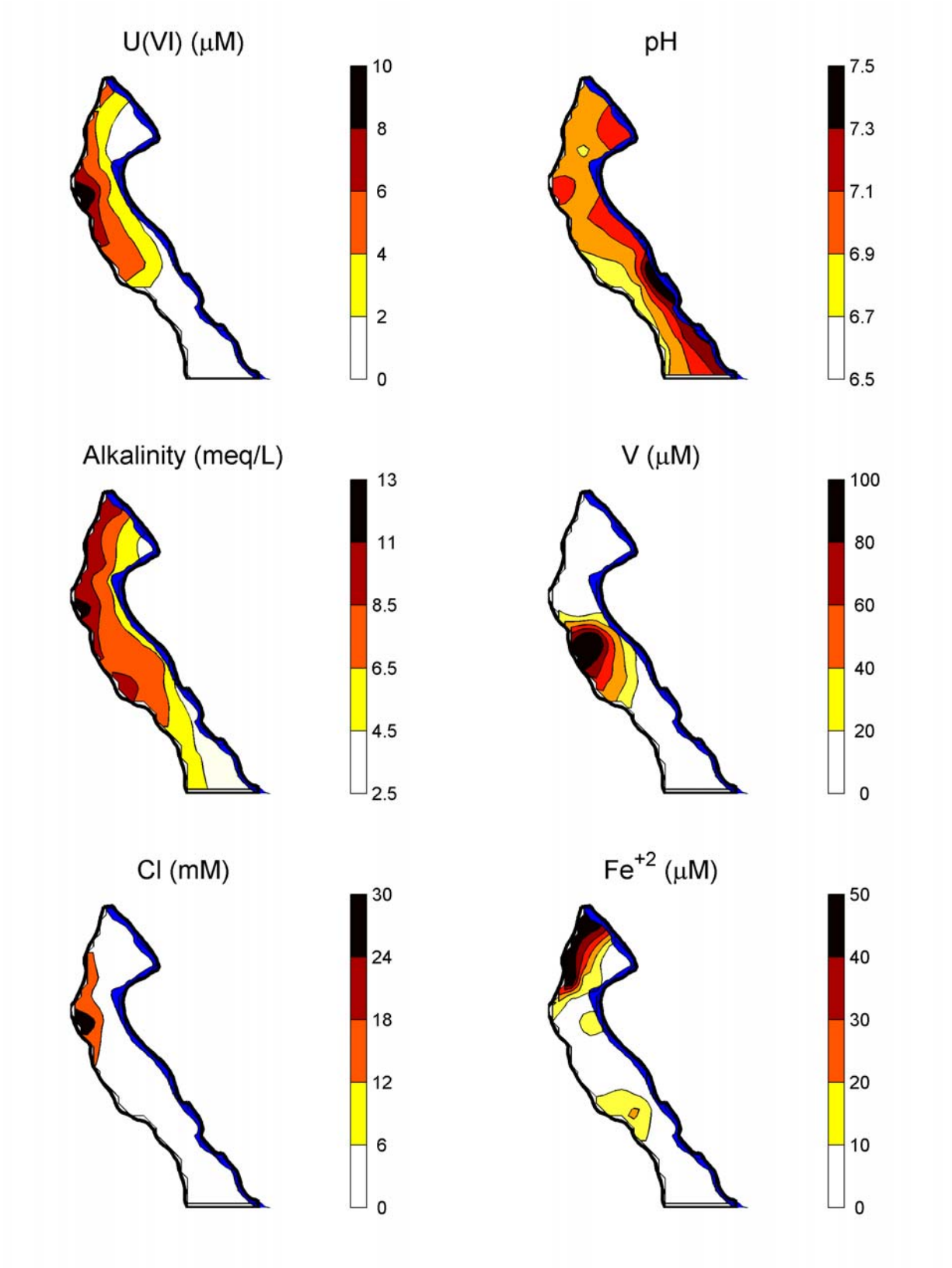

Figure A.7. Kriged Concentration of dissolved U(VI), V, Cl and Fe(II) concentrations, pH and alkalinity, observed in Naturita groundwater in September 1999.

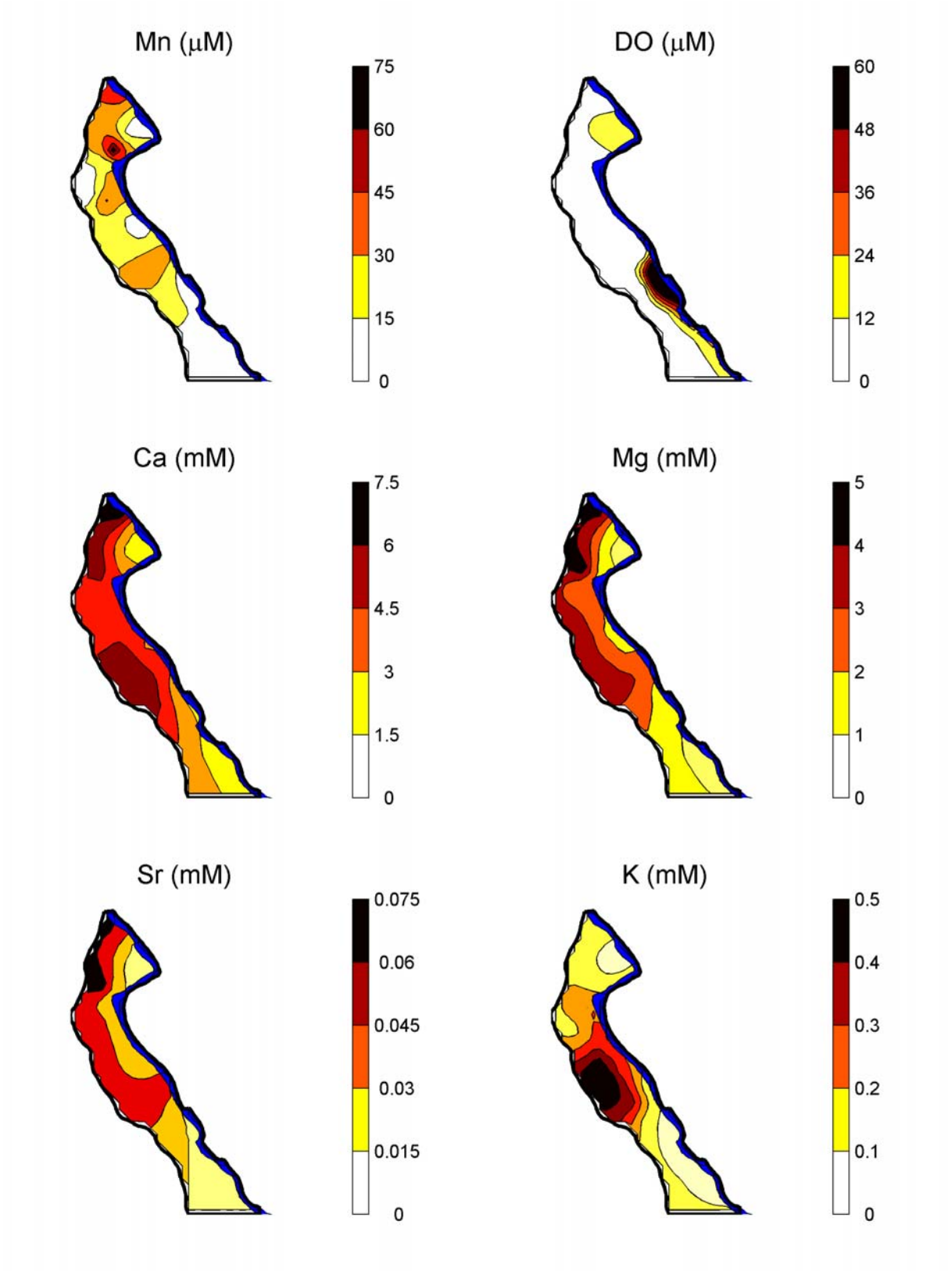

Figure A.7 (continued). Kriged concentrations of dissolved Mn, DO, Ca, Mg, Sr and K concentrations observed in Naturita groundwater in September 1999.

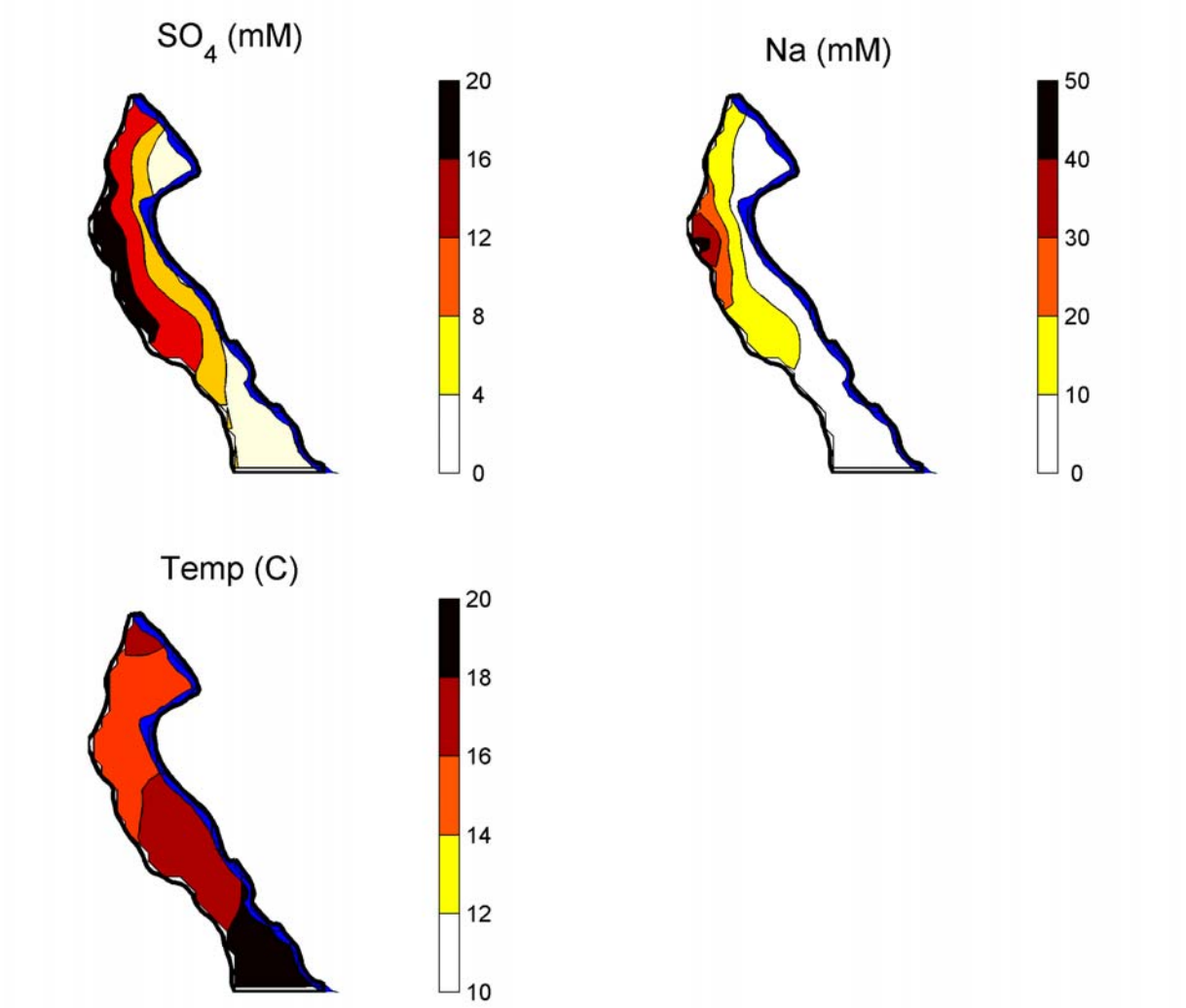

Figure A.7 (continued). Kriged concentrations of dissolved SO_4 and Na and temperature observed in Naturita groundwater in September 1999.

APPENDIX B: ESTIMATES OF HYDRAULIC CONDUCTIVITY

Groundwater head values computed from the steady state flow model for the Naturita site were insensitive to the hydraulic conductivity (K_X). This implies that the hydraulic conductivity cannot be determined from parameter estimation approaches using only the flow model, because the magnitude of the groundwater fluxes are unknown. However, K_X values are critically important for conducting solute transport simulations because of the linear dependence between solute velocity and hydraulic conductivity in Darcy's Law. Therefore, K_X values must be obtained independently of the flow model.

Several approaches were considered and are briefly summarized below. Slug tests were performed on 10 wells at the Naturita site during November 1999, when water levels in the aquifer were generally low, and in May 2000 when water levels in the aquifer were generally high. Two to four slug test replicates were done on each well (Table B.1). The Bouwer-Rice solution for unconfined aquifers was used to determine all hydraulic conductivity values. The mean K_X value obtained from the slug tests was approximately $3.5 \cdot 10^{-4}$ m/s (100 ft/d), and the data ranged by a factor of approximately 3 (Table B.2). In heterogeneous aquifers, slug test results can be biased toward high values of hydraulic conductivity, because these regions respond most rapidly to the change of volume in the well.

K_X was also estimated from the observed rate of change in aquifer head in response to a change in stream stage. This analysis was completed at 4 wells and at 4 different times. K_X values determined from this method ranged from $1 \cdot 10^{-3}$ to 0.22 m/s (290 - 63,000 ft/d). These values were very high and are considered to be inconsistent with the transport data at the site.

An empirical estimate of ground water velocity was obtained from the observed disappearance of bromide during several injection tests. The K_X values estimated from these velocities and an average gradient were highly variable, ranging from $4.6 \cdot 10^{-5}$ to nearly $3.5 \cdot 10^{-4}$ m/s.

The final method used to estimate an average K_X for the aquifer was based on tritium-helium age-dating results. This method has the advantage that the age of the groundwater is affected by many of the same processes that affect U(VI) migration, and the scale of this approach encompasses nearly the whole aquifer. The groundwater age was directly simulated in the two-dimensional transport model using a constant porosity of 0.20 and the simulated age was compared with the observed value. The K_X value was varied to minimize the sum of the squared error. The best fit (Figure B.2) was obtained with a K_X of $3.17 \cdot 10^{-4}$ m/s.

The major disadvantage of the age dating approach is that the interpretation of the age of the water is dependent on the extent of mixing in the groundwater. This may be particularly important at wells MAU-04 and MAU-07, which had water on long recharge flow paths but also exhibited low groundwater age. The steady state flow model suggested that these wells were on flow paths that entered the aquifer upgradient of well DOE-547 and passed between well NAT-23 and the San Miguel River (Figure B.2). The water elevation and chemical characteristics at well NAT-23 are impacted by the San Miguel River, and if a transient flow model were considered, it is likely that the flow simulations would show a mixing of river water with groundwater in the region of well NAT-23. In other words, water that enters the aquifer near well NAT-23 could have been transported to wells MAU-04 and MAU-07, and this would have accounted for the younger water ages at those wells.

A second limitation of the age dating results was that the flow paths show that the most of the wells are recharged by water that enters the aquifer upgradient of the mill yard and then passes below the mill yard. As this water passes below the mill yard, it apparently mixes with

Table B.1: Hydraulic Conductivity Determined from Slug Tests

Well	Hydraulic Conductivity (m/s * 10^4)				Average Hydraulic Conductivity (m/s * 10^4)
	Test 1	Test 2	Test 3	Test 4	
NAT-02		1.02	1.44		1.24
NAT-03	3.39	2.98			3.18
NAT-05	2.68	2.37			2.51
NAT-10	1.33	1.05	0.94		1.09
NAT-11	3.29	2.86	3.19	3.34	3.18
NAT-23	8.68	11.04	10.41		9.88
NAT-25	0.84	1.54	1.13		1.16
MAU-03	2.99	2.48	3.67		3.03
MAU-07	0.56	0.93	0.93		0.81
NAT-03	3.67	3.19			3.42
NAT-05	2.67	2.36			2.54
NAT-09	10.1	11.3	13.6		11.8
NAT-11	3.81	4.05	3.71		3.85
NAT-19	5.39	3.77	4.51		4.55
NAT-24	7.97	2.31	2.36		1.89
NAT-25	3.98	4.45	4.09		4.16

Table B.2 Summary of Hydraulic Conductivity Estimates

Hydraulic Conductivity (m/s)				
	Slug Tests	Stream-Aquifer Interactions	Tracer Tests[1]	Age-Dating[2]
Min	$8.1 \cdot 10^{-5}$	$1.02 \cdot 10^{-3}$	$4.59 \cdot 10^{-5}$	
Median	$3.10 \cdot 10^{-4}$	$1.03 \cdot 10^{-2}$	$1.31 \cdot 10^{-4}$	
Mean	$3.60 \cdot 10^{-4}$	$6.07 \cdot 10^{-2}$	$1.59 \cdot 10^{-4}$	$3.17 \cdot 10^{-4}$
Max	$1.17 \cdot 10^{-3}$	0.222	$3.28 \cdot 10^{-4}$	

[1] Median, Mean and Max values are based on an assumed velocity at well NAT-04-3.
[2] Values are based on the assumed shorter flow path to wells MAU-04 and MAU-07.

some water that is high in Cl concentration (Figure B.3). The observation that there is high Cl concentrations in many of the wells were where tritium helium age dating results were obtained suggests that young water may have recharged the water along with the high Cl concentrations. Thus, the average recharge path lengths would have been shorter if there was significant recharge at the Mill yard. This shorter average path length would be consistent with a smaller K_X value.

Table B.2 lists a summary of the hydraulic conductivity values estimated from the field conditions. The values estimated from the analysis of the stream aquifer interactions are generally one to two orders of magnitude larger than the results from all other tests. These results are probably biased toward the most permeable layers or regions in the aquifer and therefore these results will not be considered further. The remaining results generally agree within a factor of 20. The slug test results are uniformly larger than those estimated from the tracer tests or from the chloride results (Section

9). Again this bias towards larger values is probably because the slug tests are often biased toward high values by highly permeable regions. The age dating results generally agreed with the slug tests. However, when Cl was simulated with a K_X of $3.10 \cdot 10^{-4}$ m/s the Cl plume was transported off site by 2001 when the Cl observed in 1986 was used as initial conditions. The slug tests and the age dating results are about a factor of 2 larger than the value estimated from Cl and this agreement is considered very good for K_X. A better agreement between the Cl simulations and the slug tests if the porosity in the simulations was reduced by a factor of approximately 2. However, the resulting porosity of 0.10 was considered to be too small for the predominantly sand and gravel aquifer.

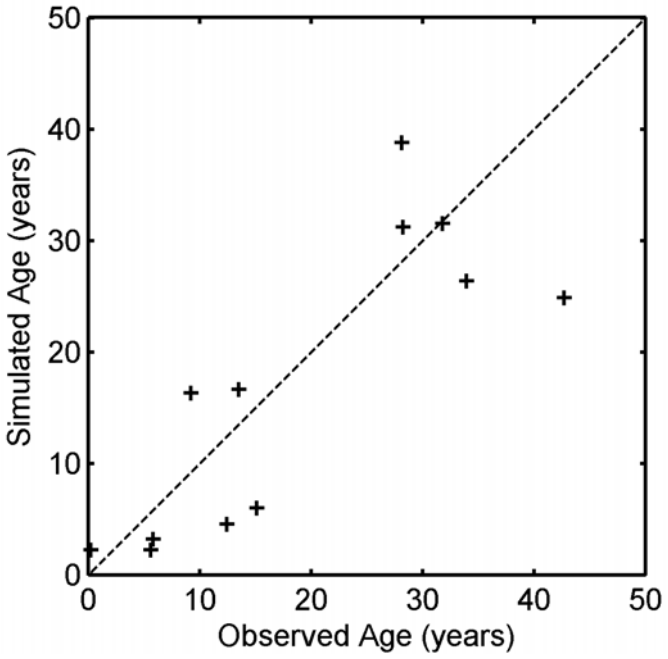

Figure B.1 Optimized fit of tritium-helium age-dating of groundwater.

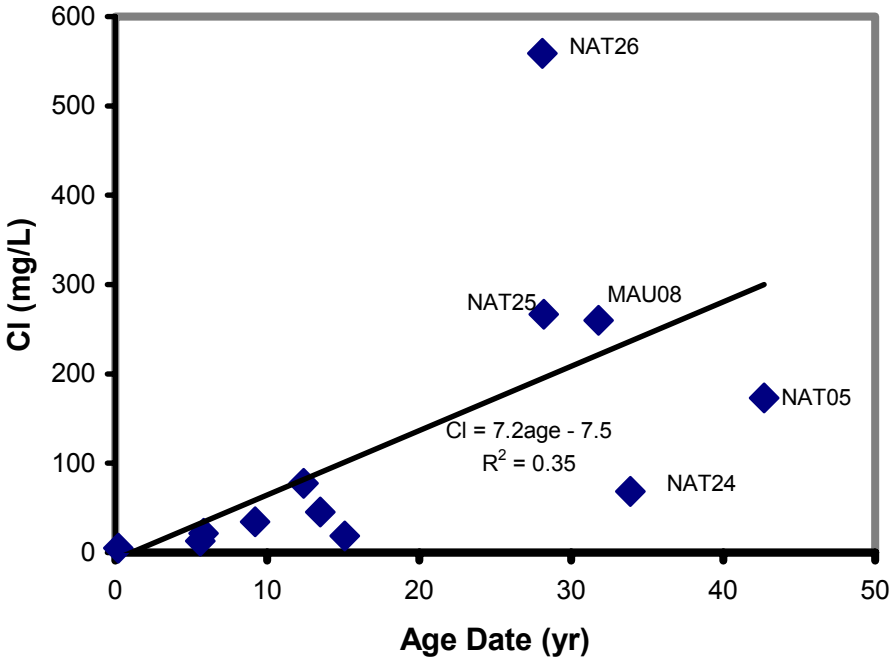

Figure B.2. Relation between measured tritium-helium groundwater age and Cl concentration.

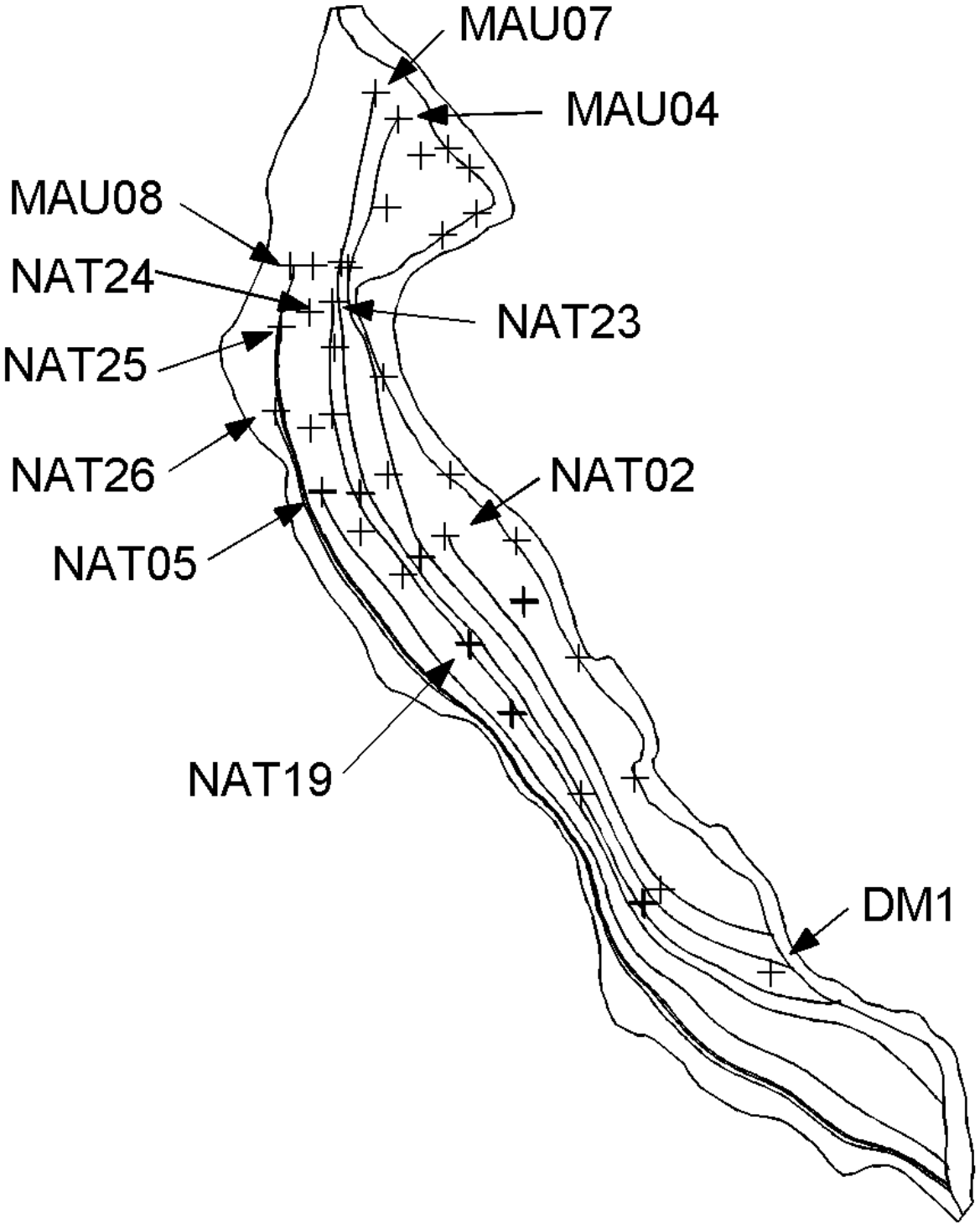

Figure B.3. Flow paths backtracked from wells where tritium-helium age-dating samples were analyzed.

APPENDIX C: ADDITIONAL CHARACTERIZATION DATA FOR THE NATURITA AQUIFER SEDIMENTS

C.1 Surface Area of Grain Size Fractions

A "washing" experiment was carried out as part of an investigation into the certainty of the values for the specific surface area of the 1-3 and 0.5-1 mm fractions of the NABS sample. The original grain size separations were performed by dry sieving the NABS sample, followed by rinsing each fraction in the sieve with an artificial groundwater, AGW-1, approximately 60% saturated with respect to calcite ($NaHCO_3$ $4.17 \cdot 10^{-4}$M, Na_2CO_3 $1.7 \cdot 10^{-6}$M, $CaSO_4 \cdot 2H_2O$ $4.5 \cdot 10^{-3}$M, KCl $3.84 \cdot 10^{-5}$M, NaCl $1.96 \cdot 10^{-3}$M, $MgCl_2$ $1.15 \cdot 10^{-3}$M). These fractions are referred to as "wet-sieved". The wet-sieved material was washed by suspending 10 g of each fraction in 10 ml AGW-1, centrifuging and decanting. This process was repeated 23 times until the supernatant remained clear. This treatment removed fines that adhered to the larger grains and disaggregated poorly cemented particles. The surface areas of the newly derived fractions are presented in Table C.1. The dry-sieved values were already presented in Section 4 (Table 4.1).

Table C.1 Specific Surface Areas (m^2/g) of washed, wet- and dry-sieved size fractions obtained from the NABS sample

Size Fraction	Washed	Wet-sieved	Dry-sieved
1-3mm	5.01	4.47	6.31
500-1000μm	4.81	4.40	5.70
250-500μm	2.48	3.09	3.95
125-250μm	3.05	3.94	5.10
63-125μm	4.52	5.33	7.19
<63μm	25.1	17.2	13.1

The washing procedure decreased the surface areas in the 250-500, 125-250, and 63-125 μm fractions, as would be expected if finer grained particles were being removed. However, the surface areas in the 1-3 mm and 500-1000 μm fractions *increased*, possibly due to disaggregation or silica dissolution. The collected <63 μm fractions were not combined, that is, the "wet-sieved" measurement was made on the material removed from the coarser fractions by wet-sieving and not combined with the dry sieved material. Similarly, the "washed" measurement was made only on the material removed by washing. These data show that the material removed in each treatment step became progressively finer.

C.2 Preparation and Characterization of a Carbonate-free NABS sample

In order to study U(VI) adsorption of U(VI) by the NABS sample in the absence of carbonate minerals, a procedure (Chao, 1984; Tessier et al., 1979) was modified slightly to dissolve the carbonate minerals from the sample. Figure C.1 shows the rate of dissolution of selected elements (Ca and Mg in C.1a and Al, Fe, Mn and Si in C.1b) into an acetic acid buffer solution from ground samples of the composite sample.

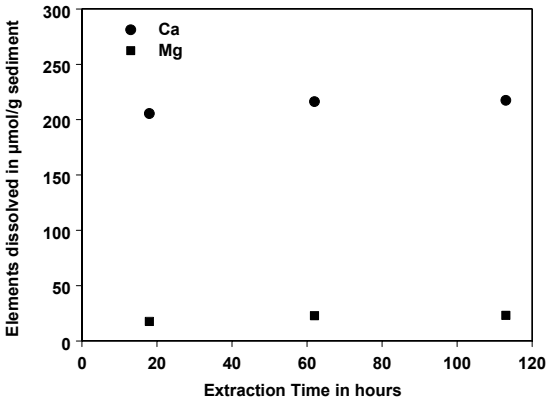

Figure C.1a. Ca and Mg extracted from 100g/L NABS sample in 1M Na-Acetate/Acetic Acid buffer pH 5.

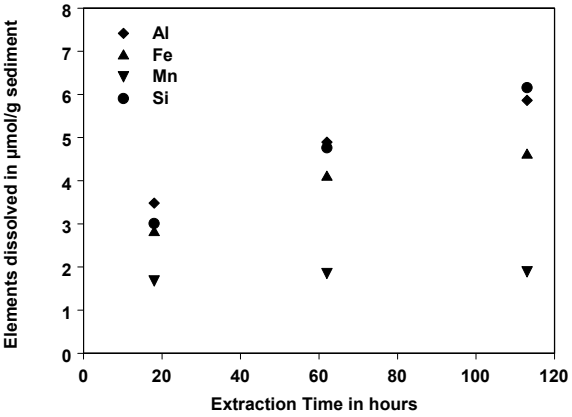

Figure C.1b. Various elements extracted from 100 g/L NABS sample in 1M Na-Acetate/Acetic Acid buffer pH 5.

A 500 g sample of "carbonate-free" material was then prepared by extraction of the NABS sample with 1M acetate buffer. As this sample was not ground, the inorganic carbon content of the material may have not been reduced completely to zero (Table C.2). Experimental procedures to study U(VI) adsorption by this sample were similar to that used for the NABS sample (described in Section 5), with the exception that a different artificial groundwater was prepared for these experiments with a lower calcium concentration (AGW-4: $NaHCO_3$ $5.38 \cdot 10^{-4}$M, Na_2SO_4 $3.267 \cdot 10^{-3}$M, $MgSO_4$ $1.515 \cdot 10^{-3}$M, NaCl $3.819 \cdot 10^{-3}$M, $CaCl_2$ $4.71 \cdot 10^{-4}$M and KCl $6.4 \cdot 10^{-5}$M).
The surface area of the "carbonate-free" material was measured as 4.47 m^2/g by BET adsorption of nitrogen gas. The results of the U(VI) adsorption by the carbonate-free sample are given in Sanpawanichakit (2002).

Table C.2 shows the results of inorganic and organic carbon analysis for the NABS sample for aliquots of the NABS sample extracted with HCl or acetic acid. The organic carbon content of the NABS sample before and after extractions by 1.2M HCl or 1M acetate buffer was 0.11 weight percent. Carbonate minerals were extracted efficiently by the acetate buffer if the sample was ground.

C.3 Characterization of the Naturita Sediment Samples

C.3.1 Extractions of the NABS and U-Contaminated Naturita Sediments with the Sodium (Bi)carbonate solution at pH 9.4 (CARB)

The CARB extraction method and results for extracted U are reported in Section 4. Here we report the concentrations of other elements in the extractions.

Figure C.2 shows the pH development during the extractions. The pH in these samples was not adjusted, except at approximately 1850 hr, when it was brought back to near its initial pH value of 9.4. After the adjustment, the pH decreased again at various rates for the different samples, but most pronounced for the NAT-06 sample.

Figures C.3 through C.7 show the moles of various elements extracted per gram of sediment (data are also given in the corresponding Tables C.5. through C.9. at the end of this appendix). Only samples NAT-03, NAT-06, NAT-08, NAT-11, NAT-12 and MAU-02 were let drift for the first 1850 hr and were then pH-adjusted. For all the other samples, the pH was adjusted more frequently and kept nearly constant during the entire course of the extraction.

Table C.2. Carbon analyses of the NABS Sample and Extracted Samples

Sample	% Carbon by weight		
	Total Carbon	Inorganic Carbon	Organic Carbon
<3 mm NABS sample	0.36	0.25	0.11
1.2M HCl-extracted	0.11	0.0	0.11
1.2M HCl-extracted (ground)	0.10	0.0	0.10
1M acetate buffer - extracted	0.14	0.03	0.11
1M acetate buffer – extracted (ground)	0.12	0.00	0.12

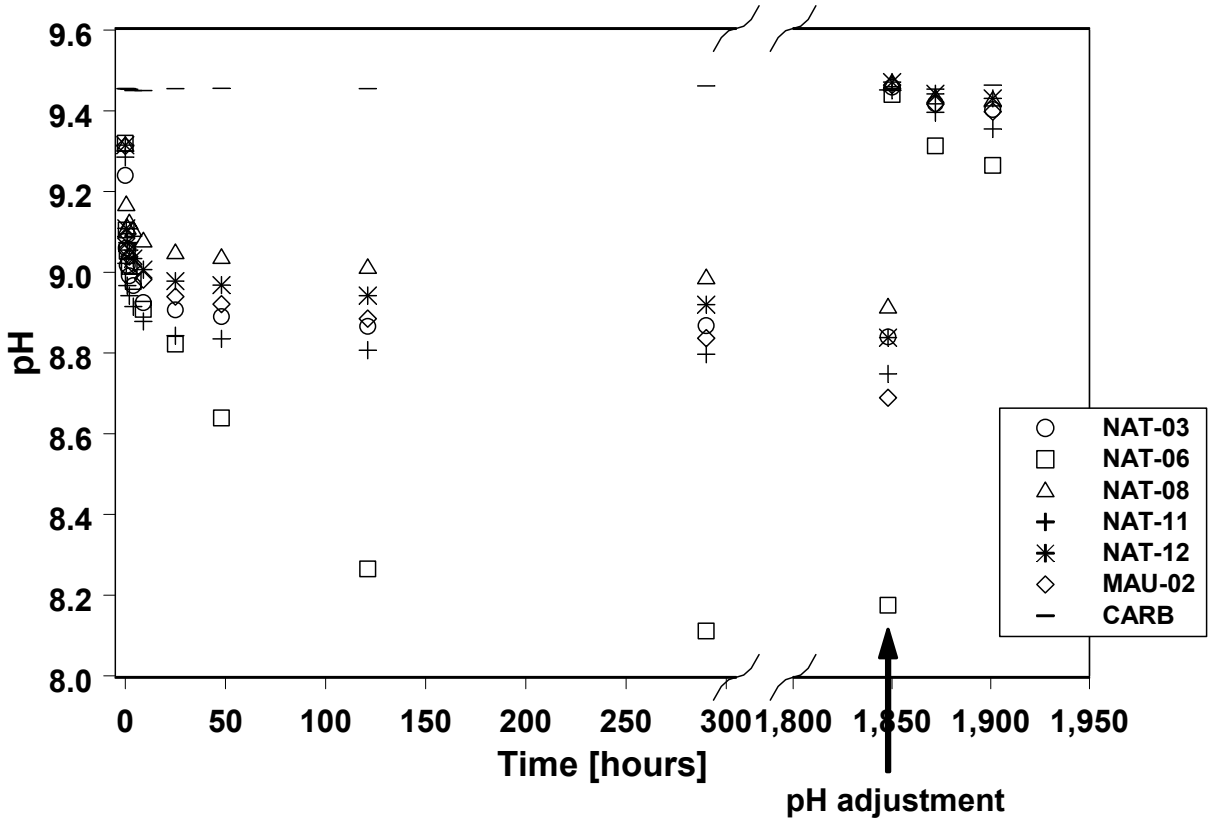

Figure C.2. pH development during extraction with the CARB solution.

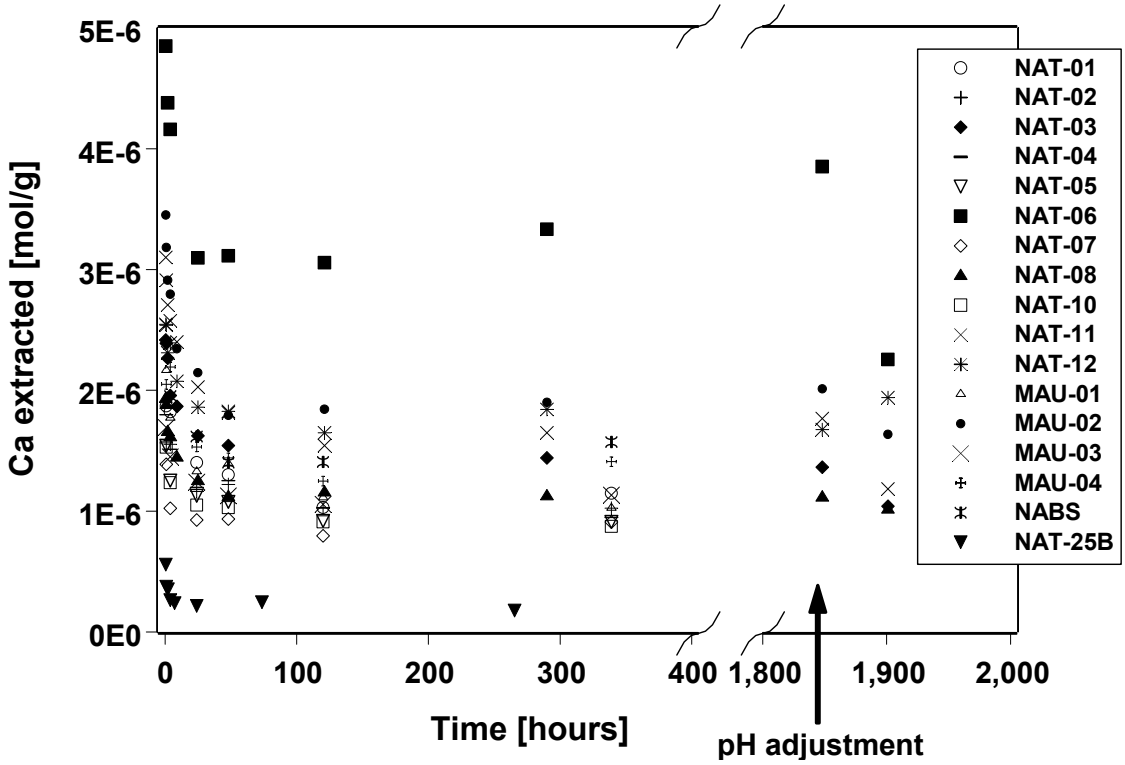

Figure C.3. Ca dissolved during the CARB extraction.

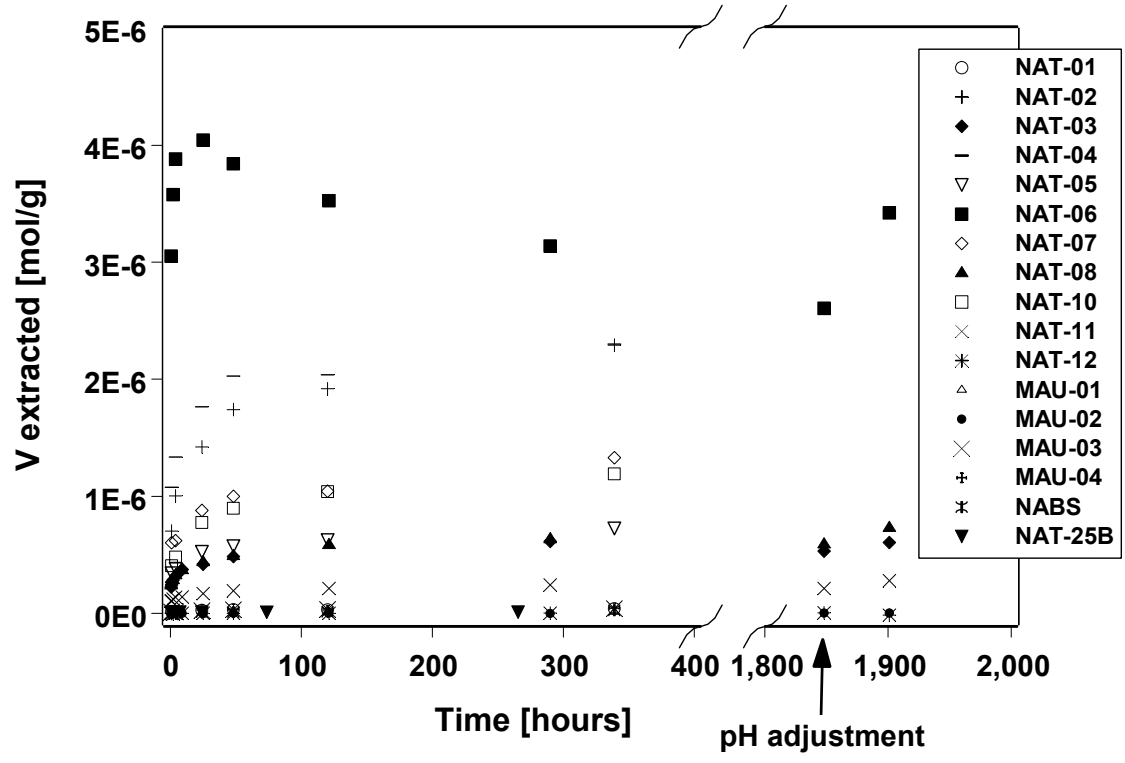

Figure C.4. Vanadium dissolved during the CARB extraction.

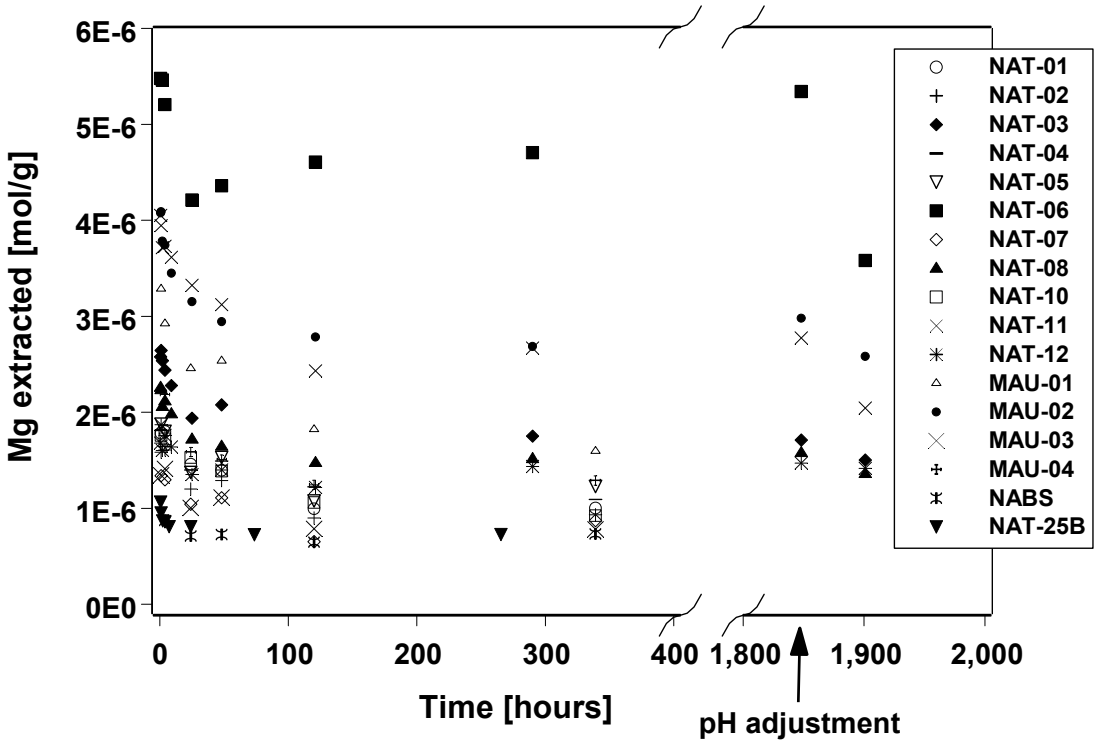

Figure C.5. Magnesium dissolved during the CARB extraction.

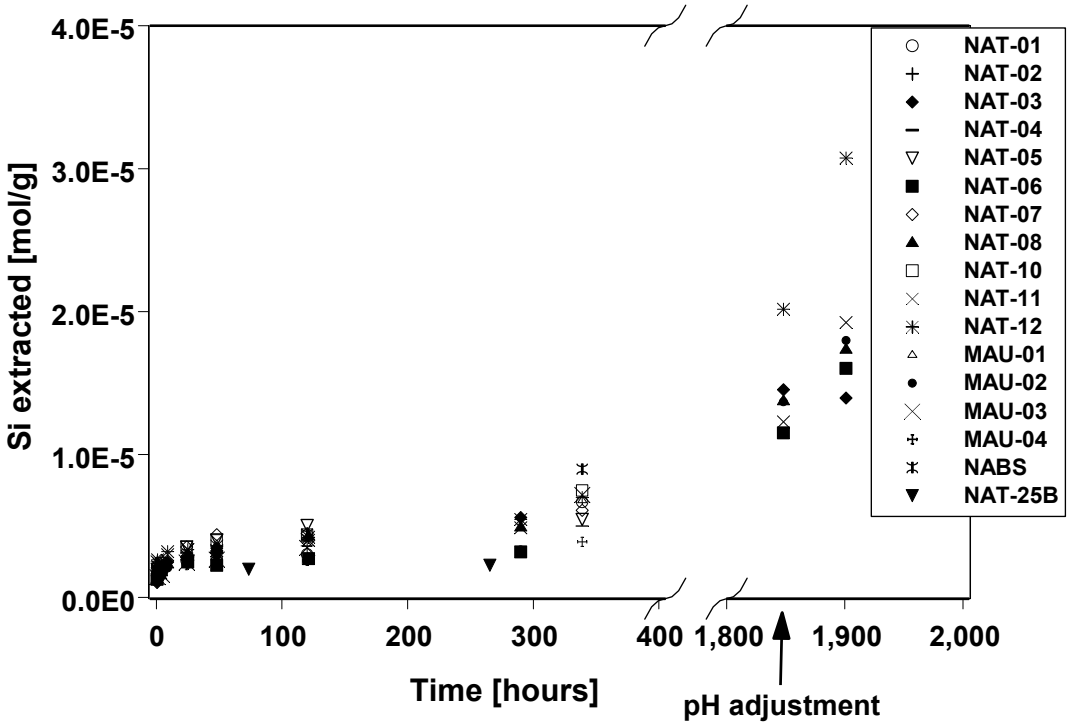

Figure C.6. Silicon dissolved during the CARB extraction.

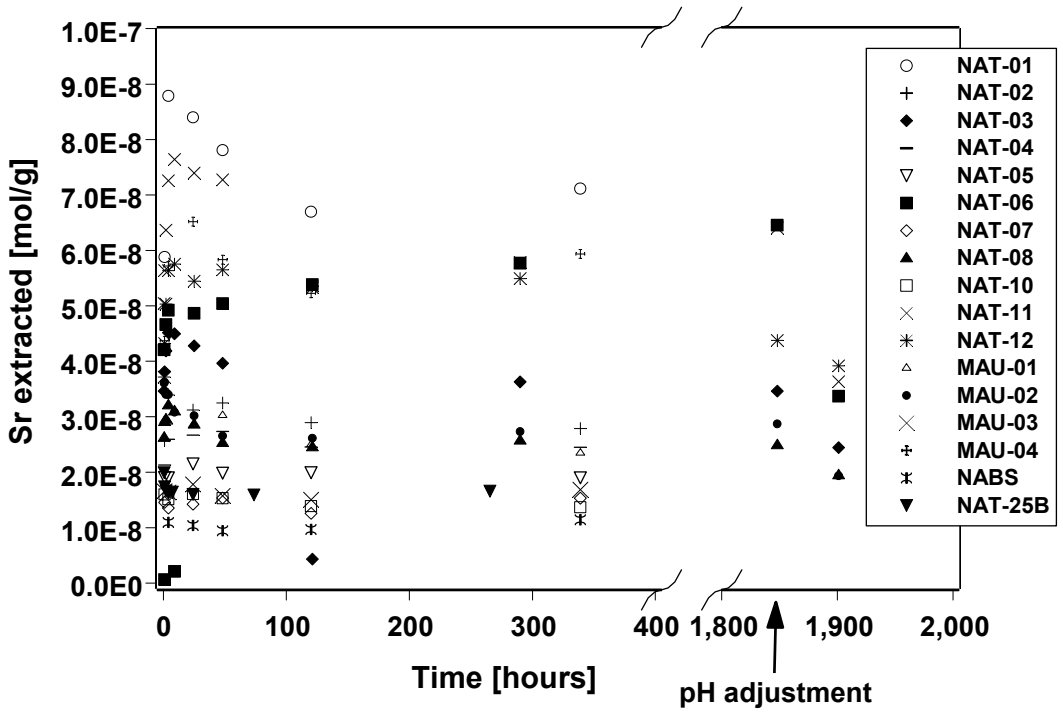

Figure C.7. Strontium extracted during the CARB extraction.

C.3.2 Extraction of the NABS Sample with Hydroxylamine Hydrochloride (HH)

The experiment was comprised of two parts: (i) a time series extraction of the <3 mm NABS sample, and (ii) 0.5 and 72 hr extractions of the <3 mm NABS sample and its grain size fractions. The available data for the time series extraction are shown below in Figures C.8a through C.8.i. The results of the 0.5 and 72 hr extractions of the grain size fractions of the NABS sample (Table C.3) show that the release of Ca, Mg and Mn was enhanced in the finer fractions, while the dissolution of Al, Si, and Fe was slower and more evenly distributed across the size spectrum. The latter curves show minima in the amount dissolved per unit mass in the 250-500 μm size fraction, as was seen in the surface area distribution (Section 4; Table 4.1).

When normalized to surface area, most of these trends disappear (Table C.4), and the relative importance of the coarser fractions as a source of Al and Fe becomes more pronounced.

C.3.3 Extraction of the U-Contaminated Samples with Hydroxylamine Hydrochloride (HH)

The method and results for extracted U are reported in Section 4. Here we report the concentrations of other elements in the extractions.

Figures C.8 a) through i) show the dissolution of several elements from the U-contaminated sediment samples during HH extractions. The data in these figures are also compiled in Table C.5.

Elements associated with carbonate minerals were rapidly dissolved and reached a steady-state concentration during the extractions (e.g., Ca, V, Sr and Mn in Figs. C.8b, d, f, and h, respectively). For other elements there was a continuous dissolution taking place (Al, Fe, K and Si in Figs. C.8a, c, e, and i, respectively). Mg dissolution appeared to have contributions from both types of mineral groups.

Table C.3. Metals dissolved (moles/g) from different grain size fractions of the NABS sample by HH extractions. Two values for each size fraction represent duplicate samples.

	Al		Ca		Fe		Mg		Mn		Si	
	0.5hrs	72hrs	0.5hrs	72hrs	0.5hrs	72hrs	0.5hrs	72hrs	0.5hrs	72hrs	0.5hrs	72hrs
1-3mm	1.43E-05	2.12E-04	1.41E-04	2.22E-04	7.18E-06	1.20E-04	5.78E-06	8.17E-05	1.00E-06	2.28E-06	1.55E-05	1.23E-04
	1.11E-05	1.62E-04	1.57E-04	2.10E-04	4.93E-06	1.12E-04	6.56E-06	8.12E-05	8.73E-07	3.14E-06	1.16E-05	8.48E-05
0.5-1mm	1.60E-05	1.61E-04	2.17E-04	2.95E-04	9.39E-06	1.26E-04	2.28E-05	1.13E-04	1.49E-06	4.00E-06	1.86E-05	9.52E-05
	1.62E-05	1.45E-04	1.61E-04	2.27E-04	7.70E-06	1.18E-04	1.65E-05	1.05E-04	1.19E-06	3.77E-06	1.79E-05	9.11E-05
0.25-0.5mm	1.64E-05	8.99E-05	1.38E-04	1.58E-04	7.26E-06	6.97E-05	2.02E-05	6.65E-05	1.95E-06	2.34E-06	2.40E-05	7.95E-05
	1.54E-05	8.83E-05	1.47E-04	1.51E-04	7.42E-06	7.02E-05	2.38E-05	6.70E-05	1.50E-06	2.23E-06	2.22E-05	7.78E-05
0.125-0.25mm	2.04E-05	8.33E-05	2.18E-04	2.25E-04	9.29E-06	6.47E-05	3.52E-05	7.74E-05	2.28E-06	3.22E-06	3.20E-05	8.63E-05
	2.02E-05	8.38E-05	2.13E-04	2.28E-04	9.29E-06	6.46E-05	3.54E-05	7.87E-05	2.27E-06	3.30E-06	3.12E-05	8.94E-05
0.063-0.125mm	2.06E-05	9.89E-05	3.64E-04	3.89E-04	1.18E-05	8.30E-05	6.58E-05	1.20E-04	3.56E-06	4.55E-06	2.93E-05	9.81E-05
	1.93E-05	9.72E-05	3.57E-04	3.80E-04	1.11E-05	8.17E-05	6.48E-05	1.19E-04	3.29E-06	4.63E-06	2.69E-05	9.99E-05
<0.063mm	2.56E-05	1.48E-04	6.54E-04	6.93E-04	1.82E-05	1.30E-04	1.26E-04	2.14E-04	5.62E-06	7.19E-06	2.88E-05	1.18E-04
	2.62E-05	1.48E-04	6.69E-04	6.87E-04	1.88E-05	1.29E-04	1.29E-04	2.13E-04	5.78E-06	7.14E-06	2.97E-05	1.17E-04
NABS	1.52E-05	1.09E-04	1.90E-04	2.02E-04	8.28E-06	1.02E-04	2.95E-05	9.23E-05	1.87E-06	2.88E-06	2.01E-05	9.03E-05
	1.75E-05	1.42E-04	1.96E-04	2.06E-04	9.14E-06	8.88E-05	3.30E-05	8.19E-05	1.90E-06	2.75E-06	2.33E-05	9.54E-05

Table C.4. Metals dissolved (moles/m^2) from different grain size fractions of the NABS sample by HH extractions. Two values for each size fraction represent duplicate samples.

mol/m2	Al		Ca		Fe		Mg		Mn		Si	
	0.5hrs	72hrs	0.5hrs	72hrs	0.5hrs	72hrs	0.5hrs	72hrs	0.5hrs	72hrs	0.5hrs	72hrs
1-3mm	3.20E-06	4.75E-05	3.15E-05	4.96E-05	1.61E-06	2.68E-05	1.29E-06	1.83E-05	2.24E-07	5.09E-07	3.47E-06	2.76E-05
	2.48E-06	3.63E-05	3.51E-05	4.70E-05	1.10E-06	2.50E-05	1.47E-06	1.82E-05	1.95E-07	7.02E-07	2.59E-06	1.90E-05
0.5-1mm	3.64E-06	3.67E-05	4.94E-05	6.71E-05	2.13E-06	2.86E-05	5.19E-06	2.57E-05	3.38E-07	9.09E-07	4.23E-06	2.16E-05
	3.69E-06	3.30E-05	3.66E-05	5.15E-05	1.75E-06	2.68E-05	3.75E-06	2.39E-05	2.70E-07	8.57E-07	4.06E-06	2.07E-05
0.25-0.5mm	5.31E-06	2.91E-05	4.48E-05	5.12E-05	2.35E-06	2.26E-05	6.53E-06	2.15E-05	6.31E-07	7.58E-07	7.75E-06	2.57E-05
	4.99E-06	2.86E-05	4.76E-05	4.88E-05	2.40E-06	2.27E-05	7.71E-06	2.17E-05	4.86E-07	7.21E-07	7.20E-06	2.52E-05
0.125-0.25mm	5.18E-06	2.11E-05	5.54E-05	5.72E-05	2.36E-06	1.64E-05	8.95E-06	1.97E-05	5.77E-07	8.18E-07	8.12E-06	2.19E-05
	5.14E-06	2.13E-05	5.39E-05	5.79E-05	2.36E-06	1.64E-05	9.00E-06	2.00E-05	5.75E-07	8.36E-07	7.92E-06	2.27E-05
0.063-0.125mm	3.87E-06	1.86E-05	6.83E-05	7.30E-05	2.21E-06	1.56E-05	1.23E-05	2.25E-05	6.68E-07	8.54E-07	5.49E-06	1.84E-05
	3.63E-06	1.82E-05	6.71E-05	7.14E-05	2.09E-06	1.53E-05	1.22E-05	2.24E-05	6.18E-07	8.69E-07	5.05E-06	1.87E-05
<0.063mm	1.95E-06	1.13E-05	4.99E-05	5.29E-05	1.39E-06	9.90E-06	9.62E-06	1.63E-05	4.28E-07	5.48E-07	2.20E-06	8.97E-06
	2.00E-06	1.13E-05	5.10E-05	5.24E-05	1.43E-06	9.86E-06	9.84E-06	1.62E-05	4.41E-07	5.45E-07	2.27E-06	8.91E-06
NABS	2.94E-06	2.12E-05	3.68E-05	3.92E-05	1.61E-06	1.98E-05	5.73E-06	1.79E-05	3.64E-07	5.60E-07	3.90E-06	1.75E-05
	3.39E-06	2.76E-05	3.80E-05	4.00E-05	1.78E-06	1.72E-05	6.42E-06	1.59E-05	3.69E-07	5.34E-07	4.52E-06	1.85E-05

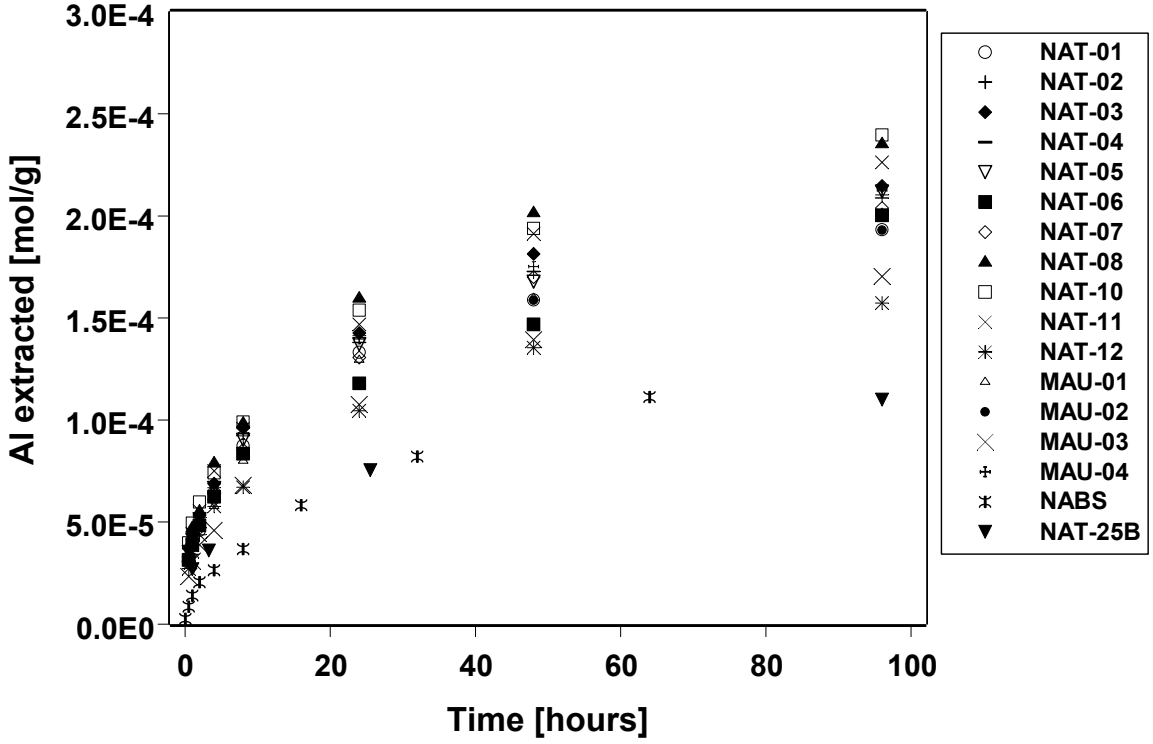

Figure C.8 a) Aluminum dissolved during HH extractions.

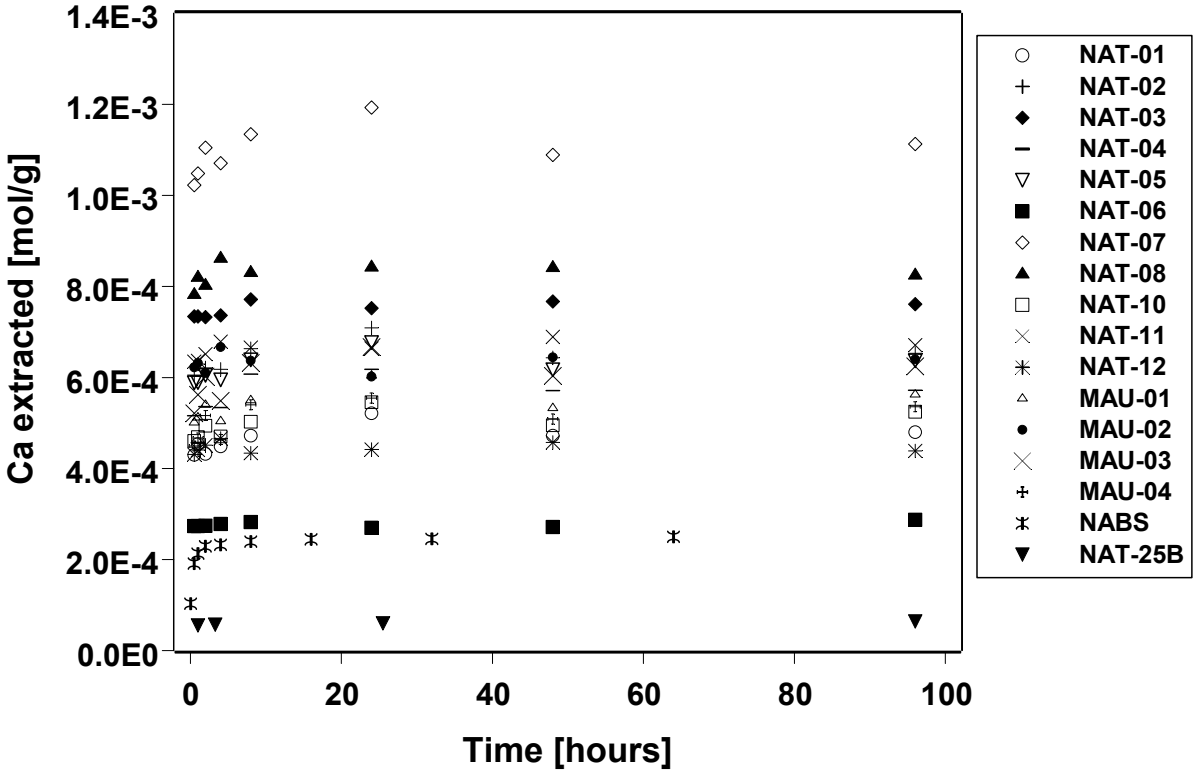

Figure C.8 b) Calcium dissolved during HH extractions.

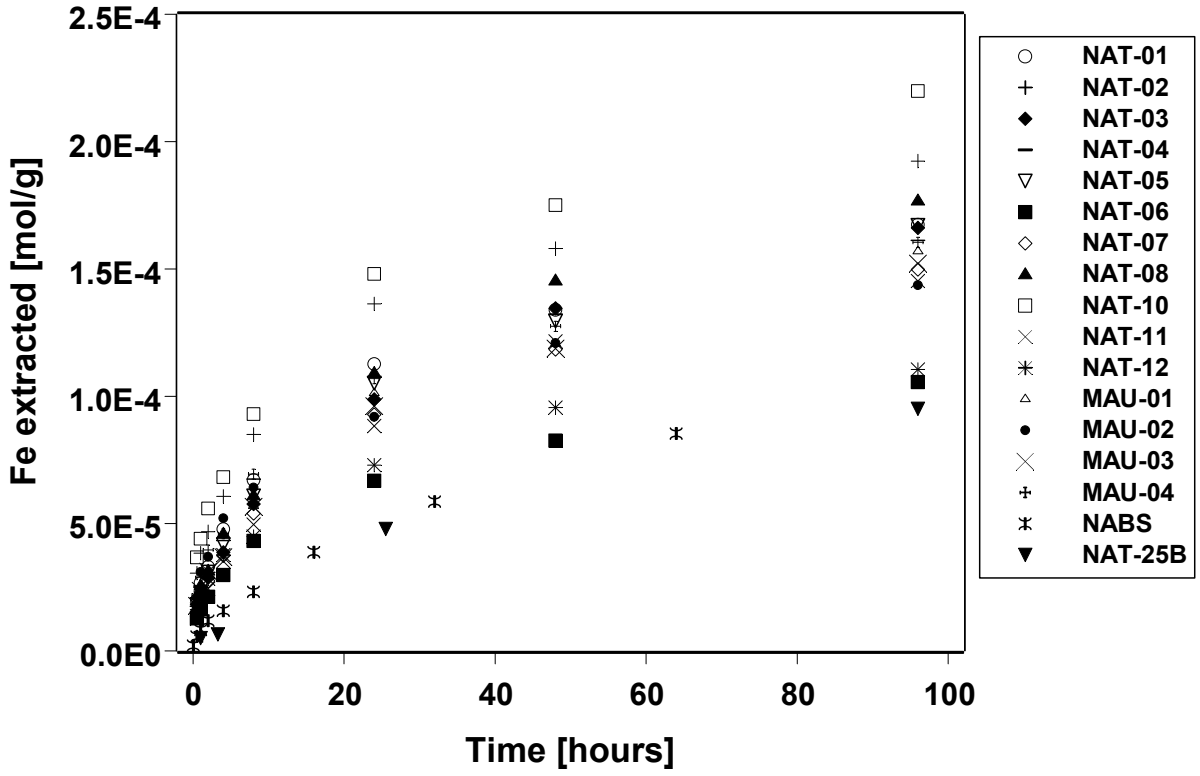

Figure C.8 c) Iron dissolved during HH extractions.

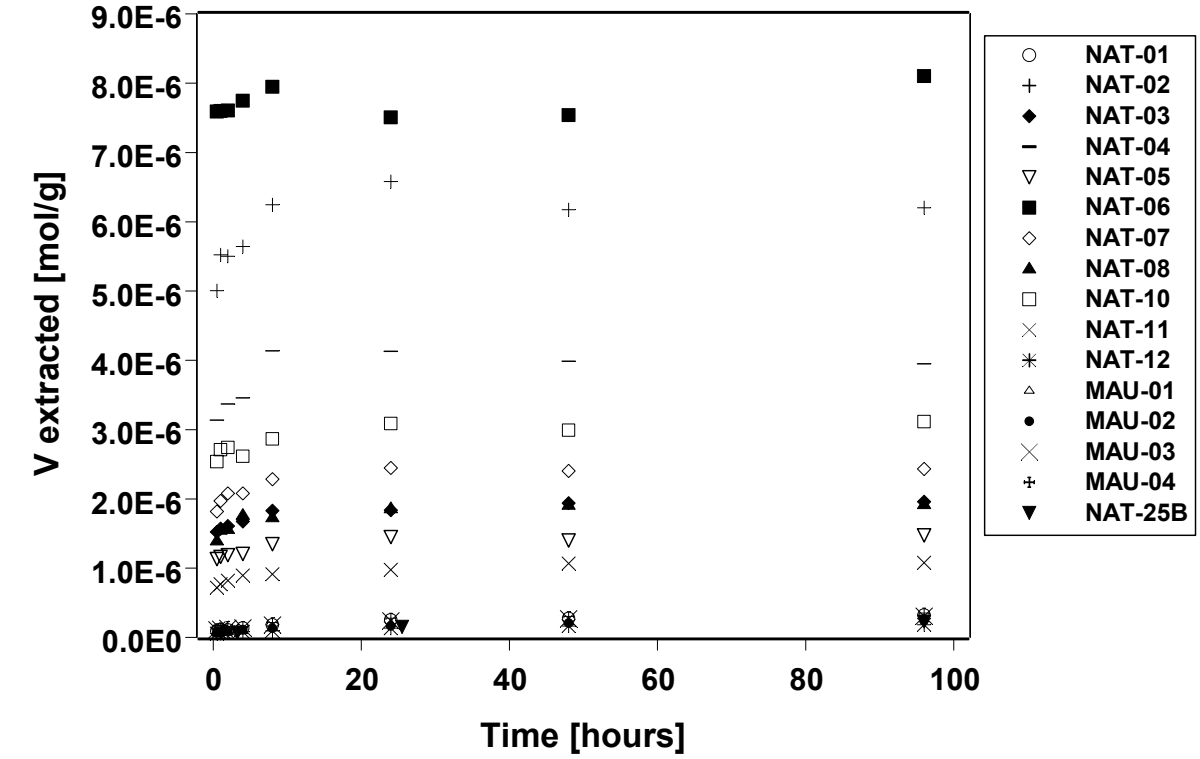

Figure C.8 d) Vanadium dissolved during HH extractions.

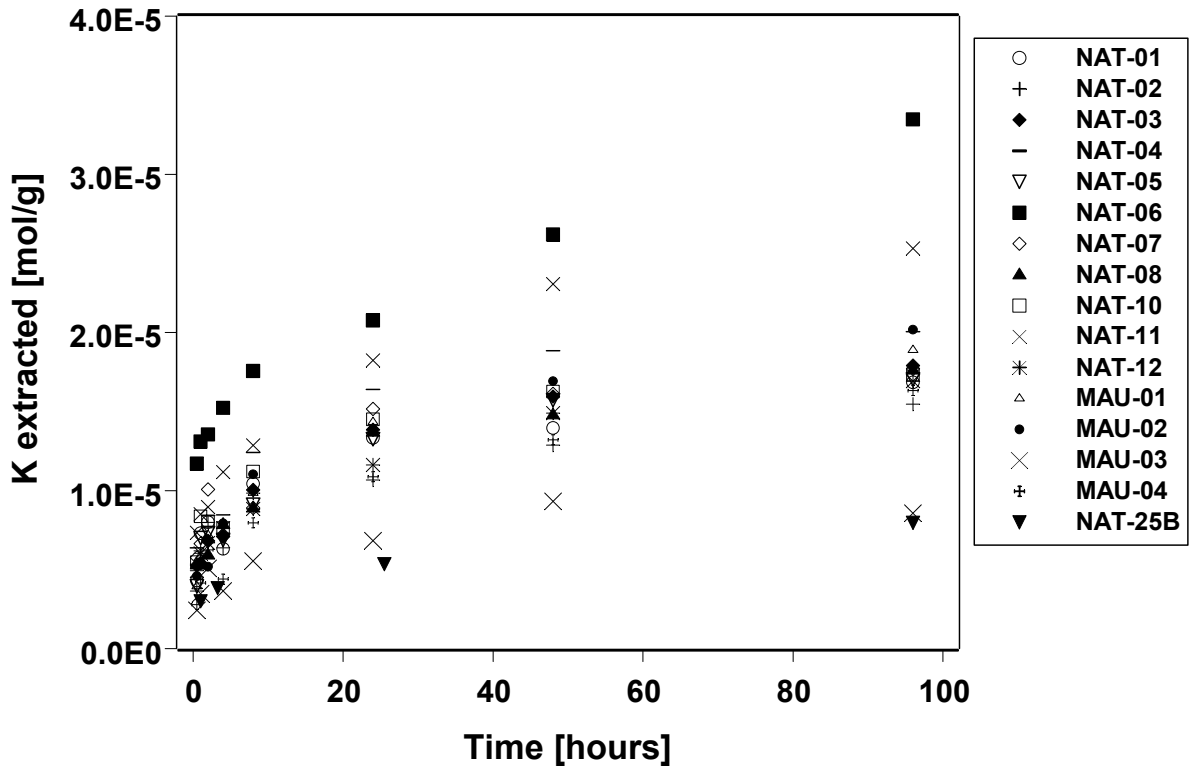

Figure C.8 e) Potassium dissolved during HH extractions.

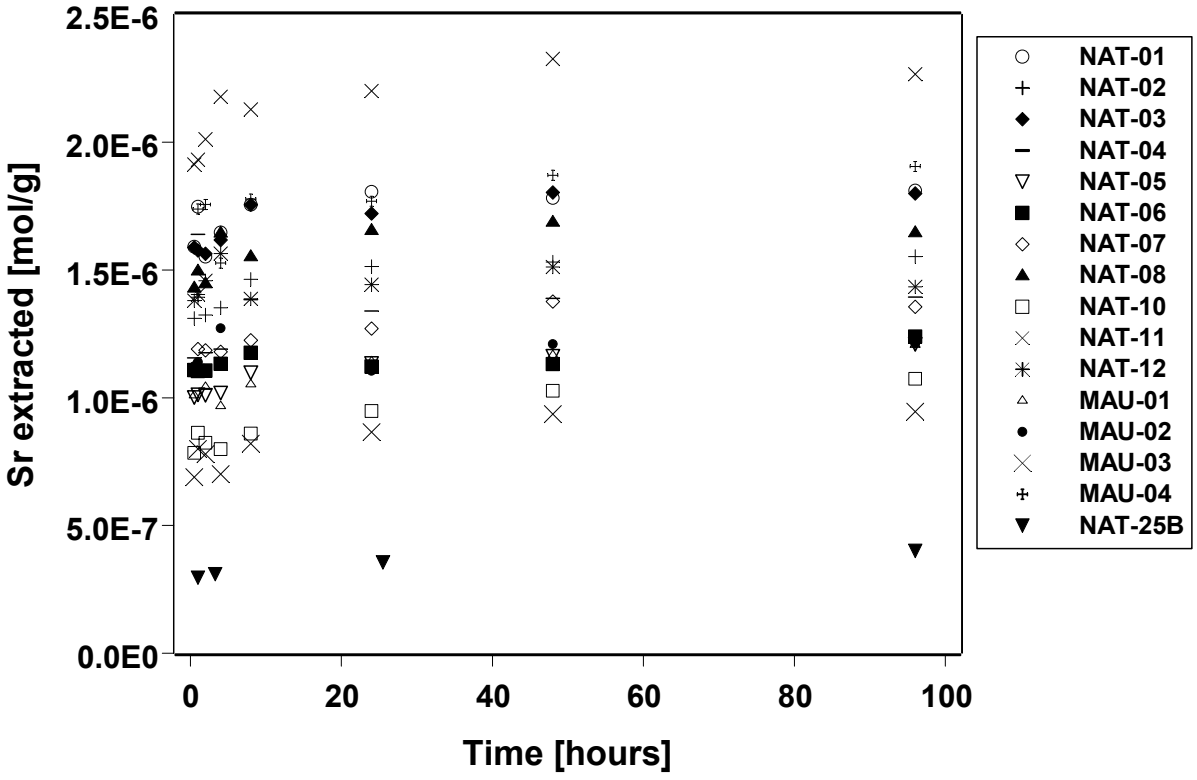

Figure C.8 f) Strontium dissolved during HH extractions.

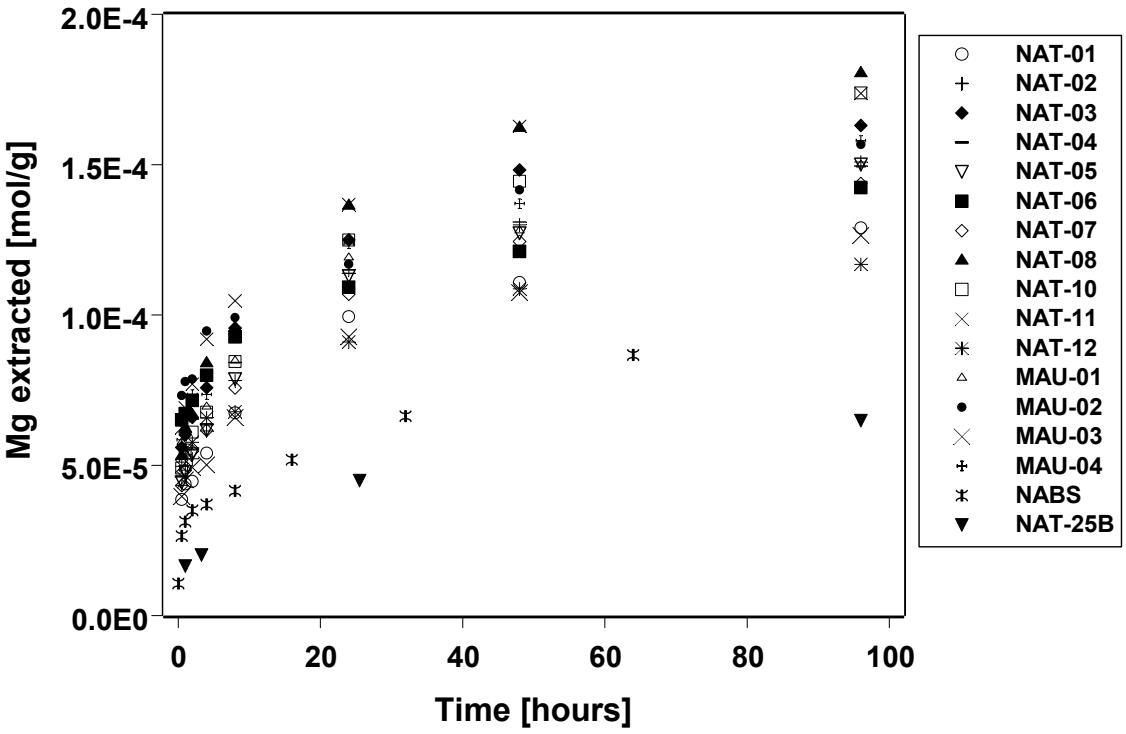

Figure C.8 g) Magnesium dissolved during HH extractions.

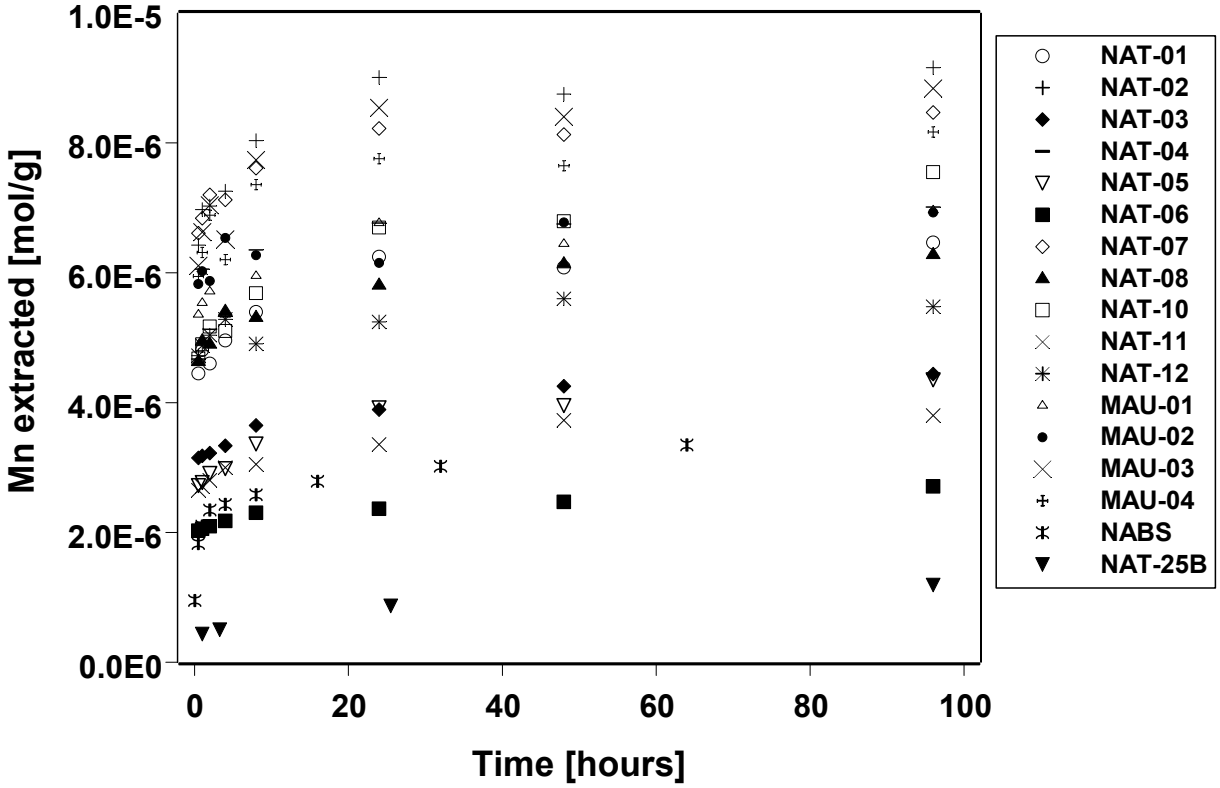

Figure C.8 h) Manganese dissolved during HH extractions.

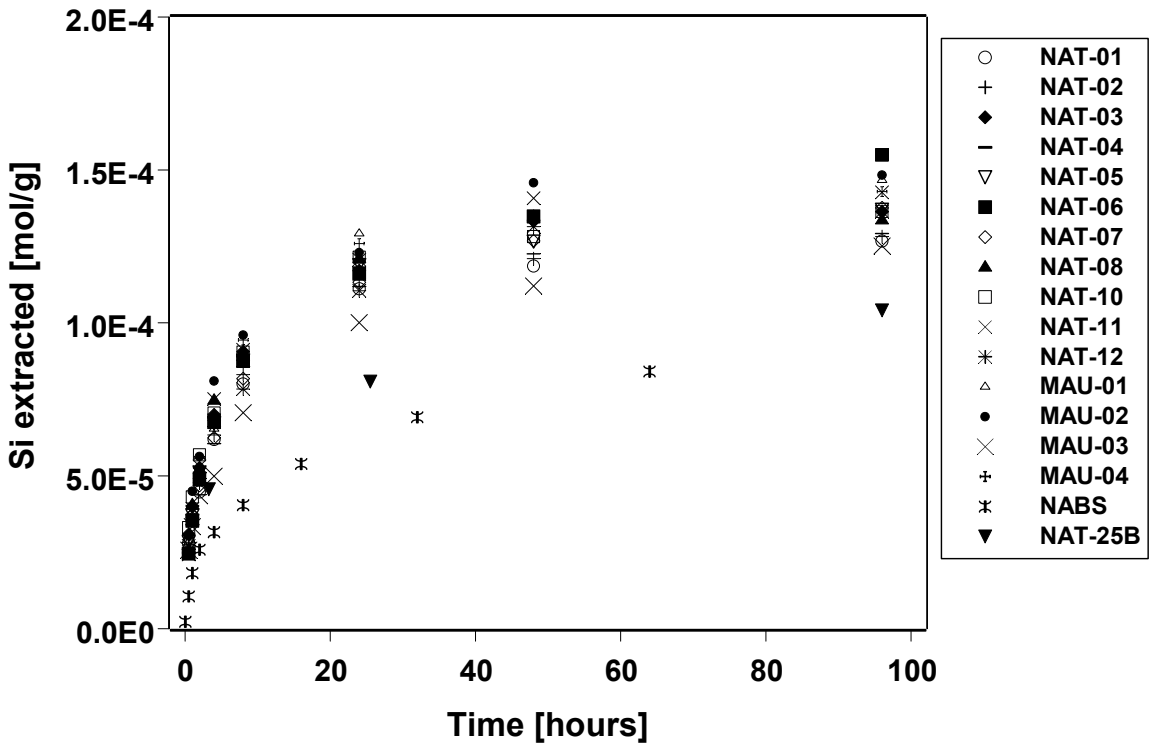

Figure C.8 i) Silicon dissolved during HH extractions.

Table C.5. CARB Extractions of U-Contaminated Sediment Samples, Ca Extracted (moles/g)

Ca	Sample	#1	#2	#3	#4	#5	#6	#7	#8	#9	#10	#11
	Time [hr]	0.5	1	2	4	9	25	48	121	290	1848	1901
NAT-03		2.42E-06	2.39E-06	2.27E-06	1.96E-06	1.87E-06	1.62E-06	1.54E-06		1.44E-06	1.36E-06	1.04E-06
NAT-06		4.85E-06		4.38E-06	4.16E-06		3.1E-06	3.11E-06	3.06E-06	3.33E-06	3.85E-06	2.26E-06
NAT-08		1.93E-06	1.88E-06	1.66E-06	1.62E-06	1.45E-06	1.25E-06	1.12E-06	1.16E-06	1.13E-06	1.12E-06	1.02E-06
NAT-11		3.1E-06	2.91E-06	2.71E-06	2.58E-06	2.4E-06	2.03E-06	1.82E-06	1.54E-06	1.65E-06	1.77E-06	1.18E-06
NAT-12		2.55E-06	2.54E-06	2.31E-06	2.39E-06	2.08E-06	1.86E-06	1.83E-06	1.65E-06	1.84E-06	1.67E-06	1.94E-06
MAU-02		3.45E-06	3.18E-06	2.91E-06	2.8E-06	2.34E-06	2.15E-06	1.79E-06	1.84E-06	1.9E-06	2.01E-06	1.64E-06

	Sample	#1	#2	#3	#4	#5	#6
	Time [hr]	1	4	24	48	120	339
NAT-01		1.87E-06	1.82E-06	1.40E-06	1.30E-06	1.03E-06	1.15E-06
NAT-02		1.56E-06	1.55E-06	1.16E-06	1.22E-06	1.03E-06	1.03E-06
NAT-04		1.80E-06	1.51E-06	1.20E-06	1.25E-06	1.03E-06	9.49E-07
NAT-05		1.54E-06	1.25E-06	1.13E-06	1.08E-06	9.19E-07	9.10E-07
NAT-07		1.39E-06	1.02E-06	9.27E-07	9.36E-07	7.96E-07	9.10E-07
NAT-10		1.53E-06	1.23E-06	1.05E-06	1.03E-06	9.12E-07	8.74E-07
MAU-01		2.17E-06	1.77E-06	1.33E-06	1.39E-06	1.11E-06	1.03E-06
MAU-03		1.69E-06	1.45E-06	1.24E-06	1.13E-06	1.06E-06	1.13E-06
MAU-04		2.05E-06	2.19E-06	1.53E-06	1.44E-06	1.25E-06	1.41E-06
NABS			1.95E-06	1.62E-06	1.40E-06	1.41E-06	1.57E-06

	Sample	#1	#2	#3	#4	#5	#6	#7	#8
	Time [hr]	0.5	1	2.167	4	7.25	24	73.5	265.5
NAT-25B		5.58E-07	3.74E-07	3.53E-07	2.64E-07	2.37E-07	2.16E-07	2.45E-07	1.77E-07

Table C.6. CARB Extractions of U-Contaminated Sediment Samples, V Extracted (moles/g)

V	Sample	#1	#2	#3	#4	#5	#6	#7	#8	#9	#10	#11
	Time [hr]	0.5	1	2	4	9	25	48	121	290	1848	1901
NAT-03		2.25E-07	2.66E-07	2.84E-07	3.18E-07	3.75E-07	4.18E-07	4.85E-07		6.14E-07	5.31E-07	6.05E-07
NAT-06		3.05E-06		3.58E-06	3.88E-06		4.04E-06	3.84E-06	3.52E-06	3.14E-06	2.61E-06	3.42E-06
NAT-08		2.42E-07	2.74E-07	2.88E-07	3.29E-07	3.72E-07	4.41E-07	4.92E-07	5.86E-07	6.38E-07	5.93E-07	7.34E-07
NAT-11		1.05E-07	1.07E-07	1.22E-07	1.36E-07	1.41E-07	1.69E-07	1.93E-07	2.12E-07	2.43E-07	2.13E-07	2.79E-07
NAT-12		1.86E-09	-2.42E-09	-3.65E-09	1.71E-09	-3.76E-11	-3.76E-11	-3.76E-11	-3.76E-11	2.15E-09	5E-09	-1.68E-08
MAU-02		-3.75E-09	-7.45E-09	-3.81E-09	-3.81E-09	-2.81E-10	-3.75E-09	-3.38E-10	1.33E-09	-1.95E-09	2.69E-09	3.09E-09

	Sample	#1	#2	#3	#4	#5	#6
	Time [hr]	1	4	24	48	120	339
NAT-01		1.6E-08	1.44E-08	2.68E-08	3.14E-08	2.99E-08	4.02E-08
NAT-02		7.03E-07	1E-06	1.42E-06	1.74E-06	1.92E-06	2.29E-06
NAT-04		1.08E-06	1.34E-06	1.76E-06	2.03E-06	2.04E-06	2.3E-06
NAT-05		3.42E-07	3.81E-07	5.26E-07	5.73E-07	6.26E-07	7.25E-07
NAT-07		6.03E-07	6.22E-07	8.8E-07	9.99E-07	1.04E-06	1.33E-06
NAT-10		4.06E-07	4.81E-07	7.76E-07	8.98E-07	1.04E-06	1.19E-06
MAU-01		1.58E-09	4.74E-09	9.39E-09	1.85E-08	1.4E-08	1.26E-08
MAU-03		9.59E-09	1.27E-08	2.2E-08	2.96E-08	3.27E-08	4E-08
MAU-04		2.24E-08	2.39E-08	3.32E-08	3.47E-08	2.72E-08	4.15E-08
NABS			9.28E-09	1.08E-08	1.08E-08	1.36E-08	2.71E-08

	Sample	#1	#2	#3	#4	#5	#6	#7	#8
	Time [hr]	0.5	1	2.167	4	7.25	24	73.5	265.5
NAT-25B		6.33E-09	7.23E-09	5.43E-09	6.72E-09	9.68E-09	9.31E-09	8.61E-09	1.07E-08

Table C.7. CARB Extractions of U-Contaminated Sediment Samples, Mg Extracted (moles/g)

Mg	Sample	#1	#2	#3	#4	#5	#6	#7	#8	#9	#10	#11
	Time [hr]	0.5	1	2	4	9	25	48	121	290	1848	1901
NAT-03		2.58E-06	2.65E-06	2.54E-06	2.44E-06	2.28E-06	1.94E-06	2.08E-06		1.75E-06	1.71E-06	1.5E-06
NAT-06		5.48E-06		5.46E-06	5.2E-06		4.21E-06	4.36E-06	4.61E-06	4.7E-06	5.34E-06	3.58E-06
NAT-08		2.26E-06	2.23E-06	2.06E-06	2.12E-06	1.98E-06	1.72E-06	1.65E-06	1.48E-06	1.52E-06	1.58E-06	1.36E-06
NAT-11		4.05E-06	3.95E-06	3.72E-06	3.73E-06	3.62E-06	3.32E-06	3.12E-06	2.43E-06	2.67E-06	2.78E-06	2.04E-06
NAT-12		1.68E-06	1.87E-06	1.6E-06	1.76E-06	1.64E-06	1.35E-06	1.4E-06	1.22E-06	1.44E-06	1.47E-06	1.42E-06
MAU-02		4.08E-06	4.09E-06	3.78E-06	3.74E-06	3.45E-06	3.15E-06	2.94E-06	2.78E-06	2.69E-06	2.98E-06	2.58E-06

	Sample	#1	#2	#3	#4	#5	#6
	Time [hr]	1	4	24	48	120	339
NAT-01		1.78E-06	1.8E-06	1.46E-06	1.39E-06	9.95E-07	1E-06
NAT-02		1.58E-06	1.61E-06	1.2E-06	1.29E-06	8.99E-07	9.33E-07
NAT-04		1.81E-06	1.64E-06	1.4E-06	1.49E-06	1.23E-06	1.09E-06
NAT-05		1.88E-06	1.8E-06	1.37E-06	1.53E-06	1.08E-06	1.23E-06
NAT-07		1.34E-06	1.3E-06	1.04E-06	1.11E-06	6.53E-07	8.74E-07
NAT-10		1.76E-06	1.72E-06	1.53E-06	1.39E-06	1.06E-06	9.23E-07
MAU-01		3.29E-06	2.93E-06	2.46E-06	2.54E-06	1.82E-06	1.6E-06
MAU-03		1.34E-06	1.41E-06	1E-06	1.11E-06	7.86E-07	7.82E-07
MAU-04		2.58E-06	2.19E-06	1.59E-06	1.51E-06	1.24E-06	1.29E-06
NABS			8.73E-07	7.11E-07	7.26E-07	6.46E-07	7.34E-07

	Sample	#1	#2	#3	#4	#5	#6	#7	#8
	Time [hr]	0.5	1	2.167	4	7.25	24	73.5	265.5
NAT-25B		1.06E-06	9.5E-07	8.67E-07	8.57E-07	8.08E-07	8.08E-07	7.25E-07	7.26E-07

Table C.8. CARB Extractions of U-Contaminated Sediment Samples, Si Extracted (moles/g)

Si	Sample	#1	#2	#3	#4	#5	#6	#7	#8	#9	#10	#11
	Time [hr]	0.5	1	2	4	9	25	48	121	290	1848	1901
NAT-03		1.04E-06	1.38E-06	1.47E-06	1.89E-06	2.47E-06	2.83E-06	3.44E-06		5.58E-06	1.45E-05	1.4E-05
NAT-06		1.25E-06		1.68E-06	1.93E-06		2.46E-06	2.23E-06	2.7E-06	3.17E-06	1.15E-05	1.6E-05
NAT-08		1.15E-06	1.47E-06	1.59E-06	1.78E-06	2.33E-06	2.86E-06	3.33E-06	4.29E-06	4.91E-06	1.37E-05	1.73E-05
NAT-11		1.93E-06	2.16E-06	2.07E-06	2.27E-06	2.99E-06	3.35E-06	3.58E-06	3.99E-06	4.86E-06	1.23E-05	1.92E-05
NAT-12		2.48E-06	2.63E-06	2.35E-06	2.37E-06	3.19E-06	3.34E-06	3.27E-06	4.19E-06	5.44E-06	2.02E-05	3.08E-05
MAU-02		1.42E-06	1.63E-06	1.9E-06	1.83E-06	2.05E-06	2.29E-06	2.88E-06	2.81E-06	3.32E-06	1.37E-05	1.8E-05

	Sample	#1	#2	#3	#4	#5	#6
	Time [hr]	1	4	24	48	120	339
NAT-01		1.64E-06	1.78E-06	2.54E-06	2.71E-06	3E-06	6.67E-06
NAT-02		1.62E-06	1.98E-06	2.65E-06	3.18E-06	3.61E-06	6.98E-06
NAT-04		2.21E-06	2.26E-06	3.1E-06	3.58E-06	3.93E-06	4.99E-06
NAT-05		1.95E-06	2.34E-06	3.52E-06	4.01E-06	5.02E-06	5.44E-06
NAT-07		2.33E-06	2.59E-06	3.52E-06	4.39E-06	4.47E-06	6.08E-06
NAT-10		1.81E-06	2.15E-06	3.51E-06	3.98E-06	4.39E-06	7.47E-06
MAU-01		1.87E-06	2.23E-06	2.82E-06	3.69E-06	3.73E-06	6.78E-06
MAU-03		1.41E-06	1.6E-06	2.43E-06	2.64E-06	3.46E-06	7.16E-06
MAU-04		1.61E-06	1.92E-06	2.24E-06	2.36E-06	2.55E-06	3.89E-06
NABS			1.61E-06	2.95E-06	3.03E-06	4.43E-06	8.97E-06

	Sample	#1	#2	#3	#4	#5	#6	#7	#8
	Time [hr]	0.5	1	2.167	4	7.25	24	73.5	265.5
NAT-25B		1.4E-06	1.78E-06	1.49E-06	2.06E-06	1.88E-06	2.38E-06	1.96E-06	2.25E-06

Table C.9. Carbonate Extraction of Contaminated Naturita Sediment, Extracted Strontium in moles/g

Sr	Sample	#1	#2	#3	#4	#5	#6	#7	#8	#9	#10	#11
	Time [hr]	0.5	1	2	4	9	25	48	121	290	1848	1901
NAT-03		3.46E-08	3.81E-08	4.19E-08	4.52E-08	4.5E-08	4.28E-08	3.97E-08	4.32E-09	3.63E-08	3.46E-08	2.44E-08
NAT-06		4.21E-08	6.31E-10	4.66E-08	4.92E-08	2.09E-09	4.87E-08	5.04E-08	5.39E-08	5.77E-08	6.46E-08	3.37E-08
NAT-08		2.62E-08	2.91E-08	2.95E-08	3.21E-08	3.1E-08	2.86E-08	2.53E-08	2.46E-08	2.57E-08	2.49E-08	1.95E-08
NAT-11		5.04E-08	5.64E-08	6.37E-08	7.26E-08	7.64E-08	7.4E-08	7.28E-08	5.32E-08	5.79E-08	6.41E-08	3.63E-08
NAT-12		3.72E-08	4.32E-08	5.03E-08	5.63E-08	5.75E-08	5.44E-08	5.65E-08	5.36E-08	5.49E-08	4.38E-08	3.92E-08
MAU-02		3.61E-08	3.62E-08	3.4E-08	3.4E-08	3.08E-08	3.02E-08	2.65E-08	2.61E-08	2.73E-08	2.87E-08	1.93E-08

	Sample	#1	#2	#3	#4	#5	#6
	Time [hr]	1	4	24	48	120	339
NAT-01		5.88E-08	8.79E-08	8.4E-08	7.81E-08	6.7E-08	7.11E-08
NAT-02		2.57E-08	3.39E-08	3.12E-08	3.25E-08	2.89E-08	2.79E-08
NAT-04		2.13E-08	2.59E-08	2.67E-08	2.74E-08	2.45E-08	2.45E-08
NAT-05		1.9E-08	1.9E-08	2.15E-08	1.98E-08	1.99E-08	1.9E-08
NAT-07		1.46E-08	1.35E-08	1.42E-08	1.53E-08	1.26E-08	1.53E-08
NAT-10		1.6E-08	1.51E-08	1.6E-08	1.53E-08	1.39E-08	1.37E-08
MAU-01		2.91E-08	2.91E-08	2.85E-08	3.02E-08	2.5E-08	2.35E-08
MAU-03		1.66E-08	1.63E-08	1.78E-08	1.57E-08	1.5E-08	1.69E-08
MAU-04		4.37E-08	5.72E-08	6.52E-08	5.83E-08	5.23E-08	5.94E-08
NABS			1.1E-08	1.04E-08	9.42E-09	9.68E-09	1.14E-08

	Sample	#1	#2	#3	#4	#5	#6	#7	#8
	Time [hr]	0.5	1	2.167	4	7.25	24	73.5	265.5
NAT-25B		1.99E-08	1.74E-08	1.66E-08	1.62E-08	1.64E-08	1.6E-08	1.59E-08	1.66E-08

Table C.10a. HH Extraction of U-Contaminated Sediment Samples, Extracted Aluminum in moles/g

Aluminum									
26.9815	Sample	#1	#2	#3	#4	#5	#6	#7	#8
Core	Time [hr]	0.5	1	2	4	8	24	48	96
NAT-01		3.02E-05	3.93E-05	4.59E-05	6.43E-05	8.75E-05	1.33E-04	1.59E-04	1.93E-04
NAT-02	mol/g	3.32E-05	4.16E-05	4.99E-05	6.68E-05	9.22E-05	1.41E-04	1.73E-04	2.10E-04
NAT-03		3.73E-05	4.41E-05	5.34E-05	6.89E-05	9.61E-05	1.43E-04	1.81E-04	2.15E-04
NAT-04		3.07E-05	3.42E-05	4.73E-05	6.42E-05	9.63E-05	1.38E-04	1.73E-04	2.09E-04
NAT-05		3.53E-05	4.15E-05	5.14E-05	6.68E-05	9.03E-05	1.37E-04	1.68E-04	2.12E-04
NAT-06		3.15E-05	3.92E-05	4.84E-05	6.24E-05	8.35E-05	1.18E-04	1.47E-04	2.00E-04
NAT-07		3.13E-05	3.92E-05	4.94E-05	6.44E-05	8.55E-05	1.31E-04	1.70E-04	2.04E-04
NAT-08		3.45E-05	4.74E-05	5.55E-05	7.91E-05	9.86E-05	1.60E-04	2.02E-04	2.35E-04
NAT-10		3.99E-05	4.95E-05	5.98E-05	7.42E-05	9.91E-05	1.54E-04	1.94E-04	2.40E-04
NAT-11		3.39E-05	4.43E-05	5.54E-05	7.51E-05	9.57E-05	1.47E-04	1.91E-04	2.26E-04
NAT-12		2.72E-05	3.56E-05	4.38E-05	5.77E-05	6.71E-05	1.05E-04	1.36E-04	1.57E-04
MAU-01		3.09E-05	3.90E-05	4.72E-05	5.78E-05	8.00E-05	1.29E-04	1.60E-04	2.01E-04
MAU-02		3.17E-05	4.17E-05	4.83E-05	6.87E-05	8.30E-05	1.18E-04	1.59E-04	1.93E-04
MAU-03		2.33E-05	3.09E-05	3.88E-05	4.60E-05	6.81E-05	1.08E-04	1.39E-04	1.70E-04
MAU-04		3.06E-05	3.97E-05	5.26E-05	6.22E-05	9.32E-05	1.40E-04	1.75E-04	2.13E-04

	Sample	#2	#4	#6	#8
	Time [hr]	1	3.3	25.5	96
NAT-25B		2.69E-05	3.61E-05	7.55E-05	1.10E-04

	#1	#2	#3	#4	#5	#6	#7	#8	#9	#10
	0.05	0.5	1	2	4	8	16	32	64	128
NABS	2.63E-06	8.60E-06	1.40E-05	2.06E-05	2.64E-05	3.67E-05	5.83E-05	8.21E-05	1.11E-04	1.42E-04

Table C.10b. HH Extraction of U-Contaminated Sediment Samples, Extracted Calcium in moles/g

Calcium									
40.078	Sample	#1	#2	#3	#4	#5	#6	#7	#8
Core	Time [hr]	0.5	1	2	4	8	24	48	96
NAT-01		4.30E-04	4.54E-04	4.32E-04	4.49E-04	4.72E-04	5.21E-04	4.72E-04	4.79E-04
NAT-02	mol/g	6.05E-04	6.29E-04	6.21E-04	6.18E-04	6.63E-04	7.09E-04	6.43E-04	6.53E-04
NAT-03		7.34E-04	7.34E-04	7.33E-04	7.36E-04	7.72E-04	7.52E-04	7.67E-04	7.61E-04
NAT-04		5.16E-04	4.57E-04	5.36E-04	5.34E-04	6.08E-04	6.18E-04	5.71E-04	5.72E-04
NAT-05		5.88E-04	5.89E-04	6.05E-04	5.95E-04	6.39E-04	6.77E-04	6.17E-04	6.36E-04
NAT-06		2.74E-04	2.73E-04	2.74E-04	2.78E-04	2.82E-04	2.70E-04	2.71E-04	2.87E-04
NAT-07		1.02E-03	1.05E-03	1.10E-03	1.07E-03	1.13E-03	1.19E-03	1.09E-03	1.11E-03
NAT-08		7.83E-04	8.21E-04	8.03E-04	8.63E-04	8.31E-04	8.43E-04	8.42E-04	8.26E-04
NAT-10		4.60E-04	4.69E-04	4.94E-04	4.71E-04	5.03E-04	5.45E-04	4.95E-04	5.25E-04
NAT-11		6.35E-04	6.37E-04	6.51E-04	6.79E-04	6.65E-04	6.64E-04	6.89E-04	6.71E-04
NAT-12		4.31E-04	4.41E-04	4.51E-04	4.66E-04	4.33E-04	4.42E-04	4.57E-04	4.39E-04
MAU-01		5.01E-04	5.12E-04	5.40E-04	5.04E-04	5.50E-04	6.04E-04	5.33E-04	5.63E-04
MAU-02		6.22E-04	6.32E-04	6.10E-04	6.67E-04	6.37E-04	6.02E-04	6.44E-04	6.40E-04
MAU-03		5.21E-04	5.62E-04	6.02E-04	5.49E-04	6.32E-04	6.67E-04	6.04E-04	6.24E-04
MAU-04		4.49E-04	4.67E-04	5.16E-04	4.64E-04	5.40E-04	5.55E-04	5.09E-04	5.36E-04

	Sample	#2	#4	#6	#8
	Time [hr]	1	3.3	25.5	96
NAT-25B		5.53E-05	5.70E-05	5.98E-05	6.42E-05

	#1	#2	#3	#4	#5	#6	#7	#8	#9	#10
	0.05	0.5	1	2	4	8	16	32	64	128
NABS	1.03E-04	1.92E-04	2.13E-04	2.29E-04	2.33E-04	2.40E-04	2.45E-04	2.45E-04	2.50E-04	2.52E-04

Table C.10c. HH Extraction of U-Contaminated Sediment Samples, Extracted Iron in moles/g

Iron									
55.847	Sample	#1	#2	#3	#4	#5	#6	#7	#8
Core	Time [hr]	0.5	1	2	4	8	24	48	96
NAT-01		1.99E-05	2.67E-05	3.30E-05	4.78E-05	6.71E-05	1.13E-04	1.34E-04	1.67E-04
NAT-02		3.05E-05	3.84E-05	4.68E-05	6.07E-05	8.50E-05	1.36E-04	1.58E-04	1.92E-04
NAT-03		1.82E-05	2.27E-05	2.88E-05	3.87E-05	5.77E-05	9.88E-05	1.35E-04	1.66E-04
NAT-04	mol/g	1.75E-05	2.49E-05	3.08E-05	4.34E-05	6.74E-05	1.08E-04	1.32E-04	1.61E-04
NAT-05		1.82E-05	2.29E-05	3.10E-05	4.17E-05	6.09E-05	1.05E-04	1.30E-04	1.67E-04
NAT-06		1.27E-05	1.63E-05	2.12E-05	2.98E-05	4.31E-05	6.67E-05	8.25E-05	1.06E-04
NAT-07		1.51E-05	1.98E-05	2.74E-05	3.74E-05	5.40E-05	9.28E-05	1.18E-04	1.50E-04
NAT-08		1.70E-05	2.56E-05	3.15E-05	4.59E-05	6.10E-05	1.09E-04	1.45E-04	1.77E-04
NAT-10		3.67E-05	4.41E-05	5.59E-05	6.82E-05	9.30E-05	1.48E-04	1.75E-04	2.20E-04
NAT-11		1.25E-05	2.08E-05	2.43E-05	3.51E-05	4.97E-05	8.83E-05	1.22E-04	1.45E-04
NAT-12		1.62E-05	2.25E-05	2.83E-05	3.76E-05	4.50E-05	7.29E-05	9.56E-05	1.11E-04
MAU-01		1.81E-05	2.35E-05	3.10E-05	3.86E-05	5.70E-05	1.01E-04	1.21E-04	1.57E-04
MAU-02		2.08E-05	3.09E-05	3.69E-05	5.21E-05	6.41E-05	9.19E-05	1.21E-04	1.44E-04
MAU-03		1.77E-05	2.36E-05	3.12E-05	3.68E-05	5.66E-05	9.61E-05	1.19E-04	1.52E-04
MAU-04		2.20E-05	2.88E-05	3.97E-05	4.60E-05	6.94E-05	1.07E-04	1.27E-04	1.60E-04

	Sample	#2	#4	#6	#8
	Time [hr]	1	3.3	25.5	96
NAT-25B		5.02E-06	6.47E-06	4.78E-05	9.50E-05

	#1	#2	#3	#4	#5	#6	#7	#8	#9	#10
	0.05	0.5	1	2	4	8	16	32	64	128
NABS	2.01E-06	5.69E-06	8.23E-06	1.19E-05	1.58E-05	2.32E-05	3.87E-05	5.87E-05	8.54E-05	1.16E-04

Table C.10d. HH Extraction of U-Contaminated Sediment Samples, Extracted Vanadium in moles/g

Vanadium									
50.9415	Sample	#1	#2	#3	#4	#5	#6	#7	#8
Core	Time [hr]	0.5	1	2	4	8	24	48	96
NAT-01		9.58E-08	1.13E-07	1.11E-07	1.39E-07	1.85E-07	2.53E-07	2.74E-07	3.24E-07
NAT-02		5.01E-06	5.52E-06	5.50E-06	5.64E-06	6.24E-06	6.58E-06	6.18E-06	6.20E-06
NAT-03		1.52E-06	1.57E-06	1.61E-06	1.67E-06	1.83E-06	1.83E-06	1.94E-06	1.96E-06
NAT-04	mol/g	3.14E-06	1.77E-07	3.37E-06	3.46E-06	4.14E-06	4.13E-06	3.98E-06	3.95E-06
NAT-05		1.13E-06	1.16E-06	1.19E-06	1.21E-06	1.35E-06	1.45E-06	1.40E-06	1.47E-06
NAT-06		7.59E-06	7.60E-06	7.61E-06	7.75E-06	7.95E-06	7.51E-06	7.54E-06	8.10E-06
NAT-07		1.82E-06	1.97E-06	2.08E-06	2.08E-06	2.28E-06	2.45E-06	2.41E-06	2.43E-06
NAT-08		1.40E-06	1.55E-06	1.56E-06	1.77E-06	1.73E-06	1.86E-06	1.91E-06	1.92E-06
NAT-10		2.54E-06	2.71E-06	2.74E-06	2.62E-06	2.87E-06	3.09E-06	2.99E-06	3.12E-06
NAT-11		7.18E-07	7.68E-07	8.21E-07	8.96E-07	9.11E-07	9.75E-07	1.07E-06	1.08E-06
NAT-12		5.46E-08	6.18E-08	7.24E-08	8.11E-08	9.65E-08	1.34E-07	1.65E-07	1.83E-07
MAU-01		5.97E-08	7.07E-08	7.51E-08	9.10E-08	1.33E-07	1.96E-07	2.23E-07	2.66E-07
MAU-02		7.29E-08	8.90E-08	9.08E-08	1.13E-07	1.34E-07	1.65E-07	2.09E-07	2.38E-07
MAU-03		1.10E-07	1.20E-07	1.32E-07	1.39E-07	1.81E-07	2.40E-07	2.66E-07	3.08E-07
MAU-04		1.27E-07	1.37E-07	1.58E-07	1.58E-07	2.17E-07	2.80E-07	3.01E-07	3.53E-07

	Sample	#2	#4	#6	#8
	Time [hr]	1	3.3	25.5	96
NAT-25B		5.61E-08	7.16E-08	1.52E-07	2.31E-07

	#1	#2	#3	#4	#5	#6	#7	#8	#9	#10
	0.05	0.5	1	2	4	8	16	32	64	128
NABS		no data available								

Table C.10e. HH Extraction of U-Contaminated Sediment Samples, Extracted Potassium in moles/g

Potassium									
39.0983	Sample	#1	#2	#3	#4	#5	#6	#7	#8
Core	Time [hr]	0.5	1	2	4	8	24	48	96
NAT-01		4.31E-06	7.30E-06	8.00E-06	6.31E-06	1.04E-05	1.33E-05	1.40E-05	1.68E-05
NAT-02		3.65E-06	6.19E-06	7.98E-06	6.38E-06	9.84E-06	1.07E-05	1.29E-05	1.55E-05
NAT-03		5.27E-06	5.40E-06	6.81E-06	7.10E-06	1.00E-05	1.38E-05	1.59E-05	1.79E-05
NAT-04	mol/g	6.38E-06	5.07E-06	8.43E-06	8.47E-06	1.24E-05	1.64E-05	1.88E-05	2.00E-05
NAT-05		3.95E-06	7.00E-06	7.32E-06	6.87E-06	9.09E-06	1.33E-05	1.57E-05	1.70E-05
NAT-06		1.17E-05	1.31E-05	1.35E-05	1.52E-05	1.76E-05	2.08E-05	2.62E-05	3.35E-05
NAT-07		5.77E-06	6.65E-06	1.01E-05	7.12E-06	8.89E-06	1.52E-05	1.61E-05	1.77E-05
NAT-08		5.31E-06	5.40E-06	5.94E-06	7.86E-06	8.91E-06	1.37E-05	1.48E-05	1.76E-05
NAT-10		5.47E-06	8.36E-06	8.04E-06	7.63E-06	1.12E-05	1.45E-05	1.63E-05	1.73E-05
NAT-11		7.33E-06	8.51E-06	8.97E-06	1.12E-05	1.29E-05	1.82E-05	2.31E-05	2.53E-05
NAT-12		4.93E-06	6.02E-06	6.69E-06	7.63E-06	8.84E-06	1.16E-05	1.49E-05	1.69E-05
MAU-01		3.95E-06	5.89E-06	7.19E-06	7.33E-06	9.85E-06	1.43E-05	1.60E-05	1.89E-05
MAU-02		4.58E-06	5.43E-06	5.18E-06	7.92E-06	1.10E-05	1.38E-05	1.69E-05	2.02E-05
MAU-03		2.43E-06	3.48E-06	5.07E-06	3.66E-06	5.54E-06	6.83E-06	9.32E-06	8.56E-06
MAU-04		2.80E-06	4.15E-06	6.25E-06	4.40E-06	7.95E-06	1.09E-05	1.32E-05	1.63E-05

	Sample	#2	#4	#6	#8
	Time [hr]	1	3.3	25.5	96
NAT-25B		3.00E-06	3.83E-06	5.34E-06	7.95E-06

	#1	#2	#3	#4	#5	#6	#7	#8	#9	#10
	0.05	0.5	1	2	4	8	16	32	64	128
NABS		no data available								

Table C.10f. HH Extraction of U-Contaminated Sediment Samples, Extracted Strontium in moles/g

Strontium

87.62	Sample	#1	#2	#3	#4	#5	#6	#7	#8
Core	Time [hr]	0.5	1	2	4	8	24	48	96
NAT-01		1.59E-06	1.75E-06	1.55E-06	1.65E-06	1.76E-06	1.81E-06	1.78E-06	1.81E-06
NAT-02		1.31E-06	1.39E-06	1.32E-06	1.35E-06	1.46E-06	1.51E-06	1.53E-06	1.55E-06
NAT-03		1.59E-06	1.58E-06	1.56E-06	1.62E-06	1.76E-06	1.72E-06	1.80E-06	1.80E-06
NAT-04	mol/g	1.16E-06	1.64E-06	1.18E-06	1.19E-06	1.38E-06	1.34E-06	1.39E-06	1.39E-06
NAT-05		1.00E-06	1.01E-06	1.01E-06	1.02E-06	1.10E-06	1.13E-06	1.16E-06	1.21E-06
NAT-06		1.11E-06	1.10E-06	1.11E-06	1.13E-06	1.18E-06	1.12E-06	1.13E-06	1.24E-06
NAT-07		1.12E-06	1.19E-06	1.19E-06	1.18E-06	1.22E-06	1.27E-06	1.38E-06	1.36E-06
NAT-08		1.43E-06	1.50E-06	1.45E-06	1.65E-06	1.55E-06	1.66E-06	1.69E-06	1.65E-06
NAT-10		7.84E-07	8.63E-07	8.23E-07	7.99E-07	8.60E-07	9.47E-07	1.03E-06	1.07E-06
NAT-11		1.91E-06	1.93E-06	2.01E-06	2.18E-06	2.13E-06	2.20E-06	2.33E-06	2.27E-06
NAT-12		1.38E-06	1.40E-06	1.46E-06	1.56E-06	1.39E-06	1.44E-06	1.51E-06	1.43E-06
MAU-01		1.01E-06	1.10E-06	1.04E-06	9.67E-07	1.05E-06	1.14E-06	1.17E-06	1.21E-06
MAU-02		1.12E-06	1.14E-06	1.10E-06	1.27E-06	1.17E-06	1.11E-06	1.21E-06	1.21E-06
MAU-03		6.89E-07	8.00E-07	7.79E-07	7.01E-07	8.20E-07	8.66E-07	9.36E-07	9.46E-07
MAU-04		1.59E-06	1.74E-06	1.76E-06	1.53E-06	1.78E-06	1.77E-06	1.87E-06	1.90E-06

	Sample	#2	#4	#6	#8
	Time [hr]	1	3.3	25.5	96
NAT-25B		2.95E-07	3.09E-07	3.55E-07	4.00E-07

	#1	#2	#3	#4	#5	#6	#7	#8	#9	#10
	0.05	0.5	1	2	4	8	16	32	64	128
NABS		no data available								

Table C.10g. HH Extraction of U-Contaminated Sediment Samples, Extracted Magnesium in moles/g

Magnesium									
24.305	Sample	#1	#2	#3	#4	#5	#6	#7	#8
Core	Time [hr]	0.5	1	2	4	8	24	48	96
NAT-01		3.86E-05	4.38E-05	4.47E-05	5.40E-05	6.75E-05	9.95E-05	1.11E-04	1.29E-04
NAT-02		4.33E-05	4.84E-05	5.22E-05	6.14E-05	7.82E-05	1.15E-04	1.30E-04	1.51E-04
NAT-03		5.59E-05	6.02E-05	6.60E-05	7.58E-05	9.57E-05	1.25E-04	1.48E-04	1.63E-04
NAT-04	mol/g	4.61E-05	6.08E-05	5.51E-05	6.34E-05	8.42E-05	1.14E-04	1.31E-04	1.50E-04
NAT-05		4.43E-05	4.77E-05	5.36E-05	6.17E-05	7.87E-05	1.13E-04	1.27E-04	1.50E-04
NAT-06		6.51E-05	6.72E-05	7.16E-05	8.00E-05	9.27E-05	1.09E-04	1.21E-04	1.42E-04
NAT-07		4.32E-05	4.83E-05	5.47E-05	6.17E-05	7.57E-05	1.07E-04	1.24E-04	1.44E-04
NAT-08		5.32E-05	6.24E-05	6.67E-05	8.41E-05	9.59E-05	1.37E-04	1.62E-04	1.81E-04
NAT-10		4.91E-05	5.51E-05	6.10E-05	6.77E-05	8.45E-05	1.25E-04	1.45E-04	1.74E-04
NAT-11		6.25E-05	6.91E-05	7.70E-05	9.20E-05	1.05E-04	1.37E-04	1.63E-04	1.74E-04
NAT-12		4.97E-05	5.35E-05	5.77E-05	6.58E-05	6.79E-05	9.10E-05	1.09E-04	1.17E-04
MAU-01		5.78E-05	6.28E-05	6.73E-05	6.95E-05	8.48E-05	1.19E-04	1.28E-04	1.50E-04
MAU-02		7.32E-05	7.79E-05	7.87E-05	9.47E-05	9.92E-05	1.17E-04	1.42E-04	1.57E-04
MAU-03		3.97E-05	4.51E-05	4.93E-05	5.01E-05	6.58E-05	9.27E-05	1.07E-04	1.26E-04
MAU-04		5.85E-05	6.48E-05	7.35E-05	7.36E-05	9.54E-05	1.24E-04	1.37E-04	1.58E-04

	Sample	#2	#4	#6	#8
	Time [hr]	1	3.3	25.5	96
NAT-25B		1.65E-05	2.01E-05	4.49E-05	6.49E-05

	#1	#2	#3	#4	#5	#6	#7	#8	#9	#10
	0.05	0.5	1	2	4	8	16	32	64	128
NABS	1.07E-05	2.65E-05	3.12E-05	3.50E-05	3.70E-05	4.15E-05	5.19E-05	6.63E-05	8.67E-05	1.06E-04

Table C.10h. HH Extraction of U-Contaminated Sediment Samples, Extracted Manganese in moles/g

Manganese									
54.938	Sample	#1	#2	#3	#4	#5	#6	#7	#8
Core	Time [hr]	0.5	1	2	4	8	24	48	96
NAT-01		4.45E-06	4.81E-06	4.60E-06	4.96E-06	5.40E-06	6.25E-06	6.08E-06	6.47E-06
NAT-02		6.43E-06	6.98E-06	7.03E-06	7.26E-06	8.04E-06	9.01E-06	8.75E-06	9.16E-06
NAT-03		3.15E-06	3.18E-06	3.22E-06	3.34E-06	3.65E-06	3.89E-06	4.25E-06	4.44E-06
NAT-04	mol/g	4.67E-06	6.06E-06	5.13E-06	5.33E-06	6.35E-06	6.77E-06	6.75E-06	7.01E-06
NAT-05		2.72E-06	2.77E-06	2.91E-06	2.98E-06	3.37E-06	3.92E-06	3.96E-06	4.35E-06
NAT-06		2.03E-06	2.06E-06	2.09E-06	2.18E-06	2.30E-06	2.36E-06	2.47E-06	2.71E-06
NAT-07		6.61E-06	6.84E-06	7.20E-06	7.12E-06	7.61E-06	8.23E-06	8.13E-06	8.47E-06
NAT-08		4.64E-06	4.96E-06	4.91E-06	5.41E-06	5.32E-06	5.82E-06	6.14E-06	6.29E-06
NAT-10		4.68E-06	4.90E-06	5.17E-06	5.10E-06	5.69E-06	6.70E-06	6.80E-06	7.55E-06
NAT-11		2.65E-06	2.71E-06	2.80E-06	3.00E-06	3.05E-06	3.36E-06	3.73E-06	3.80E-06
NAT-12		4.72E-06	4.88E-06	5.04E-06	5.28E-06	4.91E-06	5.24E-06	5.60E-06	5.48E-06
MAU-01		5.36E-06	5.54E-06	5.72E-06	5.36E-06	5.95E-06	6.77E-06	6.45E-06	6.96E-06
MAU-02		5.83E-06	6.02E-06	5.87E-06	6.54E-06	6.27E-06	6.15E-06	6.78E-06	6.93E-06
MAU-03		6.11E-06	6.62E-06	7.04E-06	6.52E-06	7.74E-06	8.54E-06	8.41E-06	8.84E-06
MAU-04		5.94E-06	6.31E-06	6.89E-06	6.20E-06	7.36E-06	7.76E-06	7.65E-06	8.17E-06

	Sample	#2	#4	#6	#8
	Time [hr]	1	3.3	25.5	96
NAT-25B		4.34E-07	5.00E-07	8.70E-07	1.19E-06

	#1	#2	#3	#4	#5	#6	#7	#8	#9	#10
	0.05	0.5	1	2	4	8	16	32	64	128
NABS	9.53E-07	1.83E-06	2.1E-06	2.34E-06	2.43E-06	2.58E-06	2.79E-06	3.02E-06	3.35E-06	3.66E-06

Table C.10i. HH Extraction of U-Contaminated Sediment Samples, Extracted Silicon in moles/g

Silicon									
28.0855	Sample	#1	#2	#3	#4	#5	#6	#7	#8
Core	Time [hr]	0.5	1	2	4	8	24	48	96
NAT-01		2.79E-05	3.66E-05	4.47E-05	6.19E-05	8.00E-05	1.11E-04	1.19E-04	1.27E-04
NAT-02		2.82E-05	3.73E-05	4.77E-05	6.33E-05	8.31E-05	1.14E-04	1.21E-04	1.28E-04
NAT-03		3.08E-05	4.00E-05	5.27E-05	6.99E-05	9.05E-05	1.17E-04	1.33E-04	1.36E-04
NAT-04	mol/g	2.60E-05	3.41E-05	4.38E-05	6.06E-05	8.57E-05	1.12E-04	1.23E-04	1.29E-04
NAT-05		2.84E-05	3.70E-05	5.10E-05	6.72E-05	8.78E-05	1.19E-04	1.27E-04	1.37E-04
NAT-06		2.45E-05	3.53E-05	4.88E-05	6.75E-05	8.75E-05	1.16E-04	1.35E-04	1.55E-04
NAT-07		2.52E-05	3.39E-05	4.69E-05	6.24E-05	8.18E-05	1.13E-04	1.27E-04	1.38E-04
NAT-08		2.58E-05	4.05E-05	5.20E-05	7.47E-05	8.90E-05	1.21E-04	1.34E-04	1.34E-04
NAT-10		3.31E-05	4.31E-05	5.68E-05	7.05E-05	9.05E-05	1.21E-04	1.28E-04	1.36E-04
NAT-11		2.43E-05	3.83E-05	5.31E-05	7.51E-05	9.12E-05	1.21E-04	1.41E-04	1.43E-04
NAT-12		2.71E-05	3.93E-05	5.12E-05	6.82E-05	7.84E-05	1.11E-04	1.32E-04	1.36E-04
MAU-01		2.84E-05	3.84E-05	5.24E-05	6.54E-05	8.83E-05	1.29E-04	1.35E-04	1.47E-04
MAU-02		3.04E-05	4.50E-05	5.63E-05	8.10E-05	9.60E-05	1.23E-04	1.46E-04	1.48E-04
MAU-03		2.57E-05	3.34E-05	4.35E-05	4.99E-05	7.07E-05	1.00E-04	1.12E-04	1.25E-04
MAU-04		2.94E-05	4.00E-05	5.58E-05	6.61E-05	9.44E-05	1.26E-04	1.34E-04	1.43E-04

	Sample	#2	#4	#6	#8
	Time [hr]	1	3.3	25.5	96
NAT-25B		3.54E-05	4.56E-05	8.08E-05	1.04E-04

	#1	#2	#3	#4	#5	#6	#7	#8	#9	#10
	0.05	0.5	1	2	4	8	16	32	64	128
NABS	2.27E-06	1.06E-05	1.82E-05	2.58E-05	3.16E-05	4.04E-05	5.39E-05	6.92E-05	8.41E-05	9.73E-05

Appendix D: Evaluation of Rate-Controlled Sorption

In Section 5, it was shown that adsorption requires approximately 3 to 6 days to approach steady-state dissolved U(VI) concentrations. The experimental conditions for those tests were: 10^{-5} M initial dissolved U(VI), pH 7.9, atmospheric partial pressure of carbon dioxide gas (pCO_2) and 25 g/L of NABS sediment. Several sets of reaction stoichiometries were considered in developing the NABS surface complexation model (see Section 5). Many more possible combination of rate controlled reactions and slow mass transfer processes could be consistent with the experimental data. The complexity results because slow sorption kinetics could be the result of one or more slow reactions between an adsorption site and one of the many dissolved U(VI) species. The development of a detailed kinetic mechanism for the adsorption of U(VI) by the NABS sample is beyond the scope of this project. However, two different approaches were compared to illustrate some of the potential effects that could be involved.

For comparison, model simulations were performed by assuming that the rate controlled reactions involved the reaction of different U(VI) species in solution. In the first case, the rate limiting reaction was assumed to involve the reaction of the UO_2^{+2} cation as illustrated by:

$$UO_2^{+2} + >WOH \underset{k_r}{\overset{k_f}{\rightleftarrows}} >WOHUO_2OH + 2H^+ \qquad \textbf{(D.1)}$$

where k_f and k_r are the forward and backward rate constants respectively. At pH 7.9, the concentration of UO_2^{+2} is very small as a result of aqueous speciation reactions. It is possible that the rate controlled sorption process could involve a more abundant aqueous species such as a uranyl-carbonate complex. For comparison, the rate-controlled reaction that produces >WOHUO$_2$OH can also be written as:

$$>WOH + UO_2(CO_3)_2^{-2} + H_2O \underset{k_r}{\overset{k_f}{\rightleftarrows}} >WOHUO_2OH + 2H^+ + 2CO_3^{-3} \qquad \textbf{(D.2)}$$

where, in this case, the predominant aqueous species, $UO_2(CO_3)_2^{-2}$, participates in the rate-controlled reaction. The complete set of reactions for the approaches illustrated by equations D.1 and D.2 is listed in Table 9.1.

In the simulations described below, the value of k_f was varied and the value of k_r was simultaneously adjusted according to the expression:

$$K_{EQ} = \frac{k_f}{k_r} \qquad \textbf{(D.3)}$$

where K_{EQ} is the equilibrium constant. This was done so that the kinetic model was consistent with the GC-SCM for the NABS sample. Because U(VI) speciation depends on solution conditions such as pH and pCO_2, reaction rates also change with speciation.

D.1 Numerical Simulations

A kinetic model was not calibrated to the observed kinetic batch data because there was insufficient data over a wide range of experimental conditions available for calibration. In particular, there were not enough data to determine the reactive U(VI) species. Consequently, the model was used to illustrate possible changes in sorption kinetics that result from changes in solution conditions for Models 1 and 2 and the chemical conditions in Table D.1. Initially, the forward rate constants were adjusted so that the K_d values reached a nearly constant value after approximately 3 to 5 days for the batch kinetic experimental conditions. In addition, it was assumed that each of the surface species reached equilibrium after approximately 3 days. This process was conducted for both model 1 and model 2, and the simulated kinetic plots are shown in Figure D.1. The results

Table D.1 Summary of Simulation Conditions

Run	pH	pCO_2	Total surface site concentration (mM)	Condition
1	7.9	Atmospheric	0.247	Batch
2	7.1	Atmospheric	0.247	
3	7.9	0.1 atm	0.247	
4	7.9	Atmospheric	28.4	
5	7.9	0.1	28.4	Field

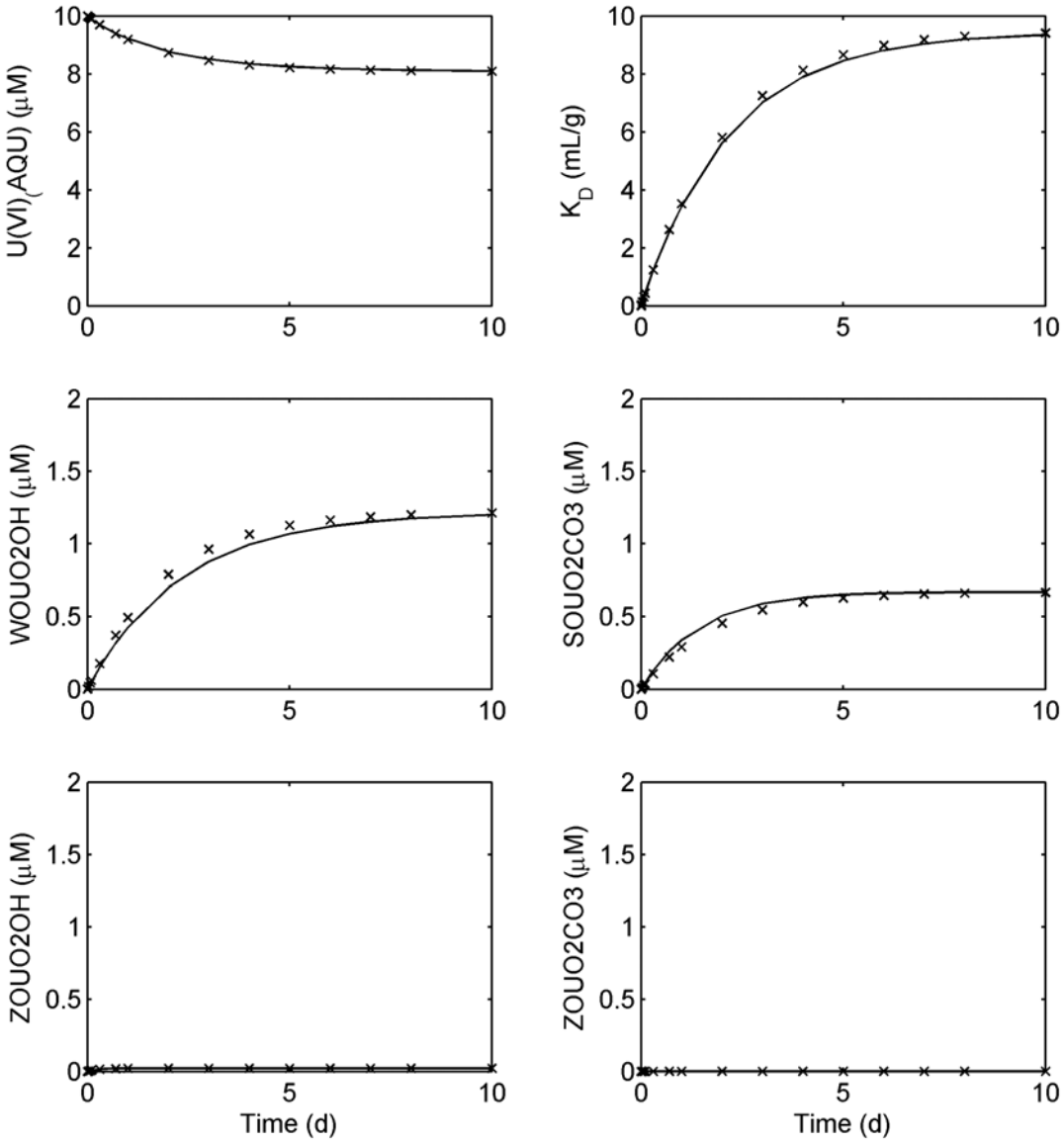

Figure D.1. Simulated concentration versus time for model 1 (solid lines) and model 2 (x) for pH 7.9, 10 μM dissolved U(VI), and atmospheric pCO_2.

illustrate that the two different kinetic models can give the same kinetic behavior.

Simulations were also conducted to illustrate the effects of different chemical conditions on the time required for the K_d values to approach a steady value. The variable included pH, pCO_2, and the sediment/water ratio. The value of each variable was set equal to that observed in the field while the remaining values were fixed at the value for the batch experiments. A final simulation was done using typical field values for each of the variables. Table D.1 contains a summary of the parameters used.

K_d values are plotted for each of the two models in Table 9.1 and each of the cases in Table D.1 in Figure D.2. The figure shows that the simulated approach to equilibrium varies with both the solution conditions and with the model formulation. Figure D.2a shows the 'calibration' results that demonstrate that the two models approach equilibrium in the batch studies at approximately the same rate. These simulation conditions are identical to those used for Figure D.1. Figures D.2b and c show that the increase in K_d with time depends on speciation. In Figure D.2b, Model 1 approaches equilibrium in a shorter time at pH 7.1 because the concentration of UO_2^{+2} increases as pH decreases (see Section 2). At increased pCO_2, Model 1 approaches equilibrium in a longer time because the concentration of UO_2^{+2} decreases as carbonate complexation increases (Fig. D.2c). At higher site concentrations, both models approach equilibrium at the same time. The initial rate of uptake is significantly faster at the higher surface concentrations with the K_d value equal to 85% of the final value after approximately 0.2 days. However, the time to reach equilibrium still requires 3 to 5 days as in the case with a smaller reactive site concentration. Finally, Figure D.2e shows that under the representative field conditions, the simulated K_d values for the models agree and reach 94% of the equilibrium value after 0.1 days; as with the other cases, however, the time to reach equilibriums is approximately 3 to 5 days. These two kinetic models are applied to the field scale transport of U(VI) in Section 9.

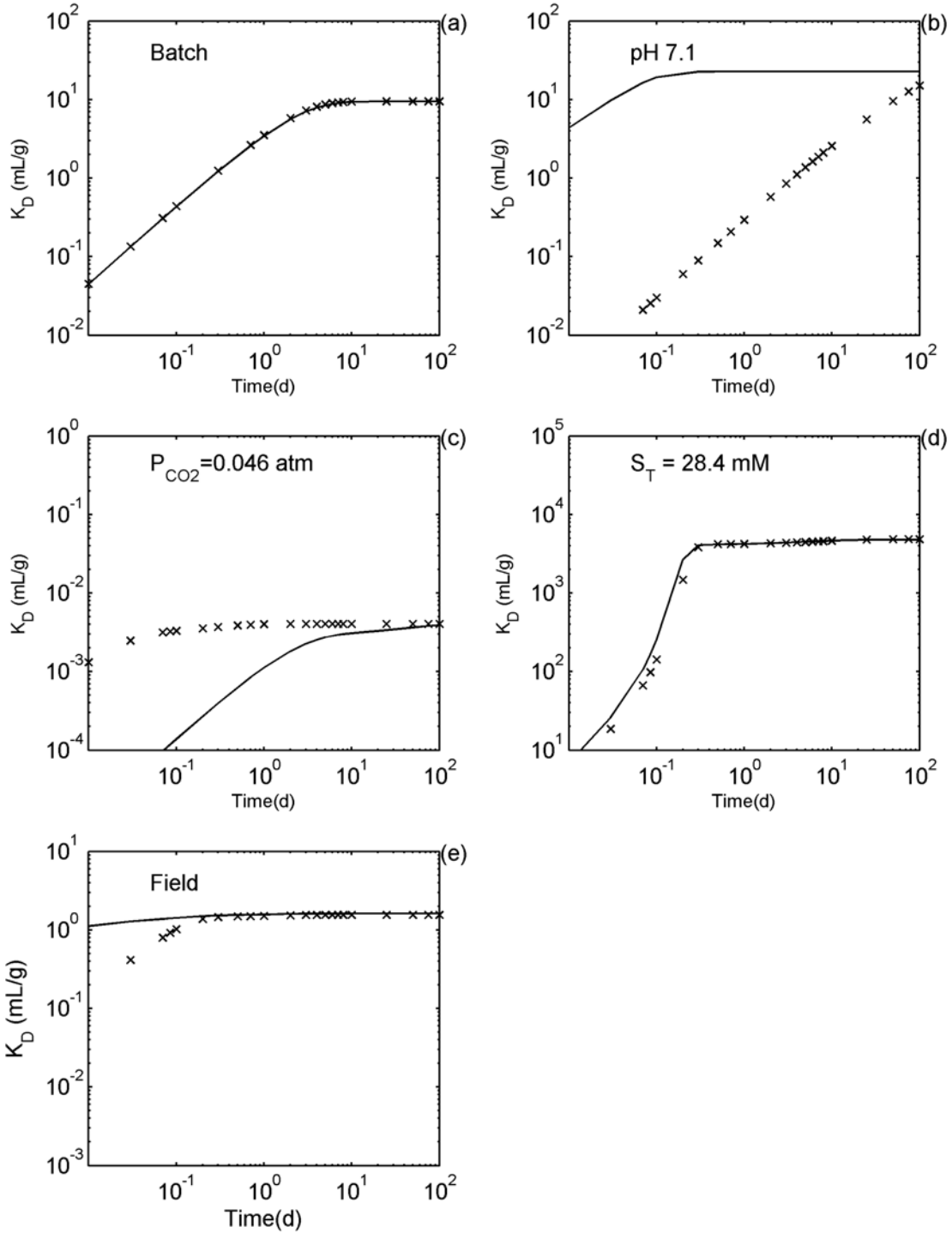

Figure D.2. Simulated K_d values for Models 1 (solid lines) and 2 (x) listed in Table 9.1. The simulation conditions are summarized in Table D.1.

Appendix E: Table of Symbols and Acronyms

a – specific surface area of a mineral, typical units of m^2/g
A - the activity of the dissolved radioisotope, ^{233}U, in experimental systems, units of dpm/mL
AGW – artificial ground water solution
Al – aluminum
A_{system} – the total activity of the radioisotope, ^{233}U, in an experimental system, units of dpm/mL
atm – unit of gas pressure, equivalent to one atmosphere
BET – analysis of nitrogen gas adsorption according to the classical method of Brunauer, Emmett, and Teller
C – the dissolved concentration of a solute
C_o – the initial dissolved concentration of a solute
^oC – degrees Celsius
Ca - calcium
CA – Component Additivity modeling approach for surface complexation models, see Davis et al. (1998) for a complete description
CARB – the sodium (bi)carbonate solution used to extract U(VI) from sediment samples, see Section 6.2.2
cfs – cubic feet per second
Cl – chloride ion
C_{labile} – the quantity of uranium in a system that participates in short-term chemical processes involving the aqueous phase and mineral surfaces, units of moles/mL
C^*_{labile} – the quantity of uranium in a system that participates in short-term chemical processes involving the aqueous phase and mineral surfaces, units of moles/g of sediment
CO_2 – carbon dioxide gas
d – unit of time, day
D_h – hydrodynamic dispersion coefficient
D_m^* - molecular diffusion coefficient
dpm – disintegrations per minute of a radioisotope
EDS – energy dispersive spectroscopy, a method of measuring element concentrations in a volume comprising the surficial 500 micrometers (approximately) of solid phases
F – fluoride ion
Fe – iron
FEMP – Fernald Environmental Management Project
FE-SEM - field-emission scanning electron microscopy
ft - foot
g –gram
g – earth gravitational force
GC – Generalized Composite modeling approach for surface complexation models, see Davis et al. (1998) for a complete description
GC-SCM – a Generalized Composite surface complexation model
HFO – hydrous ferric oxide
HH – hydroxylamine hydrochloride, a reagent used to do partial reductive dissolution of sediment coatings
HNO_3 – nitric acid
hr – hour
HRTEM – High resolution transmission electron spectroscopy
HTO – tritiated water, used as a water tracer in this study
ICP-AES – inductively coupled atomic emission spectroscopy, a method of water analysis for the concentrations of metals and certain metalloid elements

K – potassium ion
K or K_{eq} – apparent stability constant for an adsorption reaction
K_w – apparent stability constant for the reaction between the weak surface site, >WOH, and the uranyl cation
K_{SC} – apparent stability constant for the reaction between the strong surface site, >SOH, the uranyl cation, and the carbonate anion
K_{SS} – apparent stability constant for the reaction between the very strong surface site, >SSOH, and the uranyl cation
K_{SSC} – apparent stability constant for the reaction between the very strong surface site, >SSOH, the uranyl cation, and the carbonate anion
K_a – the surface-area normalized distribution coefficient, describing distribution of a molecule or element between the aqueous and solid phases in a system, units of mL/m^2, equal to K_d divided by the solid surface area
K_d – the distribution coefficient, describing distribution of a molecule or element between the aqueous and solid phases in a system, units of mL/g
keV – kilo-electron volts, 1000 electron volts
k_f – rate constant for the forward (adsorption) direction of a surface reaction
kg – kilograms, 1000 grams
km – kilometers, 1000 meters
KPA – kinetic phosphorescence analysis, a method for measuring dissolved U(VI) in aqueous samples
k_r – rate constant for the backward (desorption) direction of a surface reaction
kV – kilovolts, 1000 volts
K_x – hydraulic conductivity, units of length/time
L - liter
m - meter
M – molar concentration, units of moles/liter
mA - milliamperes
meq/L – milliequivalents/liter, a unit of measure of alkalinity or acidity in water
mg - milligram
Mg – magnesium
Milli-Q water – a trademark name for a system that produces de-ionized water for laboratory research
min - minutes
mL - milliliter
mM – millimolar concentration, units of millimoles/liter
Mo – molybdenum
n (also θ) – porosity, of an unconsolidated aquifer or of a packed column
N - nitrogen
NABS – Naturita aquifer background sediment sample
NAT-COL – the subsample of the Naturita aquifer background sediment sample (NABS) used in the column experiments
NEM – a non-electrostatic surface complexation model, meaning that the mass laws of the adsorption reactions are not corrected for calculated electrostatic attraction or repulsion
O - oxygen
PA – performance assessment
pCO_2 – partial pressure of carbon dioxide gas
PDF – probability distribution function
Pe – Peclet number
pH – negative log of the concentration of the hydrogen ion
ppm – parts per million, equivalent to mg/kg in solids and gases, and mg/L for solutes in water

Q – volumetric flow rate of water in a column experiment
r^2 – correlation coefficient between data and a linear regression through the data
RCF – centrifugal force, relative to gravity
R_f – retardation factor
RN_{ads} – adsorbed radionuclide concentration, in units of moles/gram
RN_{aq} – dissolved radionuclide concentration, in units of moles/liter
RSE – relative standard error
s – unit of time, second
SCM – surface complexation model, a model that describes chemical reactions on mineral surfaces
SEM – scanning electron microscopy
SEM-EDS – energy dispersive analysis combined with scanning electron microscopy, a semi-quantitative method of determining the presence of certain elements at the surface (several microns thick) of a solid material
Si - silicon
SI – saturation index, a calculation of the degree of under- or super-saturation of an aqueous phase with respect to the solubility of a solid phase, expressed in log units
SIMS – secondary ion mass spectroscopy, a semi-quantitative method of determining the presence of certain elements at the surface (several nm thick) of a solid material
SOH – generic, surface-hydroxyl, strong U(VI) adsorption sites in the site-binding GC model
SSOH – generic, surface-hydroxyl, very strong U(VI) adsorption sites in the site-binding GC model
Th – thorium
^{234}Th - the radioisotope of thorium with molecular weight of 234 grams
U – uranium
U_{ads} – adsorbed uranium(VI)
U_{aqu} – dissolved uranium(VI)
^{233}U – the radioisotope of uranium with molecular weight of 233 grams
^{238}U – the radioisotope of uranium with molecular weight of 238 grams
U(VI) – uranium in the +6 oxidation state
UMTRA – Uranium Mill Tailings Remediation Act
USEPA – United States Environmental Protection Agency
USDOE – United States Department of Energy
USNRC – United States Nuclear Regulatory Commission
v – linear pore water velocity, in an unconsolidated aquifer or in a packed column
V – volume of water in an experimental system, units of mL
V – vanadium, or volume of eluant in a column experiment
V_p – pore (or void) volume in a column experiment
w – mass of sediment or solid phase in an experimental system, units of grams
WOH – generic, surface-hydroxyl, weak U(VI) adsorption sites in the site-binding GC model
XRD – X-ray diffraction
Zn – zinc
α - hydrodynamic dispersivity
σ_o - net average electrical charge at a mineral surface cleavage plane
σ_β - net average electrical charge within the mean plane of adsorbed ions on a mineral surface
μg – microgram
μm – micrometer, also known as a micron
μM – micromolar concentration, units of micromoles/liter

μ-SXRF – micro-synchrotron X-ray fluorescence – a semi-quantitative method of determining the presence of certain elements at the surface (several microns thick) on a solid grain over a small spot size (e.g., 100-1000 μm^2)

μ-XANES – micro-X-ray absorption near-edge spectroscopy – a method of determining the oxidation state, and possibly structural characteristics, of certain elements in a solid grain over a small spot size (e.g., 100-1000 μm^2)

ρ_b – bulk density

θ (also *n*) – porosity, of an unconsolidated aquifer or of a packed column

REFERENCES

Allison, J. D., D. S. Brown, and K. J. Novo-Gradac, MINTEQA2/PRODEFA2, a geochemical assessment model for environmental systems; version 3.0 user's manual. 02A, General geochemistry. EPA/600/3-91/021, 1991

Altmann, S.A., J. Bruno, and C. Tweed, *Using Thermodynamic Sorption Models for Guiding Radioelement Distribution Coefficient (Kd) Investigations for Performance Assessment – A Status Report*, Nuclear Energy Agency, Paris, 2001.

Appelo, C.A.J. and D. Postma, *Geochemistry, Groundwater and Pollution*, Balkema, Rotterdam, 526, 1993.

Arnold, T. et al., "Sorption Behavior of U(VI) on Phyllite: Experiments and Modeling," *Journal of Contaminant Hydrology*, Vol. 47, No. 2, 219-231,. 2001.

Baes, C.F. and R.D. Sharp, "A Proposal for Estimation of Soil Leaching and Leaching Constants for Use in Assessment Models," *J. Environ. Quality*, Vol. 12, 17-28, 1983.

Baestlé, L., "Computational Methods for the Prediction of Underground Movement of Radionuclides," *Nuclear Safety*, Vol. 8, 576-588, 1967.

Bain, J.G. et al., "Modelling the Closure-related Geochemical Evolution of Groundwater at a Former Uranium Mine," *Journal of Contaminant Hydrology*, Vol. 52, No. 1, 109-135, 2001.

Bargar, J.R., R. Reitmeyer, and J.A. Davis, "Spectroscopic Confirmation of Uranium(VI)-Carbonato Adsorption Complexes on Hematite," *Environmental Science & Technology*, Vol. 33, No. 14, 2481, 1999.

Bargar, J.R. et al., "Characterization of U(VI)-Carbonato Ternary Complexes on Hematite: EXAFS and Electrophoretic Mobility Measurements," *Geochim. Cosmochim. Acta*, Vol. 64, No. 16, 2737-2749, 2000.

Barnett, M.O., P.M. Jardine, and S.C. Brooks, "U(VI) Adsorption to Heterogeneous Subsurface Media: Application of a Surface Complexation Model," *Environmental Science and Technology*, Vol. 36, No. 5, 937-942, 2002.

Barnett, M.O., P.M. Jardine, and H.M. Selim, "Adsorption and Transport of Uranium(VI) in Subsurface Media," *Soil Science Society of America Journal*, Vol. 64, No. 3, 908, 2000.

Bear, J., *Hydraulics of Groundwater*, McGraw-Hill, New York, 272, 1979.

Bernhard, G., et al., "Uranyl(VI) carbonate complex formation: Validation of the $Ca_2UO_2(CO_3)_3$ (aq) species", *Radiochim. Acta*, Vol. 89, 511-518, 2001.

Berry, J.A., "A Review of Sorption of Radionuclides under Near- and Far-Field Conditions of an Underground Radioactive Waste Repository: Parts I, II, and III," Oxfordshire, United Kingdom, Her Majesty's Inspectorate of Pollution/Department of the Environment, Harwell Laboratory, DOE/HMIP/RR/92/061, 1992.

Bethke, C.M. and P.V. Brady, "How the K_d Approach Undermines Group Water Cleanup," *Ground Water*, Vol. 38, No. 3, 435-443, 2000.

Bevington P.R., *Data Reduction and Analysis for the Physical Sciences*, McGraw Hill, Inc., New York, 336, 1969.

Biehler, D. and W.E. Falck, "Simulation of the Effects of Geochemical Reactions on Groundwater Quality During Planned Flooding of the Königstein Uranium Mine, Saxony, Germany," *Hydrogeology Journal*, Vol. 7, No 3, 284-293, 1999.

Borkovec, M., U. Rusch, and J.C. Westall, "Modeling of Competitive Ion Binding to Heterogeneous Materials with Affinity Distribution," *Adsorption of Metals by Geomedia*, Academic Press, 467-482, 1998.

Bostick, B.C. et al., "Uranyl Surface Complexes Formed on Subsurface Media from DOE Facilities," *Soil Science Society of America Journal*, Vol. 66, No. 1, 99-108, 2002.

Bradbury, M.H. and B. Baeyens, "A Mechanistic Description of Ni and Zn Sorption on Na-Montmorillonite. Part II: Modelling," *J. Contam. Hydrol.*, Vol. 27, 223-248, 1997.

Brooks, S.C. et al., "Inhibition of bacterial U(VI) reduction by calcium", *Environ. Sci. Tech.*, Vol. 37, 1850-1858, 2003.

Brusseau, M.L. et al., "Flow Interruption: A Method for Investigating Sorption Nonequilibrium," *Journal of Contaminant Hydrology,* Vol. 4, 223-240, 1989.

Butler, J.J.,Jr, *The Design, Performance, and Analysis of Slug Tests*, Lewis Publishers, Boca Raton, USA, 1998.

CDPHE (Colorado Department of Public health and the Environment), "Environmental Covenant," from http://www.cdphe.state.co.us/hm/convenant/covenantnaturita.pdf, 2002.

Chao, T.T. and L. Zhou, "Extraction Techniques for Selective Dissolution of Amorphous Iron Oxides from Soils and Sediments," *Soil Science Society of America Journal*, Vol. 47, 225-232, 1983.

Chao T. T., "Use of Partial Dissolution Techniques in Geochemical Exploration," *Journal of Geochemical Exploration*, Vol. 20, 101-135, 1984.

Chenowith, W.L., *Colorado Uranium Field Trip, Guidebook*; American Association of Petroleum Geologists, Energy Minerals Division, Denver, Colorado, June 1980.

Choppin, G. and J. Rydberg, *Nuclear Chemistry*, Pergamon Press, 1980.

Clark, D.L., D.E. Hobart, and M.P. Neu, "Actinide Carbonate Complexes and their Importance in Environmental Chemistry," *Chem. Rev*., Vol. 95, 25-48, 1995.

Coston, J.A., C.C. Fuller, and J.A. Davis, "Pb^{2+} and Zn^{2+} Adsorption by a Natural Aluminum- and Iron-bearing Surface Coating on an Aquifer Sand," *Geochim. Cosmochim. Acta*, Vol. 59, No. 17, 3535-3547, 1995.

Criscenti, L.J. et al., "Effects of Adsorption Constant Uncertainty on Contaminant Plume Migration," NUREG/CR-6780, Nuclear Regulatory Commission, Washington, D. C., 2003.

Crowley, K.D. and J.F. Ahearne, "Managing the Environmental Legacy of U.S. Nuclear Weapons Production," *American Scientist*, Vol. 90, 514-523, 2002.

Curtis, G. P., M. Kohler, and J.A. Davis, "Batch and Column Studies of Uranium(VI) Adsorption by Quartz in the Presence of CO_2," *Abstract Migration'99, Seventh International Conference on the Chemistry and Migration Behavior of Actinides and Fission Products in the Geosphere*, Incline Village, Lake Tahoe, Nevada/California, USA, September 26-October 1, 1999.

Curtis, G. P., "RATEQ: A Computer Program for Rate and Equilibrium Controlled Reactive Solute Transport," Unpublished Documentation, 2003.

Curtis, G.P., P. Fox, M. Kohler, and J.A. Davis, Comparison of *in-situ* uranium Kd values with a laboratory determined surface complexation model, *Applied Geochemistry*, submitted, 2003a.

Curtis, G.P., J.A. Davis, and D. L. Naftz, Simulation of reactive transport of uranium(VI) in groundwater with variable chemical conditions, *Water Resources Research*, submitted, 2003b.

Davis, J.A. and J.O. Leckie, "Effect of Adsorbed Complexing Ligands on Trace Metal Uptake by Hydrous Oxides," *Environ. Sci. Technol.*, Vol. 12, 1309-1315, 1978.

Davis, J.A., and D.B. Kent, "Surface Complexation Modeling in Aqueous Geochemistry," *Mineral-Water Interface Geochemistry*, Reviews in Mineralogy Series, Mineralogical Society of America, Vol. 23, 177-260, 1990.

Davis, J.A. et al., "Application of the Surface Complexation Concept to Complex Mineral Assemblages," *Environmental Science & Technology*, Vo. 32, No. 19, 2820-2828, 1998.

Davis J.A., "Surface Complexation Modeling of Uranium(VI) Adsorption on Natural Mineral Assemblages," U.S. Nuclear Regulatory Commission, NUREG/CR-6708, 2001.

Davis J A., T.E. Payne, and T.D. Waite, "Simulating the pH and pCO_2 Dependence of Uranium(VI) Adsorption by a Weathered Schist with Surface Complexation Models," *Geochemistry of Soil Radionuclides*, Soil Science Society America, Madison, Chap. 4, p. 61-86, 2002.

Davis, J.A. et al., "Approaches to Surface Complexation Modeling of Uranium(VI) Adsorption on Aquifer Sediments", *Geochim. Cosmochim. Acta*, submitted for publication, 2003a.

Davis, J.A. et al., "Surface Complexation Model for Carbonate and Uranyl Adsorption on Hematite Consistent with Spectroscopic Studies," *Geochim. Cosmochim. Acta*, in preparation, 2003b.

Essaid, H. I., et al., "Simulation of aerobic and anaerobic biodegradation processes at a crude oil spill site", *Water Resources Research,* Vol. 31, 3309-3327, 1995.

Faure, G., *Principles and Applications of Inorganic Geochemistry*, Macmillan Publishing, 1991.

Fuller, C.C. et al., "Characterization of Metal Adsorption Variability in a Sand and Gravel Aquifer, Cape Cod, Massachusetts," *Journal of Contaminant Hydrology*, Vol. 22, 165-187, 1996.

Gabriel U. et al., "Reactive Transport of Uranyl in a Goethite Column: An Experimental and Modelling Study," *Chemical Geology*, Vol. 151, 107-128, 1998.

Goode, D.J., "Direct Simulation of Groundwater Age," *Water Resour.Res.,* Vol. 32, 289-296, 1996.

Gadelle F., J. Wan, and T.K. Tokunaga, "Removal of Uranium(VI) from Contaminated Sediments by Surfactants," *Journal of Environ. Qual*., Vol. 30, 470-478, 2001.

Gregg, S.J. and K.S.W. Sing, *Adsorption, Surface Area, and Porosity*, Academic Press, London, 1982.

Grenthe, I. et al., *Chemical Thermodynamics of Uranium*, Elsevier, Amsterdam, 1992.

Harbaugh, A.W. and M.G. McDonald, "Programmer's Documentation for MODFLOW-96, an Update to the U.S. Geological Survey Modular Finite-difference Ground-water Flow Model," U. S. Geological Survey, Reston, VA, Open-File Rept. 96-0486, 220, 1996.

Hem J. D., "Study and Interpretation of the Chemical Characteristics of Natural Water," Water-Supply Paper 2254, U.S. Geological Survey, Reston, VA, 1985.

Herbelin, A. L. and J.C. Westall, *FITEQL: A Computer Program for the Determination of Chemical Equilibrium Constants from Experimental Data*, Version 4.0, Report 99-01, Chemistry Department, Oregon State University, Corvallis, Oregon, 1999.

Hiemstra, T. and W.H. van Riemsdijk, "Surface Structural Ion Adsorption Modeling of Competitive Binding of Oxyanions by Metal (hydr)oxides," *J. Colloid Interface Sci*., Vol. 210, 182-193, 1999.

Higgins, G., "Evaluation of the Groundwater Contamination Hazard from Underground Nuclear Explosions," *J. Geophys. Res*., Vol. 64, 1509-1519, 1959.

Honeyman, B.D., Ph.D. Thesis, Stanford University, Stanford, CA 1984.

Hsi, C.D. and D. Langmuir, "Adsorption of Uranyl onto Ferric Oxyhydroxides; Application of the Surface Complexation Site-binding Model," *Geochim. Cosmochim. Acta*, Vol. 49, No. 9, 1931-1941, 1985.

Iman, R. L. and M.J. Shortencarier, "A Fortran 77 Program and User's Guide for the Generation of Latin Hypercube and Random Samples for Use with Computer Models," NUREG/CR-3624, U. S. Nuclear Regulatory Commission, Washington, D.C., 1984.

Isherwood, D. "Geoscience Data Base Handbook for Modeling a Nuclear Waste Repository," U. S. Nuclear Regulatory Commission, NUREG/CR-0912, Vol. 1, 1981.

Jove-Colon, C.F. et al., "A Combined Analytical Study to Characterize Uranium Soil Contamination: The Case of the Naturita UMTRA Site and the Role of Grain Coatings," U.S. Nuclear Regulatory Commission, 2003.

Kalmykov, S.N. and Choppin, G.R., "Mixed $Ca^{2+}/UO_2^{2+}/CO_3^{2-}$ complex formation at different ionic strengths", *Radiochim. Acta*, Vol. 88, 603-606, 2000.

Kaplan, D.I. et al., "Gravel-Corrected K_d Values", *Groundwater*, Vol. 38(6), 851-857, 2000.

Kent, D.B. et al., "Modeling the Influence of Variable pH on the Transport of Zinc in a Contaminated Aquifer Using Semiempirical Surface Complexation Models," *Water Resour.Res*., Vol. 36, No. 12, 3411-3425, 2000.

Koch, S. and H. Flühler, "Non-reactive Solute Transport with Micropore Diffusion in Aggregated Porous Media Determined by a Flow-interruption Method," *Journal of Contaminant Hydrology,* Vol. 14, 39-54, 1993.

Kohler, M. et al., "Experimental Investigation and Modeling of Uranium(VI) Ttransport under Variable Chemical Conditions," *Water Resour.Res*., Vol. 32, No. 12, 3539-3551, 1996.

Kohler, M. et al., "Methods for Estimating Adsorbed Uranium(VI) and Distribution Coefficients of Contaminated Sediments", *Environ. Sci. Tech.*, in press, 2003.

Kohler, M., B.D. Honeyman, and J.O. Leckie, "Neptunium(V) Sorption on Hematite (α-Fe_2O_3) in Aqueous Suspension: The effect of CO_2," *Radiochim. Acta*, Vol. 85, 33-48, 1999.

Kohler, M. and J.A. Davis, "Uranium(VI) Adsorption on Crushed Quartz in $NaNO_3$/HCO_3 Systems," *Surface Complexation Modeling of Uranium(VI) Adsorption on Natural Mineral Assemblages*, U.S. Nuclear Regulatory Commission, NUREG/CR-6708, 214, 2001.

Koretsky, C., "The significance of surface complexation reactions in hydrologic systems: A geochemist's perspective", *Journal of Hydrology*, Vol. 230, 127-171, 2000.

Krupka, K.M., and J.R. Serne, "Input Vault and Sorption Values for Use in the NRC Low-Level Radioactive Waste Performance Assessment Test Case," Richland, Washington, Pacific NW Laboratory/Water and Land Resource. Dept., Task Order 1, Letter Rept., October 1, 1996.

Langmuir, D., "Uranium Solution-mineral Equilibria at Low Temperatures with Applications to Sedimentary Ore Deposits," *Geochim. Cosmochim. Acta*, Vol. 42, 547-569, 1978.

Langmuir, D., *Aqueous Environmental Chemistry*, Prentice-Hall, Upper Saddle River, NJ, 1997.

Lenhart, J. J., and B. D. Honeyman, "Uranium(VI) sorption to hematite in the presence of humic acid", *Geochim. Cosmochim. Acta,* Vol. 63, 2891-2901, 1999.

Lienert C., S.A. Short, and H.R. von Gunten, "Uranium Infiltration from a River to Shallow Groundwater," *Geochim Cosmochim. Acta*, Vol. 58, 5455-5464, 1994.

Looney, B.B. et al., "Estimation of Geochemical Parameters for Assessing Subsurface Transport at the Savannah River Plant," Aiken, S.C, Savannah River Lab., DPST-85-904, 1987.

Lovley, D. and E.J. Phillips, "Availability of Ferric Iron for Microbial Reduction in Bottom Sediments of the Freshwater Tidal Potomac River," *Applied Envrion. Microbio*, Vol. 52, No. 4, 751-757, 1986.

Lovley, D.R. and E.J.P. Phillips, "Novel Mode of Microbial Energy Metabolism; Organic Carbon Oxidation Coupled to Dissimilatory Reduction of Iron or Manganese," *Appl.Environ.Microbiol*., Vol. 54, No. 6, 1472-1480, 1988.

Mayer, K. U., S. G. Benner, E. O. Frind, S. F. Thornton, and D. N. Lerner, "Reactive transport modeling of processes controlling the distribution and natural attenuation of phenolic compounds in a deep sandstone aquifer", *J. Contam. Hydrol ,* Vol. 53, 341-368, 2001.

Mason, C.F.V. et al., "Carbonate Leaching of Uranium from Contaminated Soils," *Envrion. Sci., Technol*, Vol. 31, 2707-2711, 1997.

Matijevic, E. and P. Scheiner, "Ferrous Hydrous Oxide Sols. III. Preparation of Uniform Particles by Hydrolysis of Fe(III)-chloride, -nitrate, and -perchlorate Solutions," *J. Colloid Interface Sci.*, Vol. 63, 509-524, 1978.

McKinley, J. P., J. M. Zachara, S. C. Smith, and G. D. Turner, 1995: The influence of uranyl hydrolysis and multiple site-binding reactions on adsorption of U(VI) to montmorillonite. *Clays Clay Miner. ,* **43**, 586-598.

McFadden, K. et al., "Residual Radioactive Contamination From Decommissioning – User's Manual DandD Version 2.1," Sandia National Laboratories, NUREG/CR-5512, Vol. 2, 2001.

McKinley, I.G. and A. Scholtis, "A Comparison of Sorption Databases Used in Recent Performance Assessments," *Radionuclide Sorption from the Safety Evaluation Perspective*, NEA-OCDE, Paris, 1992.

Meeussen, J.C.L. et al., "Multicomponent Transport of Sulfate in a Goethite-Silica Sand System at Variable pH and Ionic Strength," *Environmental Science and Technology*, Vol 33, 3443-3450, 1999.

Moll, H., "Zur Wechselwirkung von Uran mit Silicat in wässrigen Systemen," Ph.D. Thesis, Technische Universität Dresden, 1997.

Morrison, S.J. and L.S. Cahn, "Mineralogical Residence of Alpha-emitting Contamination and Implications for Mobilization from Uranium Mill Tailings," *J. Contam. Hydrol.,* Vol. 8, 1-21, 1991.

Nakayama, F.S. and R.D. Jackson, "Diffusion of Tritiated Water ($H^3H^1O^{16}$) in Agar Gel and Water," *J. Phys. Chem.,* Vol. 67, 932-933, 1963.

Pabalan, R.T. and D.R. Turner, "Uranium(6+) Sorption on Montmorillonite: Experimental and Surface Complexation Modeling Study," *Aquatic Geochemistry*, Vol. 2, 203-226, 1996.

Pabalan, R.T. et al., "Uranium(VI) Sorption onto Selected Mineral Surfaces: Key Geochemical Parameters," *Adsorption of Metals by Geomedia*, Academic Press, p. 99-130, 1998.

Padmanabhan, E. and A. R. Mermut, "Submicroscopic Structure of Fe-coatings on Quartz Grains in Tropical Environments," *Clays and Clay Minerals*, Vol. 44, 801-810, 1996.

Papelis, C., K.F. Hayes, and J.O. Leckie, "HYDRAQL: A Program for the Computation of Chemical Equilibrium Composition of Aqueous Batch Systems Including Surface Complexation

Modeling of Ion Adsorption at the Oxide/solution Interface," *Technical Report No. 306*, Department of Civil Engineering, Stanford University, Stanford, CA, 1988.

Papini, M.P. et al., "Adsorption of Lead at Variable pH onto a Natural Porous Medium: Modeling of Batch and Column Experiments," *Environmental Science and Technology*, Vol 33, 4457-4464, 1999.

Parkhurst, D. L. and C. A. J. Appelo, "User's Guide to PHREEQC (Version 2); a Computer Program for Speciation, Batch-reaction, One-dimensional Transport, and Inverse Geochemical Calculations," U.S.Geological Survey, WRI 99-4259, 1999.

Payne T.E. and T.D. Waite, "Surface Complexation Modelling of Uranium Sorption Data Obtained by Isotope Exchange Techniques," *Radiochimica Acta*, Vol. 52/53, 487-493, 1991.

Payne T.E. et al., "Comparison of laboratory uranium sorption data with "in situ distribution coefficients" at the Koongarra uranium deposit, Northern Australia," *Journal of Environmental Radioactivity*, Vol. 57, 35-55, 2001.

Penn, R.L. et al., "Iron Oxide Coatings on Sand Grains from the Atlantic Coastal Plain: High-resolution Transmission Electron Microscopy Characterization," *Geology*, Vol. 29, 843-846, 2001.

Poeter, E.P. and M.C. Hill, "UCODE, a Computer Code for Universal Inverse Modeling," *Comput.Geosci.,* Vol. 25, 457-462, 1999.

Pollock, D. W., "User's Guide for MODPATH/MODPATH-PLOT, Version 3," A particle tracking post-processing package for MODFLOW, the U.S. Geological Survey Finite-Difference Ground-Water Flow Model, U.S. Geological Survey, Open-File Report 94-464, Ch 6, 1997.

Prikryl J.D. et al., "Migration Behavior of Naturally Occurring Radionuclides at the Nopal I Uranium Deposit, Chihuahua, Mexico," *Journ. Contam. Hydrol.*, Vol. 26, No. 1, 61-69, 1997.

Prikryl, J.D. et al., "Uranium(VI) Sorption Behavior on Silicate Mineral Mixtures," *J. Contam. Hydrol.*, Vol. 47, 241-253, 2001.

Reardon, E. J., "Kd's-Can They be Used to Describe Reversible Ion Sorption Reactions in Contaminant Migration," *Ground Water*, Vol. 19, 270-286, 1981.

Reilly, T.E. et al., "The Use of Simulation and Multiple Environmental Tracers to Quantify Groundwater Flow in a Shallow Aquifer," *Water Resour.Res.,* Vol. 30, 421-433, 1994.

Reisch, M. and D. M. Bearden, *Superfund Fact Book*, Committee for the National Institute for the Environment, 1997.

Rogers, J.J.W. and J. A. S. Adams, *Handbook of Geochemistry,Vol II/5.*, Wedepohl, K. H., Ed.; Vol. II/5, Springer-Verlag, Chap.92 D. Abundances in Rock Forming Minerals (I), Uranium Minerals (II), 1978.

Rubin, J., "Transport of reacting solutes in porous media; relation between mathematical nature of problem formulation and chemical nature of reactions", *Water Resour. Res. ,* Vol. 19, 1231-1252, 1983.

Sahai, N. and D. A. Sverjensky, "Solvation and Electrostatic Model for Specific Electrolyte Adsorption," *Geochim. Cosmochim. Acta*, Vol. 61, 2827-2848, 1997.

Sandino A. and J. Bruno, "The Solubility of $(UO_2)_3(PO_4)_2 \bullet 4H_2O_{(s)}$ and the Formation of U(VI) Phosphate Complexes: Their Influence in Uranium Speciation in Natural Waters," *Geochim. Cosmochim. Acta*, Vol. 56, 4135-4145, 1992.

Sanpawanitchakit, C., PhD Thesis, Colorado School of Mines, Environmental Science and Engr. Dept., Golden, Co., USA, 2002.

Sheppard, M.I. and D.H. Thibault, "Default Soil Solid/Liquid Partition Coefficients, K_ds, for Four Major Soil Types: A Compendium," *Health Physics*, Vol. 59, 471-482, 1990.

Silva, R.J., "Mechanisms for the Retardation of Uranium(VI) Migration," *Mat. Res. Soc. Symp. Proc*., Vol. 257, 323-330, 1992.

Silva, R.J. et al., "Thermodynamics 2; Chemical Thermodynamics of Americium," with an appendix on "Chemical Thermodynamics of Uranium," Nuclear Energy Agency, OECD, North-Holland, Elsevier, 1995.

Smith, R. L., S. P. Garabedian, and M. H. Brooks, "Comparison of denitrification activity measurements in groundwater using cores and natural-gradient tracer tests,", *Environ. Sci. Technol. ,* Vol. 30, 3448-3456, 1996.

Smith, R. M., and A. E. Martell, *Critical Stability Constants*, *Volume 4: Inorganic Complexes* , p. 257, 1976.

Stollenwerk, K.G., "Modeling the Effects of Variable Groundwater Chemistry on Adsorption of Molybdate," *Water Resour.Res*., Vol. 31, No. 2, 347-358, 1995.

Stollenwerk, K.G., "Molybdate Transport in a Chemically Complex Aquifer; Field Measurements Compared with Solute-transport Model Predictions," *Water Resour.Res*., Vol. 34, No. 10, 2727-2740, 1998.

Tessier, A., P. G. C. Campbell, and M. Bisson, "Sequential Extraction Procedure for the Speciation of Particulate Trace Metals," *Analytical Chemistry*, Vol. 51(7), 844-851, 1979.

Tripathi, V.S.,"Uranium (VI) Transport Modelling: Geochemical Data and Sub-models." Ph.D. Thesis, Stanford University, 1983.

Turner, D., "A Uniform Approach to Surface Complexation Modeling of Radionuclide Sorption," CNWRA Rept. 95-001, Center for Nuclear Waste Regulatory Analyses, San Antonio, TX, 1995.

Turner, D.R. and S.A. Sassman, "Approaches to Sorption Modeling for High-level Waste Performance Assessment," *J. Contam. Hydrol*., Vol. 21, 311-332, 1996.

Turner, G.D. et al., "Surface-charge Properties and UO_2^{2+} Adsorption of a Subsurface Smectite," *Geochim. Cosmochim. Acta*, Vol. 60, 3399-3414, 1996.

USDOE, "Baseline Risk Assessment of Ground Water Contamination at the Uranium Mill Tailings Site near Naturita, Colorado," U. S. Dept. of Energy, Albuquerque, DOE/AL/62350-195, Rev. 1, 190, 1995.

USDOE, "Programmatic Environmental Impact Statement for the Uranium Mill Tailings Remedial Action Ground Water Project," U.S. Department of Energy, Grand Junction Office, Vol. I, No. DOE/EIS-0198, 314, 1996.

USEPA, "Soil Screening Guidance: User's Guide," EPA/540/R-96/018, Washington, D. C., 1996.

USEPA, "Understanding Variation in Partition Coefficient, K_d, Values," Vol. 1, EPA 402-R-99-0044A, Washington, DC, 1999.

USNRC, "Decision Methods for Dose Assessment to Comply with Radiological Criteria for License Termination," NUREG-1549, U.S. Nuclear Regulatory Commission, Washington, D.C., 1998.

Villalobos, M. and J.O. Leckie, "Surface Complexation Modeling and FTIR Study of Carbonate Adsorption on Goethite," *J. Colloid Interface Sci*., Vol. 235, 15-32, 2001.

von Gunten, H. R. et al., "Seasonal Biogeochemical Cycles in Riverborne Groundwater," *Geochim. Cosmochim. Acta*, Vol. 55, No. 12, 3597-3609, 1991.

Waite, T.D. et al., "Uranium(VI) Adsorption to Ferrihydrite; Application of a Surface Complexation Model," *Geochim. Cosmochim. Acta*, Vol. 58, No. 24, 5465-5478, 1994.

Waite, T.D. et al., "Approaches to Modelling Uranium(VI) Adsorption on Natural Mineral Assemblages," *Radiochim Acta*, Vol. 88, No. 9/11, 687-699, 2000.

Weerasooriya R., D. Aluthpatabendi, and H.J. Tobschall, "Charge Distribution Multi-site Complexation (CD-MUSIC) Modeling of Pb(II) Adsorption on Gibbsite," *Colloids and Surfaces A-Physicochemical and Engineering Aspects*, Vol. 189, 131-144, 2001.

Westall, J. C., M. Cernik, and M. Borkovec, "Modeling metal speciation in aquatic systems", in *Metals in Surface Water*, Ann Arbor Press, p. 191-216, 1998.

Zachara, J.M. et al., "Oxidation and Adsorption of Co(II)$EDTA^{2-}$ Complexes in Subsurface Materials with Iron and Manganese Oxide Grain Coatings," *Geochim. Cosmochim. Acta*, Vol. 59, 4449-4464, 1995.

Zheng, C. & Wang, P.P., "MT3DMS, A Modular Three-dimensional Multi-species Transport Model for Simulation of Advection, Dispersion and Chemical Reactions of Contaminants in Groundwater Systems, Documentation and User's Guide," U.S. Army Engineer Research and Development Center Contract Report SERDP-99-1, Vicksburg, MS, 1999.

NRC FORM 335 (2-89) NRCM 1102, 3201, 3202

U.S. NUCLEAR REGULATORY COMMISSION

BIBLIOGRAPHIC DATA SHEET

(See instructions on the reverse)

1. REPORT NUMBER (Assigned by NRC, Add Vol., Supp., Rev., and Addendum Numbers, if any.)

NUREG/CR-6820

2. TITLE AND SUBTITLE

Application of Surface Complexation Modeling to Describe Uranium(VI) Adsorption and Retardation at the Uranium Mill Tailings Site at Naturita, Colorado

3. DATE REPORT PUBLISHED

MONTH: December YEAR: 2003

4. FIN OR GRANT NUMBER

W6813

5. AUTHOR(S)

James A. Davis and Gary P. Curtis

6. TYPE OF REPORT

Topical research report

7. PERIOD COVERED *(Inclusive Dates)*

1998 - 2003

8. PERFORMING ORGANIZATION - NAME AND ADDRESS *(If NRC, provide Division, Office or Region, U.S. Nuclear Regulatory Commission, and mailing address; if contractor, provide name and mailing address.)*

U. S. Geological Survey; Mail Stop 465; 345 Middlefield Rd.; Menlo Park, CA 940 25

9. SPONSORING ORGANIZATION - NAME AND ADDRESS *(If NRC, type "Same as above"; if contractor, provide NRC Division, Office or Region, U.S. Nuclear Regulatory Commission, and mailing address.)*

Division of Systems Analysis and Regulatory Effectiveness
Office of Nuclear Regulatory Research
US Nuclear Regulatory Commission
Washington, DC 20555-001

10. SUPPLEMENTARY NOTES

J.D. Randall, NRC Project Manager

11. ABSTRACT *(200 words or less)*

The objective of this study was to demonstrate a surface complexation modeling (SCM) approach at the field scale for estimating distribution-coefficient (Kd) values and the retardation of a sorbin g radionuclide with complex aqueous chemistry. SCM offers an improved way to estimate sorption in the NRC's performance assess ments of decommissioning and nuclear waste facilities. A uranium site near Naturita, Colorado, was chosen for study , because it had a well-developed and definable uranium(VI) plume in a shallow alluvial aquifer and had spatially variant chemi cal conditions that were believed to be important in influencing U(VI) transport and retardation. A generalized composite (GC) S CM was developed for the Naturita aquifer background sediments based on fitting batch U(VI) adsorption data. The GC-SCM w ithout electrical double-layer terms was able to simulate Kd values accurately for U(VI) adsorption on the Naturita aqui fer sediments over the observed range of pH and dissolved carbonate and U(VI) concentrations. At this site, alkalinity was more important than pH or U(VI) concentration in influencing U(VI) mobility. Kd values ranged from 0.29 to 22 mL/g when calcula ted for all Naturita groundwater analyses using SCM. Kd values decreased with increasing concentrations of dissolved U(VI) and alkalinity.

12. KEY WORDS/DESCRIPTORS *(List words or phrases that will assist researchers in locating the report.)*

Radionuclide Transport, Geochemistry, Soprtion, Surface-Complexation Modeling

13. AVAILABILITY STATEMENT

unlimited

14. SECURITY CLASSIFICATION

(This Page) unclassified

(This Report) unclassified

15. NUMBER OF PAGES

16. PRICE

This form was electronically produced by Elite Federal Forms, Inc.

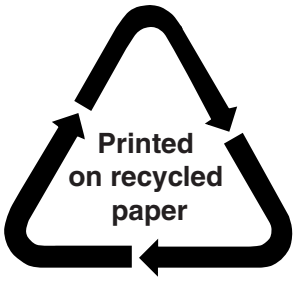

Federal Recycling Program